CONFORMATION AND FUNCTION OF GRAMICIDIN S, A PEPTIDE ANTIBIOTIC WHICH MEDIATES PHASE TRANSFER OF NUCLEOTIDES AND NUCLEIC ACIDS

Thesis by

Eric Martin Krauss, M.D.

In Partial Fulfillment of the Requirements

for the Degree of

Doctor of Philosophy

California Institute of Technology

Pasadena, California 91125

1983

(Submitted February 11, 1983)

Dedicated to the Memory of Professor Robert W. Vaughan

Acknowledgments

I wish to thank Sunney Chan for his guidance in this work. His unique perspective on biophysical chemistry and insistence on excellence in research were invaluable. I am also grateful for my many discussions with Chan group members which broadened my perspective on research and science in general. My experience at Caltech has more than vindicated my decision to devote myself to the advancement of science.

Many members of the Caltech community provided assistance at various stages of this work. Professor George Rossman and his students made available the Perkin-Elmer 180 IR spectrophotometer; Professor Judith Campbell provided instruction, advice, and laboratory space for the microbiological studies; Mr. Roger Shelton assisted with amino acid analyses; and the Schroeder, Gray, and Richards groups generously furnished needed equipment at critical stages. To all, I extend sincere thanks. I am especially grateful to Dr. Luciano Müller and the staff of the Southern California Regional NMR facility for keeping the "500" up and operating throughout the heart of this work.

Thanks are due to Professor David Cowburn of Rockefeller University for his guidance and encouragement in the early phases of the project, and to Professor Herman Wyssbrod of the Mt. Sinai School of Medicine for providing extensive preprints of his research on gramicidin S.

Mrs. Henriette Wymar is to be credited for an excellent typing job.

The support of my family has been a source of strength throughout. My wife, Anne, maintained a keen and critical interest in my work, as well as overseeing the upbringing of my daughters Miriam and Rachel (my principal avocation, as well). We acknowledge the devotion of our parents, Mr. and Mrs. K. Martin Stevenson of Santa Barbara and Mr. and Mrs. Lawrence B. Krauss of New York.

Financial assistance was provided in part by an NIH predoctoral fellowship, an Earle G. Anthony fellowship, the ARCS Foundation, and Professor Chan.

THE PLEATED SHEET

The chemists took several polypeptide chains and laid them side by side. Hydrogen and oxygen atoms bulged out here and there on the chains. And to their joy the chemists found that certain hydrogen atoms fitted neatly against oxygen atoms on adjoining chains, linking the chains snugly with a series of straight N-H-O bonds.

The linked polypeptide chains lying side by side formed a flattish pattern. But the chains did not lie perfectly flat; they zigzagged along their length and their attached groups stood out sharply, this way and that. So the pattern has been given the name of the pleated sheet.

But is there any protein that really has this structure? To answer that question, let us follow the chemists in an investigation started several years ago.

– from "The World of Science" by Jane Watson, Simon & Schuster, New York, 1958.

ABSTRACT

Gramicidin S (GrS; cyclo-(Val^1-Orn^2-Leu^3-D-Phe^4-Pro^5)$_2$) is a cyclosymmetric decapeptide antibiotic synthesized by mature cultures of the gram-positive spore former, Bacillus brevis. Its amphiphilic character and antiparallel β-pleated conformation in solution are experimentally established, but the extent of internal hydrogen bonding, the structural basis of its cytotoxicity and the physiological role in the producer organism remain unelucidated. These issues are addressed in the present investigation.

The secondary structure of GrS is studied by a combination of proton exchange kinetics and vibrational spectroscopy. Dispersion in amide proton exchange rates provides a means of synthesizing variably N-deuterated GrS congeners, the isotopic composition of which are determined quantitatively by NMR. Difference IR of Me_2SO solutions then affords isolation of residue-specific peptide group vibrations. Two pairs of equivalent hydrogen bonds with donor groups Leu NH and Val NH are identified, and their geometry and energetics characterized. The β-pleated conformation is thus shown to be stabilized by the maximum of four transannular hydrogen bonds.

The solution conformation of the functionally essential ornithine side chains is then investigated by ^1H and ^{15}N NMR spectroscopy at 11.7 Tesla. Rotational averaging of the chemical shifts of the Orn $C^{\delta}H_2$ protons is incomplete, the degree to which the apparent motility of the side chain is limited varying inversely with the ability of the solvent to compete for hydrogen bonding donor or acceptor sites. Methylation of

GrS to give [N^{δ}-trimethylornithyl$^{2,2'}$]-GrS results in an upfield shift of 3.5 ppm in the ^{15}N resonance of Pro in MeOH and abolishes the correlation of the Orn $C^{\delta}H_2$ splitting with solvent basicity. The data are consistent with the presence of intramolecular Orn $N^{\delta}H_3^+$--O=C D-Phe hydrogen bonds, each with formation constant ~1.1 in MeOH at 23° C, and exerting a substantial charge relay effect on the Pro ^{15}N chemical shift. Proton exchange kinetics and nuclear Overhauser enhancement measurements indicate that these hydrogen bonds are formed in the $\underline{i} \rightarrow \underline{i} + \underline{2}$ sense. Estimates for the Orn side chain torsional angles in the intramolecularly hydrogen bonded configuration are given, and the possible origin of the Orn $C^{\delta}H_2$ chemical shift inequivalence discussed.

The studies of the solution conformation raise the possibility that the biological actions of GrS involve complexation of polyvalent anions; Orn $N^{\delta}H_3^+$--O=C D-Phe hydrogen bonding might then ensure a critical intercationic distance (6-8 Å) which is complementary to the architecture of the anionic species. Indeed, it is shown that GrS binds nucleotides in water to yield a complex which partitions into organic solvents. The observed phase transfer efficiencies at a given pH increase in the order AMP < ADP < ATP. The lipophilic complexes have well-defined stoichiometries, which are determined to be 1:1 for ADP-GrS at pH 7 and ATP-GrS at pH 3 and 1:2 for ATP-GrS at pH 7. The interaction is primarily ionic, involving coordination of the Orn $N^{\delta}H_3^+$ groups of the peptide and the phosphoryl groups of the nucleotide, with little contribution from the nucleoside moiety. The nucleotide complexes are sparingly soluble in water, and self-associate extensively

in $CHCl_3$, most likely by cross-β aggregation, to yield large, ribbon-like aggregates which give rise to broad NMR resonances. Structures for the 1:1 and 1:2 complexes are proposed. In the latter, two GrS molecules envelop the nucleotide, orienting their apolar faces externally in opposite directions, while the lateral faces retain considerable polar character and direct aggregation in organic media. The 1:1 complex possesses a single apolar face and is less lipophilic. Binding constants are estimated by simulation of the extraction data.

A novel interaction between GrS and nucleic acids is subsequently characterized which, like that between GrS and nucleotides, exploits both the dicationic and amphiphilic properties of the peptide. Complex formation between calf thymus DNA and GrS is demonstrated by (i) phase transfer to $CHCl_3$ of ultrasonically irradiated DNA and (ii) inhibition of phase transfer to $CHCl_3$ of ATP by either native or ultrasonically irradiated DNA. The stoichiometry of the interaction is 2:1 (DNA-P/GrS) as expected for a predominantly electrostatic mode of binding. The extraction-competition data suggest that the affinity of GrS for DNA is considerably higher than it is for free nucleotides. It is proposed that during dormancy stoichiometric binding by GrS ensheaths the bacterial chromosome in a dense peptide matrix possessing a highly apolar external surface, which should constitute an effective barrier against chemical degradation.

In order to elucidate the molecular basis for GrS toxicity <u>in vivo</u> microbiological studies of GrS and analogues derivatized at ornithine are undertaken. The minimum lethal concentrations of GrS,

[N^{δ}-trimethylornithyl$^{2,2'}$]-GrS, and [N-acetylornithyl^{2}]-GrS in a standard bioassay employing Staphylococcus aureus in nutrient broth are compared. In addition, the time course of attenuation of the culture by GrS and the dependence of the minimum lethal concentration on initial cell concentration are determined. A model for GrS action is proposed involving internalization and formation of cytotoxic lipophilic complexes with polyanionic substrates, possibly nucleotides. The limiting antibiotic potencies at zero initial cell concentration and apparent extraction constants for nucleotides estimated in vitro are shown to be consistent with this model.

TABLE OF CONTENTS

Abbreviations

AcGrS, [N^{δ}-acetylornithyl^{2}]-GrS; Ac_2GrS, [N^{δ}-acetylornithyl$^{2,2'}$]-GrS; ADP, adenosine 5′-diphosphate; AMP, adenosine 5′-monophosphate; ATP, adenosine 5′-triphosphate; CD, circular dichroism; ChaGrS, [D-cyclohexylalanyl$^{4,4'}$]-GrS; CTP, cytidine 5′-triphosphate; CW, continuous wave; DMPC, dimyristoylphosphatidylcholine; DNA, deoxyribonucleic acid; DNA-P, deoxyribonucleic acid monomer phosphate; DPPC, dipalmitoylphosphatidylcholine; DPPE, dipalmitoylphosphatidylethanolamine; DS-Dabco, (N,N′-distearyl)1,4-diazabicyclo-[2.2.2]octane; EDTA, ethylenediamine tetraacetic acid; ESR, electron spin resonance; EYL, egg yolk lecithin; GrS, gramicidin S; GTP, guanosine 5′-triphosphate; H bond, hydrogen bond; HX, hydrogen (proton) exchange; IR, infrared (spectrophotometry); LG, linear gramicidin; Me_6GrS, [N^{δ}-trimethylornithyl$^{2,2'}$]-GrS; MIC, minimum inhibitory concentration; MLC, minimum lethal concentration; NADH, β-nicotinamide adenine dinucleotide; NAS, N-acetyloxysuccinimide; NBD, N-4-nitrobenz-2-oxa-1,3-diazole; NHS, N-hydroxysuccinimide; NMR, nuclear magnetic resonance; NOE, nuclear Overhauser enhancement; NTP, nucleoside triphosphate; ORD, optical rotatory dispersion; RNA, ribonucleic acid; TLC, thin-layer liquid chromatography; Tris, tris(hydroxymethyl)-aminomethane; tRNA, transfer RNA; TTP, thymidine 5′-triphosphate; UTP, uridine 5′-triphosphate; UV, ultraviolet (spectrophotometry).

CHAPTER I

INTRODUCTION

1. Gramicidin S: A Cyclodecapeptide Antibiotic Produced by Bacillus Brevis

Discovery and Characterization. In 1939, eleven years after the discovery of and two years before the first commercial production of penicillin, Dubos reported the isolation from aerobic sporogenous Bacillus brevis cultures a crude preparation, tyrothricin, which was bactericidal towards gram-positive microorganisms (1). It was subsequently shown that tyrothricin consisted of a mixture of two classes of polypeptides: the neutral gramicidins, with a high content of tryptophan and aliphatic D amino acids, and the basic, cyclic tyrocidines, containing the unusual amino acids ornithine and D-phenylalanine (2). Both substances, as well as the crude preparation, were considerably less potent towards gram-negative bacteria, and were highly lethal to animals when administered internally (2). Gause and Brazhnikova, attempting shortly thereafter to isolate tyrothricin-producing B. brevis strains from soil samples in the Soviet Union by methods similar to those employed by Dubos, discovered instead a new antibiotic substance, chemically distinct from both gramicidin and tyrocidine, which they named gramicidin S (Soviet) (3). Also a product of an aerobic sporogenous B. brevis strain, gramicidin S (GrS) was found to be bactericidal towards Staphylococus aureus in concentrations as low as 3×10^{-6} g ml^{-1}, while 5×10^{-5} g ml^{-1} was effective against Escherichia coli cultures. GrS was used extensively during the Second World War in the Soviet Union in the treatment of septic lacerations.

The method of delivery was primarily direct installation of an aqueous lavage containing 6×10^{-4} g ml^{-1} of the recrystallized peptide (3). The therapeutic use of GrS was ultimately curtailed because of its hemolytic effect (4) and the wider availability of penicillin and streptomycin.

Within a year of its discovery, the amino acid composition of the minimum stoichiometric unit had been determined to be one equivalent of each of D-Phe, Leu, Orn, Pro, and Val, and it was suggested that the molecule was cyclic (5). Synge concluded in 1945, "The relationship of gramicidin S to tyrocidine hydrochloride is emphasized, and a plea is made for renaming gramicidin S to bring out this relation" (5). His advice was not heeded, and the confusing nomenclature persists. The pentapeptide sequence was determined from partial hydrolysates to be -VOLF̂P- (6), and the molecule was thereafter shown, by an elegant application of countercurrent distribution chromatography, to be a decapeptide (7). By 1965, the primary structures of the naturally occurring tyrocidines (8-10) and linear gramicidins (11-13) had been determined. GrS was evidently a dimer of the invariant pentapeptide fragment of the tyrocidines, bearing no similarity to the linear gramicidins (Table I).

Schwyzer and Sieber, in 1957, synthesized GrS by solution-phase methods (14), the first synthesis of a naturally occurring cyclic peptide. The dihydrochloride was obtained as colorless needles from EtOH-1 N HCl (dec 277-278°, $[\alpha]_D^{24}$ = -289° (70% EtOH)) (14). The peptide has since been produced synthetically by the Merrifield method (15). It is very soluble in polar organic solvents, practically insoluble in $CHCl_3$, and insoluble in pure ethers or liquid hydrocarbons. It has been

Table I. Primary Structures of Gramicidin S and the Component of Tyrothricin[a]

1	2	3	4	5	6	7	8	9	10	11	12	13	14	15		
cyclo - (V	O	L	F̂	P	V	O	L	F̂	P)							Gramicidin S
cyclo - (V	O	L	F̂	P	F	F̂	N	Q	Y)							Tyrocidine A
cyclo - (V	O	L	F̂	P	W	F̂	N	Q	Y)							Tyrocidine B
cyclo - (V	O	L	F̂	P	W	Ŵ	N	Q	Y)							Tyrocidine C
cyclo - (V	O	L	F̂	P	W	Ŵ	N	Q	W)							Tyrocidine D
HCO - V	G	A	L̂	A	V̂	V	V̂	W	L̂	W	L̂	W	L̂	W	- NHEtOH	Val-Gramicidin A
HCO - I	G	A	L̂	A	V̂	V	V̂	W	L̂	W	L̂	W	L̂	W	- NHEtOH	Ile-Gramicidin A
HCO - V	G	A	L̂	A	V̂	V	V̂	W	L̂	F	L̂	W	L̂	W	- NHEtOH	Val-Gramicidin B
HCO - I	G	A	L̂	A	V̂	V	V̂	W	L̂	F	L̂	W	L̂	W	- NHEtOH	Ile-Gramicidin B
HCO - V	G	A	L̂	A	V̂	V	V̂	W	L̂	Y	L̂	W	L̂	W	- NHEtOH	Val-Gramicidin C
HCO - I	G	A	L̂	A	V̂	V	V̂	W	L̂	Y	L̂	W	L̂	W	- NHEtOH	Ile-Gramicidin C

[a] D residues are indicated by a caret (^).

reported that GrS is practically insoluble in water, and studies of the peptide in aqueous systems have generally utilized an admixture of 5 to 10 percent MeOH (16,17). However, aqueous solutions of 10^{-2} M are readily obtained if the dihydrochloride is first lyophilized, a manipulation which alters neither the spectral properties nor the biological activity of the peptide (18). GrS · 2HCl possesses a powerfully sweet taste (18).

Secondary Structure of GrS. In an attempt to synthesize the cyclic pentapeptide cyclo-(VO(Ts)LF̂P) from the para-nitrophenyl ester in pyridine, Schwyzer and Sieber unexpectedly obtained exclusively a cyclic decapeptide which, on deprotection, was identical to GrS (19). They proposed that the critical intermediate was a head-to-tail dimer in which the pentapeptides formed an antiparallel β-pleated structure. Simultaneously, X-ray diffraction patterns of a number of GrS salts and di-N-acylornithyl-GrS derivatives were measured by Hodgkin and coworkers (20, 21). While it was not possible, because of residual disorder in the crystal, to solve the structure, a β sheet configuration, based upon the structure proposed for β keratin by Pauling and Corey (22), was suggested (among others) to be consistent with the observed packing (23). In this model, the molecule possessed C_2 symmetry, the -VOL- fragments were extended, and Val and Leu NH were transannularly hydrogen bonded (H-bonded) to Leu and Val C=O, respectively (Figure 1a).

For a decade following the first synthesis, a number of very different conformations were considered. In part, confusion was engendered by IR dichroic (24) and CD and ORD data (25, 26) which were

Figure 1. Proposed structures for gramicidin S.

A. β sheet structure of Hodgkin and Oughton (23), 1957.

B. β sheet-β-III turn solution conformation, Stern et al. (28), 1968. The molecule is viewed along the C_2 axis, but from the side opposite that of Fig. 1A.

C. β sheet-β-II′ turn solution conformation, Ovchinnikov et al. (30), 1970. This structure was initially proposed for the [2, 2′-N-acetyl-ornithyl]-GrS analogue in organic solvents. Note that an additional H bond between Orn $N^{\delta}HC{=}O$ and Orn N′H is indicated.

D. Calculated M1 structure of Dygert et al. (56), 1975. This and more recent structures show the phenyl group of D-Phe overlying the Pro ring, as suggested by large anisotropic shielding effects observed in the ^1H NMR spectrum (34). The figure was reproduced from Scheraga, H. A. (1981) Biopolymers 20, 1877-1900.

E, F. The crystalline urea complex (59), 1978. The structures are of the β sheet-β-II′ type, but it is the GrS dimer (with associated molecules of urea) which is cyclosymmetric. A pair of intermolecular H bonds also forms (Orn NH··O=C Orn′). The ORTEP diagrams are reproduced from reference 62.

G. A schematic representation showing the β sheet-β-II′ turn structure, omitting the transannular H bonds.

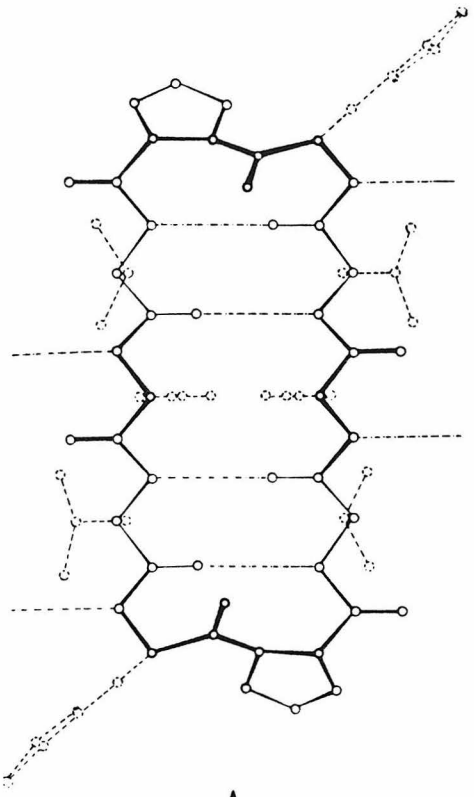

A

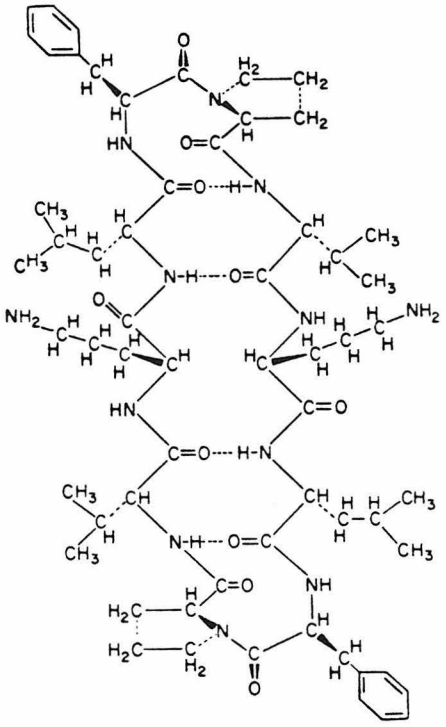

B

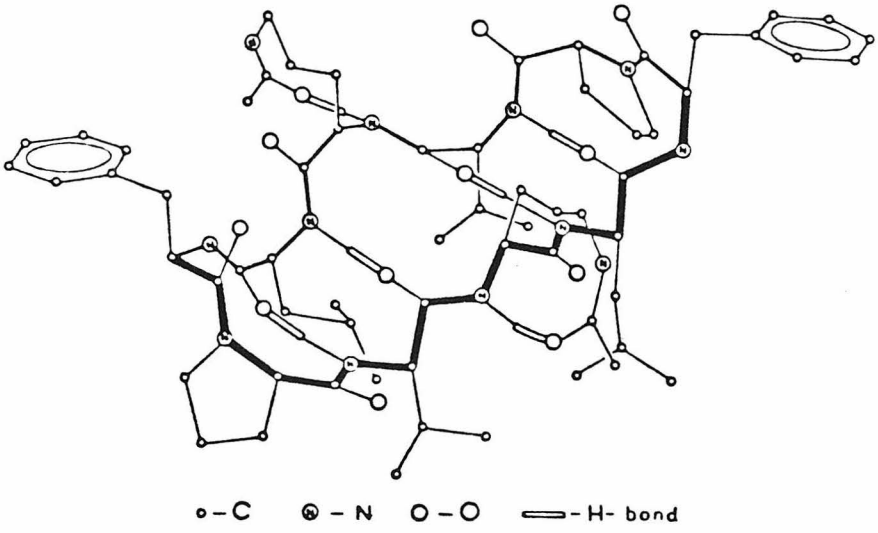

C

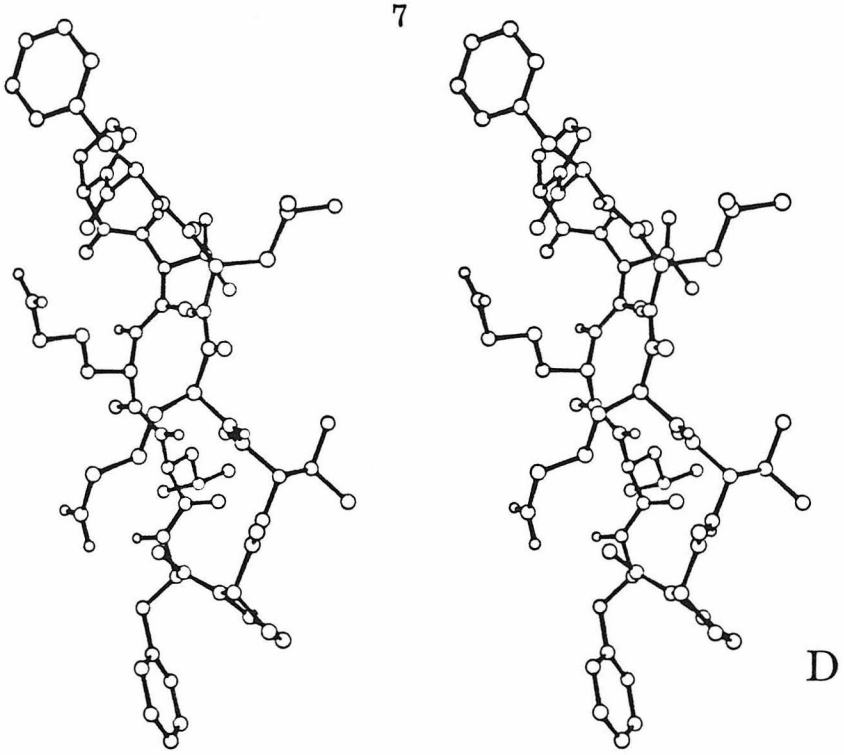

D

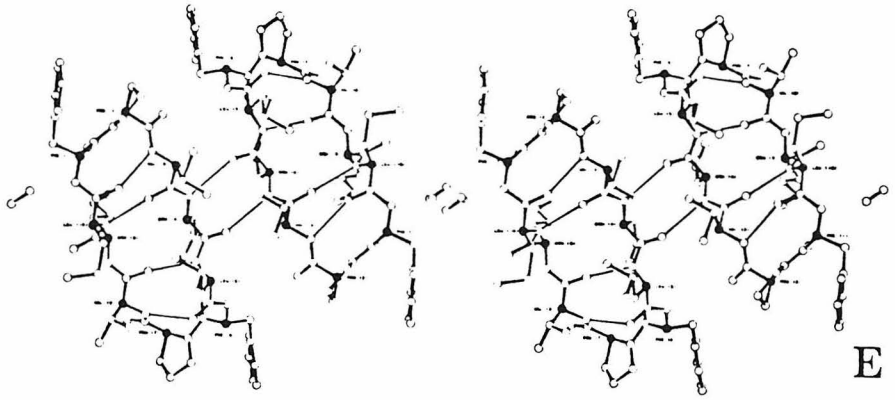

E

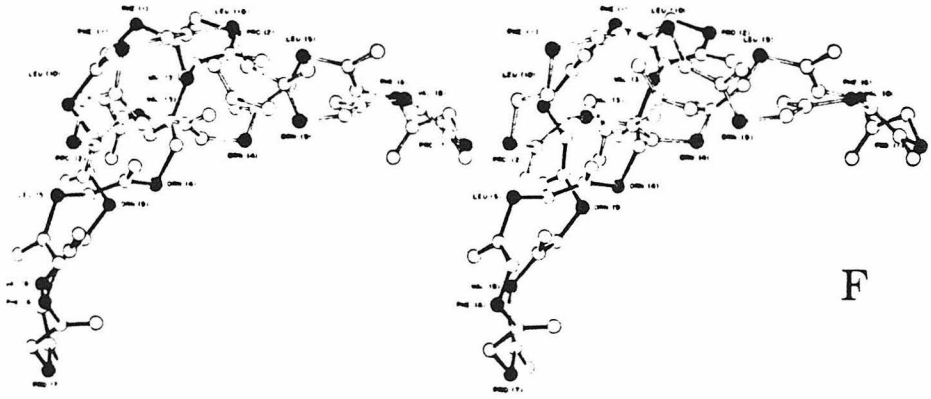

F

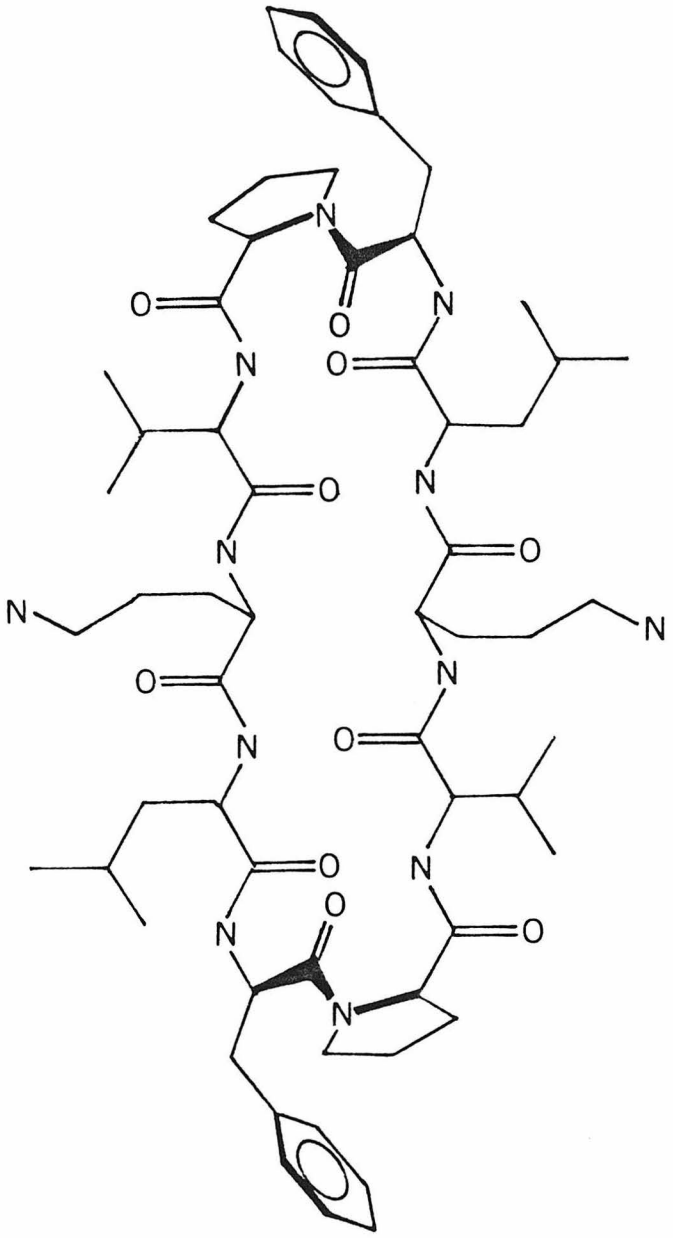

G

consistent with α-helical character, and difficulty obtaining correct ^1H NMR assignments (27). Experimental support for the β sheet model was finally provided in 1968 by Craig and coworkers (28) who performed the first systematic ^1H NMR study in Me_2SO and MeOH at 60, 100, and 220 MHz. They determined that GrS possessed twofold symmetry on the NMR timescale, and the dihedral angles ϕ for Val, Orn, and Leu were close to 150°, as indicated by comparison of the vicinal coupling constants $^3J_{NHC^\alpha H}$ ($=^3J_{NH}$) with values for model compounds. Hydrogen exchange was markedly retarded at Val and Leu NH, demonstrating that these protons were shielded from solvent. A structure of the β sheet type was proposed (28) similar to those suggested by Schwyzer and Sieber (19) and Hodgkin and Oughton (23) containing 2 pairs of internal H bonds and 2 β-III (29) turns (Figure 1b).

The proposal of Craig and coworkers was subsequently modified by Ovchinnikov et al. (30), who used a refined Bystrov-Karplus relationship in the analysis of $^3J_{NH}$ to establish that the 4 → 1 turns were type II′ (Figure 1c). NMR studies performed in the succeeding decade have confirmed the general features of this structure in Me_2SO (31-34), MeOH (35-37), $(CH_2OH)_2$ (38), F_3EtOH (39-42), and water (16, 37, 43). Evidence brought out in favor of the model included magnetization transfer measurements (31-33, 38, 44), solvent variation of amide ^1H (39, 40, 45), ^{13}C (40), and ^{15}N chemical shifts (41, 42, 46), anisotropic shielding of Pro $C^\delta H_2$ by the phenyl group of D-Phe (34), and proton exchange rates (37, 43, 47). Investigations of the dynamics of GrS in solution have confirmed that the backbone is relatively rigid (44, 48, 49), lending support to the assumption (critical in the inter-

pretation of NMR observables, such as the chemical shifts and coupling constants, which are affected by motional averaging) that a single predominant backbone conformation exists, while the side chains exhibit segmental flexibility (48, 49).

Tertiary Structure of GrS. The β sheet structure suggests a functional "sidedness" to the molecule: the positively charged side chains of Orn are directed to one side of the ring, whilst the aliphatic side chains of Val and Leu are directed to the opposite side. (The side chains of D-Phe appear to lie nearly in the ring plane). The notion of amphiphilicity was supported by the early studies of the ability of GrS to form monolayers at air-water interfaces (50, 51). However, it has proven difficult to establish the spatial orientations of the side chains experimentally by spectroscopic methods, even with the availability of high field NMR instrumentation affording satisfactory spectral dispersion. There are several major obstacles. First, no information has been obtained concerning the backbone dihedral angles ψ. Vicinal coupling constants which report on this angle ($^3J_{^{15}NC'C^{\alpha}H}$, $^3J_{^{15}NC'C^{\alpha}{}^{13}C^{\beta}}$, $^3J_{^{15}NC'C^{\alpha}{}^{15}N}$) involve the observation of rare nuclei, and are smaller in magnitude than vicinal ^1H-^1H couplings. Model compound data are generally lacking (52). Second, C^{β} of every residue save Val is bonded to 2 protons, so that 2 values of $^3J_{HC^{\alpha}C^{\beta}H}(= {}^3J_{\alpha\beta})$ are measured; no estimate of the first side chain dihedral angle χ^1 can be made until the $C^{\beta}H_2$ protons are stereospecifically assigned by ^2H substitution or other means (53, 54). Finally, side chain motions which are rapid compared to ^3J will average this parameter, so that assumptions concerning the nature of the averaging must be made in

order to describe the structures contributing to the time-averaged conformation (55).

A set of measurements of $^3J_{\alpha\beta}$ were obtained for GrS in MeOH by Gibbons and coworkers (35), and the values subjected to standard Pachler analysis (36), where it was assumed that for Val, Orn, Leu, and D-Phe only the 3 staggered rotamers ($\chi^1 = 180°, \pm 60°$) contributed to the average structure, while for Pro a fixed dihedral angle was assumed. For the reasons noted above, rotamer populations could not be determined unambiguously, although the method of analysis suggested that for each of Orn and D-Phe one of the 3 classical rotamers was dominant. The study did not extend beyond the first side chain segment. Presumably, any attempt to do so would require a means of circumventing the difficulties presented by the increase in segmental motions with increasing distance from the backbone.

Recent Studies of the Total Conformation. A symmetry-constrained energy minimization study has been performed by Scheraga and coworkers (56) and 9 minima obtained, of which the 3 lowest in energy ("M1-M3") were of the β sheet type containing β-II′ turns (Figure 1d). The calculation neglected solvation, utilized measured values of $^3J_{NH}$ in Me_2SO and MeOH as constraints, and was not exhaustive for the side chain conformations. Interestingly, in the M1-M3 conformations only a single pair of transannular H bonds was present (Leu NH—O=C Val), in contrast to previously proposed β-type models which contained 2 pairs. Here, Val NH is buried in a hydrophobic pocket and thus is inaccessible to solvent. This apparent discordance concerning the H-bonding scheme could not be experimentally

settled, since the NMR and kinetic data adduced in favor of internal H bonding of Leu and Val NH were indicative only of solvent shielding of these groups, not of H bonding per se. The M1 conformation contained, in addition, a backbone twist and a pair of Orn $N^{\delta}H_2$—O=C D-Phe H bonds in the i → i - 3 sense, which had not previously been predicted. The Scheraga model has found wide acceptance, as indicated by a tendency in later publications to develop indices of similarity to the M1-M3 structures (36,57). Such indices are of little physical significance, since many interconverting structures are present in solution, and the number of true minima (or their corresponding energies) is entirely unknown. The most recent NMR study (57) is an attempt at "proximity mapping" (58) by measurement of a large number of nuclear Overhauser enhancements. Since the saturating field was applied continuously under circumstances in which the extreme narrowing condition did not obtain (400 MHz, Me_2SO, $\tau_c \sim 10^{-9}$ s (49), $\omega\tau_c > 1$) and no allowance was made for spin diffusion (38), the analysis of the enhancements is without meaning.

The crystal structure of the hydrated urea complex was solved by Hull et al. (59). Because of the interaction of one ring edge of each GrS molecule with a molecule of urea, individual GrS molecules lacked C_2 symmetry (Figure 1e,f) so that the relation of this structure to the time-averaged solution conformation detected by other methods is difficult to assess. Loss of molecular symmetry has been observed in crystalline synthetic cyclopeptides which appear to be cyclosymmetric in solution (60,61). The structure was, however, of the β sheet type, and apparently contained the 4 transannular H bonds originally proposed

($\underline{R}_{NO}$ not published). In addition, there was one Orn $N^{\delta}H_3^+$—O=C $\underline{\underline{D}}$-Phe H bond in the $\underline{i} \rightarrow \underline{i}+2$ sense and one intermolecular H bond (Orn NH—O=C Orn′) per GrS molecule. The backbone twist, although asymmetric, was clearly in the sense opposite to that of the Scheraga structures, as determined from the ORTEP diagrams (56, 62).

Structural Comparison of GrS and the Tyrocidines. Relatively less is known of the structure of the tyrocidines. Separation of the individual species is difficult, the only methods successfully employed on a preparative scale having been countercurrent distribution procedures developed by Craig (63) or Okamoto (64). The tyrocidines aggregate extensively in aqueous solution (65) unlike GrS, which is monomeric (51). The tyrocidines form surface monolayers as well, but do not exhibit the extended low-viscosity region in which nonzero surface pressures can be obtained at high surface areas, as does GrS, a difference attributed to greater electrostatic repulsion between individual GrS molecules (50). Recent conformational studies, based on ^{1}H NMR, have suggested a secondary structure of the antiparallel β-pleated type containing one β-I and one β-II′ turn (66, 67), with a topochemistry considerably more complex than GrS (68). Studies such as these, in which a conformation is built up from interproton distances and rotamer populations determined by cross-relaxation rates and homonuclear vicinal coupling constants, respectively, have been seriously questioned on methodological grounds (69).

Interaction of GrS with Lipid Bilayers. The first studies of the interaction of GrS with synthetic phospholipid membranes were performed by Chapman and coworkers. As part of a larger effort to elucidate the

effects of proteins on membrane structure, the membranotropic behavior of the cyclic antibiotics GrS, valinomycin, alamethicin (since shown to be acyclic), and polymixin B were investigated by physical methods. An unsonicated suspension of egg yolk lethicin (EYL) and GrS, mole ratio 1:1.3 (10^{-2} g ml^{-1} lipid) gave rise to a ^1H NMR spectrum containing high-resolution features characteristic of sonicated preparations of pure phospholipid. X-ray diffraction indicated the absence of lamellar structures (70). It was thereafter shown (71) that GrS present in equimolar or greater amounts solubilized multibilayer suspensions of dipalmitoylphosphatidylcholine (DPPC), both above and below the gel-to-liquid crystalline phase transition temperature $\underline{T}_m$. The resulting particles were estimated by ultracentrifugation to have a molecular weight of $\sim 4 \times 10^4$. Addition of GrS shifted $\underline{T}_m$ to slightly lower temperatures, but the enthalpy change per mole lipid appeared unchanged, and the motional state of spin-labeled fatty acid incorporated into the DPPC suspension was unaltered by GrS. It was concluded (71) that GrS, in sufficiently high concentrations, interacted with adjacent phospholipid head groups in a purely electrostatic fashion to yield micelle- or vesicle-like particles.

Wu et al. (72), utilizing substoichiometric quantities of the antibiotic which did not result in micellization, obtained evidence claimed to be indicative of an interaction with the hydrocarbon region of the bilayer as well. The lateral diffusion coefficient $\underline{D}$ of a fluorescent-labeled derivative, [N-4-nitrobenz-2-oxa-1,3-diazole-ornithyl]-GrS (NBD-GrS) was shown by fluorescence recovery after photobleaching to decrease abruptly below $\underline{T}_m$ in dimyristoylphosphatidylcholine (DMPC)

multibilayers, while $\underline{D}$ of NBD-labeled phosphatidylethanolamine (PE) decreased 1.5-fold in the presence of 20 mole percent GrS. Cholesterol (> 20 mole percent) apparently excluded NBD-GrS from DMPC membranes (but not from EYL). The phase transition was broadened and shifted by 5° to lower temperatures over the range of 4 to 20 mole percent GrS, with a 2-fold increase in $\Delta\underline{H}$; the behavior of NBD-GrS was identical on calorimetry. The calorimetric work was subsequently extended to multibilayers of DPPC and DPPE (73) with qualitatively similar results, but approximately twice as much GrS in DPPC was required relative to DMPC or DPPE to produce the $\underline{T}_m$ shift, and the estimated $\Delta\underline{H}$'s were only 1.0 to 1.5-fold larger. A laser Raman study of DMPC multibilayers containing 25 mole percent GrS revealed an apparent disordering of acyl chains below $\underline{T}_m$, as indicated by decreased relative intensity of the 1062 cm^{-1} "trans" band, with little change above $\underline{T}_m$; on differential scanning calorimetry, the transition was broadened and shifted 5-10° to lower temperature, and there was a 5-fold <u>decrease</u> in ΔH (74).

While the results of the more recent investigations may be consistent with incorporation of GrS into the bilayer, they are not conclusive. If, for example, GrS formed a sufficiently tight chelate with the head groups of neighboring phospholipid molecules, as had been proposed originally, it is plausible that $\underline{D}$ of NBD-GrS would still change abruptly at $\underline{T}_m$, and the increase in $\underline{D}$ of the phospholipid in the presence of GrS would arise simply because the diffusing entity is a phospholipid dimer. The exclusion effect of cholesterol can be rationalized by a direct interaction of the latter with the phospholipid head group, which

interferes with the electrostatic binding of GrS. The decrease in cooperativity in the phase transition might derive from altered packing consequent to head group chelation by GrS, since the surface area of the antibiotic (150 - 200Å (21,52)) is more than twice that of the phospholipid; the degree to which the packing of the hydrocarbon chains is affected should then vary with the size of the head group and the length of the alkyl chains, as observed.

The question of whether GrS is physically incorporated into phospholipid bilayers thus remains, despite major efforts, unsettled. The principal objection to the hypothesis of simple electrostatic binding derives from consideration of the known biological role of the hydrophobic face of the peptide; studies of analogues have demonstrated that substitution at positions 1 or 3 with hydrophilic residues yields a conformationally similar, but completely inactive, compound (75). If the binding of GrS to synthetic membrane bilayers is indeed purely electrostatic, the model membrane studies will have revealed at most a single facet of a considerably more complex interaction occurring in vivo. There are two additional difficulties with the synthetic membrane studies: (i) The concentrations employed, because of the inherently low sensitivities of methods such as NMR, Raman scattering, and differential scanning calorimetry, are 10^3 to 10^4-fold higher than encountered physiologically or in the bioassay, and (ii) pure phospholipid bilayers, particularly those containing phosphatidylcholine, are poor models for bacterial membranes, which lack phosphatidylcholine and typically contain only 20 to 30 percent lipids.

Antibiotic Action of GrS. The mechanism of action of GrS against sensitive microorganisms is poorly characterized; the collected observations of the past two decades do not form a coherent whole. It is generally acknowledged that less sensitive bacteria, such as E. coli, are relatively impermeable to the drug (17, 77), and that GrS does not induce the transmembrane transport of cations (78).

It was shown by the Osaka group that incubation of susceptible strains of several species with ^{14}C-labelled GrS for 20 min resulted in almost quantitative labelling of a 140,000 g fraction associated with ribonucleoprotein (77). When the monodansyl derivative of GrS was used, fluorescent granules were observed in the sensitive strains of B. megatherium, but not resistant strains (79). Subsequent studies focused on events attributed to a membranolytic action of the antibiotic. Exposure of sensitive strains of Micrococcus pyogenes to the minimum lethal concentration (10^{-6} M) of GrS for 1 to 10 min at temperatures between 0 and 24° C resulted in the release of acid-soluble nucleotides into the medium (80), while tenfold higher concentrations caused lysis of M. lysodeikticus protoplasts (81). Treatment of mitochondria with concentrations ranging from 1 to 200×10^{-6} M was associated with a variety of nonspecific toxic effects ranging from swelling to release of oxidative enzymes (4). Reports of inhibition of membrane-bound enzyme systems at relatively high concentrations of antibiotic were made by several groups (4).

The membranolytic effect of GrS was ascribed to its detergent-like character before the topochemical features of the β sheet structure were established (4). As noted above, the close relationship of GrS to

the tyrocidines was recognized shortly after their discovery. In the first biological studies of tyrocidine, it was found (82) that these peptides and a number of cationic surfactants exerted similar effects on microorganisms, and at similar concentrations (which were actually considerably higher than the minimum lethal concentrations for tyrocidines reported in recent studies (64, 83)), and that the cationic character of the antibiotic was essential for bactericidal activity. Tyrocidine was then proposed to function as a cationic detergent (82), and GrS was presumed to act similarly (4).

Once the solution structure had been grossly characterized and the initial studies on the interaction with synthetic membranes carried out, Ostrovskii and coworkers proposed that the molecular basis for the bactericidal effect of GrS was in fact the electrostatic interaction between GrS and the head groups of adjacent phospholipids, which altered the mobility of the lipids in the bacterial membrane and thereby indirectly interfered with oxidative phosphorylation (84). In vitro, GrS was shown to inhibit the activities of membrane-bound malate and lactate dehydrogenase from M. lysodeikticus (85), with maximal effect observed after 30 min, and render NADH dehydrogenase more susceptible to proteolysis. The enzyme inhibition was not reversed by excess micrococcal lipids added after GrS treatment. Triton X-100 (1 percent) eliminated the inhibitory effect on malate dehydrogenase. ESR spectra of spin-labeled fatty acids incorporated into the membrane preparation suggested a slight (1.5 to 2.8-fold) increase in apparent rotational correlation times. These results were interpreted by the authors as compatible with the electrostatic binding hypothesis, and it was

proposed that enzyme inactivation was mediated by a condensation of boundary lipid induced by GrS (85, 86).

Later experiments failed to show any inhibitory effect of Ca^{++} or aliphatic diamines on the respiratory enzymes of M. lysodeikticus, and these investigators conceded that hydrophobic interactions between GrS and the target site were also of importance (87). The reported disappearance of ^{1}H NMR signals from the peptide in the presence of perdeuterated M. lysodeikticus membranes in phosphate buffer (88) is compatible with either total intramembrane incorporation, tight electrostatic binding to head groups, or gross precipitation as a phosphate salt. Overall, Ostrovskii et al. provide no compelling evidence to support the hypothesis that the immobilization of boundary lipid in the bacterial membranes underlies its antibiotic effect, other than to cite the well-established fact that M. lysodeikticus membrane lipids are primarily anionic (76).

Yonezawa et al. recently reported the synthesis by solid phase methods of a GrS congener labeled with ^{14}C at Pro (17). Bacteria were treated with the labeled antibiotic for brief periods ($\leq$ 20 min), collected by filtration, and the radioactivity remaining on the filter quantitated. No ^{14}C-GrS was adsorbed by GrS-resistant species. Substantial radioactivity was retained by the GrS-sensitive strain, which these workers estimated (according to the specific activity of the peptide and the estimated surface area of the cell) to be equivalent to a monomolecular layer of antibiotic covering the cell surface ($\sim 1.3 \times 10^{6}$ molecules $cell^{-1}$). Even if the authors' assumption of surface adsorption were valid, the membrane of the microorganism in

question (B. subtilis), which contains only ~16% lipids (76) (predominantly neutral), should be incapable of binding this large a quantity of peptide. One must then reconsider the first observations of the Osaka group, which suggested internalization and binding of the antibiotic in the cytosol.

Structure-Function Correlations: Synthetic Analogues of GrS. Many GrS analogues, produced by de novo synthesis or chemical derivatization, have been structurally characterized (generally by chiroptical methods alone or in conjunction with ^{1}H NMR) and assayed for antibiotic activity, in order to gain an intuitive understanding of the relationship of structure to biological function in the native peptide. Such studies have consistently shown that, for full activity, an analogue must be dicationic, possess a conformationally rigid secondary structure, and exhibit amphiphilicity. Since a comprehensive racapitulation of this work is not possible, analogues will be considered by classes and general trends noted. A complete review has been published (89), from which the following has been distilled.

1. Linear peptides related to GrS: The acyclic decapeptides are weak agonists. The activity of $(VOL\hat{F}P)_n$ polymers increases slightly with n, while the pentapeptide is inactive. Random copolymers exhibited nearly the same activity as GrS in one study utilizing synthetic media, but 5 to 10-fold lower activities were observed in nutrient broth.

2. Cyclic peptides related to GrS: The cyclic pentapeptide is inactive, as are cyclic peptides containing the pentapeptide sequence and an adjacent spacer of Gly residues. Cyclo-$(VOL\hat{F}P)_n$, n = 3 or 4, are weak agonists.

3. Cyclic decapeptides with perturbed secondary structure: Peptides whose ORD spectra lack the characteristic trough at 233 nm are invariably inactive or very weakly active. Examples are depsipeptide analogues, retro analogues, and analogues containing an L amino acid or Gly at position 4. By chiroptical criteria, such peptides possess a disordered solution structure. The full potency of enantio-GrS (cyclo-($\hat{V}\hat{O}\hat{L}F\hat{P}$)$_2$) is strong evidence against a stereospecific interaction of GrS with a biological receptor.

4. Side chain substitution at positions 1, 3, or 4: Reducing the hydrophobicity of the side chains at these sites is associated with decreased potency; analogues containing a hydrophilic side chain are inactive. Aromaticity at position 4 is not essential.

5. Side chain substitution or derivatization at position 2: Neutral, zwitterionic, or anionic derivatives are inactive; analogues containing a single positive charge are moderately active. [His]$_2$-GrS is of comparable activity to the monocationic analogues, while the Arg$^{2,2'}$ congener is fully active, indicating that this side chain should ideally be at least as basic as an alkylamine. The Lys$^{2,2'}$ and diaminoisobutyric acid$^{2,2'}$ analogues are slightly less active than GrS, while stretched dicationic analogues such as [N^{δ}-(6-aminohexanoyl)ornithyl]$_2$-GrS are only moderately active, suggesting that the side chain of Orn is in fact of optimum length.

6. Side chain substitution at position 5: Whereas substitution of an L amino acid or Gly for D-Phe at the first position of the β turn abolishes activity, a variety of nonpolar L-α-residues (including Gly and sarcosine) may be substituted for Pro.

A striking anomaly is the full potency of mono- and diacylornithyl derivatives in which the acyl group contains 10 to 12 C atoms. While the activity of these compounds has never been rationalized, it is entirely possible that these derivatives readily penetrate the inner cell membrane of sensitive strains and are converted to GrS by an intracellular enzyme which catalyzes the hydrolysis of fatty acid amides in this range of acyl chain lengths.

Biosynthesis of GrS and Physiological Role in the Producer. The mode of enzymatic biosynthesis of GrS in producer strains of B. brevis has been well characterized (90). Synthesis commences with racemization and activation of L-Phe by an enzyme designated fraction II or light enzyme. The process requires Mg^{++} and ATP, which is cleaved to AMP and PP_i, leaving D-Phe covalently attached to the enzyme by a thioester linkage. Pro, Val, Orn, and Leu are thioester-linked to separate sites on a second enzyme complex containing 4-phosphopantetheine designated fraction I or heavy enzyme; these activations similarly require Mg^{++} and involve cleavage of ATP to AMP and PP_i. Free peptide intermediates have not been detected in the synthesis. Elongation begins with peptide bond formation between the activated carboxyl group of D-Phe and the NH group of Pro. Subsequent reactions are confined to the heavy enzyme. The activated dipeptide $\hat{F}P$ is transferred by the pantetheine arm from the Pro site to the amino group of Val to yield the bound tripeptide, and the transfers repeated until the pentapeptide is obtained. The process of cyclization to yield the cyclodecapeptide remains undetermined; it is believed to occur either by interaction of two heavy enzyme complexes bearing activated penta-

peptides or by condensation on a single heavy enzyme complex bearing 2 pentapeptides, the second thioester-linked at a "holding" site.

Some 167 different antibiotic substances are known to be elaborated by sporulating Bacillus species (91). These are generally small peptides, of which most are cyclic (90). Antibiotic synthesis is commonly observed at the end of the logarithmic phase of vegetative growth (t_o), as is the case with GrS (90). Neither the physiological role of these antibiotics in general, nor their relation to the process of sporulation, is presently understood.

The strains of B. brevis which produce GrS (Gause-Brazhnikova or G-B, and Nagano) are insensitive to exogenously added GrS at concentrations of 10^{-4} M during vegetative growth (81). Producer strains actively synthesizing the peptide exhibit a nearly complete loss of extractable nucleoside di- and triphosphates (92) accompanied by a brisk efflux of nucleotides into the medium (93) and a loss of ^{31}P NMR signals from intracellular ATP (94), without evidence of destruction of the culture. These changes are not observed when an inhibitor of GrS synthesis, β-phenyl-β-alanine, is added to the medium (92). B. brevis G-B mutants incapable of GrS production do not undergo nucleotide depletion unless GrS is added exogenously (93). The effects on phosphate metabolism were tentatively attributed to an inhibition of membrane bound respiratory enzymes (87) and GrS-induced permeability changes which are evidently not lethal (94). Evidence for a direct connection between the in vitro inhibition of respiration in the producer by GrS and nucleotide depletion and efflux have not been obtained, however.

Whereas it was initially believed that GrS production was essential to sporulation it has since been demonstrated that mutants lacking synthetase activity can nevertheless produce normal quantities of morphologically normal spores (95,96). The GrS content of the wild type spore is typically 5×10^{-14} g (96), which represents some 25% of the GrS synthesized in the parent cell (97). The fate of the remainder is unknown. Nandi and Seddon (96) have shown that both the mutant and wild-type spores germinate similarly, but outgrowth (the rapid onset of RNA synthesis triggering vegetative growth) is substantially slower in the GrS-containing spores (8 h vs. 80 min). Addition of GrS to germinating cultures of the mutant strains delayed outgrowth, as did addition of the peptide to mutant spores at a final concentration of $\geqslant 2 \times 10^{-14}$ g spore^{-1}. Conversely, extraction of GrS from wild-type spores with EtOH resulted in rapid outgrowth (98).

During germination, virtually all of the GrS present in the wild-type spore is hydrolyzed to the free amino acids, which are detectable in the culture medium. The intact antibiotic is not secreted, suggesting that GrS does not persist in the spore in order to serve a protective function in the nascent culture (97). GrS synthesis commences after outgrowth, and accelerates again at the end of logarithmic phase.

Antibiotic Action and Physiological Role of Tyrothricin. The antibacterial properties of the tyrocidines and their analogues have been less thoroughly investigated than GrS. The purified species are generally roughly half as potent as GrS (64,83), the difference being attributed to the weaker basicity of the tyrocidines. The role of the invariant Asn and Gln residues is unknown. On a molar basis, the

structurally dissimilar linear gramicidins (LG's) are more than 10 times as potent as GrS or tyrocidine (89). LG's have been shown to form cation-conducting channels in phospholipid bilayers (99) most likely as head-to-head helical dimers (100), which may underlie their toxicity *in vivo*.

The role of tyrothricin in the producer organism has, in contrast, been under active study. As with GrS, tyrothricin content increases substantially after t_o. The energy charge of tyrothricin-producing strains is, however, apparently normal during antibiotic synthesis (101). In addition, sporogenesis can under conditions of nitrogen deprivation be induced by exogenous tyrocidine (102), and mutants deficient in LG have been reported which are unable to produce heat-resistant spores unless supplied with LG exogenously (103). Consequently, in the case of tyrothricin, unlike GrS, there is evidence that antibiotic synthesis and sporulation are causally linked (102-104).

Attempts to characterize the possible role of tyrothricin in triggering the change from vegetative growth to sporulation have centered upon an inhibition of RNA synthesis by the antibiotic, first noted by Sarkar and Paulus (104). These investigators observed that DNA transcription was blocked partially *in vivo* and completely *in vitro* by 50×10^{-6} g ml^{-1} of either tyrocidine or LG, a concentration comparable to that achieved by the mature culture of the producer. GrS had only a slight effect on RNA synthesis *in vitro*. The inhibition, which was observed with DNA templates of diverse origins, was attributed to a specific interaction with RNA polymerase. A subsequent study (105) revealed that the *in vitro* inhibition by LG was, at most,

partial, and evidence was presented in support of a specific effect of LG on the formation of the polymerase-promoter complex.

Ristow et al. (106) demonstrated that excess polymerase indeed reversed the LG-induced inhibition of RNA synthesis, but were unable to obtain direct evidence of complex formation between LG and the enzyme. On the other hand, they showed that the inhibition by tyrocidine was reversed only by additional template, and that a complex formed between DNA and tyrocidine which was detectable by nitrocellulose filtration (107), uv spectrophotometry (108), and fluorescence quenching (108). This interaction with DNA was nonspecific, occurring with either single- or double-stranded species as well as with synthetic copolymers (108). Surprisingly, DNA binding did not require the presence of a positive charge, formyltyrocidine exhibiting similar affinity for the nucleic acid; however, only native tyrocidine formed a complex which was nuclease-resistant (102). There was no evidence of a preferred nucleotide sequence for tyrocidine binding (102). Interestingly, the inhibition of RNA synthesis in vitro by tyrocidine was partially reversed by LG (106, 108), an effect which could be mimicked by low (2 to 8 percent) concentrations of $HCONH_2$ (102).

Based on these results, Ristow et al. have suggested that tyrocidine and LG function antagonistically in the regulation of spore formation (102), tyrocidine serving primarily to inhibit vegetative growth by blocking RNA synthesis whilst LG (subsequently?) permits transcription of late genes encoding spore-specific products. Paulus and coworkers have emphasized the inhibition of RNA synthesis by LG itself, which they assert (on the basis of very preliminary evidence)

is selective, and, therefore, potentially regulatory (103). The issues of the disposition of the components of tyrothricin in the spore and their fate during germination and outgrowth have not been addressed.

In summary, for neither GrS nor tyrothricin has a physiological function been proven, although for the latter a primary role in the triggering of sporulation appears likely. There is presently no evidence to suggest that either antibiotic is secreted as a biological weapon. The observation that tyrocidine binds to DNA is of significance for GrS, in view of the structural similarity between these peptides; however, formyltyrocidine binds DNA equally well, which may indicate that the invariant Asn and Gln residues, which are absent in GrS, are in fact necessary for this interaction.

2. Aims of the Present Investigation

This study was initiated as an experimental inquiry into intramolecular H bonding in peptides in solution. As an object of such an endeavor, GrS uniquely presented three distinct advantages; (i) a high probability of internal H bonding in solution; (ii) a unique secondary structure, at once prototypical of β-pleated regions and $4 \leftarrow 1$ hairpin turns in proteins; and (iii) the potential for selective observation of H bond donor and acceptor sites. At the time the work was undertaken, this writer was aware of no site-selective solution phase study of intramolecular H bonds in a heteropolypeptide.

As part of this inquiry, experimental protocols for the definitive elucidation of backbone-backbone and side chain-backbone H bonds in polypeptides in solution are developed which should prove particularly

useful in conformational studies of other small, biologically active peptides, where the influence of solvent on structure is large (109). In addition, information concerning the energetics of specific types of intrapeptide H bonds can for the first time be gained, shedding light on the degree to which such bonds contribute to the stabilization of structural domains in proteins. Previous experimental approaches to the thermodynamics of H bonding in proteins have been limited either to studies of intermolecular association of model compounds (typically amides or carbamides) (110) where, because of the coexistence of many different associated species at equilibrium, the geometry of the H-bonded complex cannot be determined (111), or to calorimetric measurements of denaturation enthalpies in globular proteins, which yield what is at best an average value of the enthalpy change per H bond on complete unfolding, subject to important assumptions concerning the hydration of hydrophobic groups and the magnitude of the van der Waals interactions in the native structure (112). Finally, theoretical studies of H bonding have yet to resolve, even for the simplest systems, such fundamental questions as the effect of bonding on the anharmonicity of the molecular potential of the donor (113) and the nature of the coupling of vibrational transitions in the H-bonded complex to external modes in condensed media (114); for systems as complex as amides or peptides, it is necessary to resort to empirical H bonding potentials calibrated primarily against geometric parameters from crystal structures (115,116). Clearly, a technique for identifying specific H bonds in peptides can provide a powerful check of the theoretical methodologies.

The final chapters of this work center upon the mechanism of antibacterial action and the possible physiological role of GrS in the producer, both of which were at the outset, despite the efforts of many investigations, complete enigmas. This part of the study did not, as initially anticipated, make use of model membranes in order to determine the site of interaction with phospholipid bilayers and the spatial orientation of the membrane-bound peptide. Rather, it was possible to delineate certain novel intermolecular interactions in which GrS participates in vitro that appear to be the crucial determinants of many, if not all, of its biological effects.

The determination of the solution conformation of the ornithyl residues (Chapter III) suggested that the intercationic spacing might be an important determinant of biological potency in GrS. This in turn raised the possibility that GrS could (unlike the univalent tyrocidines) bind polyvalent anions such as organic phosphates in solution. Such anion complexes would then be lipophilic by virtue of the antibiotic's amphiphilicity. It is shown in Chapter IV that GrS indeed functions as a nucleotide complexone and phase transfer agent. In this section, several nucleotide-GrS complexes are characterized structurally and estimates of binding constants are obtained. The analysis of binding is complicated by the tendency of the complex to associate, but it is apparently the colligative properties and surface characteristics of the complexes, rather than significant differences in intrinsic binding affinities, which are responsible for the selectivity of GrS for particular nucleotides in the phase transfer process. In contrast to membrane binding, nucleotide-GrS interactions are easily detected in vitro

in the range of physiologically active concentrations of peptide.

If GrS binds and induces phase transfer of nucleotides it might do so as well with nucleic acids, and this is in fact observed. The fifth chapter reports experiments which characterize the GrS-nucleic acid interaction. The stoichiometry is defined, and uv spectra of DNA in $CHCl_3$ obtained for the first time. The interaction of GrS with DNA is of major significance in understanding the physiological role. The final section reports the results of preliminary microbiological studies on the antibiotic action. The time course of the bactericidal effect, relative potencies of GrS analogues derivatized at ornithine, and the effect of bacterial cell density on the minimum lethal concentration are determined. These data support a model for GrS action involving internalization of the peptide and formation of a relatively small number of cytotoxic complexes, possibly with nucleotides.

REFERENCES

1. Dubos, R. J. (1939) J. Exptl. Med. 70, 249-256.
2. Hotchkiss, R. L., & Dubos, R. J. (1940) J. Biol. Chem. 132, 791-792.
3. Gause, G. F., & Brazhnikova, M. G. (1944) Nature 154, 703.
4. Hunter, F. E., & Schwartz, L. S. (1967) in Antibiotics: Mechanism of Action (Gottlieb, D., & Shaw, P. D., eds) pp 636-641, Springer-Verlag, New York.
5. Synge, R. L. M. (1945) Biochem. J. 39, 363-367.
6. Consden, R., Gordon, A. H., Martin, A. J. P., & Synge, R. L. M. (1947) Biochem. J. 41, 596-602.
7. Battersby, A. R., & Craig, L. C. (1951) J. Am. Chem. Soc. 73, 1887-1888.
8. Paladini, A., & Craig, L. C. (1954) J. Am. Chem. Soc. 76, 688-692.
9. King, T. P., & Craig, L. C. (1955) J. Am. Chem. Soc. 77, 6627-6631.
10. Ruttenberg, M. A., King, T. P., & Craig, L. C. (1965) Biochemistry 4, 11-18.
11. Sarges, R., & Witkop, B. (1965) J. Am. Chem. Soc. 87, 2011-2020.
12. Sarges, R., & Witkop, B. (1965) J. Am. Chem. Soc. 87, 2027-2030.
13. Sarges, R., & Witkop, B. (1965) Biochemistry 4, 2491-2494.
14. Schwyzer, R., & Sieber, P. (1957) Helv. Chim. Acta 40, 624-639.
15. Klostermeyer, H. (1968) Chem. Ber. 101, 2823-2831.

16. Fischman, A. J., Live, D. H., Wittbold, W. M., & Wyssbrod, H. R. (1980) J. Magn. Reson. 40, 527-537.

17. Yonezawa, H., Kaneda, M., Tominaga, N., Higashi, S., & Izumiya, N. (1981) J. Biochem. 90, 1087-1091.

18. Krauss, E. M. Unpublished observations.

19. Schwyzer, R., & Sieber, P. (1958) Helv. Chim. Acta 41, 2186-2189.

20. Schmidt, G. M. J., Hodgkin, D. C., & Oughton, B. M. (1957) Biochem. J. 65, 744-750.

21. Synge, R. L. M. (1957) Biochem. J. 65, 750-752.

22. Pauling, L., & Corey, R. B. (1951) Proc. Natl. Acad. Sci. U.S.A 37, 729-740.

23. Hodgkin, D. C., & Oughton, B. M. (1957) Biochem. J. 65, 752-756.

24. Abbott, N. B., & Ambrose, S. J. (1953) Proc. Roy. Soc. A 219, 17-32.

25. Quadrifoglio, F., and Urry, D. W. (1967) Biochem. Biophys. Res. Comm. 29, 785-791.

26. Balasubramanian, D. (1967) J. Am. Chem. Soc. 89, 5445-5449.

27. Liquori, A. M., & Conti, F. (1968) Nature 217, 635-637.

28. Stern, A., Gibbons, W. A., and Craig, L. C. (1968) Proc. Nat. Acad. Sci. U.S.A. 61, 734-741.

29. Venkatachalam, C. M. (1968) Biopolymers 6, 1425-1436.

30. Ovchinnikov, Yu. A., Ivanov, V. T., Bystrov, V. F., Miroshnikov, A. I., Shepel, E. N., Abdullaev, N. D., Efremov, E. S., & Senyavina, L. B. (1970) Biochem. Biophys.

Res. Comm. 39, 217-225.

31. Gibbons, W. A., Crepaux, D., Delayre, J., Dunand, J., Hajdukovic, G., & Wyssbrod, H. R. (1975) in Peptides: Chemistry, Structure and Biology, Proc. Am. Peptide Symp. Fourth (Walter, R., & Meienhofer, J., eds.) pp. 127-137, Ann Arbor Science, Ann Arbor.

32. Jones, C. R., Sikakana, C. T., Kuo, M., & Gibbons, W. A. (1978) J. Am. Chem. Soc. 100, 5960-5961.

33. Jones, C. R., Sikakana, C. T., Hehir, S., Kuo, M., & Gibbons, W. A. (1978) Biophys. J. 24, 815-832.

34. Rae, I. D., & Scheraga, H. A. (1978) Biochem. Biophys. Res. Comm. 81, 481-485.

35. Kuo, M., Jones, C. R., Mahn, T. H., Miller, P. R., Nicholls, L. J. F., & Gibbons, W. A. (1979) J. Biol. Chem. 254, 10301-10306.

36. Jones, C. R., Kuo, M., & Gibbons, W. A. (1979) J. Biol. Chem. 254, 10307-10312.

37. Wyssbrod, H. R., Wittbold, W. M., & Fischman, A. J. (1982). The Mount Sinai Medical Center, personal communication.

38. Bothner-By, A. A., & Johner, P. E. (1978) Biophys. J. 24, 779-790.

39. Pitner, T. P., & Urry, D. W. (1972) J. Am. Chem. Soc. 94, 1399-1400.

40. Urry, D. W., Long, M. M., Mitchell, L. W., & Okamoto, K. (1975) in Peptides: Chemistry, Structure, and Biology, Proc. Am. Peptide Symp. Fourth (Walter, R. & Meienhofer, J., eds.)

pp. 113-126, Ann Arbor Science, Ann Arbor.

41. Khaled, M. A., Urry, D. W., Sugano, H., Miyoshi, M., & Izumiya, N. (1978) Biochemistry 17, 2490-2494.

42. Hawkes, G. E., Randall, E. W., Hull, W. E., & Convert, O. (1980) Biopolymers 19, 1815-1826.

43. Philson, S. B., & Bothner-By, A. A. (1979) in Peptides: Chemistry, Structure, and Biology, Proc. Am. Peptide Symp. Sixth (Gross, E. & Meienhofer, J., eds.) pp. 209-212, Pierce Chemical, Rockford, Illinois.

44. Bleich, H. E., Easwaran, K. R. K., & Glasel, J. A. (1978) J. Magn. Reson. 31, 517-522.

45. Schwyzer, R., & Ludescher, U. (1969) Helv. Chim. Acta 52, 2033-2040.

46. Kricheldorf, H. R. (1981) Org. Magn. Reson. 15, 162-177.

47. Laiken, S. L., Printz, M. P., & Craig, L. C. (1969) Biochemistry 8, 519-526.

48. Allerhand, A., & Komoroski, R. A. (1973) J. Am. Chem. Soc. 95, 8226-8231.

49. Komoroski, R. A., Peat, I. R., & Levy, G. C. (1975) Biochem. Biophys. Res. Commun. 65, 272-279.

50. Few. A. V. (1956) Trans. Faraday Soc. 848-859.

51. Craig, L. C. (1964) Science 144, 1093-1099.

52. Bystrov, V. F. (1976) Prog. NMR Spectrosc. 10, 41-81.

53. Cowburn, D., Fischman, A. J., Live, D. H., Agosta, W. C. & Wyssbrod, H. R. (1977) in Peptides: Chemistry, Structure, and Biology, Proc. Am. Peptide Symp. Fifth (Goodman, M. &

Meienhofer, J., eds.) pp. 322-324, Wiley, New York.

54. Fischman, A. J., Live, D. H., Wyssbrod, H. R., Agosta, W. C., & Cowburn, D. (1980) J. Am. Chem. Soc. 102, 2533-2539.

55. Jardetzky, O., & Roberts, G. C. K. (1981) NMR in Molecular Biology, pp. 126-142, Academic Press, New York.

56. Dygert, M., Go., N., & Scheraga, H. A. (1975) Macromolecules 8, 750-761.

57. Huang, D., Walter, R., Glickson, J. D. & Krishna, N. (1981) Proc. Natl. Acad. Sci. U.S.A. 78, 672-675.

58. Reference 55, p. 290.

59. Hull, S. E., Karlsson, R., Main, P., Woolfson, M. M., & Dodson, E. J. (1978) Nature 275, 206-207.

60. Kostansek, E. C., Lipscomb, W. N. & Thiessen, W. E. (1979) J. Am. Chem. Soc. 101, 834-837.

61. Kostansek, E. C., Thiessen, W. E., Schomburg, D., & Lipscomb, W. N. (1979) J. Am. Chem. Soc. 101, 5811-5815.

62. Rackovsky, S., & Scheraga, H. A. (1980) Proc. Natl. Acad. Sci. U.S.A. 77, 6965-6967.

63. Battersby, A. R., & Craig, L. C. (1952) J. Am. Chem. Soc. 74, 4019-4023.

64. Okamoto, K., Yonezawa, H., & Izumiya, N. (1974) J. Chromatogr. 92, 147-156.

65. Ruttenberg, M. A., King, T. P., & Craig, L. C. (1965) J. Am. Chem. Soc. 87, 4196-4198.

66. Kuo, M., Drakenberg, T., & Gibbons, W. A. (1980) J. Am. Chem. Soc. 102, 520-524.

67. Kuo, M., & Gibbons, W. A. (1980) Biophys. J. 32, 807-836.

68. Kuo, M., & Gibbons, W. A. (1979) Biochemistry 18, 5855-5867.

69. Jardetzky, O. (1980) Biochim. Biophys. Acta 621, 227-232.

70. Finer, E. G., Hauser, H., & Chapman, D. (1969) Chem. Phys. Lipids 3, 386-392.

71. Pache, W., Chapman, D., & Hillaby, R. (1972) Biochim. Biophys. Acta 255, 358-364.

72. Wu, E.-S., Jacobson, K., Szoka, F., & Portis, A. (1978) Biochemistry 17, 5543-5549.

73. Nakagaki, M., Handa, T., & Sehara, C. (1981) Yakugaku Zasshi 101, 774-779.

74. Susi, H., Sampugna, J., Hampson, J. W., & Ard, J. S. (1979) Biochemistry 18, 297-301.

75. Iwai, M., Nakajima, A., Uno, S., Hase, I., Takeuchi, I., & Okawa, K. (1970) Bull. Chem. Soc. Japan 43, 3246-3251.

76. Gel'man, N. S., Lukoyanova, M. A., & Ostrovskii, D. N. (1975) Biomembranes, Vol. VI (Manson, L.A., ed.), Chapter 2, Plenum, New York.

77. Uemura, I., Chern, C. J., Saito, T., & Hashimoto, Y. (1960) Osaka Shiritsu Daigaku Igaku Zasshi 9, 3625-3632; Chem. Abstr. (1962), 55, 10587d.

78. Pressman, B. C. (1965) Proc. Natl. Acad. Sci. U.S.A. 53, 1076-1083.

79. Izumiya, N., Kato, T., Aoyagi, H., Waki, M., & Kondo, M. (1979) Synthetic Aspects of Biologically Active Cyclic Peptides: Gramicidin S and Tyrocidines, p. 102, Wiley, New York.

80. Miki, Y. (1960) Osaka Shiritsu Daigaku Igaku Zasshi 9, 4005-4017; Chem. Abstr. (1962), 55, 10587h.

81. Hiramatsu, T. (1961) Osaka Shiritsu Daigaku Igaku Zasshi 10, 267-273; Chem. Abstr. (1962) 56, 14720h.

82. Hotchkiss, R. D. (1944) Adv. Enzymology 4, 153-199.

83. Okamoto, K., Nonaka, K., & Izumiya, N. (1977) Bull. Chem. Soc. Japan 50, 231-236.

84. Ovchinnikov, Yu. A., & Ivanov, V. T. (1975) Tetrahedron 31, 2177-2209.

85. Ostrovskii, D. N., Bulgakova, V. G., Zhukova, I. G., Kaprel'-yants, A. S., Rozantsev, E. G., & Simakova, I. M. (1976) Biokhimiya 41, 175-182.

86. Kaprel'yants, A. S., Nikiforov, V. V., Miroshnikov, A. I., Snezhkova, L. G., Eremin, V. A., & Ostrovskii, D. N. (1977) Biokhimiya 42, 329-337.

87. Dergunov, A. D., Kaprel'yants, A. S., & Ostrovskii, D. N. (1981) Biokhimiya 46, 1499-1509.

88. Eremin, V. A., Sepetov, N. F., Sibeldina, L. A., Lordkipanidze, A. E., & Ostrovskii, D. N. (1979) Dokl. Akad. Nauk SSSR 245, 994-997.

89. Reference 79, Chapters 4, 6.

90. Katz, E., & Demain, A. L. (1977) Bacteriol. Rev. 41, 449-474.

91. Berdy, J. (1974) Adv. Appl. Microbiol. 18, 309-406.

92. Silaeva, S. A., Glazer, V. M., Shestakov, S. V., & Prokof'ev, M. A. (1965) Biokhimiya 30, 947-955.

93. Glazer, V. M., Silaeva, S. A., & Shestakov, S. V. (1966) Biokhimiya 31, 1135-1141.

94. Vostroknutova, G. N., Bulgakova, V. G., Udalova, T. P., Sepetov, N. F., Sibel'dina, L. A., & Ostrovskii, D. N. (1981) Biokhimiya 46, 657-666.

95. Kambe, M., Sakamato, Y., & Kurahashi, K. (1974) J. Biochem. 75, 481-493.

96. Nandi, S., & Seddon, B. (1978) Bioch. Soc. Trans. 6, 409-411.

97. Egorov, N. S., Vypiyach, A. N., & Zharikova, G. G. (1970) Microbiologiya 39, 331-336.

98. Seddon, B., & Nandi, S. (1978) Bioch. Soc. Trans. 6, 412-413.

99. Hladky, S. B. & Haydon, D. A. (1970) Nature 225, 451-453.

100. Urry, D. W., Goodall, M. C., Glickson, J. D., & Mayers, D. F. (1971) Proc. Natl. Acad. Sci. U.S.A. 68, 1907-1911.

101. Fynn, G. H. & Davison, J. A. (1976) J. Gen. Microbiol. 94, 68-74.

102. Hansen, J., Pschorn, W., & Ristow, H. (1982) Eur. J. Biochem. 126, 279-284.

103. Mukherjee, P. K. & Paulus, H. (1977) Proc. Natl. Acad. Sci. U.S.A. 74, 780-784.

104. Sarkar, N., & Paulus, H. (1972) Nature 239, 228-230.

105. Sarkar, N., Langley, D., & Paulus, H. (1977) Proc. Natl. Acad. Sci. U.S.A. 74, 1478-1482.

106. Ristow, H., Schazschneider, B., Bauer, K., & Kleinkauf, H. (1975) Biochim. Biophys. Acta 390, 246-252.

107. Schazschneider, B., Ristow, H., & Kleinkauf, H. (1974) Nature 249, 757-759.

108. Ristow, H., Schazschneider, B., Vater, J., & Kleinkauf, H. (1975) Biochim. Biophys. Acta 414, 1-8.

109. Craig, L. C., Cowburn, D., & Bleich, H. (1975) Ann. Rev. Biochem. 44, 477-490.

110. Kauzmann, W. (1959) Adv. Protein Chem. 14, 1-63.

111. Toniolo, C. (1980) CRC Crit. Rev. Biochem. 1-44.

112. Privalov, P. R. (1979) Adv. Protein Chem. 33, 167-241.

113. Sandorfy, C. (1976) in The Hydrogen Bond (Schuster, P., Zundel, G., & Sandorfy, C., eds.) Vol. II, Chapter 12, Elsevier, New York.

114. Besnainou, S. (1980) Adv. Mol. Relax. Interact. Proc. 16, 81-100.

115. McGuire, R. F., Momany, F. A., & Scheraga, H. A. (1972) J. Phys. Chem. 76, 375-393.

116. Momany, F. A., McGuire, R. F., Burgess, A. W., & Scheraga, H. A. (1975) J. Phys. Chem. 79, 2361-2381.

CHAPTER II

INTRAMOLECULAR HYDROGEN BONDING IN GRAMICIDIN S: THE PEPTIDE BACKBONE

1. Introduction

The identification of intramolecular hydrogen bonds (H bonds) in solution has been a major aim of conformational studies of peptides. A variety of experimental methods has been applied to the task (1), including high resolution NMR, IR spectrophotometry, and hydrogen exchange (HX) kinetics. Both NMR and HX can be highly selective, but these methods do not differentiate between intramolecular H bonding and solvation differences in a particular solvent (2, 3). While IR is exquisitely sensitive to the effects of H bonding on vibrations of both the donor and acceptor moieties (4) there is generally insufficient dispersion of frequencies for a given vibrational mode to render the method useful in any but the simplest oligo- and homooligopeptides (5, 6), and even in these compounds band assignment is not straightforward (2). In this chapter, a novel combination of all these three methods is reported which affords the necessary sensitivity and selectivity to provide definitive assignment of vibrational bands and a direct view of residue-specific intramolecular H bonding in GrS.

2. Experimental Section

Gramicidin S dihydrochloride (Sigma) was dissolved in H_2O:dioxane (5:2, v/v), filtered and lyophilized prior to use. It yielded a single spot on TLC in n-BuOH:AcOH:H_2O, 4:1:5 (upper phase) and $CHCl_3$:MeOH:AcOH:H_2O, 25:15:4:2. NMR spectra were identical to those published previously (7). It was therefore judged $>99\%$ pure.

Reagent grade Me_2SO (Baker) was distilled under reduced pressure over CaH_2. p-Dioxane (Eastman) was distilled over Na metal in the presence of benzophenone. p-Dioxane-$^2H_8$, 99.5% g-atom ^2H (Merck) was used without further purification.

Exchange-in of ^2H for ^1H was accomplished by the addition of D_2O:dioxane (5:2, v/v), adjusted to the desired glass electrode reading with DCl and NaOD, to a sample of the lyophilized peptide. The final peptide concentration was 0.016 M. The solvent mixture was selected because of the availability of HX rate data for GrS (8) and the high solubility of the peptide. Exchange was terminated after 30 min by freezing in a dry ice-EtOH bath. The frozen samples, representing a distribution of pH's, were placed in a single vacuum flask and lyophilized. The flask was removed from the lyophilizer without venting and transferred to a glove box under He (Vacuum Atmospheres Co.). Preparation of all samples for spectroscopic measurements were performed in this environment.

For exchange-in of ^1H for ^2H, the peptide was initially per-N-deuterated in D_2O:dioxane and lyophilized. Aliquots were divided out under He, sealed to exclude moisture, and removed from the glove

box. The procedure was thereafter identical to that outlined above save that protonated solvents were used.

^1H-^2H exchange rates of poly-D, L-alanine, type I (Sigma) in D_2O:dioxane-$^2H_8$ (5:2, v/v) were obtained by monitoring the integrated intensity of the amide proton NMR resonance as a function of time at 24°C. The peptide concentration was 2 mg/ml. The kinetic analysis was carried out as previously described (9).

^1H NMR spectroscopy was performed on a Bruker WM-500 spectrometer operating in the Fourier transform mode. The lock signal was provided by the solvent. The peptide concentration was typically 8 mM GrS in Me_2SO-$^2H_6$ or methanol-$^2H_4$. The chemical shifts of the NH protons, in ppm relative to internal Me_4Si, were: in Me_2SO-$^2H_6$, Val, 7.22; Leu, 8.34; Orn N'H, 8.68; Orn $N^{\delta}H$, 8.07; D-Phe, 9.11; in methanol-$^2H_4$, Val, 7.73; Leu, 8.80. The determination of isotope composition was based on the integrated intensities of the proton resonances.

IR spectra were obtained on a Beckman 4240 grating spectrophotometer calibrated against polystyrene. Resolution was better than 1.4 cm^{-1} at 3000 cm^{-1}. Adjustable-pathlength CaF_2 cells (Perkin-Elmer) were employed for the measurement of transmittance between 4000 and 1200 cm^{-1}. Absorbances were obtained by logarithmic scaling. In a typical difference spectrum, the peptide concentration was 0.037 M in Me_2SO and the path length was 0.085 cm.

For the determination of integrated IR band intensities, a Perkin-Elmer 180 grating spectrophotometer was employed and the path length reduced to 0.045 cm to ensure linearity. The intensities

were measured by cutting and weighing the peaks obtained by subtraction of the digitized spectra. Interference from solvent absorbances in spectral regions of interest was negligible, and there was no measurable absorbance change indicative of rehydration during IR spectral acquisition.

3. Results

The dispersion in base-catalyzed amide proton exchange rates (8) provided a means of synthesizing variably N-deuterated GrS analogues, the isotopic composition of which were determined quantitatively by NMR. Difference IR of Me_2SO solutions of these analogues then afforded isolation of residue-specific amide group vibrations. Me_2SO was selected because (I) it is aprotic; (ii) it has been employed frequently in studies of the solution structure of GrS (3,10-20); and (iii) non-H-bonded, intramolecularly H-bonded, and solvent H-bonded peptide NH groups are readily differentiated by their amide A frequencies (21,22; Table I).

HX conditions were adjusted so that for a given pair of isotopic analogues as large a difference in degree of N-deuteration as possible be achieved for a specific residue, with minimal differences incurred in the remainder. Rate constants for base-catalyzed HX are known to increase in the order $\underline{k}_{Val}$, $\underline{k}_{Leu}$, $\underline{k}_{Orn}$, $\underline{k}_{Phe}$ (8) because of the combined influences of conformation and the inductive effects of side chain substituents. The rate law above pH 3 (uncorrected glass electrode reading) is $-\underline{d}[NH]/\underline{dt} = \underline{k}[NH]/[H]$. If $\underline{f}_V$ is defined as the fraction of Val NH not deuterated in the synthesis of an analogue in

Table I. Trans Amide Group Vibrations[a]

Amide mode (NH)	Amide mode (ND)	Approximate frequency (-CONH-) (cm^{-1})	
A	A′	3300	$\bar{\nu}$ or valence modes; NH stretch in Fermi
B		3100	resonance with first overtone of amide II
I	I′	1650	$\bar{\delta}$ or in-plane deformation modes; amide I
II	II′	1550	predominantly C=O stretch, amide II and
III	III′	1300	amide III predominantly C-N stretch and
IV	IV′	625	N-H in-plane bend
V	V′	650	$\bar{\gamma}$ or out-of-plane deformation modes
VI	VI′	550	
VII	VII′	200	

[a]From reference 30.

which all NH groups are deuterated save that of Val, then at a time $\underline{t}$ after initiation of HX, $\underline{f}_V = \exp(-\underline{k}_{Val}\underline{t}/[H])$. Similarly, for Leu, $\underline{f}_L = \exp(-\underline{k}_{Leu}\underline{t}/[H]) = \exp(\underline{k}_{Leu}\ln(\underline{f}_V/\underline{k}_{Val}))$. Thus if $\underline{k}_{Leu}/\underline{k}_{Val} \equiv \rho$, $\underline{f}_L = \underline{f}_V^{\rho}$ and it is necessary just to maximize $\underline{f}_V - \underline{f}_L$ with respect to $\underline{f}_V$ to determine the optimal exchange conditions, assuming that deuteration of all residues exchanging more rapidly than Leu will be essentially complete. This analysis yields $pH_{optimal} = \log(\ln \rho/((\rho - 1)\underline{k}_{Val}\underline{t}))$; with the available data for $\underline{k}_{Val}$ and $\underline{k}_{Leu}$, allowing HX to proceed 30 min at 25°C requires that the pH be 5.4 for a product 93% deuterated at Leu and 21% deuterated at Val NH. The actual isotope dispersion in a typical run is displayed in Figures 1 and 2.

Figure 3a shows the difference spectrum between GrS and per-N-^{2}H-GrS across the entire amide A band. It reveals a featureless resonance centered at 3300 cm^{-1} with a bandwidth $\Delta\bar{\nu}_{\frac{1}{2}} = 120$ cm^{-1}. This is similar to the spectra previously recorded for the di-N-acetylornithyl (23) and di-N-benzyloxycarbonylornithyl (24) derivatives in $CHCl_3$. The amide A′ band at 2300-2500 cm^{-1} obtained by subtracting the spectrum of GrS from the spectrum of per-N-^{2}H-GrS (Fig. 3b) is broader and appears more complex.

Because of an intense absorption by methyl CH near 3000 cm^{-1}, the amide B band was not observed; it was assigned to the shoulder appearing at 3050 cm^{-1} in the simple spectrum. The sharp ($\Delta\bar{\delta}_{\frac{1}{2}} =$ 25 cm^{-1}) amide I band shifts from 1655 to 1650 cm^{-1} on complete deuteration.

Amide vibrations for specific residues were obtained from the

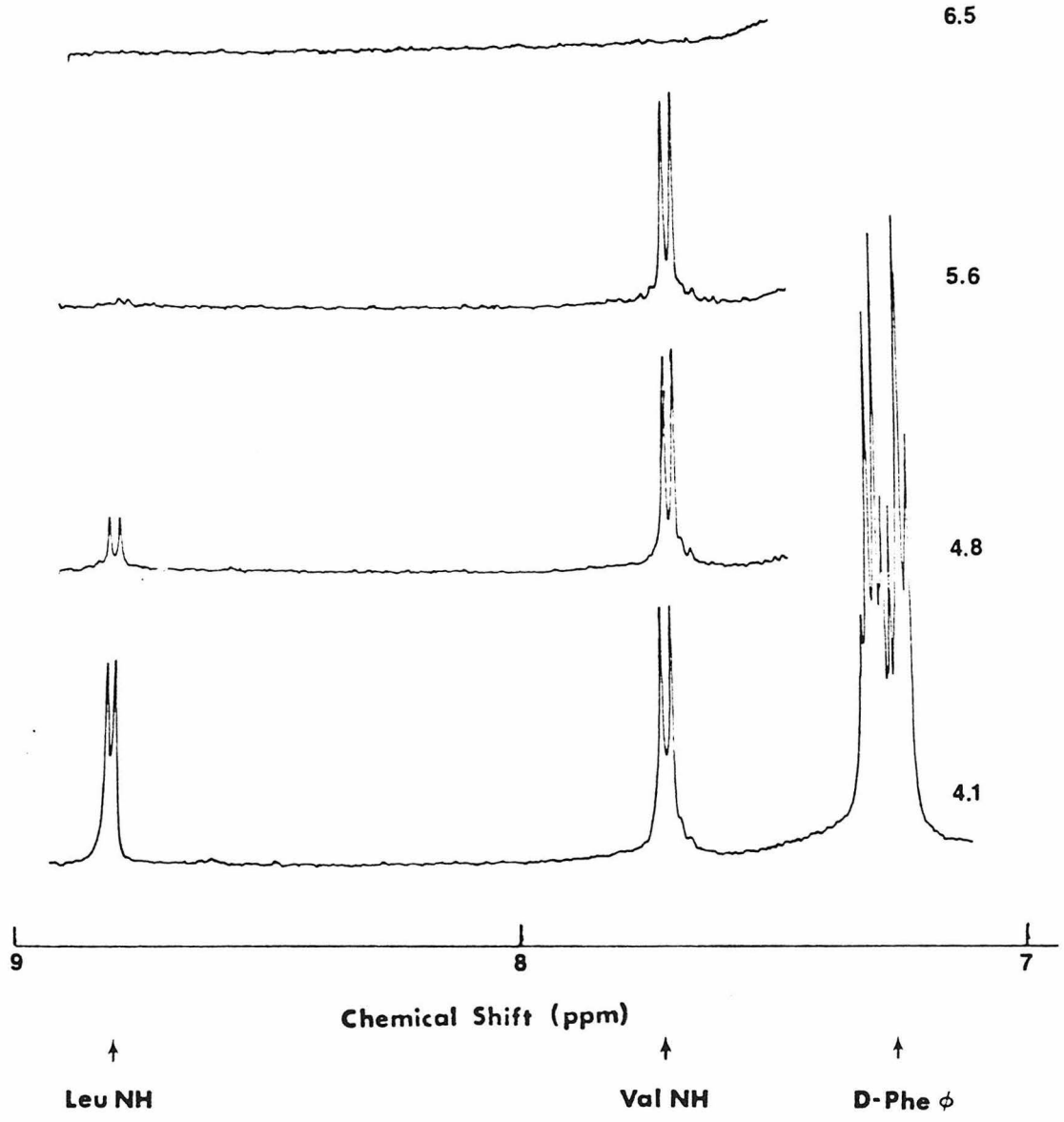

Figure 1. 500 MHz ^{1}H NMR spectra of GrS analogues produced by exchange-in of ^{2}H. Solvent: Methanol-$^{2}H_4$. The pH of the exchange medium (glass electrode reading) for each analogue is given on the right.

Figure 2. Isotope dispersion in a single run (forward exchange). Plot of integrated NMR peak intensities for the indicated NH protons in methanol-$^2H_4$ (solid line) or Me_2SO-$^2H_6$ (broken line) vs. pH of the exchange medium. A relative intensity of 1.0 corresponds to 2.0 equiv mol^{-1} for each of Leu and Val NH, and 2.2 equiv mol^{-1} for D-Phe NH, Orn NH, and Orn $N^{\delta}H_3^+$ collectively.

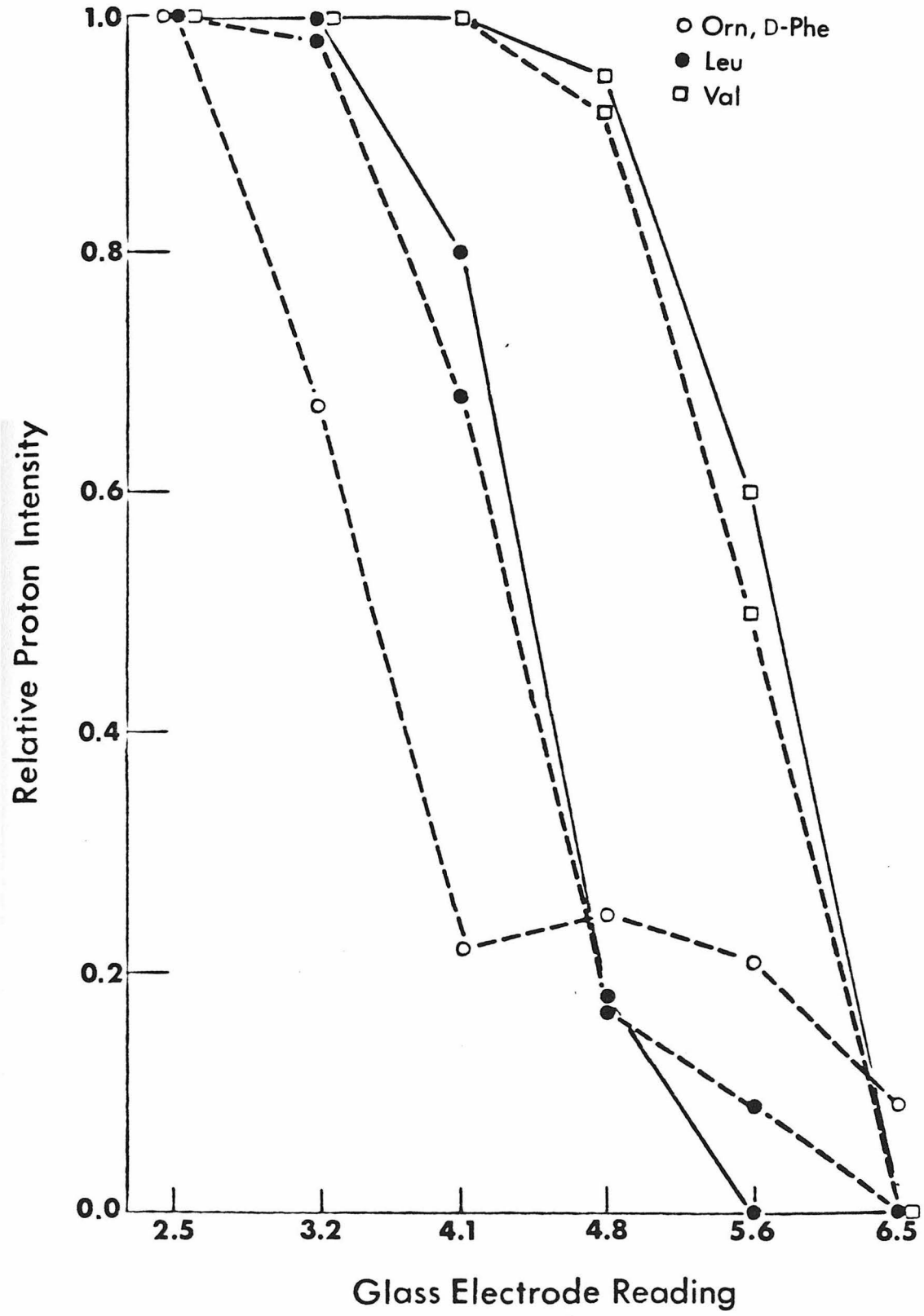
Orn, D-Phe
Leu
Val
1.0
0.8
0.6
0.4
0.2
0.0
Relative Proton Intensity
2.5
3.2
4.1
4.8
5.6
6.5
Glass Electrode Reading

Figure 3. IR difference spectra between the spectra of GrS (i) and per-N-^{2}H-GrS (ii). (a) i-ii, displaying the complete amide A band; (b) ii-i, displaying the complete amide A′ band.

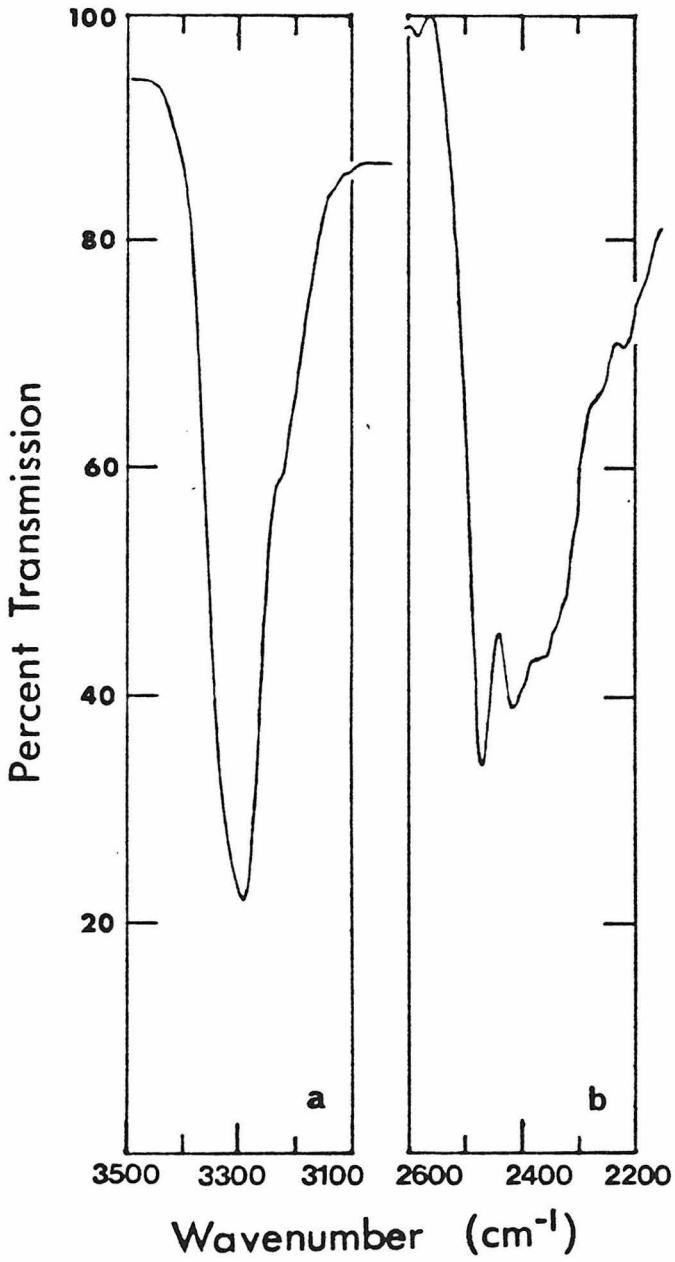
100
80
60
40
20
Percent Transmission
a
b
3500
3300
3100
2600
2400
2200
Wavenumber (cm-1)

IR difference spectra of partially deuterated analogues (Figs. 4, 5). The spectrum displayed in Fig. 4a was obtained by subtraction of the spectrum of an analogue prepared at pH 6.5, which was totally N-deuterated, from the spectrum of an analogue prepared at pH 5.5, which was N-deuterated at Leu, Orn, and D-Phe and partially N-deuterated at Val. The two analogues differed only in the degree of deuteration at Val NH, and the amide A band calculated in the difference spectrum was unambiguously assigned to this residue. This band is Gaussian, with $\bar{\nu}_A$(Val) = 3334 cm^{-1} and $\Delta\bar{\nu}_{\frac{1}{2}}$(Val) = 75 cm^{-1}. To calculate the spectrum shown in Fig. 4b, the spectrum of an analogue synthesized at pH 4.8 was subtracted from the spectrum of an analogue synthesized at pH 4.0. These analogues differed in degree of N-deuteration at Leu (90%) and Val (10%). It is clear that, relative to Val, the valence band assigned to Leu (Fig. 4b) is substantially narrower and more red-shifted: $\bar{\nu}_A$(Leu) = 3281 cm^{-1} and $\Delta\bar{\nu}_{\frac{1}{2}}$ (Leu) = 56 cm^{-1}. The amide A bands of D-Phe and Orn, isolated together (Fig. 4c) in the difference spectrum of analogues synthesized at pH 3.2 and 2.5, lie to lower frequency than those of Val or Leu. Accurate recording or the amide A bandshape for D-Phe and Orn was hindered by the strong methyl CH absorbance.

Isolation of the amide A′ bands (Fig. 5) was accomplished in similar fashion, except that the spectrum of the analogue prepared at the lower pH was subtracted from that of the analogue prepared at the higher pH. The broad absorbance centered at 2350 cm^{-1} appearing in difference spectra in which D-Phe and Orn were N-deuterated (Figs. 5a, b) was attributed to error in the computation of transmission

Figure 4. IR difference spectra between the spectra of partially deuterated GrS analogues prepared at pH 6.5 (i), 5.5 (ii), 4.8 (iii), 4.0 (iv), 3.2 (v), and 2.5 (vi). See text for details. (a) ii-i, amide A (Val); (b) iv-iii, amide A (Leu); (c) vi-v, amide A (D-Phe, Orn).

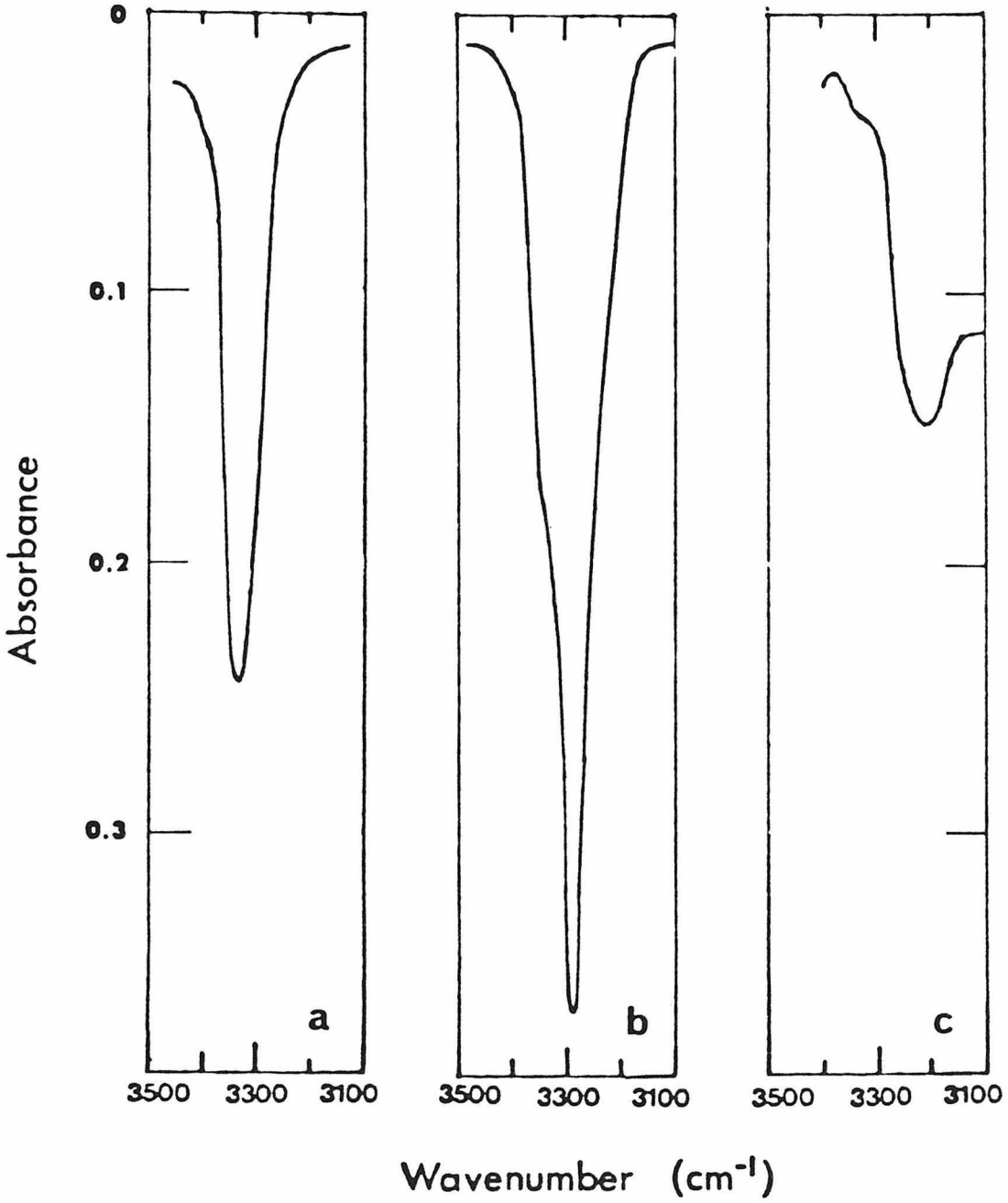
0
0.1
0.2
0.3
Absorbance
a
b
c
3500
3300
3100
3500
3300
3100
3500
3300
3100
Wavenumber (cm-1)

Figure 5. IR difference spectra; labelling as in Figure 4. (a) i-ii, amide A′ (Val); (b) iii-iv, amide A′ (Leu); (c) v-vi, amide A′ (D-Phe, Orn).

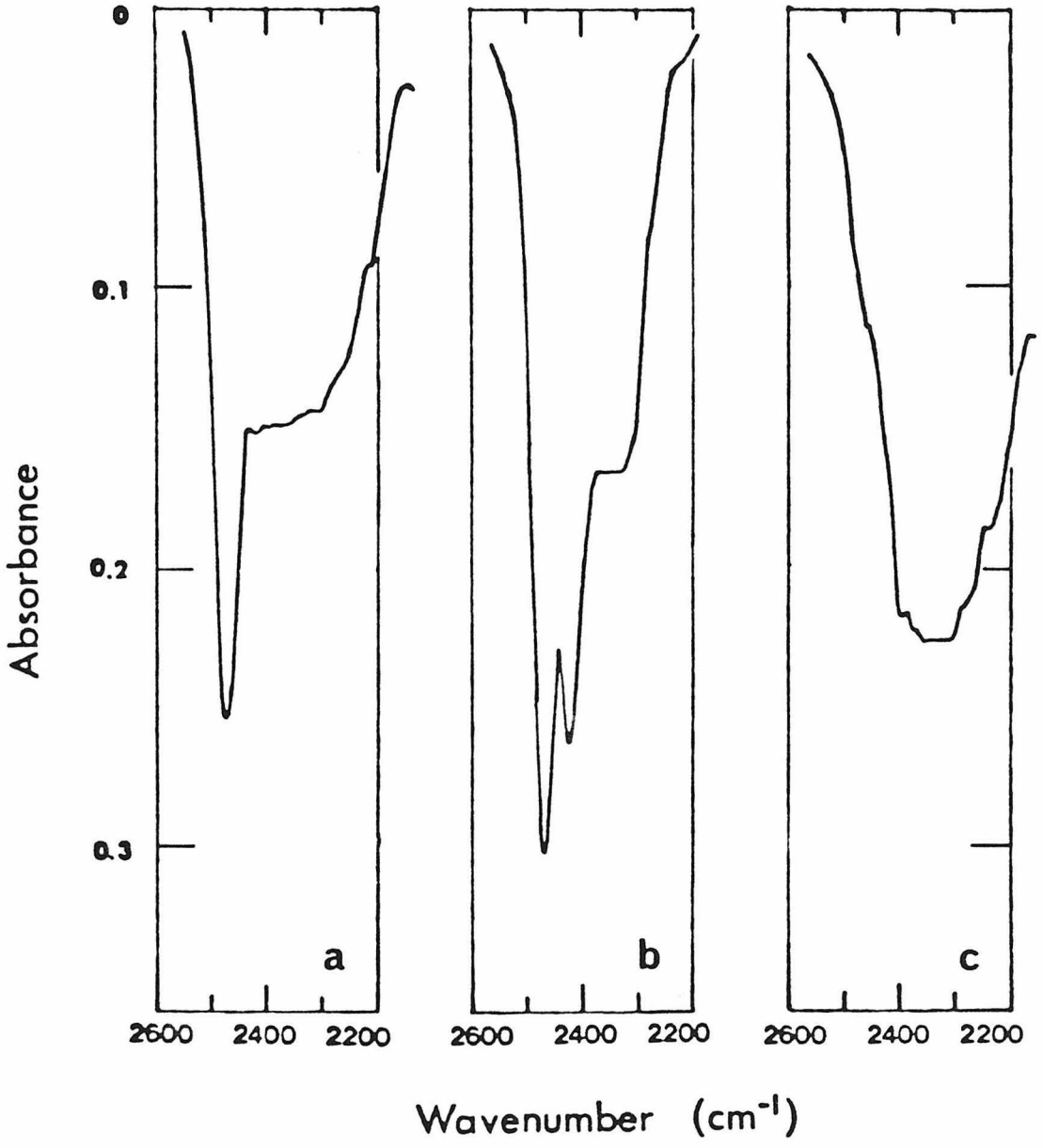
0
0.1
0.2
0.3
Absorbance
a
b
c
2600
2400
2200
Wavenumber (cm⁻¹)

differences when sample and reference absorbances were high, and was eliminated by initially per-N-deuterating the peptide and thereafter exchanging in ^1H. The isotope dispersion achieved for back exchange is illustrated in Figures 6 and 7. In this manner, it was possible to delineate the band structure to the low frequency side of the Val (Fig. 8a) and Leu (Fig. 8b) amide A′ vibrations.

The complete set of IR band assignments is summarized in Table II. D-Phe and Orn are clearly differentiated from Leu and Val on the basis of the valence vibration frequencies $\bar{\nu}_A$ and $\bar{\nu}_{A'}$. For the former, $\bar{\nu}_A$ is close to that reported for secondary amides in Me_2SO (22) and it is concluded that these NH groups are completely H-bonded to solvent. The amide A frequencies of Leu and Val are characteristic of NH-O=C H bonds (21). The latter set of bonds must be intramolecular, since ^{13}C NMR relaxation times measured (20) at higher peptide concentrations than employed here demonstrated a lack of intermolecular association in this solvent. In no instance was a band assignable to a non-H-bonded NH group observed.

4. Discussion

The novel combination of proton exchange, NMR, and IR spectroscopy employed here has afforded the unambiguous demonstration of two pairs of equivalent intramolecular H bonds in GrS, with donor groups provided by Leu and Val NH, distinguishable on the basis of characteristic vibrational frequencies when isolated isotopically in solution. Previous NMR studies of GrS in solution (7, 10-20, 25, 26) have generally supported a cyclosymmetric conformation of the anti-

Figure 6. 500 MHz ^{1}H NMR spectra of GrS analogues produced by exchange-in of ^{1}H following per-N-deuteration, to facilitate observation of Fermi splitting. The pH of the exchange medium is given on the right. (A) Solvent: methanol-$^{2}H_4$. Exchange-in of ^{2}H from solvent occurred at Orn NH during spectral acquisition, so that Orn NH could not be determined quantitatively in ths solvent. (B) Solvent: Me_2SO-$^{2}H_6$.

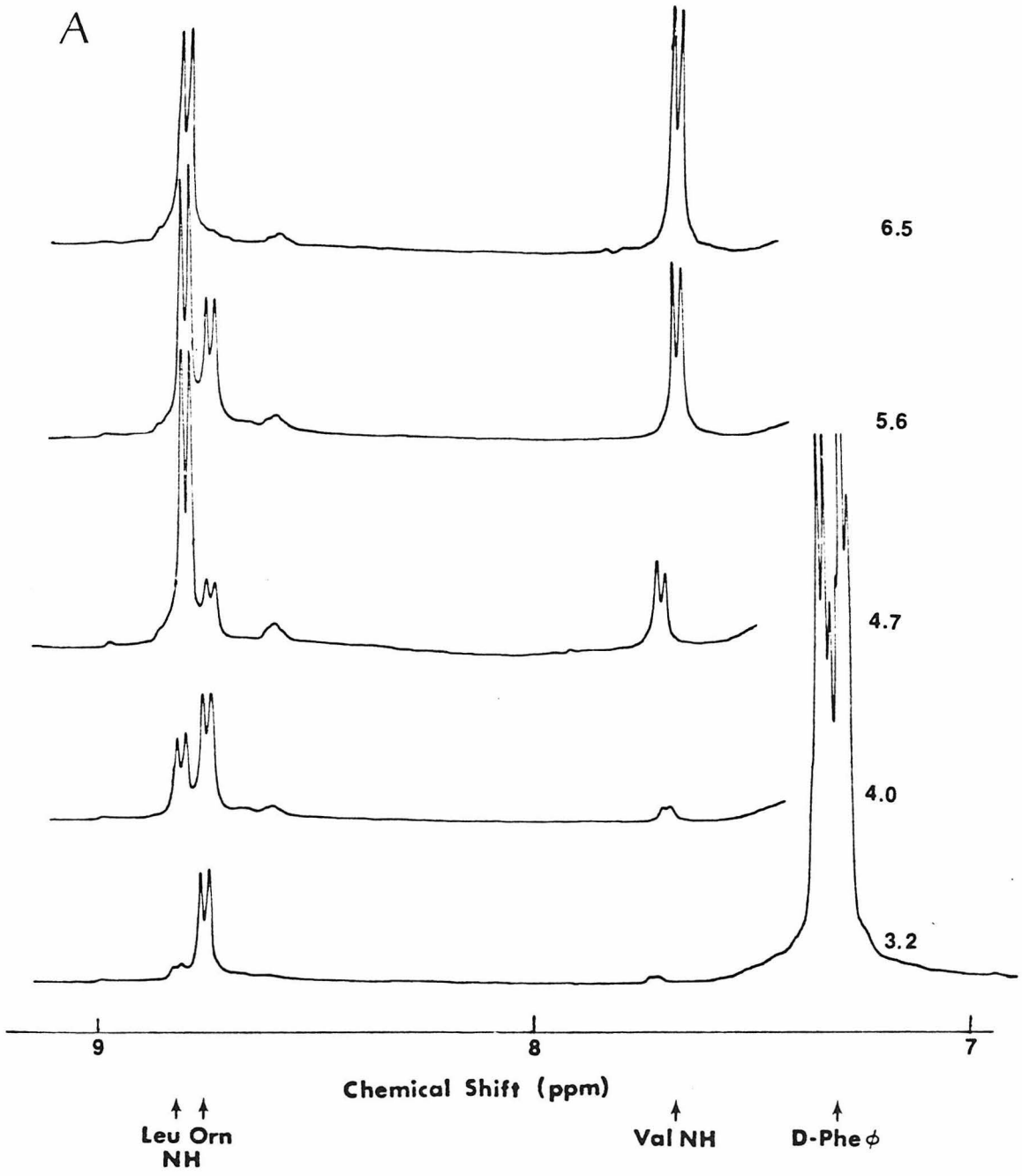
A
6.5
5.6
4.7
4.0
3.2
9
8
7
Chemical Shift (ppm)
Leu Orn NH
Val NH
D-Phe ϕ

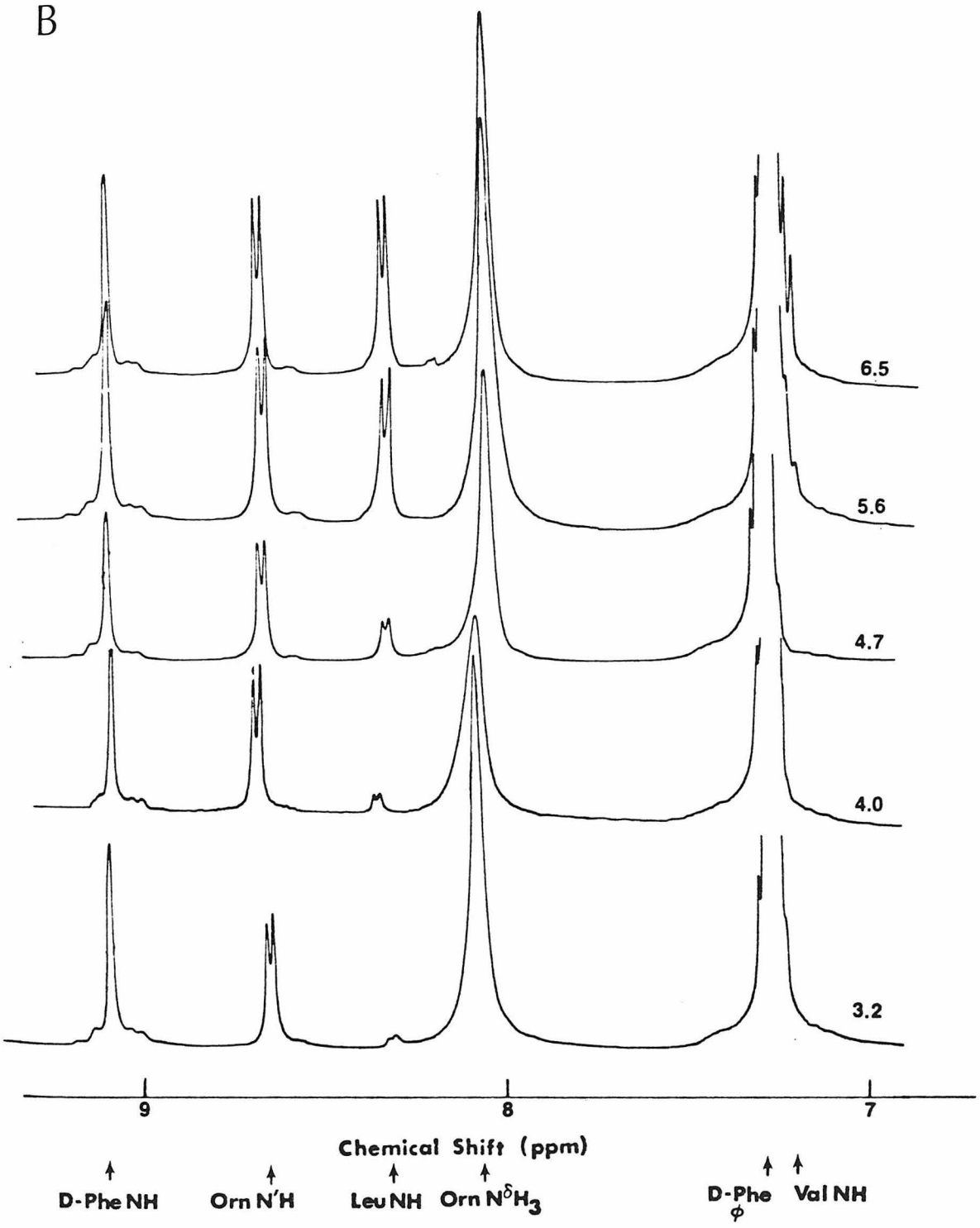
B
6.5
5.6
4.7
4.0
3.2
9
8
7
Chemical Shift (ppm)
D-Phe NH
Orn N'H
Leu NH
Orn N$^{\delta}$H$_3$
D-Phe ϕ
Val NH

Figure 7. Isotope dispersion in a single run (back exchange). Plot of integrated NMR peak intensities for the indicated NH protons in methanol-$^2H_4$ (solid line) or Me_2SO-$^2H_6$ (broken line) vs. pH of the exchange medium. A relative intensity of 1.0 corresponds to 2.0 equiv mol^{-1} for each of Leu and Val NH, and 10 equiv mol^{-1} for D-Phe NH, Orn NH, and Orn $N^{\delta}H_3^+$ collectively.

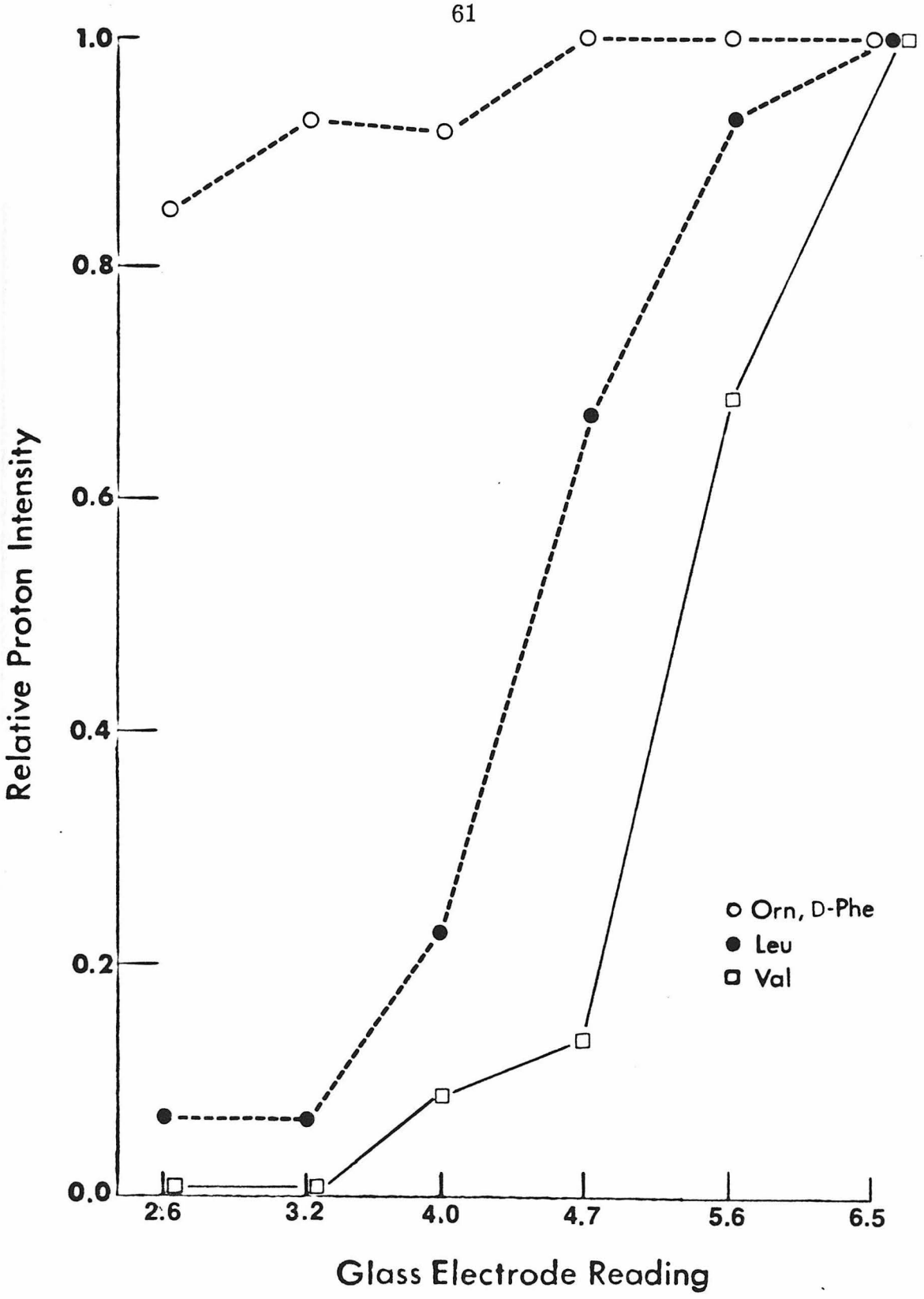
1.0
0.8
0.6
0.4
0.2
0.0
Relative Proton Intensity
2.6
3.2
4.0
4.7
5.6
6.5
Glass Electrode Reading
Orn, D-Phe
Leu
Val

Figure 8. IR difference spectra between the spectra of partially deuterated GrS analogues prepared by exchange-in of ^{1}H following complete N-deuteration, to facilitate observation of Fermi splitting, at pH 6.5 (i), 5.6 (ii), 4.7 (iii), 4.0 (iv). (a) i-ii, amide A′ (Val); (b) iii-iv, amide A′ (Leu).

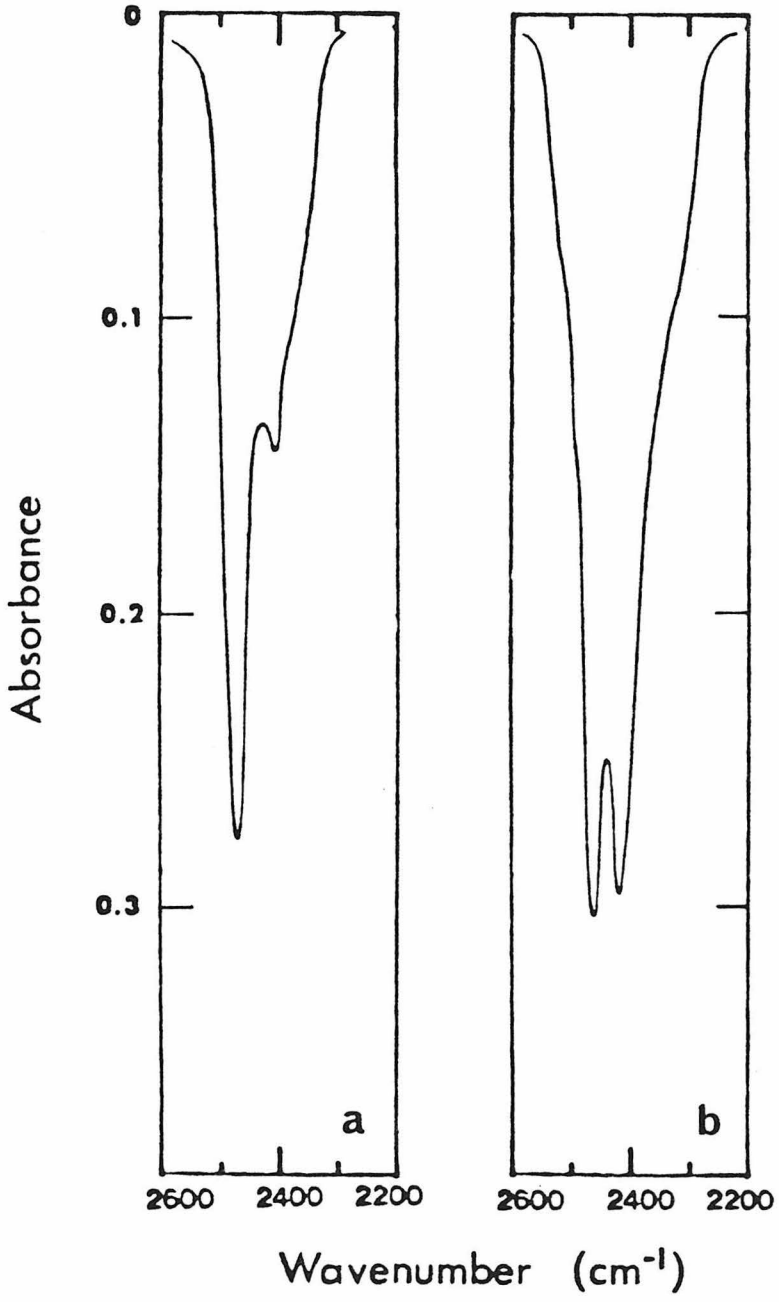
0
0.1
0.2
0.3
Absorbance
a
b
2600
2400
2200
2600
2400
2200
Wavenumber (cm⁻¹)

Table II. Specific Peptide Group Vibrations in Gramicidin S in Me_2SO Solution[a]

Vibrational Mode	Leu			Val			D-Phe, Orn	
	$\bar{\nu}$	$\Delta\bar{\nu}_{\frac{1}{2}}$	$\underline{A}$	$\bar{\nu}$	$\Delta\bar{\nu}_{\frac{1}{2}}$	$\underline{A}$	$\bar{\nu}$	$\Delta\bar{\nu}_{\frac{1}{2}}$
A	3281	56	2.2	3334	75	2.4	~3250	
A′	2423, 2465	39		2410, 2477	61		~2350	>200
II	1535	62		1521	32			
II′				1460	38			

[a]Observed positions $\bar{\nu}$ and bandwidths $\Delta\bar{\nu}_{\frac{1}{2}}$ are in cm^{-1}; intensities $\underline{A}$ are in 10^7 mol^{-1} cm.

parallel β-pleated type containing extended Val-Orn-Leu sequences connected to D-Phe-Pro fragments forming β-II′ (27) turns, but could not establish whether Leu and Val NH, manifestly solvent-shielded (8,18), were in fact internally H-bonded. The present study, taken in conjunction with ^{13}C (3) and ^{15}N NMR (17,28) investigations which have clearly indicated the sequestration of Val and Leu C=O, provides conclusive evidence that GrS possesses in solution a β-pleated structure containing the maximum of four transannular H bonds: one pair with donor Leu NH and acceptor Val C=O (Leu NH-O=C Val) and a second pair, closing the β turns, with donor Val NH and acceptor Leu C=O (Val NH-O=C Leu). The selective delineation of the vibrational bands in this decapeptide not only serves to identify these intramolecular H bonds but also permits us to characterize them in terms of their geometry and thermodynamics.

H bond lengths. It is possible to estimate the NO distance, r_{NO}, from $\bar{\nu}_{NH}$ through application of an empirical relationship proposed for NH-O H bonds (29) once the observed amide A frequency is corrected for the effects of Fermi resonance, which influences the ν_{NH} fundamental through interaction with the first overtone of the amide II vibration (δ_{02}) (30). Assignment of the amide B band by difference IR was not possible, and the unperturbed δ_{02} frequency is unknown. An approximate correction can be made if δ_{02} is taken as twice the observed amide II fundamental (31) (Table II) and $\bar{\nu}_B = 3050\ cm^{-1}$ (see Results), in which case the unperturbed stretch frequency $\bar{\nu}_{NH}$(Leu) is $\sim 20\ cm^{-1}$ lower than $\bar{\nu}_A$, while the Fermi resonance effect on $\bar{\nu}_{NH}$(Val) is negligible. Invoking the relationship proposed by Pimentel

and Sederholm (29) and using $\bar{\nu}_{NH}$ (free) = 3457 cm^{-1} for EtNHCOEt (32), we obtained $r_{NO} = 2.85 \pm 0.06$ Å for Leu and 2.98 ± 0.06 Å for Val. These estimates fall near the mode of the distribution function of collected values of r_{NO} in crystalline peptides (33, 34).

Considering specifically the solution conformation of GrS, several examples of geometrically similar H bonds in model compounds have been well elucidated structurally and spectroscopically. The NH stretch frequency of Leu observed here is typical of polypeptides in the β conformation (21). Crystallographically determined NO distances are 2.83, 2.76, and 2.88 Å in $(\underline{\underline{L}}\text{-Ala})_n$ in the β form (30), silk fibroin (35), and dimeric t-BuCO-Gly-NH$\underline{i}$Pr (36), respectively; in solid MeCO-Gly-NHEt, $\bar{\nu}_A = 3276$ cm^{-1} (37). A survey of antiparallel β sheet structures in oligopeptide crystals (38) yielded an average r_{NO} of 2.88 ± 0.09 Å (IR data not available). These H bonds tend to be linear, with the NHO angle, θ, greater than 170° (36, 39). Overall, good agreement is found with the projected r_{NO}, warranting an estimate of 2.80 to 2.90 Å for the Leu NH-O=C Val H bond.

For Val NH, the angular dependence of the H bonding interaction must be taken into account. Nonlinearity is characteristic of intramolecular H bonds closing β turns. For the ten lowest energy minima found (40) for closed ($r_{NO} < 3.2$ Å) β-II turns in a blocked $\underline{\underline{LD}}$-type dipeptide, $\langle r_{NO} \rangle = 2.96 \pm 0.06$ Å and $\langle \theta \rangle = 156° \pm 10°$ (calculated for $r_{NH} = 1.00$ Å). Considering crystalline peptides (excluding depsipeptides) containing closed β-II or β-II′ turns for which published values of θ (39, 41, 42) or the dihedral angles ϕ and ψ within the turn (43-46) necessary for the calculation (47) of θ are available, $\langle \theta \rangle = 149° \pm 5°$.

This degree of distortion should be accompanied by a 10 to 20 cm^{-1} increase in $\bar{\nu}_{NH}$ above the value expected for a linear H bond with r_{NO} in the usual range (48). (The dependence of $\Delta\bar{\nu}$ on θ was determined for OH--O H bonds. That this applies reasonably well to the trend in angle dependence for NH--O bonds is inferred from the similarity in slopes of the lines relating the bandshift to H bond length in the two types of bond (49).) Unfortunately, accompanying IR measurements are seldom available, primarily because of the difficulty of making specific band assignments in the amide A region. An additional complication is that C_2 symmetry is sometimes lost in crystalline cyclosymmetric peptides (39, 50).

The most useful comparisons were noted for the following compounds. cyclo-(Gly_6) retains C_2 symmetry in the solid state (43) and contains transannular 4→1 H bonds (r_{NO} = 2.96 Å; θ_{calcd} = 155°), which most likely correspond to the strong 3333 cm^{-1} band observed in the IR spectrum of the Nujol mull (51). Dihydrochlamydocin (52) has two 3→1 H bonds with r_{NO} = 2.95 and 2.84 Å and θ = 145° and 138°, respectively. [Ala^4]-desdimethylchlamydocin has similar secondary structure (53) and demonstrates a bulk $\bar{\nu}_A$ in $CHCl_3$ of 3335 cm^{-1}. NH stretch frequencies of hydrated tropocollagens and isomorphic synthetic polytripeptides (54, 55) range from 3320 to 3345 cm^{-1}, attributed in part to deviation from linearity (55) since r_{NO} = 2.90 Å for the collagen model (56) and 2.96 Å for $(Gly\text{-}Pro\text{-}Pro)_n$ (57). For these peptides, r_{NO} is consistently shorter than predicted by the Pimentel-Sederholm relationship. If θ assumes a value typical of 4→1 intramolecular H bonds, r_{NO} for the Val NH-O=C Leu bonds closing the β

turns in GrS should lie between 2.90 and 3.00 Å.

Enthalpies. Whereas H bond enthalpies have been determined spectroscopically for complexes of simple amides (4), difficulties arise when attempting to measure ΔH° from the temperature dependence of the association constant in polypeptides containing intramolecular H bonds. GrS demonstrates no free ν_{NH} resonance for Leu or Val at 25°C. Peptide unfolding is a cooperative process, and the temperature dependences should be complex. GrS is soluble only in polar media, thus introducing the additional complications of specific interactions with the solvent (58) and hydrophobic effects (59).

Spectroscopic-thermodynamic correlations, such as the regression of ΔH° on the bandshift $\Delta\bar{\nu}_{XH} \equiv \bar{\nu}_{XH}$(H-bonded) - $\bar{\nu}_{XH}$(free) for analogous complexes (60), can provide estimates of ΔH° and circumvent the difficulties of direct measurement. However, the Badger-Bauer relationship is not established for trans secondary amides. Amide A bands of the intermolecular complexes of suitable model compounds are characteristically broad ($\Delta\bar{\nu}_{\frac{1}{2}} > 120$ cm^{-1}) and non-Gaussian (61), and it is difficult to assign $\bar{\nu}_{NH}$(H-bonded) precisely; e.g., for associated MeCONHMe in CCl_4 at ambient temperature, $\bar{\nu}_{NH}$ was reported to be 3325 cm^{-1} by Jones (61) and 3280 cm^{-1} by Miyazawa et al. (62). Such inconsistencies result in part from polymerization (63, 64). A survey of experimentally determined enthalpies for complexes of model amides (65-69) ranging from -2.1 to -4.7 kcal mol^{-1} revealed no systematic variation with $\Delta\bar{\nu}_{NH}$ (61, 62, 67, 68, 70) of predictive value.

A second approach to the estimation of ΔH° from IR data for

model compounds is based on the integrated band intensity, $\underline{A}$. Iogansen (71) successfully applied the relation $-\Delta\underline{H}^\circ = \underline{C}\Delta\Gamma^{\frac{1}{2}}$ to a series of phenol adducts, where $\Gamma \equiv (\underline{cl})^{-1} \int_{\bar{\nu}} \ln(\underline{I}_0/\underline{I})\, \underline{d}(\ln\bar{\nu}) \simeq \underline{A}/\bar{\nu}_{XH}$, $\Delta\Gamma^{\frac{1}{2}} = \Gamma^{\frac{1}{2}}$(H-bonded) - $\Gamma^{\frac{1}{2}}$(free), and $\underline{C}$ is an empirically derived constant. It was proposed that Γ is proportional to the square of the dipole moment of the XH valence fundamental, to which the H bond makes an additive contribution (71). This method is advantageous in that the entire envelope of the valence band, rather than the point of maximal absorptivity alone, is utilized. Previous intensity measurements in simple amides (61) show a direct variation with $-\Delta\underline{H}^\circ$ (66, 67, 69).

In GrS, band intensities for Leu and Val are readily determined from the IR difference spectra (Table II) since the amide A bands are discrete and closely approximated by Gaussians. Using values of 3.9×10^6 mol^{-1} cm and 73 cal mol$^{-\frac{1}{2}}$ cm^{-1}, respectively, for $\underline{A}$(free) and $\underline{C}$ suggested by the model compound spectra (61, 66, 67, 69) and $\bar{\nu}_{NH}$(free) = 3457 cm^{-1}, we obtain estimates of $-\Delta\underline{H}^\circ$ = 3.5 kcal mol^{-1} (Leu NH-O=C Val) and 3.7 kcal mol^{-1} (Val NH-O=C Leu) from the Iogansen equation. The error in the estimates is $\simeq$ 0.5 kcal mol^{-1} and is attributable primarily to uncertainties in $\Delta\underline{H}^\circ$ for the model compounds. The intramolecular H bonds in GrS are thus of moderate strength (60).

Free Energies and the HX Barriers. Estimates of the free energies of formation of the transannular H bonds in GrS, $\Delta\underline{G}^\circ_{hb}$, can be obtained by joint analysis of the HX kinetics of the peptide protons and the IR data. It is then possible to discuss quantitatively the

contributions of intramolecular H bonding and steric hindrance to the measured kinetic barriers to HX at Leu and Val NH.

For a two-state system in the high motility limit (72, 73), the observed HX rate constant, $\underline{k}_{obsd}$, is given by (9) Eq. 1

$$\frac{\underline{k}_{obsd}}{\underline{k}_u} = \frac{(\underline{k}_r/\underline{k}_u)\,\underline{K}+1}{\underline{K}+1} \tag{1}$$

where $\underline{k}_u$ and $\underline{k}_r$ are the pseudo-first order rate constants for the unrestricted (U) and restricted (R) conformers and $\underline{K} \equiv [R]/[U]$. Here, $\underline{k}_u$ is the random-coil HX rate constant, which is calculable from model compound data (74), and $\underline{k}_r < \underline{k}_u$. In the case of intramolecular H bonding, $\underline{k}_r \ll \underline{k}_u$ (75) and (72) $\underline{k}_{obsd}/\underline{k}_u \simeq (1+\underline{K})^{-1}$. Defining $\Delta\Delta\underline{G}^{\ddagger} = -\underline{RT}\ \ln(\underline{k}_{obsd}/\underline{k}_u)$ as the apparent kinetic barrier to HX, we obtain, for an H-bonded system with $\underline{K}$ large,

$$\Delta\Delta\underline{G}^{\ddagger}_{hb} \simeq -\Delta\underline{G}^{\circ}_{hb}. \tag{2}$$

If, on the other hand, HX is blocked in the R state by steric factors in the absence of intramolecular H bonding, this approximation can not generally be made, and Eq. 1 holds (9).

It is very likely that both H bonding and steric hindrance will contribute to reduce $\underline{k}_{obsd}$. To treat this situation we shall consider a simple model in which four formally discrete conformational states are in rapid equilibrium, each with a characteristic rate constant: fully solvent exposed (U; $\underline{k}_u$), H-bonded (R_1; $\underline{k}_1$), solvent shielded (R_2; $\underline{k}_2$), and both H-bonded and solvent shielded (R_{12}; $\underline{k}_{12}$). Defining

$\underline{K}_1 = [R_1]/[U] \simeq [R_{12}]/[R_2]$ and $\underline{K}_2 = [R_2]/[U] \simeq [R_{12}]/[R_1]$, and allowing that $\underline{k}_1/\underline{k}_u$, $\underline{k}_{12}/\underline{k}_u \ll 1$,

$$\frac{\underline{k}_{obsd}}{\underline{k}_u} = \frac{(\underline{k}_2/\underline{k}_u)\,\underline{K}_2 + 1}{\underline{K}_1 + \underline{K}_2 + \underline{K}_1\underline{K}_2 + 1} \quad . \tag{3}$$

Combining Eqs. 2 and 3, we obtain

$$\Delta\Delta\underline{G}^{\ddagger} \simeq \underline{RT}\ \ln\left[\frac{\underline{K}_2 + 1}{(\underline{k}_2/\underline{k}_u)\,\underline{K}_2 + 1}\right] - \Delta\underline{G}^{\circ}_{hb} \tag{4}$$

indicating that in the general case the experimentally determined $\Delta\Delta\underline{G}^{\ddagger}$ is an upper limit to $-\Delta\underline{G}^{\circ}_{hb}$.

It was shown previously (8) that the HX kinetics of GrS, summarized in Table III, are consistent with the high motility limit. It had not been possible to account for the substantially reduced HX rates at Leu and Val NH in terms of specific conformational interactions, however, since $\underline{k}_{obsd}/\underline{k}_u$ must depend on $\underline{k}_2$, $\underline{K}_1$, and $\underline{K}_2$, which were unknown. In this context, the following conclusions based on the IR data greatly facilitate the interpretation of the HX kinetics: (i) Leu and Val NH participate in intramolecular H bonds. (ii) The absence of a non- or solvent-H-bonded vibrational band for these residues requires that $\underline{K}_1 > 30$, given the quantitative precision of the absorbance measurements. Thus a lower limit of 2 kcal mol^{-1} to $-\Delta\underline{G}^{\circ}_{hb}$ is imposed by the IR difference spectra. (iii) $-\Delta\underline{H}^{\circ}_{hb}$(Leu) $\simeq$ 3.5 kcal mol^{-1} and $-\Delta\underline{H}^{\circ}_{hb}$(Val) $\simeq$ 3.7 kcal mol^{-1}. These are significantly greater in magnitude than $\Delta\Delta\underline{G}^{\ddagger}$ (Table III) for each residue.

Table III. Hydrogen Exchange Kinetics of the Amide Protons of Gramicidin S in Aqueous Media[a]

Solvent:	D_2O:dioxane-$^2H_8$, 5:2 (v/v), 25°C; ϵ = 52.6[b]			D_2O, 20°C; ϵ = 79.8[b]		
Residue	$\underline{R}'_{obsd}$[c]	$\underline{R}'_{pred}$[d]	$\Delta\Delta\underline{G}^{\ddagger}$	$\underline{R}'_{obsd}$[e]	$\underline{R}'_{pred}$[f]	$\Delta\Delta\underline{G}^{\ddagger}$
Val	0.0106	2.22	3.15	0.128	5.97	2.23
Orn	0.495	1.32	0.58	2.33	3.60	0.25
Leu	0.0256	1.98	2.57	0.307	5.32	1.65
$\underline{\underline{D}}$-Phe	1.77	1.57	0	4.49	4.24	0

[a]Definitions: $\underline{R}'_{obsd} \equiv 2(\underline{k}_D \underline{k}_{OD} \underline{K}_w)^{\frac{1}{2}}$, in $(10^2 \text{ min})^{-1}$, is the minimum HX rate as a function of pD at a given temperature (9). $\underline{R}'_{pred}$, in $(10^2 \text{ min})^{-1}$, is the projected minimum HX rate for a hypothetical random coil peptide of corresponding primary structure (74). $\Delta\Delta\underline{G}^{\ddagger} \equiv -\underline{RT} \ln (\underline{k}_{obsd}/\underline{k}_{pred}) \simeq -\underline{RT} \ln (\underline{R}'_{obsd}/\underline{R}'_{pred})$, in kcal mol^{-1}. [b]Refs. 76, 77. [c]Ref. 8. [d]Based on poly-$\underline{\underline{D}}$, $\underline{\underline{L}}$-alanine HX parameters measured in the present study: $\underline{k}_D$ = 16.0 mol^{-1} min^{-1}, $\underline{k}_{OD}\underline{K}_w = 6.37 \times 10^{-6}$ mol min^{-1} at 24°C. [e]Ref. 78. [f]The average of several earlier determinations of $\underline{R}'$ for poly-$\underline{\underline{D}}$, $\underline{\underline{L}}$-alanine was used in the calculation.

Since the activation energy difference $\Delta\underline{G}^{\ddagger}_{1} - \Delta\underline{G}^{\ddagger}_{u}$ for HX between the R_1 and U states should vary directly with the strength of the internal H bond (75), $\underline{k}_1\underline{K}_1/\underline{k}_u \ll 1$, and the use of Eqs. 2 through 4 is justified for GrS.

For the Leu NH-O=C Val bond, the upper (1.65-2.57 kcal mol^{-1}) and lower (2 kcal mol^{-1}) limits indicated by the HX and IR experiments, respectively, establish that $-\Delta\underline{G}^{\circ}_{hb}(\text{Leu}) \simeq 2.0$ kcal mol^{-1}. H bond cleavage therefore accounts entirely for the apparent kinetic barrier to HX at Leu NH.

$\Delta\underline{G}^{\circ}_{hb}(\text{Val})$ is not as well specified, since $\Delta\Delta\underline{G}^{\ddagger} > 2$ kcal mol^{-1}. To characterize better the components of the kinetic barrier, the effect of variation of the dielectric constant, ϵ, on HX kinetics was investigated (Table III). As expected (59), $\Delta\Delta\underline{G}^{\ddagger} \simeq -\Delta\underline{G}^{\circ}_{hb}$ varies as ϵ^{-1} in the case of Leu NH. The sensitivity of $\Delta\Delta\underline{G}^{\ddagger}(\text{Val})$ to ϵ^{-1} is slightly less, but sufficient to show that H bond cleavage contributes the major portion of the kinetic barrier at Val NH. Modeling of the β turn region of GrS shows the Val NH proton to be shielded from solvent by the peptide group linking $\underline{\underline{D}}$-Phe and Pro and the side chains of Leu and Val. A small steric term accounting for ≤ 1 kcal mol^{-1}, or ~ 30%, of $\Delta\Delta\underline{G}^{\ddagger}(\text{Val})$ is consistent with the IR data and HX kinetics.

Fermi Resonance. The pair of peaks assigned to each of Leu and Val in the amide A′ region (Figure 8) could represent separate conformers or Fermi interaction of ν_{ND} with other amide vibrations. The first possibility seems unlikely, since the NH stretch fundamentals are not doubled. Alternatively, Fermi resonance of ν_{ND} with the combination mode amide II′ + III′ has been demonstrated in N-deuterated

amides and trans-polyamides (79-81). The occurrence of $\bar{\delta}_{II'}$(Val) at 1460 cm^{-1} suggests that the amide II′ frequencies do not differ appreciably from the model compounds (80).

Fermi resonance arises when close-lying stationary states of the unperturbed vibrational Hamiltonian are connected by an anharmonic perturbing potential, $\mathcal{H}'$. Here, the states in question are $\phi_f \equiv \phi_{A'}^{(1)} \phi_{II'}^{(0)} \phi_{III'}^{(0)}$ and $\phi_c \equiv \phi_{A'}^{(0)} \phi_{II'}^{(1)} \phi_{III'}^{(1)}$, corresponding to unperturbed reduced frequencies $\bar{\nu}_f \equiv \bar{\nu}_{ND}$ and $\bar{\nu}_c \equiv \bar{\delta}_{II'} + \bar{\delta}_{III'}$ for the transitions from the vibrational ground state. The dominant term in $\mathcal{H}'$ is proportional to the product $Q_{A'} Q_{II'} Q_{III'}$ of the normal coordinates of the coupled vibrations (82), so that $\langle \phi_f | \mathcal{H}' | \phi_f \rangle = \langle \phi_c | \mathcal{H}' | \phi_c \rangle = 0$ and $\langle \phi_f | \mathcal{H}' | \phi_c \rangle = \langle \phi_c | \mathcal{H}' | \phi_f \rangle \equiv \underline{h}\ (cm^{-1})$, where $\underline{h} \sim |\bar{\nu}_f - \bar{\nu}_c|$. Letting ψ_1 and ψ_2 be the perturbed wavefunctions corresponding to the observed reduced frequencies $\bar{\nu}_1$ and $\bar{\nu}_2$ (choosing $\bar{\nu}_1 > \bar{\nu}_2$), one obtains from first-order perturbation theory (79, 82)

$$\psi_n = c_{nf} \phi_f + c_{nc} \phi_c \qquad n = 1, 2$$

yielding the following secular equation for the $\bar{\nu}_n$

$$\begin{vmatrix} \bar{\nu}_n - \bar{\nu}_f & -\underline{h} \\ -\underline{h} & \bar{\nu}_n - \bar{\nu}_c \end{vmatrix} = 0$$

from which it is found that

$$\bar{\nu}_1 = \bar{\nu}_c + \tfrac{1}{2}(\underline{x} + \underline{y}) \qquad \bar{\nu}_2 = \bar{\nu}_c + \tfrac{1}{2}(\underline{x} - \underline{y})$$

where $\underline{x} = \bar{\nu}_f - \bar{\nu}_c$ and $\underline{y} = (\underline{x}^2 + 4\underline{h}^2)^{\frac{1}{2}}$. Returning to the secular

equation to obtain the c's,

$$\psi_1 = (\sqrt{1 + \underline{x}/\underline{y}}\ \phi_f \pm \sqrt{1 - \underline{x}/\underline{y}}\ \phi_c)/\sqrt{2}$$

$$\psi_2 = (\sqrt{1 - \underline{x}/\underline{y}}\ \phi_f \mp \sqrt{1 + \underline{x}/\underline{y}}\ \phi_c)/\sqrt{2}$$

The intensity ratio of the low- to the high-frequency peak, $\underline{B}$, is

$$\underline{B} = \frac{|\psi_2|^2}{|\psi_1|^2} = \frac{(\underline{y} + \underline{x})|\phi_f|^2 + (\underline{y} - \underline{x})|\phi_c|^2}{(\underline{y} - \underline{x})|\phi_f|^2 + (\underline{y} + \underline{x})|\phi_c|^2} \approx \frac{\underline{y} + \underline{x}}{\underline{y} - \underline{x}} = \frac{\bar{\nu}_c - \bar{\nu}_2}{\bar{\nu}_1 - \bar{\nu}_c}$$

where it is assumed (as is reasonable (83)) that the intensity of the unperturbed combination band is much less than that of the unperturbed fundamental. Thus the unperturbed frequencies are

$$\bar{\nu}_c = \frac{\underline{B}\bar{\nu}_1 + \bar{\nu}_2}{\underline{B} + 1}\ ;\ \bar{\nu}_f = \bar{\nu}_1 + \bar{\nu}_2 - \bar{\nu}_c \qquad (5)$$

and $\underline{h}$ is found, after algebraic rearrangement, to be

$$\underline{h} = \frac{\underline{B}^{\frac{1}{2}}(\bar{\nu}_1 - \bar{\nu}_2)}{\underline{B} + 1}\ . \qquad (6)$$

For Leu, $\underline{B} \approx 1$, $\bar{\nu}_1 = 2465\ cm^{-1}$, $\bar{\nu}_2 = 2423\ cm^{-1}$, and from Eqs. 5 and 6, $\bar{\nu}_f = \bar{\nu}_{ND} = 2444\ cm^{-1}$, $\bar{\nu}_c = \bar{\delta}_{II'} + \bar{\delta}_{III'} = 2444\ cm^{-1}$, and $\underline{h} = 21\ cm^{-1}$. For Val, $\underline{B} \approx 0.4$, $\bar{\nu}_1 = 2477\ cm^{-1}$, and $\bar{\nu}_2 = 2410\ cm^{-1}$, so that $\bar{\nu}_f = 2458\ cm^{-1}$, $\bar{\nu}_c = 2429\ cm^{-1}$, $\bar{\delta}_{III'}$ (calcd) $= \bar{\nu}_c - \bar{\delta}_{II'}$ (obsd) $= 969\ cm^{-1}$, and $\underline{h} = 30\ cm^{-1}$. The isotope ratio $\bar{\nu}_{NH}/\bar{\nu}_{ND}$ calculated for the corrected valence vibration frequencies is 1.33 for Leu and 1.35 for Val (free NH oscillator, 1.37). These suggest that the vibrational potential

in which the H atom resides is of the single minimum type in both complexes (84, 85). Study of the overtone region is, however, essential to elucidating the shape of the potential (84). The estimated values of $\underline{h}$ are comparable to those calculated for N-deuterated amides for which $\bar{\delta}_{II'}$ and $\bar{\delta}_{III'}$ are known (80).

Bandwidths. Comparison of the bandwidths reveals that $\Delta\bar{\nu}_{\frac{1}{2}}(\text{Val}) > \Delta\bar{\nu}_{\frac{1}{2}}(\text{Leu})$ for amide A and A'. Larger bandwidths in H-bonded complexes of weak to moderate strength have been attributed (86) to greater degrees of mechanical anharmonicity in the valence vibration. However, an increase in anharmonicity is generally associated with a larger fractional bandshift (87); in GrS, $\Delta\bar{\nu}_{NH}(\text{Leu}) > \Delta\bar{\nu}_{NH}(\text{Val})$. It is possible to rationalize this apparently paradoxical result in terms of stochastic processes modulating the spectral linewidths in solution (88) and conformational constraints. The NH stretch vibration is strongly coupled to the $\sigma_{NH\text{-}O}$ mode of the complex in the far IR. This, in turn, is perturbed by random intermolecular potentials as well as, in GrS, slow conformational librations. The correlation times involved are long on the IR time-scale (88) so that what is observed is a statistical ensemble of wave-number shifts produced by the couplings, approximately normally distributed about the most probable value (87). One source of the dispersion is induced fluctuation in θ. In intermolecular complexes, θ can assume any value with $\langle\theta\rangle = 180°$ (for acyclic amides), and $\Delta\bar{\nu}_{\frac{1}{2}}$ is dominated by the anharmonicity. In GrS, θ is constrained to possess different equilibrium values for the two pairs of H bonds, and $|\underline{d}\bar{\nu}/\underline{d}\theta|$, which increases rapidly with decreasing θ (48), determines

the relative linewidths. The observed trend in $\Delta\bar{\nu}_{\frac{1}{2}}$ may thus be consistent with nonlinearity of the Val NH-O=C Leu bonds. The $\mu^{-\frac{1}{2}}$ dependence of $\Delta\bar{\nu}_{\frac{1}{2}}$ (μ = reduced mass) predicted by the strong coupling theories (89) is verified by comparison of the amide A and A′ bandwidths.

The amide II frequencies confirm the $\bar{\nu}_{NH}$ bandshift difference between the H bonds (87). The composite nature of the in-plane deformation mode (Table I) precludes for the present a straightforward interpretation of the observed disparity in the amide II bandwidths.

Conclusion. This approach to the identification of intramolecular H bonds in peptides should, at the outset, resolve once and for all the persistent uncertainties associated with the solution conformation of GrS. ^{1}H nuclear Overhauser enhancements (NOE's) (10,11,19,90) had abundantly corroborated the β sheet structure for very short interproton vectors, but the r^{-6} dependence of the NOE and the problem of spin diffusion (14) precluded quantitation of the distance between the Val-Orn-Leu strands. Neither HX rates (8,18,78), NMR chemical shift temperature coefficients (3,78), nor the solvent variation of NMR chemical shifts (3,17,28) were definitive, since all were equally consistent with transannular H bonding or steric shielding of Val and Leu NH from bulk solvent. Consequently, the important question of whether the conformation was constrained by one or two pairs of intramolecular H bonds (91) remained, until the present study, unsettled.

In peptides less throughly investigated than GrS, the identification

of specific intramolecular H bonds by vibrational spectroscopy should clearly provide a powerful constraint in conformational analysis. It is shown that the IR spectrum of a peptide bond thus isolated readily furnishes information concerning the structure and energetics of the H bond not obtainable by methods conventionally employed with polypeptides. Thus, the experimental protocol outlined here should form a basis for the systematic study of the role of intramolecular H bonding in the stabilization of polypeptide conformation.

5. References

1. Craig, L. C.; Cowburn, D.; Bleich, H. Ann. Rev. Biochem. 1975, 44, 477-490.
2. Von Dreele, P. H.; Stenhouse, I. A. J. Am. Chem. Soc. 1974, 96, 7546-7549.
3. Urry, D. W.; Long, M. M.; Mitchell, L. W.; Okamoto, K. in "Peptides: Chemistry, Structure, and Biology", Proc. American Peptide Symp. Fourth; Walter, R.; Meienhofer, J., Eds.; Ann Arbor Science: Ann Arbor, 1975: pp. 113-126.
4. Vinogradov, S. N.; Linnell, R. H. "Hydrogen Bonding"; Van Nostrand Reinhold: New York, 1971; Chapter 3.
5. Néel, J. Pure Appl. Chem. 1972, 3, 201-225.
6. Boussard, G.; Marraud, M.; Aubry, A. Biopolymers 1979, 18, 1297-1331.
7. Wyssbrod, H. R.; Gibbons, W. A. Surv. Prog. Chem. 1973, 6, 209-325.
8. Philson, S. B.; Bothner-By, A. A. In "Peptides: Chemistry, Structure, and Biology", Proc. American Peptide Symp. Sixth; Gross, E.; Meienhofer, J., Eds.; Pierce: Rockford, 1979; pp. 209-212.
9. Krauss, E. M.; Cowburn, D. Biochemistry 1981, 20, 671-679.
10. Jones, C. R.; Sikakana, C. T.; Hehir, S. P.; Gibbons, W. A. Biochem. Biophys. Res. Comm. 1978, 83, 1380-1387.
11. Jones, C. R.; Sikakana, C. T.; Kuo, M.; Gibbons, W. A. J. Am. Chem. Soc. 1978, 100, 5960-5961.

12. Jones, C. R.; Sikakana, C. T.; Hehir, S.; Kuo, M.; Gibbons, W. A. Biophys. J. 1978, 24, 815-832.

13. Gibbons, W. A.; Crepaux, D.; Delayre, J.; Dunand, J.; Hajdukovic, G.; Wyssbrod, H. R. in "Peptides: Chemistry, Structure, and Biology", Proc. American Peptide Symp. Fourth; Walter, R.; Meienhofer, J., Eds.; Ann Arbor Science: Ann Arbor, 1975; pp. 127-137.

14. Rae, I.D.; Stimson, E. R.; Scheraga, H. A. Biochem. Biophys. Res. Comm. 1977, 77, 225-229.

15. Rae, I.D.; Scheraga, H. A. Biochem. Biophys. Res. Comm. 1978, 81, 481-485.

16. Bleich, H. E.; Easwaran, K. R. K.; Glasel, J. A. J. Magn. Reson. 1978, 31, 517-522.

17. Khaled, M. A.; Urry, D. W.; Sugano, H.; Miyoshi, M.; Izumiya, N. Biochemistry 1978, 17, 2490-2494.

18. Stern, A.; Gibbons, W. A.; Craig, L. C. Proc. Natl. Acad. Sci. U.S.A. 1968, 61, 734-744.

19. Huang, D.; Walter, R.; Glickson, J. D.; Rama Krishna, N. Proc. Natl. Acad. Sci. U.S.A. 1981, 78, 672-675.

20. Komoroski, R. A.; Peat, I. R.; Levy, G. C. Biochem. Biophys. Res. Comm. 1975, 65, 272-279.

21. Bamford, C. H.; Elliott, A.; Hanby, W. E. "Synthetic Polypeptides"; Academic Press: New York, 1956; pp. 148-159.

22. Paul, R. C.; Singh, P.; Chadha, S. L. Ind. J. Chem. 1968, 6, 673-674.

23. Ovchinnikov, Yu. A.; Ivanov, V. T.; Bystrov, V. F.;

Miroshnikov, A. I.; Shepel, E. N.; Addullaev, N. D.; Efremov, E. S.; Senyavina, L. B. Biochem. Biophys. Res. Comm. 1970, 39, 217-225.

24. Miroshnikov, A. I.; Snezhkova, L. G.; Sichev, S. V.; Chervin, I.I.; Senyavina, L. B.; Ivanov, V. T.; Ovchinnikov, Yu. A. Bioorg. Khim. 1977, 3, 180-191.

25. Kuo, M.; Jones, C. R.; Mahn, T. H.; Miller, P. R.; Nicholls, L. J. F.; Gibbons, W. A. J. Biol. Chem. 1979, 254, 10301-10306.

26. Jones, C. R.; Kuo, M.; Gibbons, W. A. J. Biol. Chem. 1979, 254, 10307-10312.

27. Venkatachalam, C. M. Biopolymers 1968, 6, 1425-1436.

28. Hawkes, G. E.; Randall, E. W.; Hull, W. E.; Convert, O. Biopolymers 1980, 19, 1815-1826.

29. Pimentel, G. C.; Sederholm. C. H. J. Chem. Phys. 1956, 24, 639-641.

30. Fraser, R. D. B.; MacRae, T. P. "Conformation in Fibrous Proteins"; Academic Press: New York, 1973; p. 96.

31. Miyazawa, T. J. Mol. Spectrosc. 1960, 4, 168-172.

32. Reference 30, p. 205.

33. Ramakrishnan, C.; Prasad, N. Int. J. Protein Res. 1971, 3, 209-231.

34. Vinogradov, S. N. Int. J. Peptide Protein Res. 1979, 14, 281-289.

35. Marsh, R. E.; Corey, R. B.; Pauling, L. Biochem. Biophys. Acta 1955, 16, 1-34.

36. Aubry, A.; Marraud, M.; Protas, J.; Néel, J. C.R. Acad. Sci. Sect. C 1973, 276, 1089-1092.

37. Avignon, M.; Lascombe, J. In "Conformation of Biological Molecules and Polymers"; Bergmann, E. D.; Pullman, B., Eds.; Academic Press: Jerusalem, 1973; pp. 97-105.

38. Ashida, T.; Tanaka, I.; Yamana, T. Int. J. Peptide Protein Res. 1981, 17, 322-329.

39. Kostansek, E. C.; Lipscomb, W. N.; Thiessen, W. E. J. Am. Chem. Soc. 1979, 101, 834-837.

40. Chandresakaran, R.; Lakshminarayanan, A. V.; Pandya, U. V.; Ramachandran, G. N. Biochim. Biophys. Acta 1973, 303, 14-27.

41. Kostansek, E. C.; Lipscomb, W. N.; Yocum, R. R.; Thiessen, W. E. J. Am. Chem. Soc. 1977, 99, 1273-1274.

42. Yang, C.; Brown, J. N.; Kopple, K. D. J. Am. Chem. Soc. 1981, 103, 1715-1719.

43. Karle, I. L.; Karle, J. Acta Crystallogr. 1963, 16, 969-975.

44. Norrestam, R.; Stensland, B.; Brändén, C.-I. J. Mol. Biol. 1975, 99, 501-506.

45. Brahmechari, S. K.; Bhat, T. N.; Sudhakar, V.; Vijayan, M.; Rapaka, R. S.; Bhatnagar, R. S.; Ananthanarayanan, V. S. J. Am. Chem. Soc. 1981, 103, 1703-1708.

46. Aubry, A.; Protas, J.; Boussard, G.; Marraud, M. Acta Crystallogr. Sect. B 1977, 33, 2399-2406.

47. Momany, F. A.; McGuire, R. F.; Burgess, A. W.; Scheraga, H. A. J. Phys. Chem. 1975, 22, 2361-2381.

48. Luck, W. A. P. In "The Hydrogen Bond"; Schuster, P.; Zundel, G.; Sandorfy, C., Eds.; North Holland-Elsevier: New York, 1976; Vol. II, Chapter 11.

49. Pimentel, G. C.; McClellan, A. L. "The Hydrogen Bond"; Freeman: San Francisco, 1960; pp. 87-88.

50. Kostansek, E. C.; Thiessen, W. E.; Schomburg. D.; Lipscomb, W. N. J. Am. Chem. Soc. 1979, 101, 5811-5815.

51. Schwyzer, R.; Iselin, B.; Rittel, W.; Sieber, P. Helv. Chim. Acta 1956, 39, 872-883.

52. Flippen, J. L.; Karle, I. L. Biopolymers 1976, 15, 1081-1092.

53. Rich, D. H.; Jasensky, R. D. J. Am. Chem. Soc. 1980, 102, 1112-1119.

54. Doyle, B. B.; Bendit, E. G.; Blout, E. R. Biopolymers 1976, 14, 937-957.

55. Lazarev, Y. A.; Lazareva, A. V.; Shibnev, A.; Esipova, N. G. Biopolymers 1978, 17, 1197-1214.

56. Ramachandran, G. N. In "Treatise on Collagen"; Ramachandran, G. N., Ed.; Academic Press: London, 1967; Vol. I, pp. 103-183.

57. Yonath, A.; Traub, W. J. Mol. Biol. 1969, 43, 461-477.

58. Susi, H.; Ard, J. S. Arch. Biochem. Biophys. 1966, 117, 147-153.

59. Franzen, J. S.; Stephens, R. E. Biochemistry 1963, 2, 1321-1327.

60. Joesten, M. D.; Schaad, L. J. "Hydrogen Bonding"; Marcel Dekker: New York, 1974; Chapter 4.

61. Jones, R. L. Spectrochim. Acta 1966, 22, 1555-1562.

62. Miyazawa, T.; Shimanouchi, T.; Mizushima, S. J. Chem. Phys. 1956, 24, 408-418.

63. Løwenstein, H.; Lassen, H.; Hvidt, A. Acta Chem. Scand. 1970, 24, 1687-1696.

64. Bernard-Houplain, M.; Sandorfy, C. Can. J. Chem. 1973, 51, 3640-3646.

65. Spencer, J. N.; Garrett, R. C.; Mayer, F. J.; Merkle, J. E.; Powell, C. R.; Tran, M. T.; Berger, S. K. Can. J. Chem. 1980, 58, 1372-1375.

66. Graham, L. L.; Chang, C. Y. J. Phys. Chem. 1971, 75, 776-783.

67. Bhaskar, K. R.; Rao, C. N. R. Biochim. Biophys. Acta 1967, 136, 561-562.

68. Mizuno, K.; Nishio, S.; Shindo, Y. Biopolymers 1979, 18, 693-708.

69. Klotz, I. M.; Franzen, J. S. J. Am. Chem. Soc. 1962, 84, 3461-3466.

70. Cutmore, E. A.; Hallam, H. E. Spectrochim. Acta, Part A 1969, 25, 1767-1784.

71. Iogansen, A. V. Dokl. Akad. Nauk SSSR 1965, 164, 610-613.

72. Hvidt, A.; Nielsen, S. O. Adv. Protein Chem. 1966, 21, 287-386.

73. Rama Krishna, N.; Goldstein, G.; Glickson, J. D. Biopolymers 1980, 19, 2003-2020.

74. Molday, R. S.; Englander, S. W.; Kallen, R. G. Biochemistry 1972, 11, 150-158.

75. Eigen, M.; Kruse, W.; Maass, G.; De Maeyer, L. Progr. Reaction Kinetics 1964, 2, 285-318.

76. Harned, H. S.; Owen, B. B. "The Physical Chemistry of Electrolytic Solutions", 3rd Ed.; Reinhold: New York, 1958; p. 161.

77. "Handbook of Chemistry and Physics", 52nd Ed.; Weast, R. C., Ed.; CRC Press: Cleveland, 1971; p. E-49.

78. Fischman, A. J.; Wittbold, W. M.; Wyssbrod, H. R., The Mount Sinai Medical Center, personal communication, 1981.

79. Pivcová, H.; Schneider, B.; Stokr, J.; Jakes, J. Coll. Czech. Chem. Comm. 1964, 29, 2436-2448.

80. Pivcová, H.; Schneider, B.; Stokr, J. Coll. Czech. Chem. Comm. 1965, 30, 2215-2231.

81. Dementjeva, L. A.; Iogansen, A. V.; Kurkchi, G. A. Opt. Spektrosk. 1970, 29, 868-875.

82. Wilson, E. G.; Decius, J. C.; Cross, P. C. "Molecular Vibrations"; McGraw-Hill: New York, 1955; Chapter 8.

83. Hertzberg, G. "Molecular Spectra and Molecular Structure"; Van Nostrand: New York, 1945; Vol. II, Chapter 2.

84. Fung, B. M. Ph.D. Dissertation, California Institute of Technology, 1967.

85. Novak, A. In "Infrared and Raman Spectroscopy of Biological Molecules"; Proc. NATO Adv. Study Inst.; Theophanides, T. M., Ed.; Reidel: Dordrecht, 1979; pp. 279-303.

86. Sandorfy, C. In "The Hydrogen Bond"; Schuster, P.; Zundel, G.; Sandorfy, C., Eds.; North-Holland-Elsevier: New York, 1976; Vol. II, Chapter 13.

87. Hadzi, D.; Bratos, S. In "The Hydrogen Bond"; Schuster, P.; Zundel, G.; Sandorfy, C., Eds.; North-Holland-Elsevier: New York, 1976; Vol. II, Chapter 12.

88. Bratos, S. J. Chem. Phys. 1975, 63, 3499-3509.

89. Sakun, V. P.; Sokolov, N. D. Chem. Phys. 1980, 50, 287-290.

90. Bothner-By, A. A.; Johner, P. E. Biophys. J. 1978, 24, 779-790.

91. Dygert, M.; Gō, N.; Scheraga, H. A. Macromolecules 1975, 8, 750-761.

CHAPTER III

INTRAMOLECULAR HYDROGEN BONDING AND SOLUTION CONFORMATION OF THE ORNITHYL RESIDUES

1. Introduction

While the elucidation of the secondary structure of GrS has for the first time afforded the selective observation of internal H bonds in a heteropolypeptide in solution, the relationship of conformation to biological function remains undetermined. In order to broach the latter question for this molecule, it is necessary to undertake a study of the solution conformation of the functionally essential Orn residues.

Earlier attempts to define the tertiary structure of Orn have been deterred by the flexibility of the aminopropyl side chain (diagrammed in Fig. 1). The presence of rapid rotational isomerism in solution renders estimation of dihedral angles or interatomic distances by conventional NMR methods extremely difficult without making major assumptions concerning the rotational potential (1), and when isomerism obtains along a flexible chain of several segments' length the problem becomes all but intractable. The most comprehensive NMR study of the solution structure of GrS published to date (2) does not treat the side chain dihedral angles beyond χ^1. Pachler analysis (3) of the $H^{\alpha}H^{\beta}$ vicinal coupling constants of Orn indicated a predominance (~70%) of one of the classical staggered rotamers, corresponding either to $\chi^1 = 180°$ or $\chi^1 = -60°$ (3), but without stereoselective ^2H labeling it was not possible to distinguish between them.

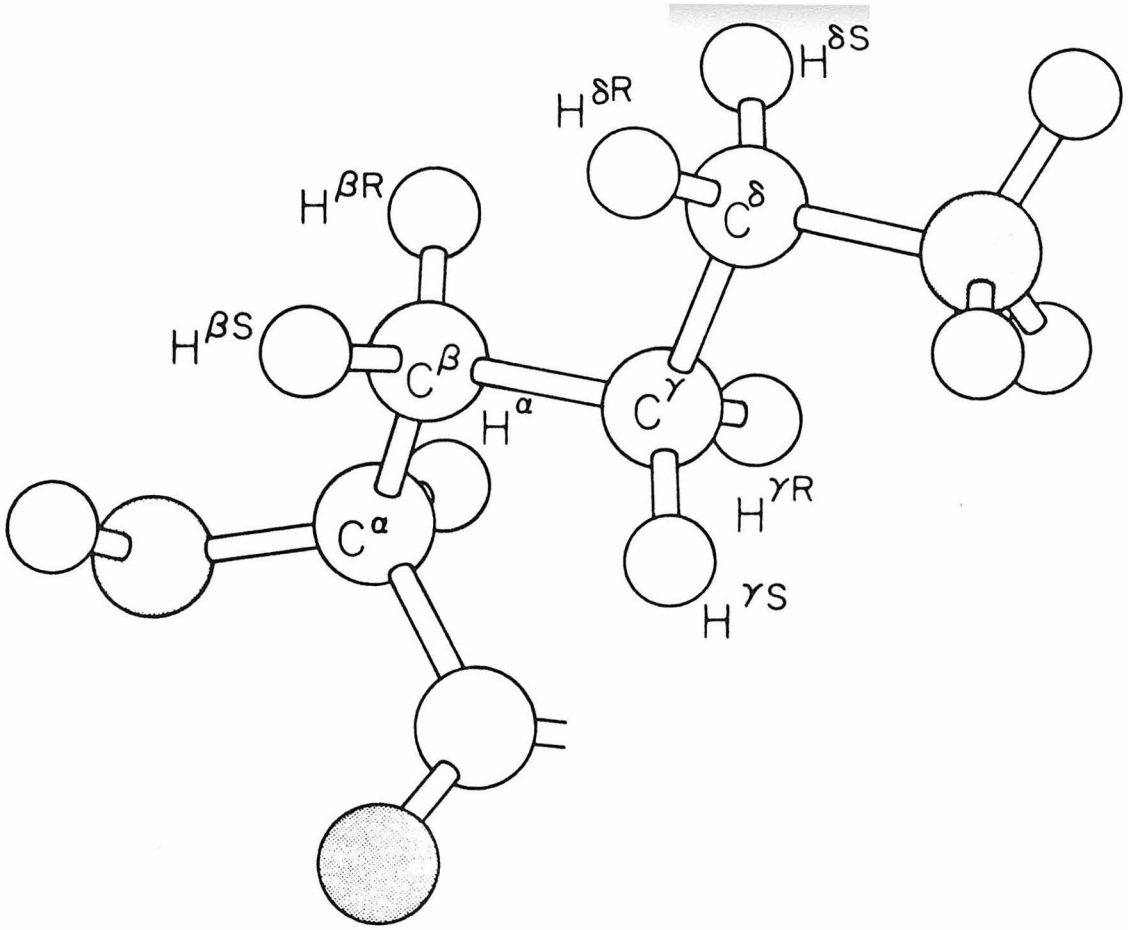

Figure 1. The ornithine side chain (all side chain dihedral angles are 180°) with stereochemical labels.

Several lines of evidence have suggested that, interestingly, there exists a preferred conformation for the distal portion of the Orn side chain. Levels of potency of GrS analogues were found to be related to the ability of spin-labeled polar side chains to achieve spatial proximity (4). ^{13}C spin-lattice relaxation times in MeOH and Me_2SO (5, 6) showed an appreciable decrease in apparent rotational correlation time only between C^{β} and C^{γ}; this may be contrasted, for example, to the highly mobile Lys side chain in lysine vasopressin (7). Finally, a significant chemical shift difference between the Orn $C^{\delta}H_2$ protons was observed in MeOH (2) which can only arise from incomplete averaging about χ^3.

The possibility of intramolecular H bonds involving Orn $N^{\delta}H_2$ was discussed in the semiempirical calculation of Dygert et al. (8). The lowest energy conformation contained a pair of Orn $N^{\delta}H_2$--O=C $\underline{\underline{D}}$-Phe H bonds formed in the $\underline{i} \rightarrow \underline{i} - \underline{3}$ sense, while other low energy conformations lacked the bonds. The minimization was not exhaustive for the side chains; an additional difficulty with the structures proposed by Dygert et al. is that the transannular H bonds involving Val NH and Leu C=O, demonstrated in the previous chapter, were not predicted. The crystalline urea complex of GrS contained a single $\underline{i} \rightarrow \underline{i} + \underline{2}$ Orn $N^{\delta}H_3^+$--O=C $\underline{\underline{D}}$-Phe H bond per molecule, but backbone distortion induced by the urea diminished the symmetry (9).

Whether the terminal amino groups of Orn are actually intramolecularly H-bonded in solution remains to be experimentally verified. Steric factors (10) or the formation of relatively long-lived complexes with the solvent could equally well explain the apparent

decrease in motility of the side chain. Selecting from these alternatives is difficult because the necessary experimental criteria are not readily available. Proton exchange rates are useful for identifying potential amide H bond donors in peptides, but model compound data are not available for amines. IR spectrophotometry should also be less helpful here than with amides, both because of the impracticality of isotopically isolating the amine vibrations and the likelihood that the vibrational bands will be broadened by coupling of the NH oscillators and interactions with the solvent (11). The study of solvent-induced NMR chemical shift changes in amide group resonances can identify solvent-shielded amide groups in peptides as long as the conformational perturbations caused by the solvents are minor. On the other hand, when the stability of an intramolecular H bond itself varies with the solvent, the variation of these chemical shifts with solvent should equal or exceed those of fully exposed amides. The latter assertion is warranted by the observation that when an NH group in an oligopeptide becomes solvent-exposed with increasing temperature, the corresponding resonance exhibits a normal or larger than expected temperature dependence (12). The discrimination between solvent-shielded and solvent-exposed groups by the temperature or solvent variation of NMR chemical shifts alone is reliable only when the conformation is invariant, an unwarranted assumption in the case of the side chains of Orn in GrS.

In view of these difficulties, this study begins not by attempting a direct demonstration of H bonding, but rather by probing its likely consequences: motional limitation at the donor site, as evidenced by

the chemical shift inequivalence of the Orn $C^{\delta}H_2$ protons (ΔO^{δ}_{obsd}), and charge relay effects on the chemical shift of ^{15}N at the acceptor site (13). It is found that when GrS is exhaustively methylated to give [N^{δ}-trimethylornithyl$^{2,2'}$]-GrS (Me_6GrS; Fig. 2), a derivative in which Orn remains ionized but cannot function as an H bond donor, the Pro ^{15}N resonance in MeOH shifts significantly upfield. Concomitantly, the observed relationship of ΔO^{δ}_{obsd} to the acid/base properties of the solvent is abolished. These results are strongly indicative of the presence of solvent-labile Orn $N^{\delta}H_3^+$--O=C D-Phe H bonds in GrS. The thermodynamics of formation of the H bonds in MeOH and their spatial orientation relative to the backbone are then investigated by NMR-based methods. The bonds, once characterized, provide a major constraint on the conformations accessible to the Orn side chain, and side chain torsional angles for the H-bonded configuration can be estimated by standard analysis of the vicinal coupling constants.

2. Experimental Section

Materials. GrS dihydrochloride (Sigma) was dissolved in H_2O-dioxane (5:2 v/v), filtered and lyophilized prior to use. It migrated as a single spot on TLC in several solvent systems. Other chemicals were reagent grade and used without further purification.

[N^{δ}-trimethylornithyl$^{2,2'}$]-GrS Chloride (Me_6GrS). The title compound was synthesized according to a modification of the method of Granados and Bello (14). GrS (Sigma, 3.29×10^{-4} mol) was dissolved in 10 ml 50% aqueous EtOH containing 0.010 M $Na_2B_4O_7(H_2O)_{10}$. The

Figure 2. Diagrammatic representations of the structures of GrS and Me_6GrS.

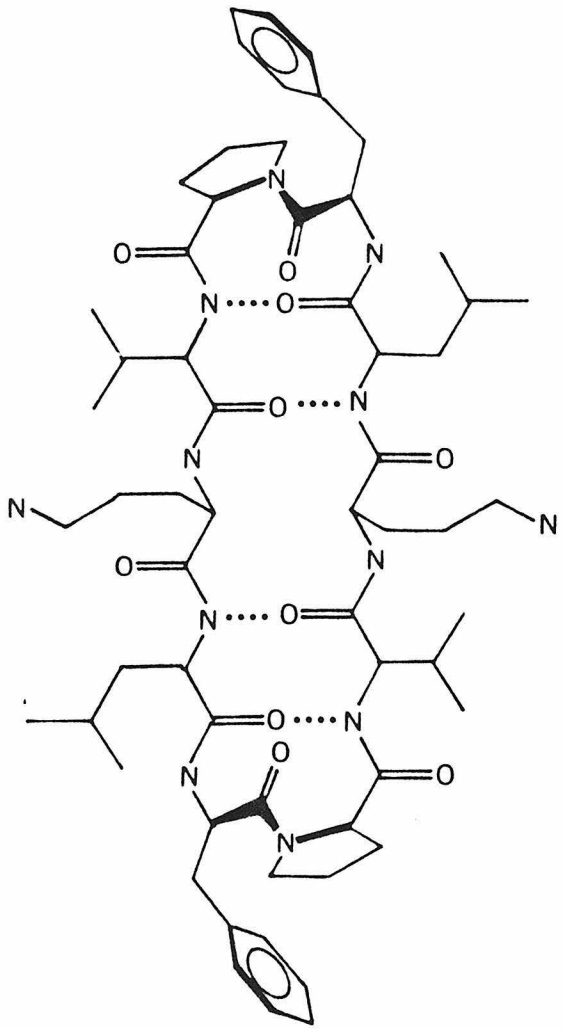

Me_2SO_4, OH^-

1:1 $EtOH/H_2O$

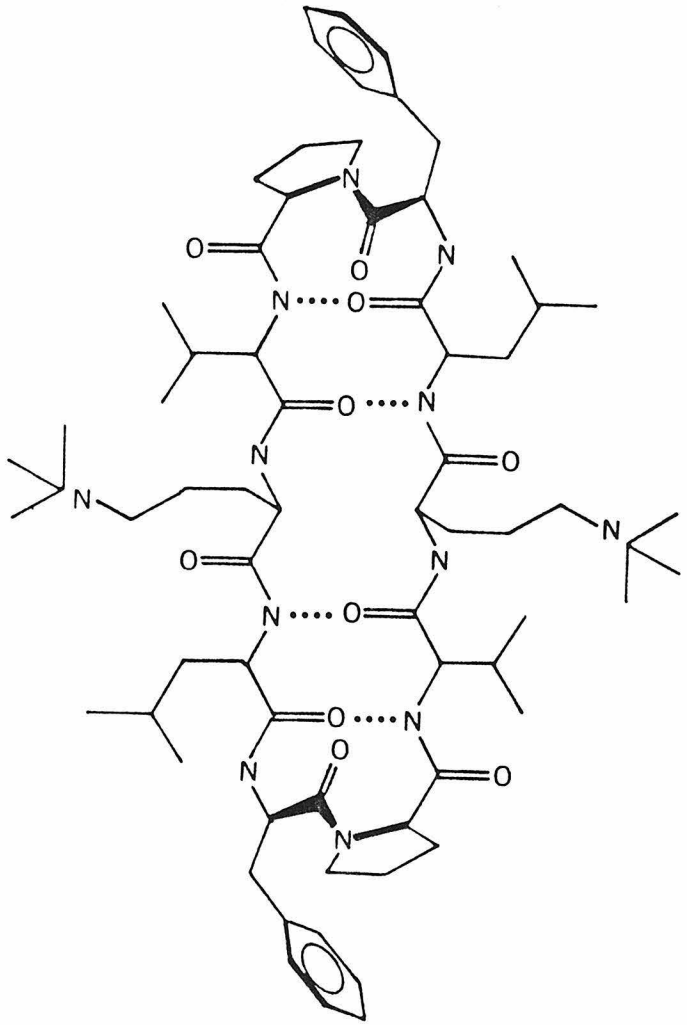

GRAMICIDIN S

[N^{δ}-TRIMETHYLORNITHYL$^{2,2'}$]-GRAMICIDIN S

(Me_6GrS)

solution was adjusted to glass electrode reading =10.0 on a pH-stat with solvent A (50 ml 10 N NaOH + 50 ml EtOH, with sufficient water to obtain a single phase). Me_2SO_4 (0.0296 mol) was added, and the solution maintained at an apparent pH of 10.0 with additional alkali. The initial and final delivery rates of solvent A were 35 and 5 μl min^{-1}, respectively. The solution was then diluted fourfold with 40% EtOH and chromatographed on Sephadex G-10 in 40% aqueous EtOH containing 0.020 M NH_4Cl. The protein-containing fractions were rechromatographed on Sephadex G-15 in 40% aqueous EtOH containing 1×10^{-3} M HCl. Removal of solvents yielded a white powder which on TLC migrated as a single ninhydrin-negative spot in several solvent systems. A ^1H NMR spectrum at 500.13 MHz in Me_2SO-$\underline{d}_6$ was consistent with a single species with the structure of the title compound, containing a singlet at 3.15δ (18 protons) assigned to Orn $N^{\delta}Me_3$, and devoid of Orn amino protons. Yield: 325 mg (76%).

NMR Spectroscopy. All spectra were obtained on a Bruker WM-500 multinuclear NMR spectrometer employing an Oxford Instruments 11.7 T superconducting magnet and an Aspect 2000 computer. ^1H spectra at 500.13 MHz were obtained on 0.02 M solutions of peptide in the indicated solvent, with the exception of ^2H_2O, in which the concentration was 5×10^{-3} M. For variable temperature runs the thermocouple was calibrated against MeOH. NOE difference spectra were acquired by alternating on- and off-resonance single frequency CW irradiation, both with and without truncation. To ensure selectivity the decoupler power was set well below saturating levels, and the NH protons exchanged with ^2H to circumvent the problem of

magnetization transfer within the peptide backbone at low temperatures.

Natural abundance ^{15}N spectra at 50.68 MHz were obtained on MeOH solutions of GrS and Me_6GrS containing 10% MeOH-$\underline{d}_4$ for internal locking. The recycle time was 3.41 s, including a 3 s relaxation delay between pulses. Chemical shifts were measured without NOE to avoid nulling the Pro resonance (15,16). There was no detectable concentration effect on the shifts for solutions up to 0.15 M. Peak assignments in Me_6GrS were confirmed by single-frequency ^1H decoupling. The chemical shift reference was external Me_2NCHO, which was assigned (17) a shift of 82.2 ppm downfield from the NH_4^+ resonance of 5 M $^{15}NH_4NO_3$ in 2 M HNO_3.

3. Results

NMR Spectra of GrS and Me_6GrS at 11.7 T. The ^1H NMR shifts of GrS and Me_6GrS, displayed in Tables I and II, were obtained by standard decoupling techniques. For either compound, a number of solvent dependences are evident, particularly in the amide NH resonances which are strongly influenced by the capacity of the solvent to donate or accept protons (18). The pleated backbone conformation of GrS is little affected by the medium, and the shift variations in the non-exchangeable resonances are thus predominantly the result of solvent screening interactions not related to H bonding (19) and induced tertiary structural effects. The solvent dependences of individual absolute ^1H shifts are not readily analyzable in terms of specific contributions and are not treated in detail at present. The ^{13}C chemical

Table I. Proton NMR Chemical Shifts of GrS[a]

Residue	Resonance	Solvent				
		Me_2SO	H_2O	MeOH	F_3EtOH	AcOH
Val	NH	7.22	7.62	7.73	7.86	7.59
	α	4.42	4.13	4.17	3.98	4.18
	β	2.08	2.16	2.26	2.37	2.26
Orn	NH	8.68	8.61	8.70	7.66	8.36
	α	4.77	4.97	4.97	5.11	5.10
	β_d	1.75	1.96	2.05	2.18	1.99
	β_u	1.60	1.66	1.64	1.65	1.75
	γ_d	1.65	1.70	1.79	1.92	1.90
	γ_u	1.65	1.70	1.79	1.81	1.84
	δ_d	2.85	3.01	3.05	3.16	3.10
	δ_u	2.75	2.99	2.91	2.94	3.10
Leu	NH	8.34	8.81	8.80	8.92	9.03
	α	4.58	4.64	4.66	4.71	4.78
	β_d	1.34	1.48	1.55	1.59	1.59
	β_u	1.34	1.41	1.41	1.55	1.51
	γ	1.41	1.38	1.50	1.51	1.51
D-Phe	NH	9.11	8.99	8.90	7.82	8.50
	α	4.36	4.67	4.50	4.53	4.53
	β_d	2.99	3.12	3.10	3.10	3.14
	β_u	2.88	2.97	2.96	3.01	3.08
Pro	α	4.32	4.40	4.35	4.29	4.66
	β_d	1.96	1.94	2.00	1.98	2.08
	β_u	1.49	1.85	1.69	1.89	1.73
	γ_d	1.52	1.69	1.71	1.80	1.70
	γ_u	1.52	1.64	1.59	1.63	1.61
	δ_d	3.60	3.68	3.73	3.77	3.76
	δ_u	2.48	2.59	2.48	2.48	2.46

Table I (continued)

---

[1] In ppm downfield of Me_4Si at 295 K in the deuterated solvents; t-BuOH was present in the aqueous sample, and the shifts corrected to Me_4Si.

Table II. Proton NMR Chemical Shifts of Me_6GrS[a]

Residue	Resonance	Solvent				
		Me_2SO	H_2O	MeOH	F_3EtOH	AcOH
Val	NH	~7.2	7.61	7.54	7.81	7.66
	α	4.40	4.04	4.10	4.01	4.28
	β	2.05	2.18	2.25	2.36	2.25
Orn	NH	8.74	8.52	8.46	7.42	8.33
	α	4.88	4.81	4.95	5.08	5.18
	β_d	1.70	1.91	1.87	1.90	1.92
	β_u	1.37	1.73	1.64	1.73	1.74
	γ_d	1.70	1.78	1.80	1.88	1.90
	γ_u	1.60	1.78	1.80	1.88	1.82
	δ_d	3.67	3.35	3.57	3.38	3.66
	δ_u	3.31	3.35	3.33	3.25	3.53
Leu	NH	8.32	8.50	8.62	8.81	8.96
	α	4.62	4.54	4.54	4.63	4.78
	β_d	1.34	1.46	1.55	1.65	1.59
	β_u	1.34	1.40	1.40	1.50	1.46
	γ	1.42	1.35	1.55	1.56	1.50
D-Phe	NH	9.17	8.99	8.75	7.61	8.64
	α	4.34	4.56	4.37	4.53	4.56
	β_d	2.95	3.03	3.06	3.05	3.12
	β_u	2.80	2.97	2.87	2.89	3.05
Pro	α	4.23	4.38	4.21	4.35	4.52
	β_d	1.91	1.89	1.98	1.99	2.04
	β_u	1.51	1.85	1.68	1.82	1.80
	γ_d	1.55	1.67	1.68	1.74	1.72
	γ_u	1.55	1.67	1.63	1.61	1.62
	δ_d	3.55	3.61	3.66	3.70	3.74
	δ_u	2.49	2.60	2.43	2.43	2.48

[a]Chemical shift referencing as in Table I.

shifts of GrS and Me_6GrS in MeOH are listed in Table III.

It is clear from examination of the NMR spectra that quaternization of Orn does not introduce substantial or long-range conformational perturbations. This is supported by the following observations: (a) With the exception of Orn, the root mean square (rms) deviation of the methylene and methyne ^1H shifts in Me_6GrS from GrS is small and demonstrates no significant solvent dependence. The rms deviations are, in 10^{-3} ppm (values for Orn α, β, and γ protons in parentheses): Me_2SO, 40 (120); water, 56 (96); MeOH, 60 (80); F_3EtOH, 57 (136); AcOH, 51 (49). (b) With the exception of Orn, the ^{13}C shifts of the proton-bearing C atoms of Me_6GrS in MeOH are identical to within 1 ppm of the corresponding resonances in GrS. Orn C^{δ} moves downfield by 20.2 ppm, Orn C^{γ} moves upfield by 4.6 ppm, and a singlet at 53.0 ppm (downfield of Me_4Si), assigned to Orn NMe_3, appears in the derivative. (c) Checks of the vicinal ^1H coupling constants $^3J_{N\alpha}$ and $^3J_{\alpha\beta}$ in the five solvents employed revealed no significant differences between GrS and its derivative.

In order to test whether the two pairs of transannular H bonds were affected by derivatization, amide hydrogen exchange (HX) rates for Me_6GrS were measured in water (Table IV; Fig. 3). Rates were measured directly by ^1H NMR in D_2O as a function of pD, and rate constants for specific acid- and base-catalyzed exchange fitted as previously described (20). The rate-pD profiles (Fig. 3) show an almost exact concordance between GrS and Me_6GrS for the internally H-bonded residues Leu and Val NH, indicating that the internal H bonds remain intact. The Orn NH profile exhibits a small shift,

Table III. ^{13}C NMR Chemical Shifts of GrS and Me_6GrS[a]

Residue	Resonance	GrS[b]	Me_6GrS
Val	α	60.18	59.33
	β	31.92	31.67
	γ_1	19.64	19.19
	γ_2	19.49	18.70
Orn	α	52.58	52.69
	β	30.89	30.22
	γ	24.57	20.01
	δ	40.49	66.70
	ϵ		53.02
Leu	α	51.46	51.07
	β	41.88	41.76
	γ	25.67	25.11
	δ_1	23.29	22.63
	δ_2	23.14	22.47
D-Phe	α	55.85	55.03
	β	37.30	36.75
Pro	α	61.95	61.15
	β	30.57	29.89
	γ	24.43	23.89
	δ	47.88	46.79

[a]In MeOH at 22°C, in ppm downfield of Me_4Si. The C′=O and aromatic resonances were not assigned. [b]Reference 6.

Table IV. Proton Exchange Parameters for GrS and Me_6GrS[a]

	GrS[b]				Me_6GrS			
Residue	$\underline{k}_D$	$\underline{k}_{OD} \times 10^{10}$	$\underline{R}'$	$p\underline{D}'$	$\underline{k}_D$	$\underline{k}_{OD} \times 10^{10}$	$\underline{R}'$	$p\underline{D}'$
Val	1.34	0.0453	0.154	3.24	1.49	0.0290	0.130	3.36
Orn	10.5	1.13	2.15	2.99	11.7	0.573	1.62	3.16
Leu	0.907	0.256	0.301	2.78	0.836	0.215	0.265	2.80
D-Phe	7.30	7.13	4.51	2.51	3.98	2.95	2.14	2.57

[a]In D_2O at 294 K. The rate law is $\underline{R} = \underline{k}_D[D^+] + \underline{k}_{OD}[OD^-]$, where $\underline{k}_D$ and $\underline{k}_{OD}$ are the pseudo-first order rate constants for specific acid and specific base catalyzed exchange, respectively, in L mol^{-1} min^{-1}, and $\underline{R}$ is the macroscopically observed exchange rate. $\underline{R}' = 2(\underline{k}_D\underline{k}_{OD}\underline{K}_{D_2O})^{\frac{1}{2}}$ in $(10^2 \text{ min})^{-1}$ is the calculated minimum value of $\underline{R}$ with respect to $p\underline{D}$; $p\underline{D}'$ is the $p\underline{D}$ at which $\underline{R} = \underline{R}'$.

[b]Ref. 23, corrected to 294 K.

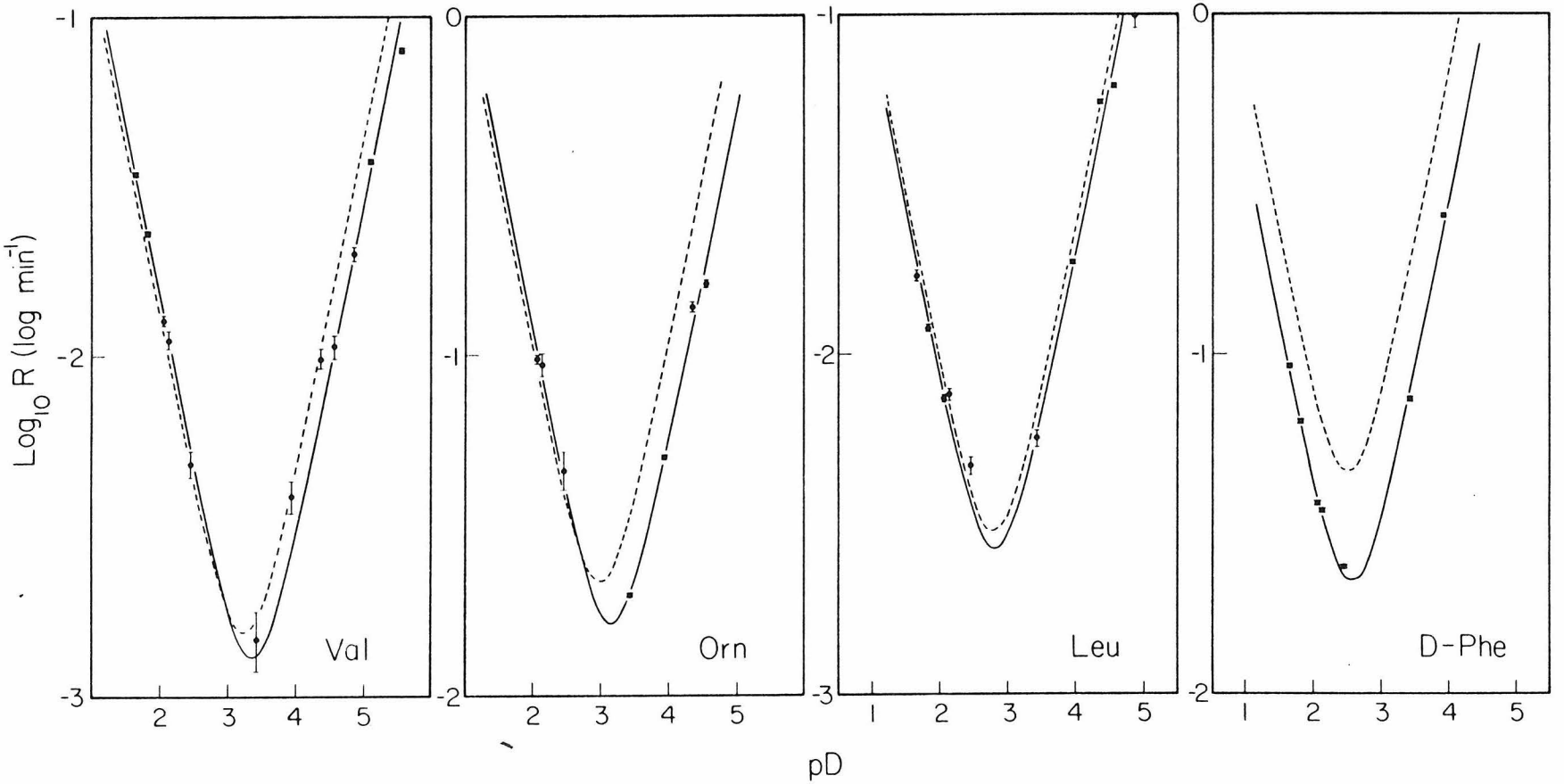

Figure 3. Observed proton exchange kinetics for Me_6GrS in D_2O: experimental values are shown with standard errors. The exchange profiles (solid lines) were fitted by a weighted nonlinear least squares routine. Exchange profiles measured previously in D_2O for GrS (Ref. 23) are also shown (dashed lines).

which is most likely the consequence of side chain modification (21). HX at D-Phe NH is retarded approximately twofold in Me_6GrS; the possible conformational significance of this is discussed below.

The observations indicate that the conformational perturbation introduced by methylation is minor, limited primarily to the Orn side chain, and not disparately large in any particular solvent. This is not unexpected; the β sheet-β-II′ turn structure is itself maintained in a considerable variety of solvents (Chapter I), and is not affected by other derivatizations at Orn N^{δ}, such as acetylation (22). The conformational effects on the remaining side chains should be negligible as well, since Orn is confined to one side of the ring, spatially isolated from the pendant hydrophobic side chains of Val, Leu, and D-Phe.

Orn-D-Phe H Bonding in Solution: Identification by NMR. ^{15}N chemical shifts in MeOH were determined for both GrS and the derivative. The Me_6GrS spectrum is shown in Fig. 4. The assignments were confirmed by single-frequency ^{1}H decoupling (Fig. 5) and are given in Table V. The chemical shifts for GrS were in good agreement with a previous determination at slightly higher temperature (24). Comparison of the amide ^{15}N shifts of GrS and Me_6GrS reveals that quaternization of Orn has induced a substantial 3.5 ppm upfield shift of ths Pro resonance, while the remaining amide chemical shifts are virtually unchanged. The Pro ^{15}N chemical shift in Me_6GrS, 112.0 ppm, is identical to that predicted for Pro in GrS in MeOH on the basis of primary structure alone (5). Since the NMR data cited above do not suggest a significant conformational change in the β turn region, it is

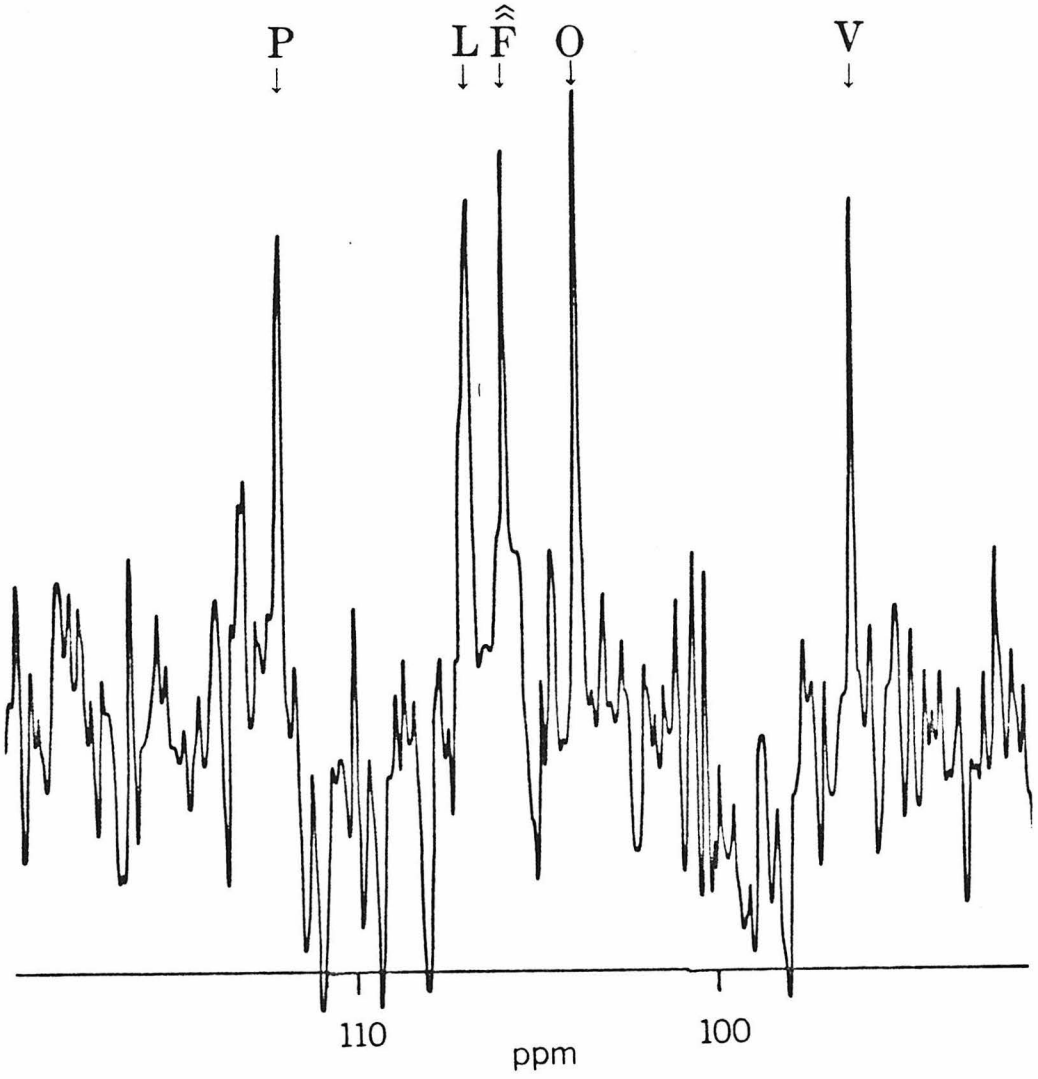

Figure 4. Natural abundance ^{15}N NMR spectrum of 0.07 M Me_6GrS in MeOH at 298 K. The spectrum was acquired with broadband ^{1}H decoupling without NOE. The chemical shifts are referenced to the NH_4^+ resonance of 5 M $^{15}NH_4NO_3$ in 2 M HNO_3. The Orn N^{δ} resonance appears at 27.2 ppm (not shown).

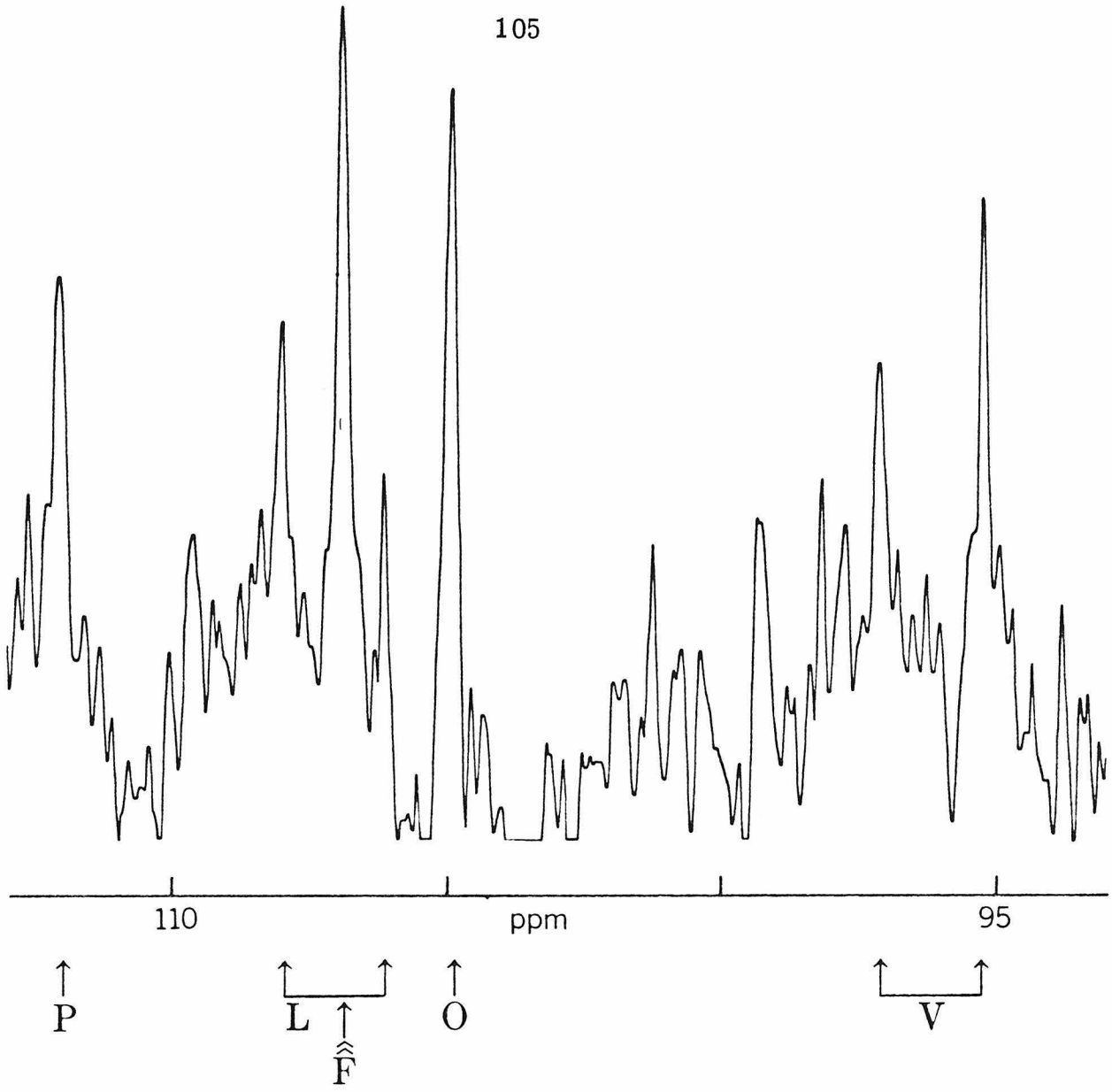

Figure 5. ^{15}N NMR spectrum of 0.07 M Me_6GrS in MeOH at 298 K with single frequency decoupling of Orn NH. Pro N is a singlet (no NH proton); Leu and Val N are doublets, $^2J_{NH} \approx 90$ Hz (each coupled to a slowly exchanging NH proton); and D-Phe N is a singlet (exchange-decoupled; Ref. 24). Shifts are referenced as in Fig. 4.

Table V. ^{15}N NMR Chemical Shifts of GrS and Me_6GrS[a]

	GrS	Me_6GrS
Val	97.3	96.2
Orn N′	105.0	104.2
Orn N^{δ}	10.8	27.2
Leu	106.7	106.8
D-Phe	106.2	105.9
Pro	115.5	112.0

[a]In ppm downfield of $^{15}NH_4NO_3$ in 2 M HNO_3 at 298 K in MeOH.

necessary to consider possible charge relay effects on the amide group comprised of Pro N and D-Phe C=O which may be exerted by a direct interaction with the cationic side chain.

It has been shown that ^{15}N NMR chemical shifts in amides are sensitive to H bonding (25). The effect is most pronounced when the carbonyl group interacts with proton donors, in which case a decrease in electron density on the adjacent nitrogen (26) is accompanied by a low-field shift of the corresponding ^{14}N or ^{15}N resonance (26-29). Downfield shifts as large as 10.6 ppm have been reported (30) in model peptides on transfer from Me_2SO to F_3AcOH, and shifts of 2.8 to 7.5 ppm were observed on transfer from Me_2SO to F_3EtOH of alumichrome (13) and GrS (24, 31, 32). ^{15}N resonances adjacent to solvent-shielded amide C=O groups, such as D-Phe and Orn ^{15}N in GrS (24), exhibit little or no dependence on solvent acidity.

The observed upfield shift of Pro ^{15}N in Me_6GrS is precisely what would be expected were an Orn $N^{\delta}H_3^+$--O=C D-Phe H-bond disrupted by Orn N^{δ} quaternization. In terms of charge relay effects, substitution of a weaker acid (MeOH) for a stronger one (Orn $N^{\delta}H_3^+$) as the H bond donor to D-Phe C=O has resulted in a relatively higher degree of diamagnetic shielding of the Pro N atom and an upfield shift of the corresponding resonance in Me_6GrS relative to GrS. The remaining amide ^{15}N resonances should be unaffected, as observed (a shift change would also be expected at D-Phe $^{13}C=O$, but the carbonyl ^{13}C shifts could not be assigned in Me_6GrS).

Examination of molecular models indicates that Orn $N^{\delta}H_3^+$--O=C D-Phe H bonds can be reversibly formed in either the

$\underline{i} \rightarrow \underline{i} + 2$ or $\underline{i} \rightarrow \underline{i} - 3$ sense with minimal perturbation of the remaining structure. Thus, it is entirely plausible that permethylation should eliminate this side chain-backbone interaction without introducing chemical shift anomalies in either the ^{1}H or ^{13}C spectra. It is also clear from the models that these H bonds would be solvent exposed (in contrast to the transannular H bonds) and thus exist to greater or lesser degree depending on the ability of the solvent to compete for H bonding moieties.

The question of solvent lability is best approached from the donor side of the interaction, where the chemical shift difference between the Orn $C^{\delta}H_2$ protons observed previously (2) demonstrates that internal motions in the distal portion of the Orn side chain are limited. The ease with which this inequivalence is measured at 500.13 MHz is illustrated in Fig. 6. If the nonvanishing ΔO^{δ}_{obsd} arises from the existence of intramolecularly H-bonded conformers in which the motility of the Orn side chain is hindered, in rapid exchange with a fully solvated state in which the intramolecular motion is unrestricted, it is possible to deduce the solvent dependence expected for this quantity. If, on the other hand, there is no intramolecular interaction, it is very unlikely that ΔO^{δ}_{obsd} (if of measurable magnitude) will conform to the pattern predicted for internal H bonding.

The form of solvent dependence for ΔO^{δ}_{obsd} is derived as follows for the H-bonded case: Because NMR detects the time-averaged chemical shifts, $\Delta O^{\delta}_{obsd} = \sum_{\underline{i}} \underline{f}_b(\underline{i})\, \Delta O^{\delta}_{b}(\underline{i})$, where $\underline{f}_b(\underline{i})$ and $\Delta O^{\delta}_{b}(\underline{i})$ refer to the probability of occupancy and the $C^{\delta}H_2$ chemical shift inequivalence of the $\underline{i}^{th}$ hypothetical bound state involving the side

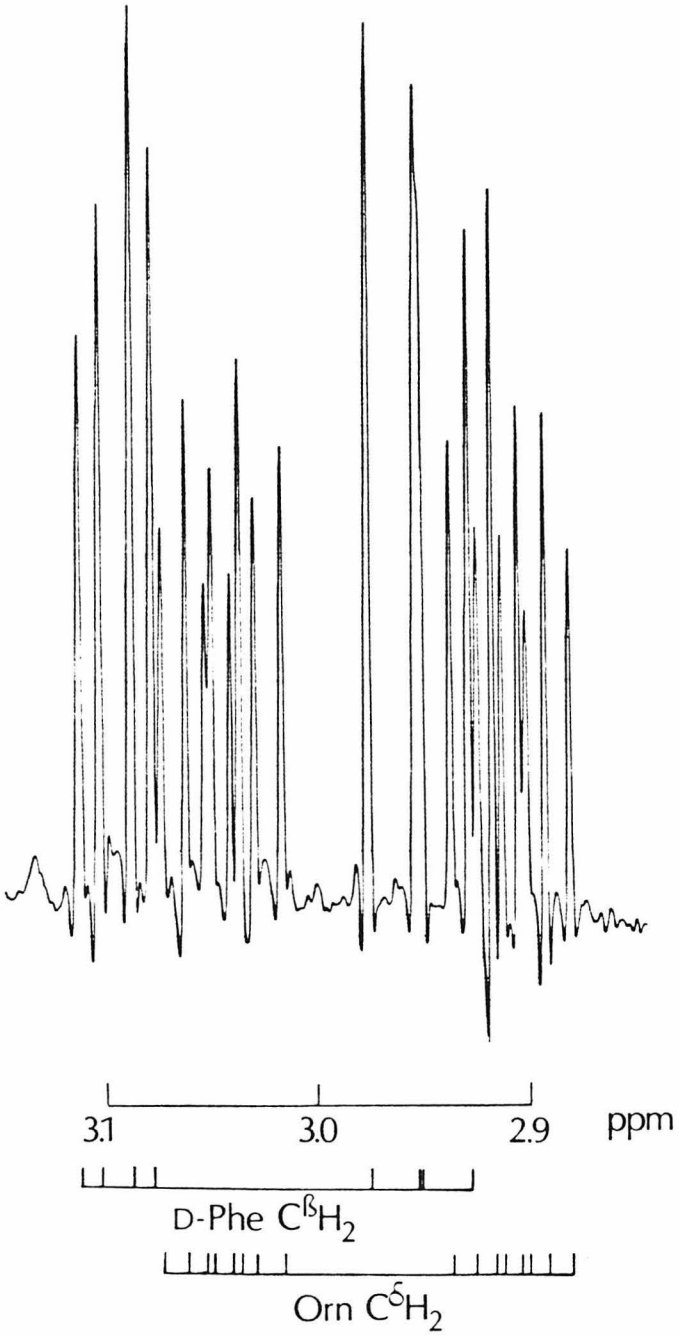

Figure 6. 500.13 MHz ^1H NMR spectrum of the D-Phe $C^{\beta}H_2$ and Orn $C^{\delta}H_2$ resonances in GrS in MeOH-d_4 at 295 K, with resolution enhancement.

chain of Orn, respectively. We take $\Delta O^{\delta} = 0$ in the fully solvated state (occupancy = $1 - \sum_{\underline{i}} \underline{f}_b(\underline{i})$). ΔO^{δ}_{obsd} is affected by solvent both through changes in the formation constants of the H-bonded conformers and by conformational and solvent influences on the absolute shifts. For the purposes of comparison between solvents, and to allow computation of thermodynamic quantities (v. i.), two simplifications are made: first, the intramolecularly H-bonded states are described by their ensemble average, e.g., $\overline{\Delta O}^{\delta}_b \equiv \sum_{\underline{i}} \underline{f}_b(\underline{i})\,\Delta O^{\delta}_b(\underline{i}) / \sum_{\underline{i}} \underline{f}_b(\underline{i}) = \sum_{\underline{i}} \underline{f}_b(\underline{i})\,\Delta O^{\delta}_b(\underline{i})/\underline{F}_b$, and thus $\Delta O^{\delta}_{obsd} = \underline{F}_b \overline{\Delta O}^{\delta}_b$; and second, $\overline{\Delta O}^{\delta}_b$ is taken (to first order only) to be independent of solvent, so that ΔO^{δ}_{obsd} is influenced chiefly by variation in $\underline{F}_b$. The apparent free energy change per H bond for the transition from the solvated to the intramolecularly H-bonded state (Eq. 1), as determined by the

$$RNH_2^+\text{-}H\text{--}SH + SH\text{--}O{=}CHNR'R'' \rightarrow RNH_2^+\text{-}H\text{--}O{=}CNHR'R'' + SH\text{--}SH \qquad (1)$$

partially averaged chemical shift difference, is then
$\Delta \underline{G}^0_b = RT \ln(\overline{\Delta O}^{\delta}_b / \Delta O^{\delta}_{obsd} - 1) \equiv RT\ \underline{g}(\Delta O^{\delta})$.

The more acidic (than RNH_3^+) or the more basic (than O=CNHR'R") the solvent, the more effectively it will compete for the acceptor or donor moieties in the peptide. In the case of intramolecular H bonding, a direct relationship should then exist between the apparent free energy change for Eq. 1 and solvent-peptide p$\underline{K}$ differences, and it should be possible to establish a correlation between $\underline{g}(\Delta O^{\delta})$ and some function $\underline{h}(\underline{K})$ of the p$\underline{K}$'s. This must take into account both the donor and acceptor roles of the solvent ($p\underline{K}_{ap} - p\underline{K}_{as}$ and $p\underline{K}_{bp} - p\underline{K}_{bs}$, where p

denotes peptide, s solvent, and $p\underline{K}_{ap} = pK_a(RNH_3^+) \sim 10.2$, $p\underline{K}_{bp} = p\underline{K}_b$ (O=CNHR'R") $\sim$ -2.1 (33, 34)) and should not be dominated by contributions from conjugate species (such as $MeC(OH)_2^+$ in AcOH) which are in effect invisible in the H-bonding transition. A simple function which meets these requirements is $\underline{h}(\underline{K}) = \log(\underline{K}_{as}/\underline{K}_{ap} + \underline{K}_{bp}/\underline{K}_{bs})$, which scales as the free energies of deprotonation and is linear in the free energies for the set of monofunctional solvents used. (In the case of solvent-labile amide-amide H bonds, solvents such as water and MeOH might behave in a bifunctional manner and the dependence on $\underline{h}(\underline{K})$ would necessarily be more complex.)

Measurements of ΔO^{δ}_{obsd}, with the corresponding solvent $p\underline{K}$'s, are listed in Table VI. For GrS, ΔO^{δ}_{obsd} is largest in F_3EtOH, which is substantially weaker as an acid than Orn $N^{\delta}H_3^+$ and as a base than O=CNHR'R", while no chemical shift difference could be resolved in AcOH (pK_{as} = 4.75) or pyridine (pK_{bs} = 5.2). Intermediate values of ΔO^{δ}_{obsd} are measured in the remaining solvents. A nonvanishing ΔO^{δ}_{obsd} is detected for Me_6GrS in most cases. Here, ΔO^{δ}_{obsd} increases with solvent in the order $F_3EtOH < MeOH < Me_2SO$, which is the reverse of the trend observed for GrS, and a 63 Hz difference is detected in AcOH.

In order to determine whether ΔO^{δ}_{obsd} exhibits the predicted variation with solvent acid/base properties, a correlation coefficient ρ was calculated by linear regression of $\underline{g}(\overline{\Delta O}^{\delta})$ against $\underline{h}(K)$. In the case of GrS, ρ = 0.908 for $\overline{\Delta O}^{\delta}_b$ = 120 Hz (estimated in MeOH, below).

Table VI. Solvent Dependence of ΔO^{δ}_{obsd}

Solvent[c]	$p\underline{K}_a$	$p\underline{K}_b$	$\underline{h}(\underline{K})$[b]	$\Delta O^{\delta}_{obsd}(GrS)$[a]	$\Delta O^{\delta}_{obsd}(Me_6GrS)$[a]
Pyridine		5.2	7.3	1[d]	
AcOH	4.75	-6.1	5.4	1[d]	63
Me_2SO	31	0	2.1	48	183
H_2O	15.7	-1.7	0.4	10	1[d]
MeOH	16	-2.2	-0.1	68	109
F_3EtOH	12.4	-8.2	-2.2	107	65

[a] In Hz at 295 K.

[b] See text for definition.

[c] Dissociation constants are representative values from Ref. 18 and refs. therein; Noller, C. R. "Chemistry of Organic Compounds"; W. B. Saunders: Philadelphia, 1965; Gordon, A. J.; and Ford, R. A. "The Chemists' Companion"; Wiley-Interscience: New York, 1972, Chapter 1, and refs. therein.

[d] No $C^{\delta}H_2$ chemical shift inequivalence was detected, and a value of 1 Hz assigned for computational purposes.

The logarithmic dependence of $\underline{g}$ on $\overline{\Delta O}_b^{\delta}$ ensures that the precise magnitude of the limiting shift inequivalence is not critical; thus, if $\overline{\Delta O}_b^{\delta}$ = 250 Hz is assumed, ρ = 0.906. It is concluded that variation in ΔO_{obsd}^{δ} is for GrS correlated with this elementary measure of the capacity of solvents to disrupt solute-solute H bonds (significance level $P < 0.01$ for the two-tailed $\underline{t}$ test). In contrast, for Me_6GrS, in which the putative H bond donor site is blocked, no correlation exists: ρ = -0.181 ($\overline{\Delta O}_b^{\delta}$ = 184 Hz, the maximum ΔO_{obsd}^{δ} plus 1 Hz; if $\overline{\Delta O}_b^{\delta}$ = 250 Hz is assumed here, ρ = -0.146). The nonzero Orn $C^{\delta}H_2$ chemical shift inequivalences in the quaternary derivative most likely derive from the bulkiness of the $RNMe_3^+$ groups and solvent mediated dipolar interactions.

The ^{1}H NMR data are thus shown to be consistent with solvent-labile Orn NH_3^+ to backbone H bonds as the principal source of motional limitation in the Orn side chain in GrS. The displacement of the Pro ^{15}N resonance in Me_6GrS and the ^{1}H NMR chemical shift inequivalence of the Orn $C^{\delta}H_2$ protons emerge as complementary manifestations of the same intramolecular interaction. Taken in concert, the ^{15}N and ^{1}H NMR measurements provide compelling evidence for the existence of Orn $N^{\delta}H_3^+$--O=C $\underline{\underline{D}}$-Phe H bonds in the native peptide.

Thermodynamics and Limiting Shifts. To investigate the thermodynamics of the transition given in Eq. 1 subject to the assumptions noted above, the temperature dependence of ΔO_{obsd}^{δ} was measured for GrS between -91 and 30°C in MeOH (Fig. 7a, b). The limiting chemical shift inequivalence $\overline{\Delta O}_b^{\delta}$ and the standard enthalpy and entropy change on intramolecular H bond formation were fitted according to the

Figure 7a. Temperature variation of the Orn $C^{\delta}H_2$ and $\underline{D}$-Phe $C^{\beta}H_2$ proton resonance in GrS in MeOH-d_4.

Figure 7b. Measured values (circles) of ΔO^{δ}_{obsd} in GrS in MeOH-d_4. The dashed line is a plot of $\Delta O^{\delta}_{obsd} = \overline{\Delta O}^{\delta}_{b}/(1 + \exp(\Delta \underline{H}^{0}/RT - \Delta \underline{S}^{0}/R))$ for $\overline{\Delta O}^{\delta}_{b}$ = 120 Hz, $\Delta \underline{H}^{0}$ = -2.3 kcal mol^{-1}, and $\Delta \underline{S}^{0}$ = -7.5 cal deg^{-1} mol^{-1}.

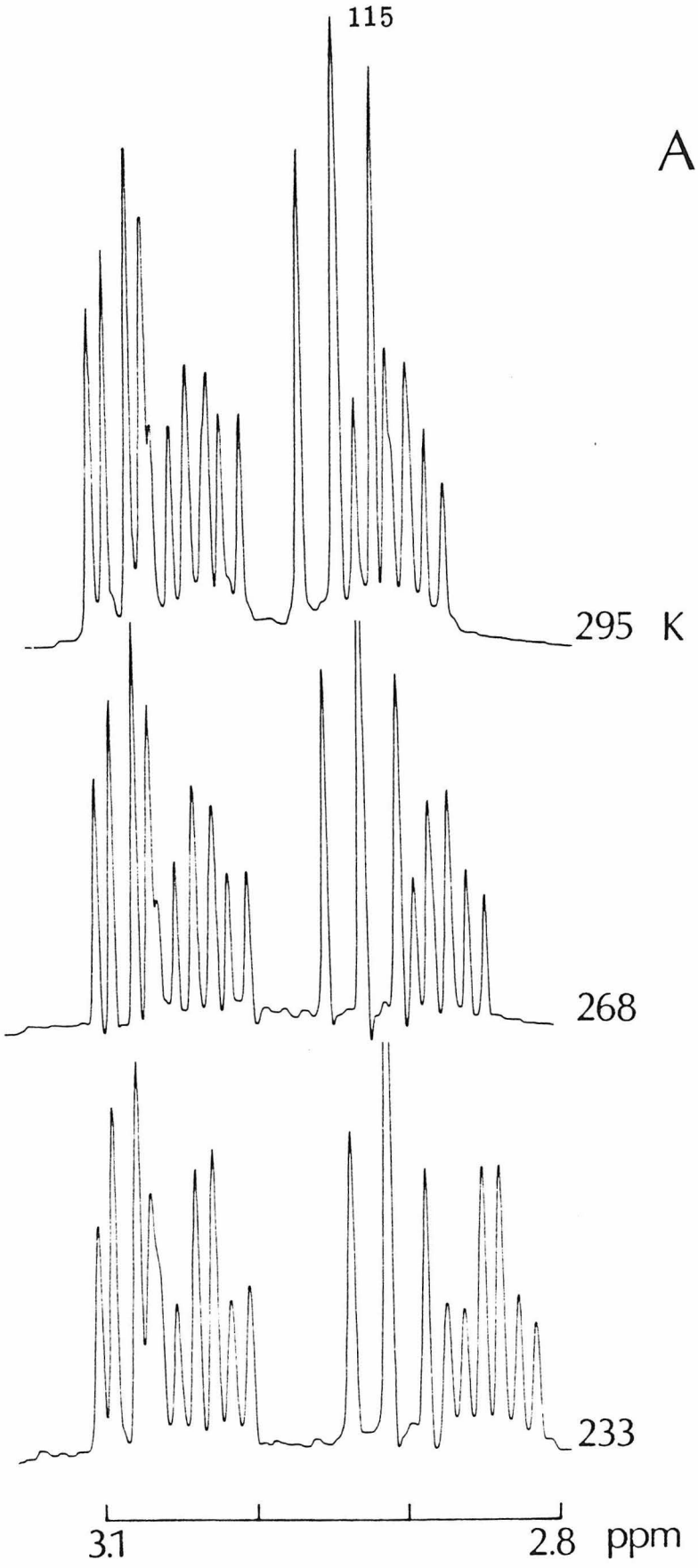
115
A
295 K
268
233
3.1
2.8 ppm

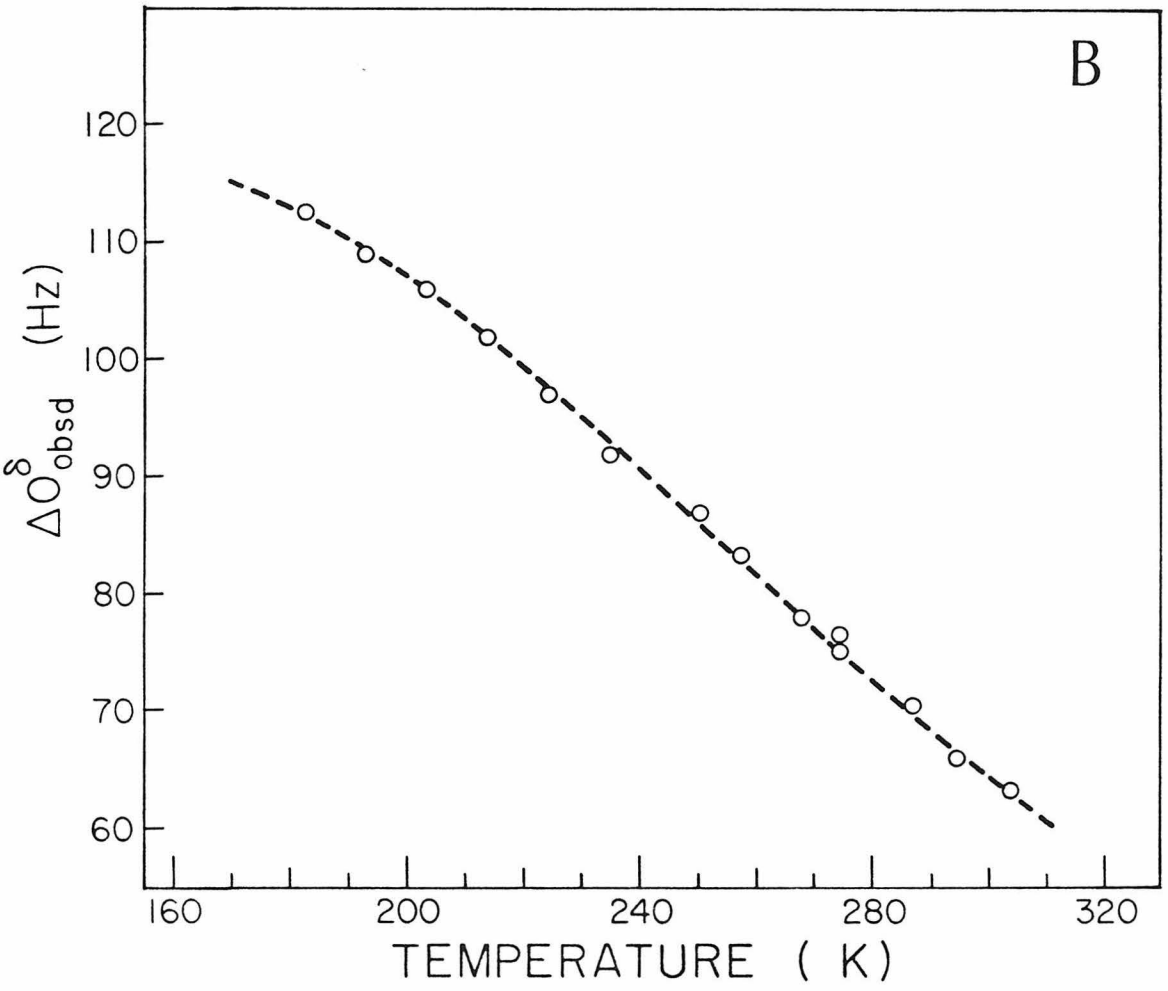
B
120
110
100
90
80
70
60
ΔO^{δ}_{obsd} (Hz)
160
200
240
280
320
TEMPERATURE (K)

relation $\Delta O^{\delta}_{obsd} = \overline{\Delta O}^{\delta}_{b}/(1 + \exp(\Delta \underline{H}^{0}/RT - \Delta \underline{S}^{0}/R))$, yielding values of $-\Delta \underline{H}^{0} = 2.3 \pm 0.4$ kcal mol^{-1}, $-\Delta \underline{S}^{0} = 7.5 \pm 1.0$ cal deg^{-1} mol^{-1}, and $\overline{\Delta O}^{\delta}_{b} = 120$ Hz. From these, a standard free energy change of -0.08 kcal mol^{-1} at 25°C is calculated, corresponding to a simple formation constant $\underline{K}_b = \underline{F}_b/(1 - \underline{F}_b)$ of 1.1. The thermodynamic quantities contain contributions both from the donor/acceptor couples (Eq. 1) and from changes in the rotamer populations about single bonds in the Orn side chain.

From the calculated thermodynamic parameters, the averaged Pro ^{15}N shift in the Orn $N^{\delta}H_3^+$--O=C $\underline{\underline{D}}$-Phe complex can be estimated. The observed shift $\delta_{obsd} = \underline{F}'_b \bar{\delta}_{intra} + (1 - \underline{F}'_b)\delta_{solv}$, where the primes indicate that the ensemble average is taken with respect to the ^{15}N shift. Making the approximation $\underline{F}'_b = \underline{F}_b = \underline{K}_b/(1 + \underline{K}_b)$, and using $\delta_{solv} = 112.0$ ppm (as indicated by the spectrum of Me_6GrS and supported by model compound studies (24)) and $\delta_{obsd} = 115.5$ ppm in MeOH, we calculate $\bar{\delta}_{intra} = 118.6$ ppm. Observed and calculated Pro ^{15}N shifts for a variety of possible donors to $\underline{\underline{D}}$-Phe C=O are diagrammed in Fig. 8. In the absence of any H bonding to $\underline{\underline{D}}$-Phe C=O, a shift of 108.5 ppm was predicted, and a shift of 112.7 ppm observed in Me_2SO (24). If the Orn $N^{\delta}H_3^+$ interaction accounts entirely for the downfield shift and $\bar{\delta}_{intra}(Me_2SO) = \bar{\delta}_{intra}(MeOH)$, a limiting $\overline{\Delta O}^{\delta}_{b}$ of 115 Hz is projected for GrS in Me_2SO from $\Delta O^{\delta}_{obsd} = 48$ Hz (Table VI), in reasonable agreement with the estimate of ΔO^{δ}_{b} for MeOH. The calculated magnitude of the Pro ^{15}N shift change from the non-H-bonded to the fully intramolecularly H-bonded state, 10.1 ppm, is comparable to the largest solvent-induced amide ^{15}N shifts recorded (30).

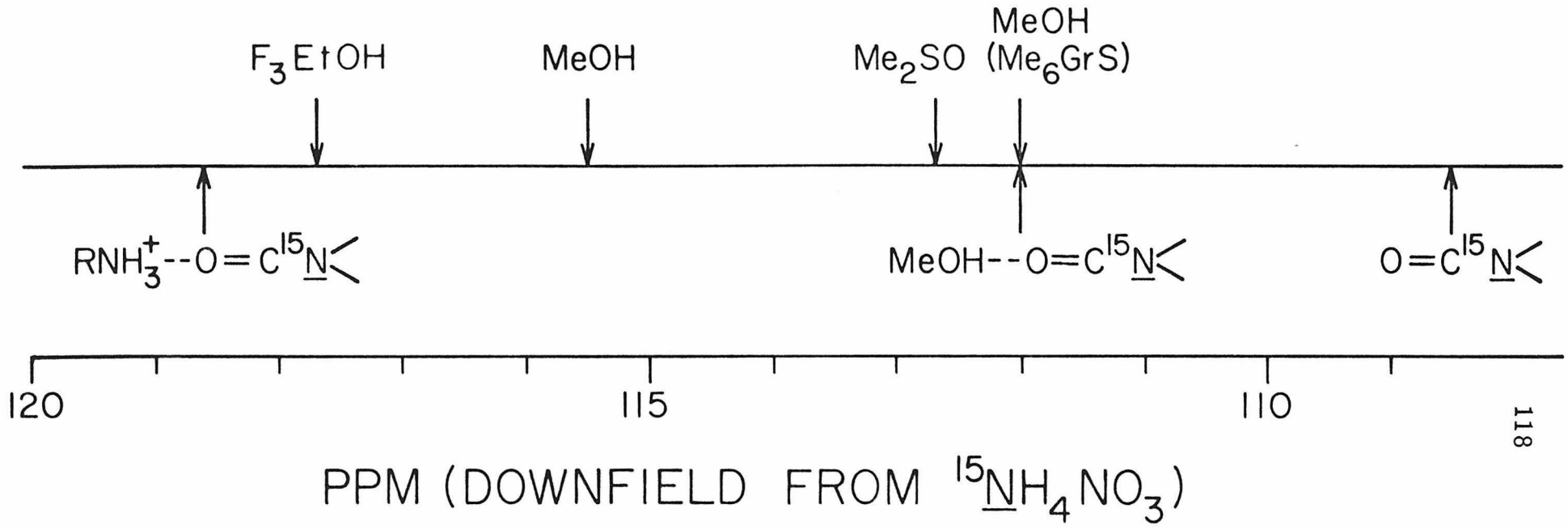

Figure 8. Pro ^{15}N shifts for several associational states of D-Phe C=O. Markers above and below the line indicate observed and computed shifts, respectively. The observed shifts in F_3EtOH and Me_2SO and the computed shifts of the MeOH and non-H-bonded complexes are from Ref. 24.

Spatial Orientation of the Orn Side Chains. It is possible to orient the Orn NH_3^+--O=C D-Phe H bonds in either the $\underline{i} \rightarrow \underline{i} + 2$ or the $\underline{i} \rightarrow \underline{i} - \underline{3}$ sense. Since the preceding work could not differentiate between the two alternatives, additional experiments were performed in which it was possible to identify specific regions of the peptide backbone in close proximity to the Orn side chain. The evidence obtained supports the $\underline{i} \rightarrow \underline{i} + \underline{2}$ orientation observed for the single H-bonded Orn in the crystalline urea complex (9) rather than the $\underline{i} \rightarrow \underline{i} - \underline{3}$ orientation proposed earlier (8).

As described above, study of the HX kinetics in D_2O revealed a single anomaly, the twofold slowing of exchange in Me_6GrS (Table IV; Fig. 3). D-Phe NH is too far from the site of modification to manifest an altered primary structure effect on HX (21). The existence of a preferred conformation in which the quaternary ammonium group shields D-Phe NH from the solvent could conceivably retard HX, but there is no evidence to support such an interaction, and the high degree of mobility of the Orn side chains of Me_6GrS in D_2O indicated by $\Delta O^{\gamma}_{obsd} = \Delta O^{\delta}_{obsd} = 0$ argues against it. The most plausible explanation is that in the unmodified peptide the terminus of the Orn side chain is, on average, sufficiently close to D-Phe NH that a general catalytic effect is exerted on HX which accelerates it twofold. Some evidence exists for such effects exerted by nitrogenous bases on amide HX kinetics, but it is generally difficult to achieve sufficiently high activities of potentially catalytic agents in pure water. NH_2OH has nonetheless been shown to accelerate both acid- and base-catalyzed HX in AcNHMe in D_2O (35). In the intramolecularly H-bonded

configuration Orn $N^{\delta}H_3^+$ achieves sufficient proximity to D-Phe NH to influence its HX kinetics (3-4 Å) only when the bonds form in the $\underline{i} \rightarrow \underline{i} + 2$ sense, as shown in Fig. 9.

Additional support for the $\underline{i} \rightarrow \underline{i} + \underline{2}$ orientation derives from the observation of a specific nuclear Overhauser enhancement (NOE) at Leu H^{α} when the Orn H^{γ} resonance is irradiated in MeOH below -25°C (Fig. 10). Working at low temperatures facilitates detection of the NOE by increasing its maximum magnitude, controlled by the solvent viscosity (36), and by increasing the population of the intramolecularly H-bonded conformers. Cross-relaxation effects become especially significant outside the extreme narrowing limit, however (36), and no calculation of internuclear distances from NOE data is attempted. Rather, it is the qualitative pattern of NOE's observed upon Orn side chain irradiation which is considered here; only in the $\underline{i} \rightarrow \underline{i} + \underline{2}$ case is the Orn H^{γ} - Leu^{α} enhancement expected ($r_{HH} < 4$ Å; Fig. 9), while in the $\underline{i} \rightarrow \underline{i} - \underline{3}$ case, either no NOE or an Orn-Val H^{α} NOE would be observed.

Solution Conformation of the Orn Side Chain. Once the H bonds involving Orn NH_3^+ are demonstrated and their orientation known, it is possible to estimate the side chain torsional angles in the H-bonded configuration by application of the Bystrov-Karplus equation to the measured vicinal coupling constants. It should be noted, however, that even in the H-bonded state there is residual motional freedom, particularly about χ^2.

Determinations of vicinal ^3J's and geminal ^2J's were made in F_3EtOH, MeOH, and Me_2SO by analysis of the H^{α}, $H^{\beta d}$, and H^{δ}

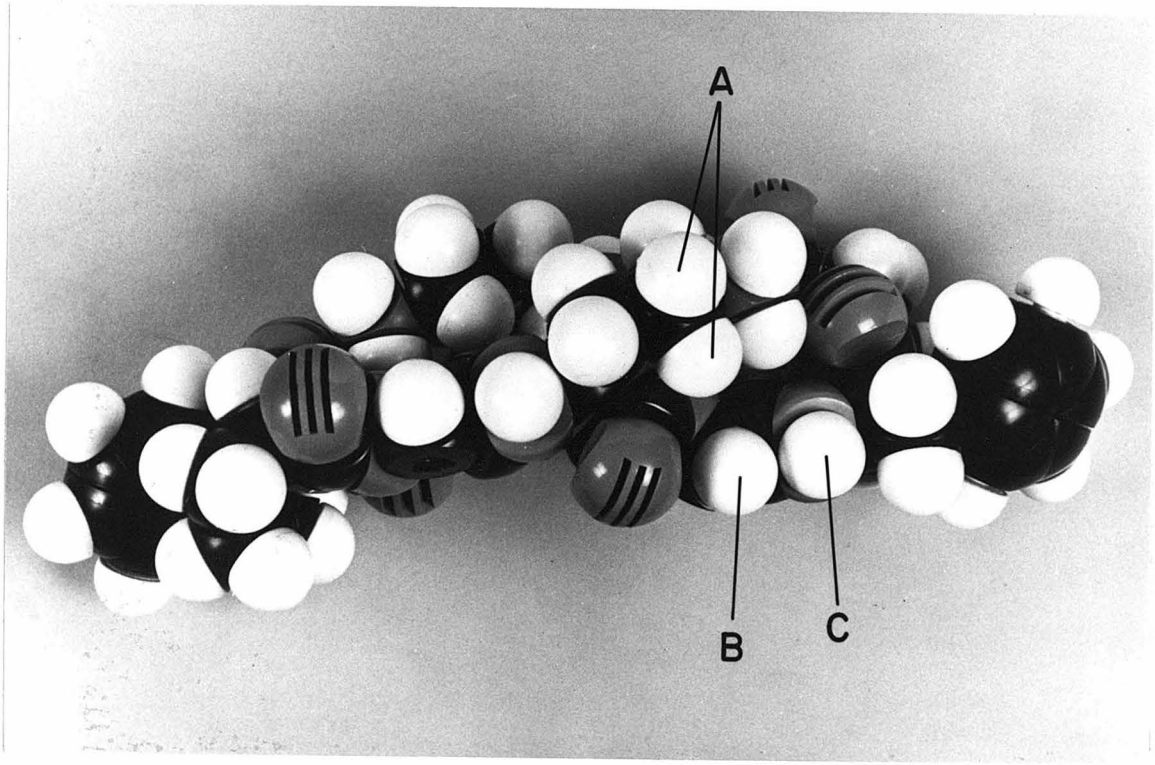

Figure 9. CPK model of GrS, viewed perpendicularly to the C_2 axis, with the Orn $N^{\delta}H_3^+$..O=C D-Phe H bonds oriented in the $\underline{i} \rightarrow \underline{i}+\underline{2}$ sense. The side chains of valine and leucine are omitted. The torsional angles estimated below are assumed for ornithine residues and the backbone contains the twist observed in the crystal (Ref. 9). The proximity of Orn $C^{\gamma}H_2$(A), Leu $C^{\alpha}H$(B), D-Phe NH(C), and the terminal amino group of ornithine is evident.

Figure 10. (Upper trace) NOE difference spectrum of GrS (per-N-deuterated) in MeOH at 226.5 K: irradiation of Orn $C^{\gamma}H_2$ at sub-saturating levels for 1 sec. Acquisition time = 1.64 sec. Intraornithyl enhancements are indicated by circles and the Orn $C^{\gamma}H_2$-Leu $C^{\alpha}H$ NOE is identified by an arrow. A small NOE at Pro $C^{\alpha}H$ (asterisk) is the result of decoupler spillover into the nearby Pro $C^{\beta}H_2$ resonance. (Lower trace) Spectrum of GrS for comparison of chemical shifts; vertical scale much reduced.

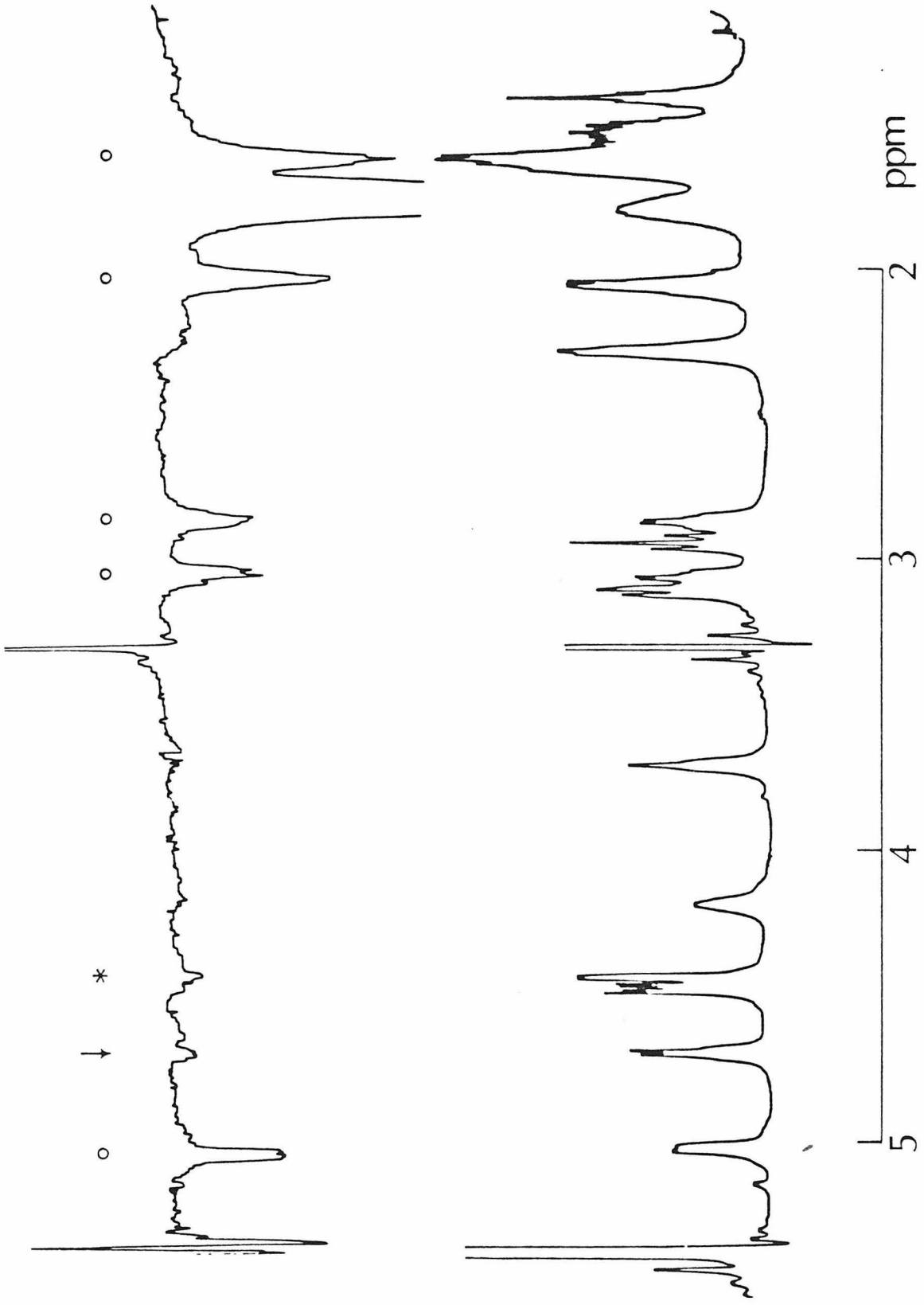
ppm
5
4
3
2

multiplets. The $H^{\beta\underline{u}}$ and H^{γ} resonances were generally too poorly isolated to permit thorough study (as was true of $H^{\beta\underline{d}}$ in Me_2SO). In all instances, ΔO^{β} was sufficiently large at 500.13 MHz that the splitting of the H^{α} multiplet was first order, allowing direct measurement of $^3J_{\alpha\beta_{\underline{d}}}$ and $^3J_{\alpha\beta_{\underline{u}}}$ from the spectra in conjunction with selective homonuclear decoupling of the separate H^{β} resonances.

The procedure used for F_3EtOH, in which all multiplets are weakly coupled, will be outlined in detail. The coupling constants $^3J_{\alpha\beta_{\underline{u}}}$, $^3J_{\alpha\beta_{\underline{d}}}$, $^2J_{\beta_{\underline{d}}\beta_{\underline{u}}}$, $^3J_{\beta_{\underline{d}}\gamma_{\underline{d}}}$, and $^3J_{\beta_{\underline{d}}\gamma_{\underline{u}}}$ were obtained by first-order analysis of the H^{α} and $H^{\beta\underline{d}}$ multiplets (Fig. 11). The two $\beta_{\underline{d}}\gamma$ coupling constants are identical to within experimental error. The $\gamma\delta$ and $\delta\delta$ coupling constants were likewise estimated by analysis of the H^{δ} multiplets (Fig. 12) with decoupling of $H^{\delta\underline{d}}$, $H^{\delta\underline{u}}$, and H^{γ}. Specific assignment of the $^3J_{\gamma\delta}$'s by selective decoupling of $H^{\gamma\underline{d}}$ and $H^{\gamma\underline{u}}$ is diagrammed in Fig. 13, from which it is clear that $^3J_{\gamma_{\underline{u}}\delta_{\underline{u}}} = {}^3J_{\gamma_{\underline{d}}\delta_{\underline{d}}} > {}^3J_{\gamma_{\underline{u}}\delta_{\underline{d}}} = {}^3J_{\gamma_{\underline{d}}\delta_{\underline{u}}}$. The measured coupling constants are compiled in Table VII.

Coupling constants were obtained in similar fashion for MeOH at ambient temperature (Figs. 14 and 15) and 233 K (H^{δ} multiplets only; Fig. 16) and for Me_2SO (H^{α} and $H^{\delta\underline{u}}$ multiplets only; Fig. 17). In these solvents the $C^{\gamma}H_2$ protons are strongly coupled, which requires small corrections to the $\gamma\delta$ coupling constants estimated by first order analysis. Correction of the $^3J_{\beta_{\underline{d}}\gamma}$'s in MeOH is unnecessary since these coupling constants are identical (37). It is possible to estimate the chemical shift difference ΔO^{γ} by

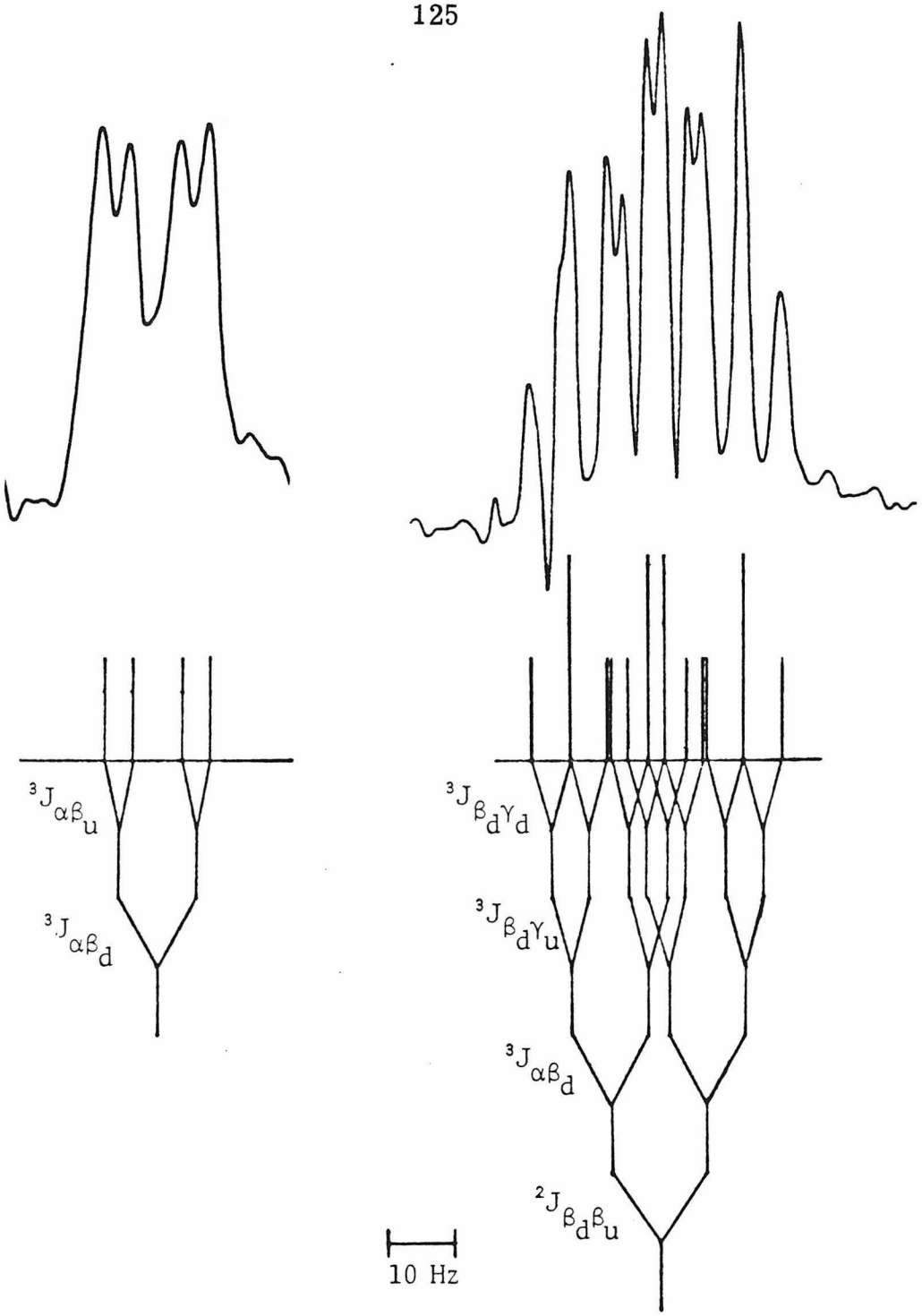

Figure 11. The O^{α} (left) and $O^{\beta d}_{-}$ (right) multiplets in GrS in F_3EtOH, with resolution enhancement. The dendrite diagram illustrates the approximate splittings, which were assigned to specific resonances by selective homonuclear decoupling. The spectra were obtained at ambient temperature.

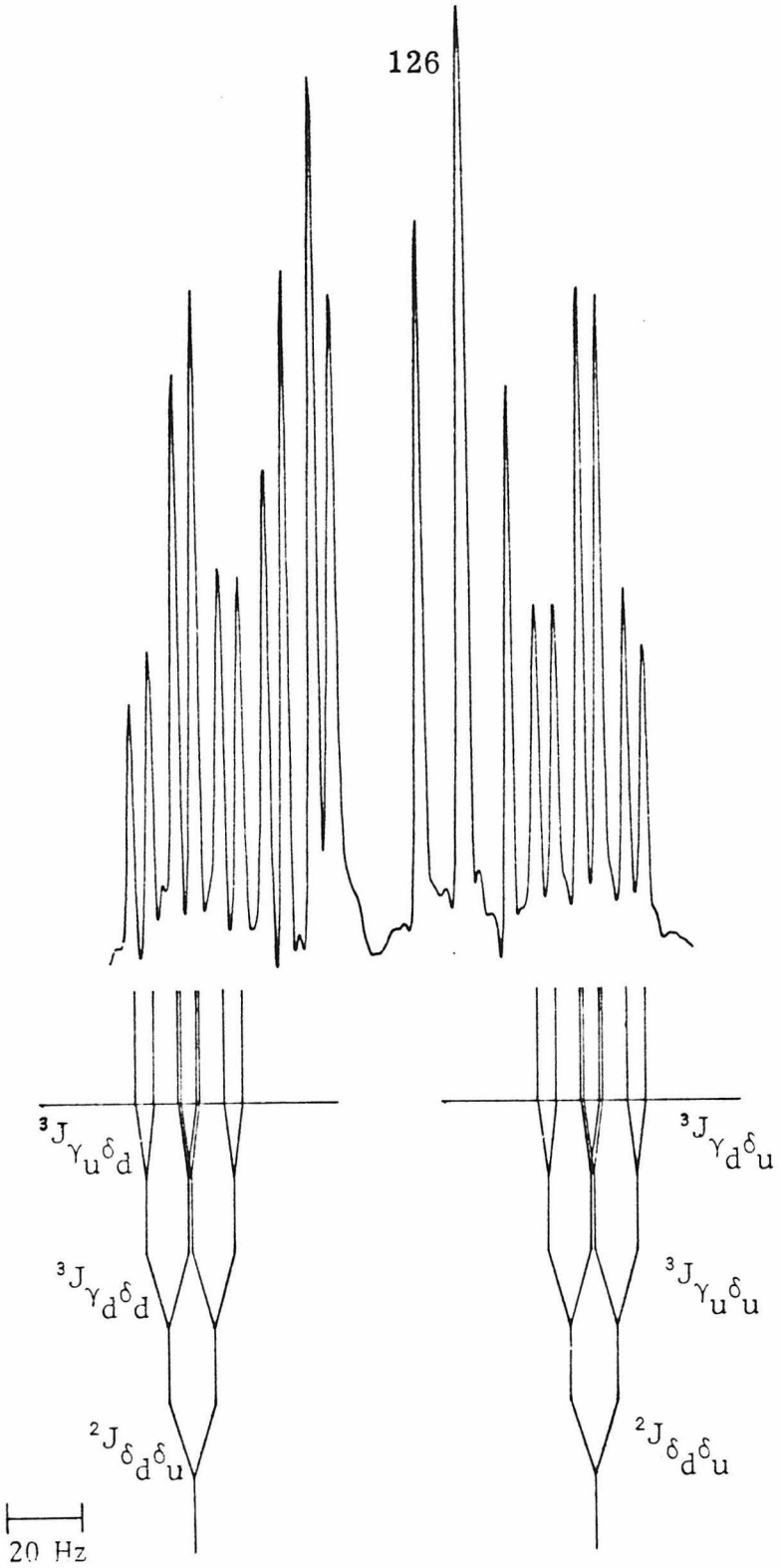

Figure 12. As in Fig. 11, for the $O^{\delta\underline{d}}$ and $O^{\delta\underline{u}}$ multiplets in F_3EtOH. The $\hat{F}^{\beta\underline{d}}$ and $\hat{F}^{\beta\underline{u}}$ resonances lie between the O^{δ} signals.

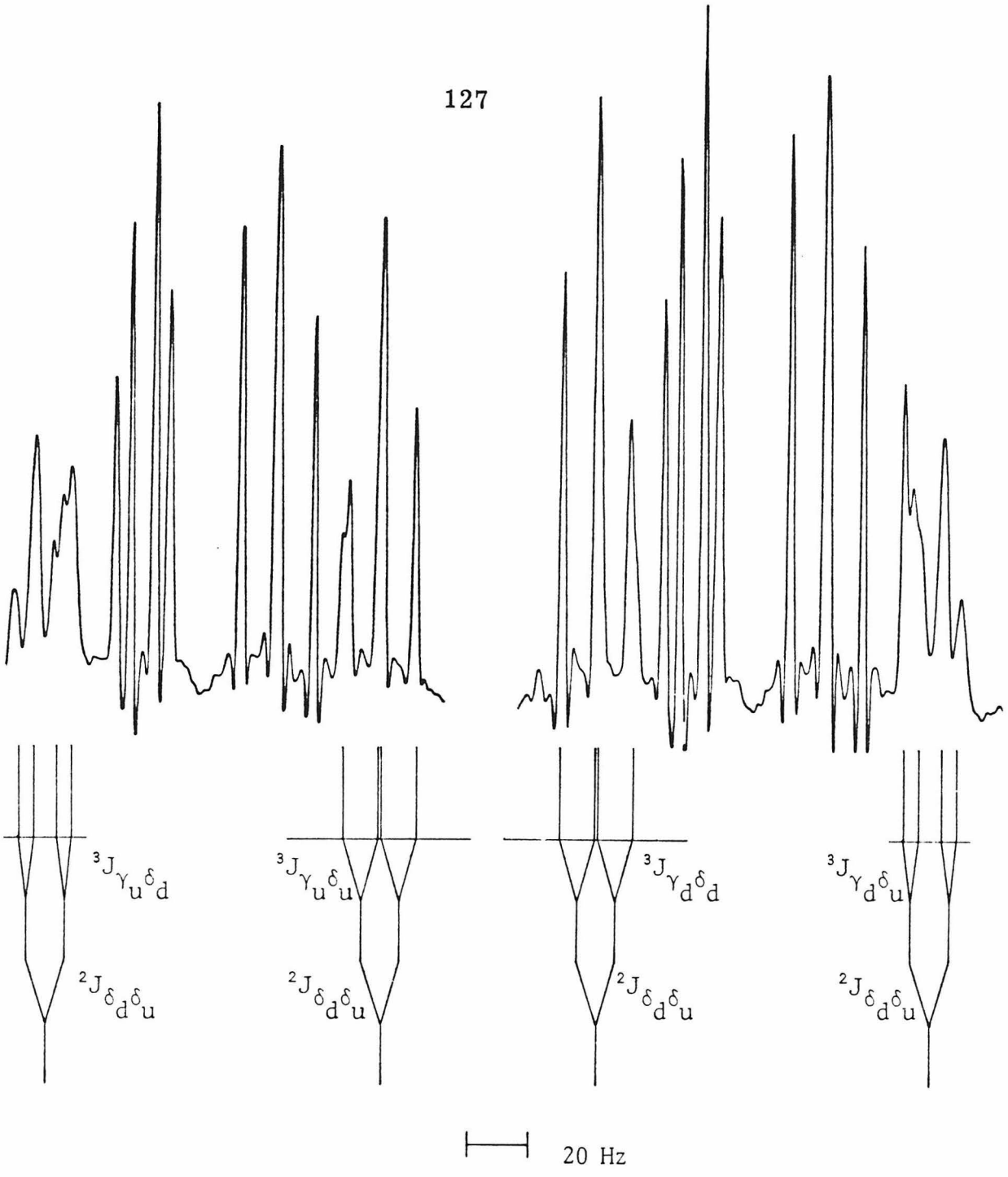

Figure 13. Assignment of the $\gamma\delta$ splittings in F_3EtOH. (Left), decoupling $O^{\gamma\underline{d}}$; (right), decoupling $O^{\gamma\underline{u}}$.

Table VII. Ornithine ^1H-^1H NMR Coupling Constants in GrS[a]

Solvent	Temperature (K)	ΔO^{δ}_{obsd}	$^3J_{\alpha\beta_d}$	$^3J_{\alpha\beta_u}$	$^2J_{\beta_d\beta_u}$	$^3J_{\beta_d\gamma}$	$^3J_{\gamma_d\delta_d}$ ($=^3J_{\gamma_u\delta_u}$)	$^3J_{\gamma_d\delta_u}$ ($=^3J_{\gamma_u\delta_d}$)	$^2J_{\delta_d\delta_u}$
Me_2SO	296	48	8.5	6.0			9.0	6.8	-12.3
MeOH	295	68	10.3	5.2	-12.5	6.5	9.8	5.8	-12.5
MeOH	233	94	11.0[b]	4.2[b]			10.9	5.3	
F_3EtOH	295	109	11.5	4.2	-14.0	5.5	11.5	4.9	-12.5

[a]All splittings in Hz at 500.13 MHz. The sign of the geminal coupling constants is assumed. The chemical shift difference between the $C^{\gamma}H$ protons was unmeasurably small in Me_2SO and MeOH and in these solvents the labeling of these protons is arbitrary.

[b]Ref. 3, at 229 K.

$(\Delta O^{\gamma})^2 \approx (W_{app} - J_{\gamma\gamma} - \frac{1}{2}\sum_{i,j=1}^{2}(J_{\gamma_i\beta_j} + J_{\gamma_i\delta_j}))^2 - J_{\gamma\gamma}^2$ (where W_{app} is the apparent width of the O^{γ} resonance), which is obtained from the formula for the total spectral width of an AB multiplet. In MeOH, $W_{app} \approx 70$ Hz, and the actual difference $^3J_{\gamma_{\underline{u}}\delta_{\underline{u}}} - {}^3J_{\gamma_{\underline{u}}\delta_{\underline{d}}}$ ($= {}^3J_{\gamma_{\underline{d}}\delta_{\underline{d}}} - {}^3J_{\gamma_{\underline{d}}\delta_{\underline{u}}}$) is computed to be ~0.6 Hz larger than the apparent (first order) difference (using the ABX formalism(37), $\delta_{\underline{d}}\delta_{\underline{u}}$ splitting removed; the sums of the $^3J_{\gamma\delta}$'s are unaffected). In Me_2SO the H^{γ} and $H^{\beta\underline{u}}$ protons are strongly coupled (Table I) and ΔO^{γ} is more difficult to gauge. Homodecoupling experiments suggest an effective width of ~50 Hz for O^{γ}, corresponding to a likely ΔO^{γ} of 5-15 Hz. If 10 Hz is assumed here, 0.3 Hz corrections are again estimated to each of the $\gamma\delta$ coupling constants. Overlap of Orn $H^{\delta\underline{d}}$ with $\underline{\underline{D}}$-Phe $H^{\beta\underline{u}}$ precluded measurement of $^3J_{\gamma\delta_{\underline{d}}}$'s in Me_2SO; it is assumed that they are numerically equal to the $^3J_{\gamma\delta_{\underline{u}}}$'s, as observed in MeOH and F_3EtOH.

Examination of the ^1H-^1H coupling constants reveals that as the fractional population of the H-bonded conformers decreases, as indicated by ΔO^{δ}_{obsd}, the ^3J's approach the fully averaged value of 6-7 Hz (38). The ^3J's in F_3EtOH, in which Orn $N^{\delta}H_3^+$--O=C $\underline{\underline{D}}$-Phe H bonding is maximally favored, are presumed close to the values corresponding to the fully H-bonded state. In the following, these are used to obtain estimates of torsional angles in the intramolecular H-bonded conformation in general.

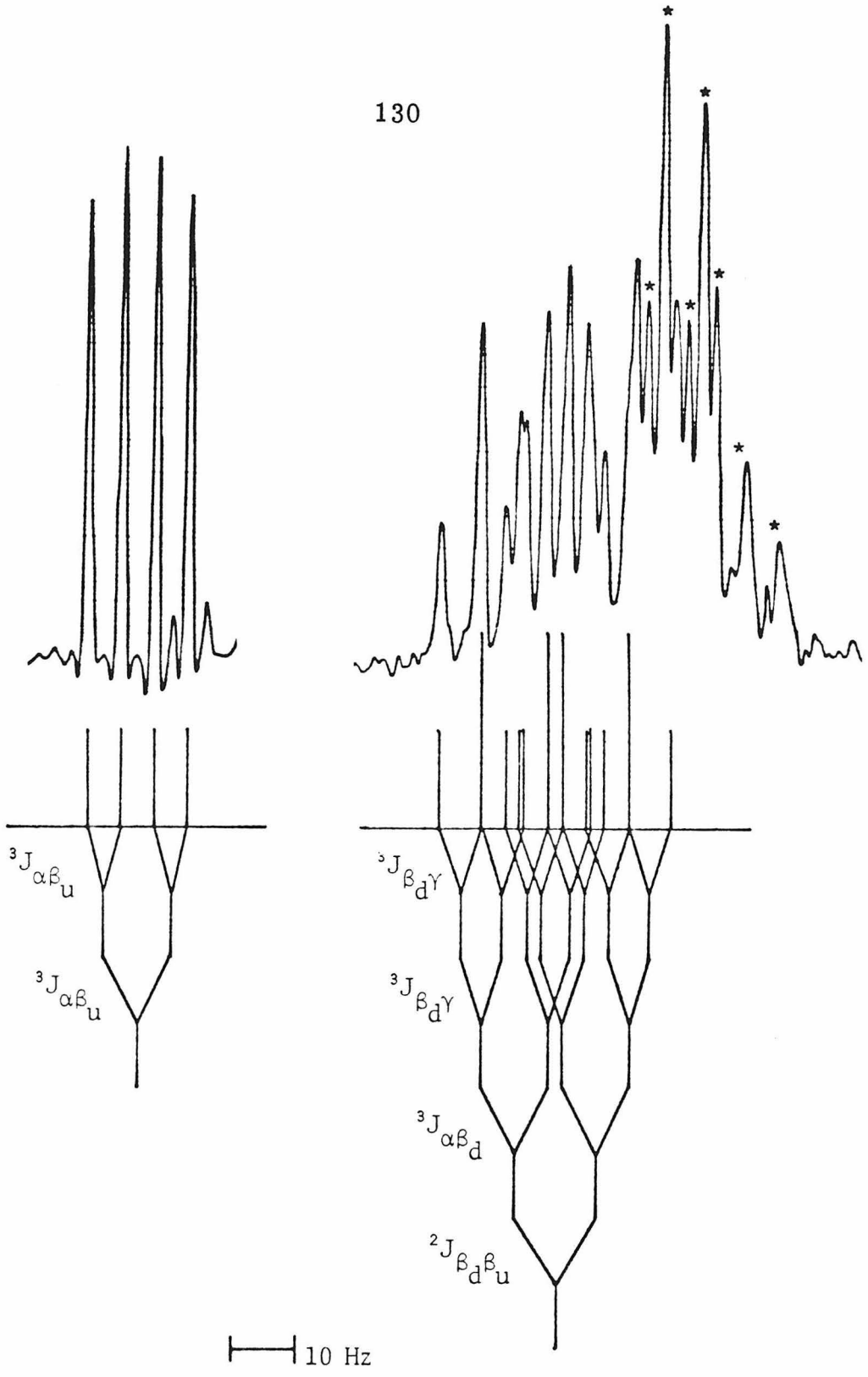

Figure 14. As in Fig. 11, for the O^{α} and $O^{\beta d}_{-}$ multiplets in MeOH. $P^{\beta d}_{-}$ transitions are identified by asterisks.

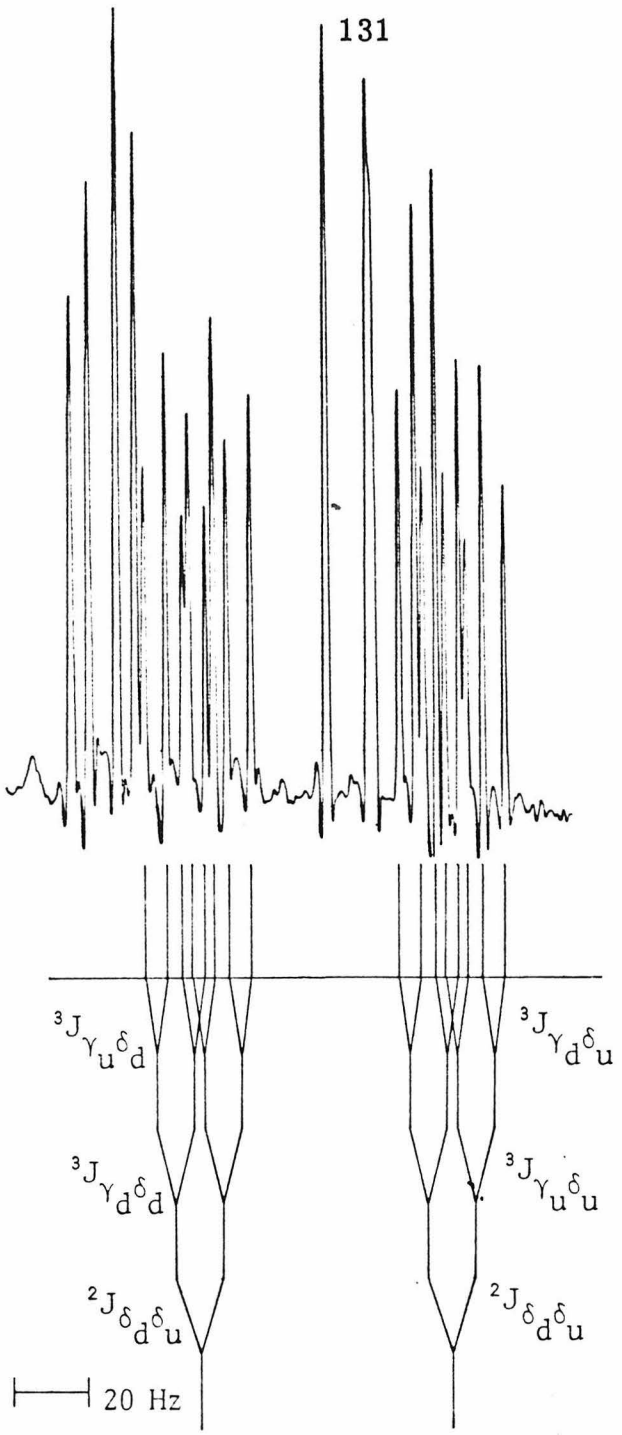

Figure 15. As in Fig. 11, for the $O^{\delta\underline{d}}$ and $O^{\delta\underline{u}}$ multiplets in MeOH. The $\hat{F}^{\beta}$ resonances lie just downfield of the O^{δ} signals.

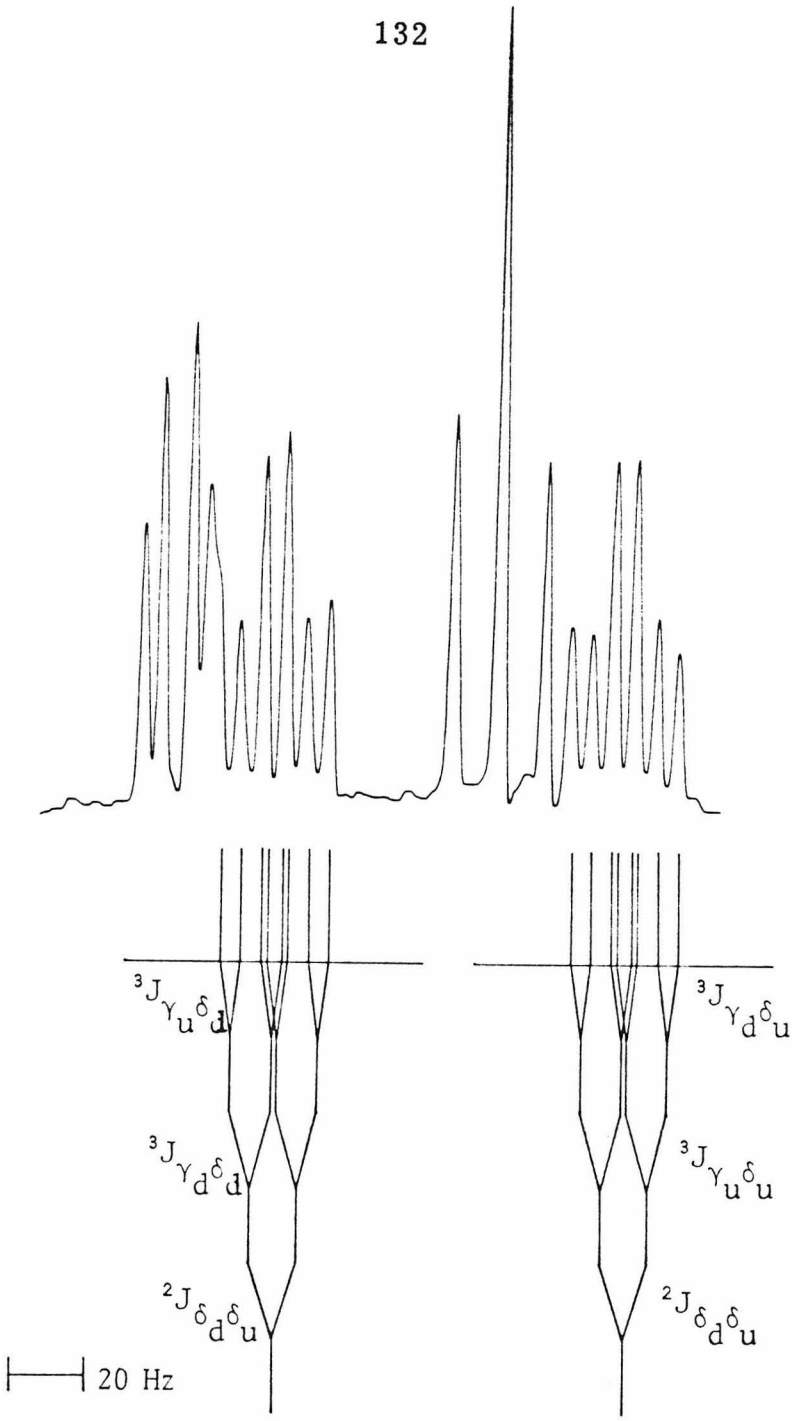

Figure 16. As in Fig. 15; 233 K.

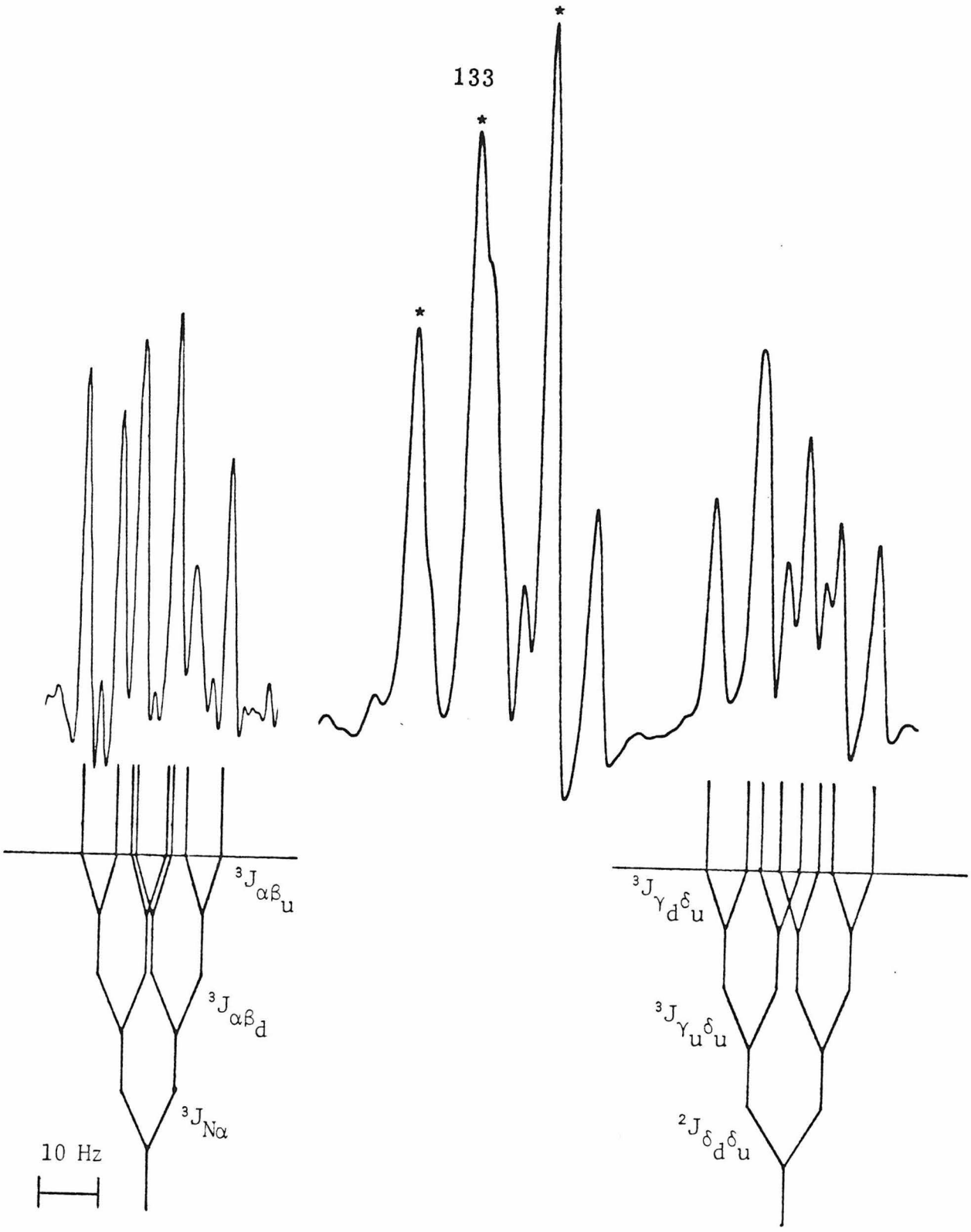

Figure 17. As in Fig. 11, for the O^{α} and $O^{\delta\underline{u}}$ multiplets in Me_2SO. The overlapping $\hat{F}^{\beta\underline{u}}$ signals are identified by asterisks.

The $H^{\alpha}H^{\beta}$ coupling constants have been subjected to Pachler analysis (3) and a statistical weight of 0.67 calculated for $\chi^1 = -60°$ or 180° in MeOH. Since the H bond forms in the $\underline{i} \rightarrow \underline{i}+\underline{2}$ sense, $\chi^1 = 180°$ is the proper choice (the form of averaging of ^3J cannot actually be specified by NMR) and the $H^{\beta\underline{d}}$ and $H^{\beta\underline{u}}$ resonances are assigned to $H^{\beta S}$ and $H^{\beta R}$, respectively (R and S denoted the stereochemical position in the geminal pair; see Fig. 1). In F_3EtOH, values of $^3J_{\alpha\beta_{\underline{d}}} = 4.2$ Hz and $^3J_{\alpha\beta_{\underline{u}}} = 11.5$ Hz indicate that $\chi^1 = 180°$ is more heavily weighted than in MeOH.

The large difference between the measured $H^{\gamma}H^{\delta}$ coupling constants for each H^{δ} resonance in F_3EtOH demonstrates, as does the large ΔO^{δ}_{obsd}, that there is considerable constraint on the motility of the terminal side chain segment. That $^3J_{\gamma_{\underline{d}}\delta_{\underline{d}}} = {}^3J_{\gamma_{\underline{u}}\delta_{\underline{u}}}$ and $^3J_{\gamma_{\underline{d}}\delta_{\underline{u}}} = {}^3J_{\gamma_{\underline{u}}\delta_{\underline{d}}}$ can only be explained by a major contribution from $\chi^3 = 180°$ in the H-bonded configuration, regardless of the precise magnitude of the coefficients used in the Karplus equation (38).

Extensive rotational averaging of the $H^{\beta}H^{\gamma}$ coupling constants is expected in light of the twofold increase in ^{13}C NT_1 on proceeding from C^{β} to C^{γ} (5, 6), and this is observed in MeOH. However, in F_3EtOH the relatively high stability of the Orn $N^{\delta}H_3^+$--O=C $\underline{\underline{D}}$-Phe H-bonds is associated with the existence of preferred conformers even about the $C^{\beta}C^{\gamma}$ bond, as indicated by the large chemical shift inequivalence of the Orn $C^{\gamma}H_2$ protons. The $^3J_{\beta_{\underline{d}}\gamma}$'s in F_3EtOH are both smaller than the fully averaged value. If it is assumed that the Karplus relationship $^3J(\theta) = 9.4\cos^2\theta - 1.4\cos\theta + 1.6$ for the $NCCHCH_2C$ fragment is reasonable for χ^2, simple rotamer analysis (39) yields

$\underline{p}$ (180°) = $\underline{p}$ (-60°) = 0.25 and $\underline{p}$ (60°) = 0.50, i.e. $\chi^2 = 60°$, in which $H^{\beta S}$ is gauche to both H^{γ} protons, is predominant. Further evidence for this preferred conformation derives from the observation of an NOE at the H^{δ} resonances when $H^{\beta\underline{u}}$, but not $H^{\beta\underline{d}}$, is irradiated (Fig. 18). The spatial relationship of the $H^{\beta\underline{u}}$ and H^{δ} protons when $\chi^2 \sim 60°$ is diagrammed in Fig. 19.

The origin of the chemical shift difference between the $C^{\delta}H_2$ protons has not been explicitly treated in the discussions of its temperature and solvent variation, but it is possible, by modeling the environment of these protons, to relate the phenomenon to the preferred torsional angles of the side chain. When χ^1 and $\chi^3 \sim 180°$ and χ^2 takes any value near +60°, one of the $C^{\delta}H_2$ protons ($H^{\delta S}$) becomes closely apposed to the C=O group of Val in the internally H-bonded network, and should thus be expected, upon formation of the Orn $N^{\delta}H_3^+$--O=C $\underline{\underline{D}}$-Phe bond, to manifest increased diamagnetic shielding (Fig. 20). Comparison of the absolute shifts of the H^{δ} resonances in MeOH at several temperatures (Fig. 7a) reveals that the increase in ΔO^{δ}_{obsd} is almost entirely attributable to an upfield shift of $H^{\delta\underline{u}}$. The $H^{\delta\underline{u}}$ resonance is therefore assigned to $H^{\delta S}$, and since, as indicated by the $^3J_{\gamma\delta}$'s, $H^{\delta\underline{u}}$ and $H^{\gamma\underline{d}}$ are gauche, the $H^{\gamma\underline{d}}$ resonance in F_3EtOH is assigned to $H^{\gamma R}$. A proposed conformation for the Orn side chain in the H-bonded state, with stereospecific assignment of the ^{1}H NMR resonances, is depicted in Fig. 20. It may be summarized as follows: $\chi^1 \sim 180°$; $\chi^2 \sim 60°$, with residual motional averaging; $\chi^3 \sim 180°$. When viewed along the symmetry axis (Fig. 21) it is seen that the intercationic distance lies between 7 and 8 Å.

Figure 18. NOE difference spectra of GrS (O^{δ} and F^{β} signals only) in F_3EtOH at 296 K. Upper trace, irradiation of $O^{\beta\underline{d}}$; middle trace, irradiation of $O^{\beta\underline{u}}$; lower trace, raw ^1H spectrum (reduced scale). The scale of the upper trace is increased two fold over the middle trace. There is a negative NOE at $O^{\delta\underline{d}}$ and $O^{\delta\underline{u}}$ upon irradiation of $O^{\beta\underline{u}}$ (compare lower trace with spectrum in Fig. 12) while such an NOE is either absent or very much reduced in the case of $O^{\beta\underline{d}}$ irradiation.

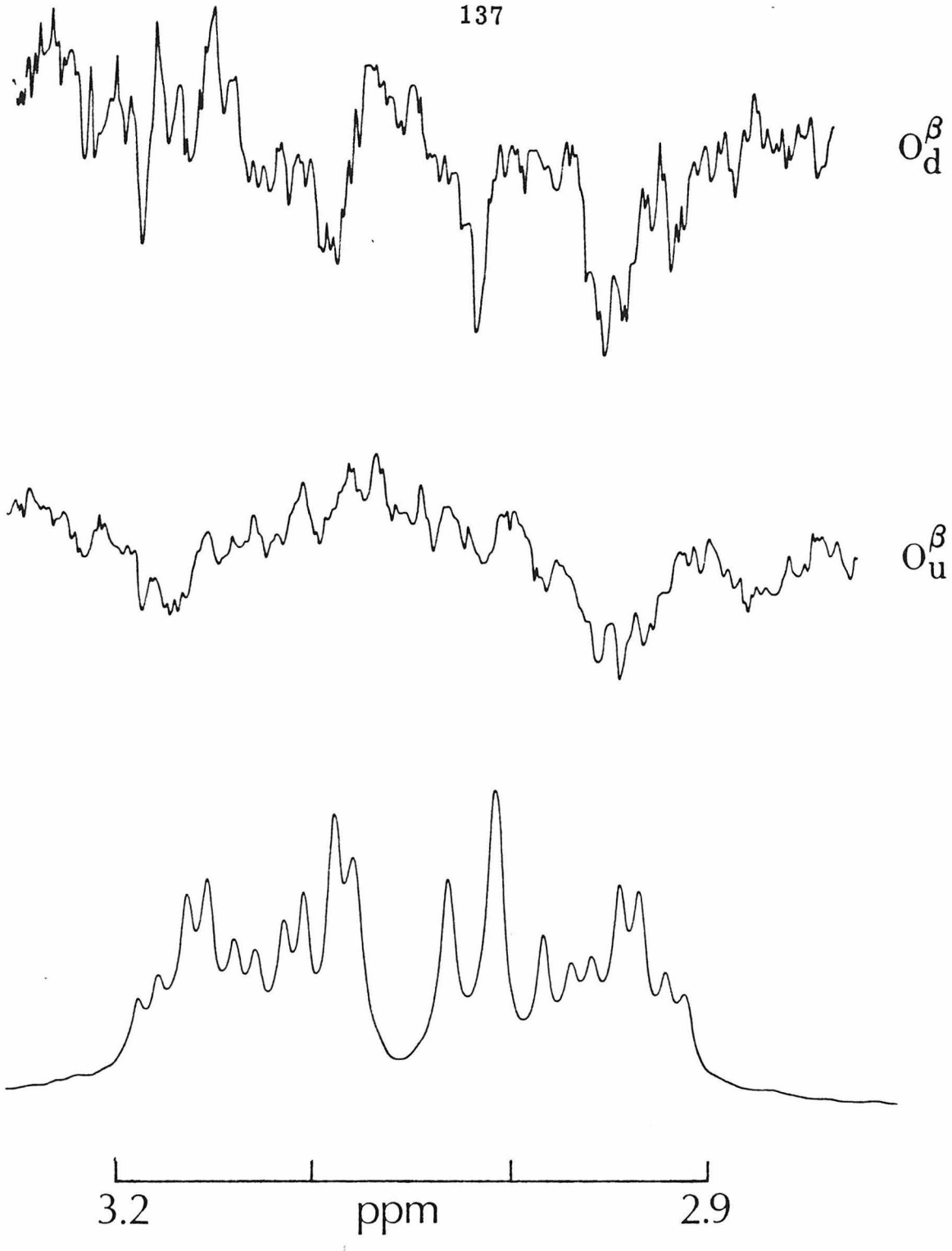
O_d^β
O_u^β
3.2
ppm
2.9

Figure 19. Ball and stick representation of the Orn side chain showing proximity of $O^{\beta u}$ and O^{δ} protons (indicated by arrows) when $\chi^2 \sim 60°$ and $\chi^3 \sim 180°$.

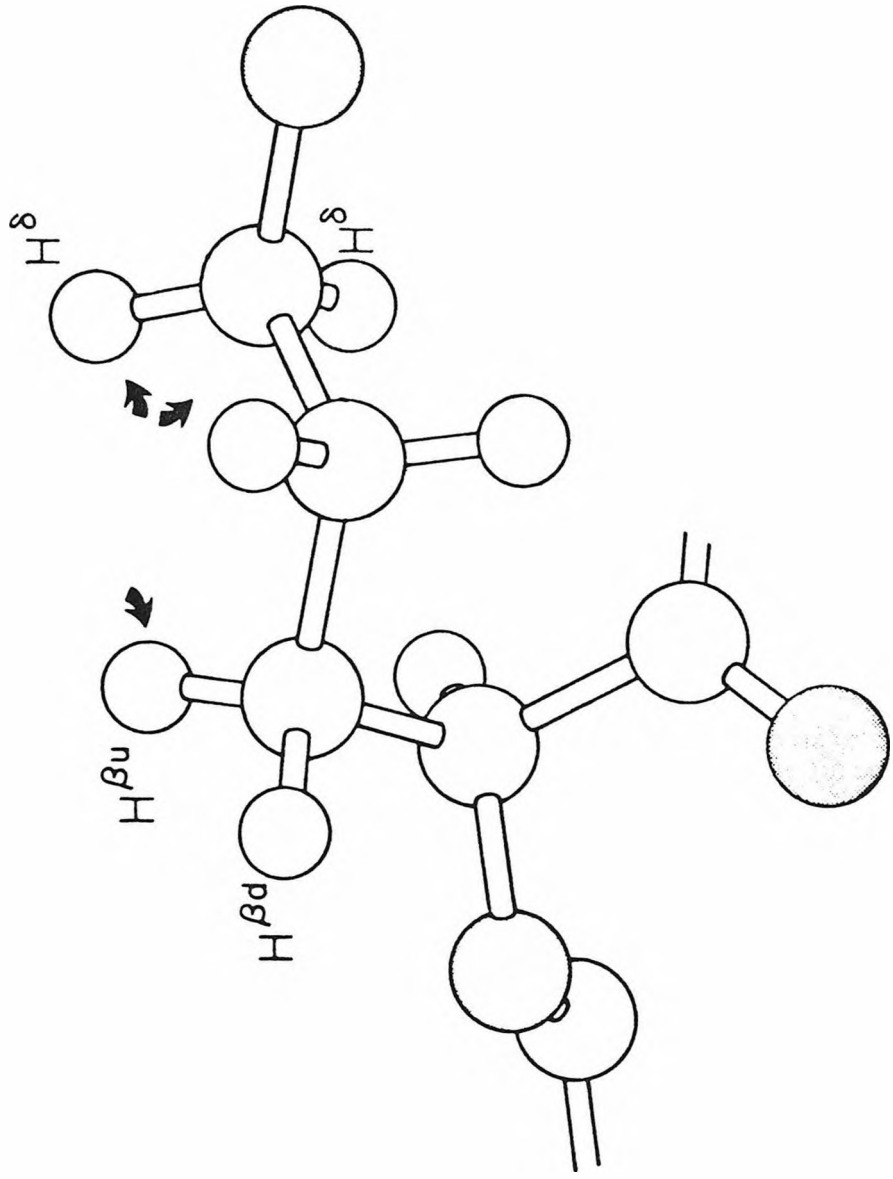
H^{δ}
H^{δ}
$H^{\beta u}$
$H^{\beta d}$

Figure 20. A proposed conformation for the Orn side chain in the presence of the Orn $N^{\delta}H_3^+$--O=C D-Phe H bond. χ^1 and χ^3 are fixed at ~180°. Motility about the second side chain segment is extensive in solution, but there is a predominance of the $\chi^2 = 60°$ conformer (see text). This is represented here by shadowing of the γ and δ protons. With minimal changes in χ^1 and χ^3, χ^2 can assume any of the staggered values ($\pm 60°$, 180°) without disrupting the H bond. Because of steric constraints the transition from $\chi^2 = -60°$ to $\chi^2 = +60°$ must proceed via $\chi^2 = 180°$. Thus, only $H^{\delta S}$ can experience anisotropic shielding by the underlying Val C=O (shown), and the resonant frequency of this proton is upfield of $H^{\delta R}$.

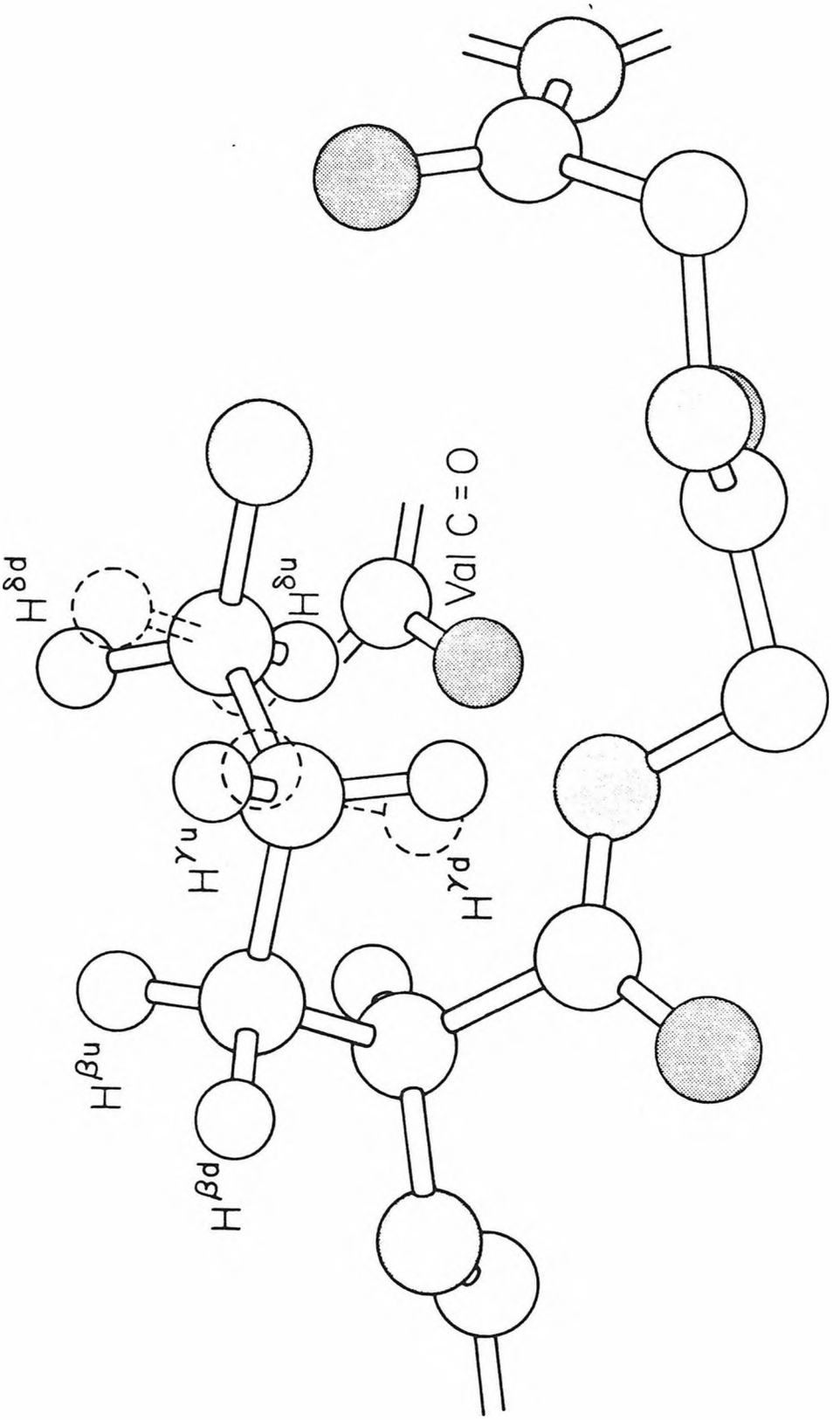
Val C=O
$H^{\delta d}$
$H^{\delta u}$
$H^{\gamma u}$
$H^{\gamma d}$
$H^{\beta u}$
$H^{\beta d}$

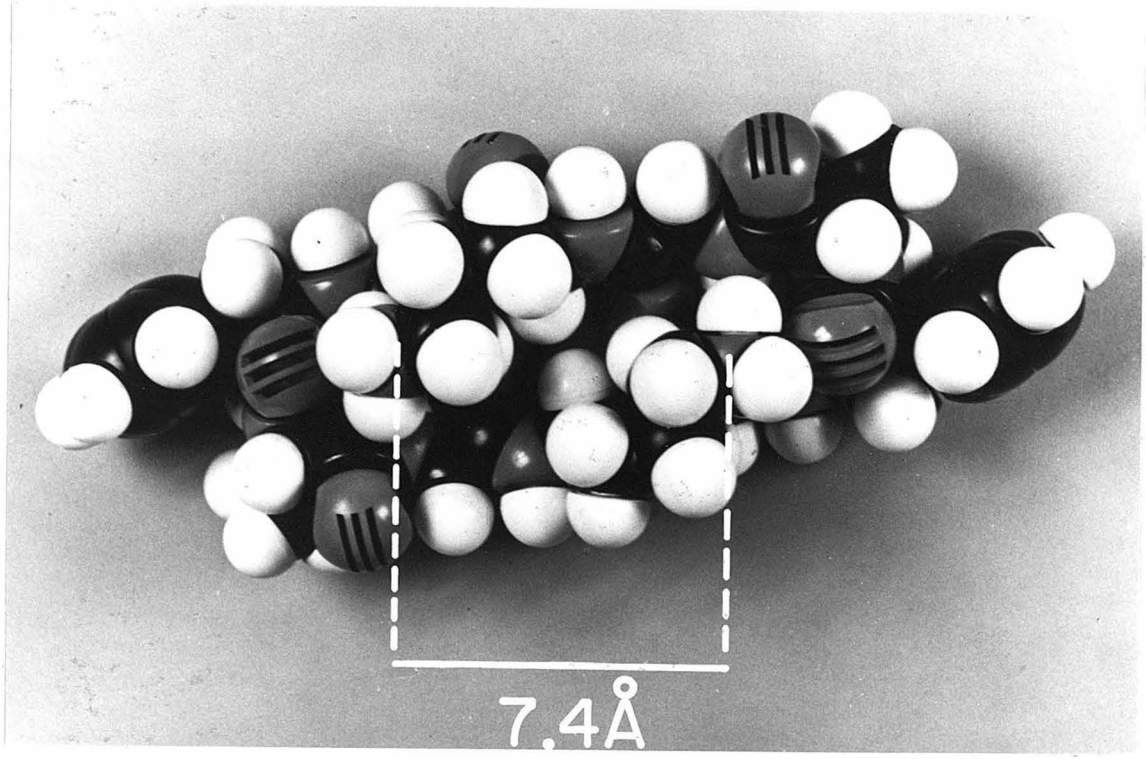

Figure 21. CPK model of GrS viewed along the C_2 axis. The Orn side chains assume the conformation shown in solid lines in Fig. 9. The exact intercationic distance measured from the model is indicated.

4. Discussion

By systematically probing both the donor and acceptor sites, a pair of side chain-to-backbone H bonds in GrS not previously known to exist in solution has been identified. These H bonds provide constraints on the torsional angles that might be accessible to the side chains of the two Orn residues and greatly facilitated the delineation of the conformation of the Orn side chains in solution by high resolution NMR methods even in the presence of residual rotational averaging.

Studies of the solution structure of GrS have revealed the extraordinary prevalence of intramolecular H bonding in this small peptide. Two pairs of symmetry-related interamide H bonds, the first between Leu NH and Val C=O and the second between Val NH and Leu C=O, were proposed in the initial conformational studies and demonstrated experimentally in the previous chapter. Elimination of these internal bonds by alteration of the primary structure yields a peptide with dramatically altered chiroptical properties, NMR spectra, and reduced or absent antibiotic activity (4,40). There is, in addition, a pair of solvent-labile H bonds between Orn $N^{\delta}H_3^+$ and D-Phe C=O. In contrast to the transannular bonds, stability is strongly solvent dependent, and the backbone conformation shows little if any change when the bonds are eliminated by covalent modification.

The question of the biological importance of the Orn $N^{\delta}H_3$--O=C D-Phe bonds is not readily resolved. Levels of activity of analogues are altered by modification of the backbone-Orn N^{δ} distance, but the side chain conformation in the analogues is unknown. Thus, shortening or

lengthening the cationic side chains by one CH_2 group results in a ~50% decrease in potency (41), and further increases in chain length are associated with still lower relative activities (42). While it would be very helpful to examine the biological effect of blocking formation of the Orn $N^{\delta}H_3^+$--O=C D-Phe bonds at the acceptor sites, it is difficult to accomplish this by covalent modification of the β-II′ turns without perturbing the interamide H bonds. In this context, two analogues substituted at position 5 should be noted. [$Gly^{5,5'}$]-GrS contains an intact internal network of H bonds (40) but is only ~0.4 as potent as GrS (43). The greater flexibility of Gly relative to Pro permits ϕ_5 to assume values approaching -100° (vs. ϕ_5 ~ -70° in GrS), which should rotate D-Phe C=O toward the external margin of the ring and away from the Orn side chain. Modeling of the β turn region suggests that when the N atom of Gly is methylated, this rotation is hindered, and indeed the biological activity of [$Sar^{5,5'}$]-GrS (Sar = sarcosine) is the same as GrS (44).

The data suggest a relatively small fraction of intramolecular H-bonded conformers in water (Table VI), but it is not essential that the H bonds exist to a major extent in aqueous solution in order for them to be functionally relevant. It is possible, for example, that the peptide readily assumes the H-bonded conformation upon transfer to a less polar environment; there is considerable evidence that GrS is membrane active (Chapter I). Alternatively, the antibiotic action of GrS may involve the formation of a complex in solution with a polyvalent anion, such as an organic polyphosphate. In this case, Orn $N^{\delta}H_3$--O=C D-Phe H bonding might facilitate binding by ensuring that

a critical intercationic distance is maintained (Fig. 21) which is complementary to the architecture of the anionic species.

5. References

1. Jardetzky, O. Biochim. Biophys. Acta 1980, 621, 227-232.
2. Kuo, M.; Jones, C. R.; Mahn, T. H.; Miller, P. R.; Nicholls, L. J. F.; Gibbons, W. A. J. Biol. Chem. 1979, 254, 10301-10306.
3. Jones, C. R.; Kuo, M.; Gibbons, W. A. J. Biol. Chem. 1979, 254, 10307-10312.
4. Ovchinnikov, Yu. A.; Ivanov, V. T. Tetrahedron 1975, 31, 2177-2209.
5. Allerhand, A.; Komoroski, R. A. J. Am. Chem. Soc. 1973, 95, 8228-8231.
6. Komoroski, R. A.; Peat, I. R.; Levy, G. C. Biochem. Biophys. Res. Comm. 1975, 65, 272-279.
7. Deslauriers, R.; Smith, I. C. P.; Walter, R. J. Am. Chem. Soc. 1974, 96, 2289-2291.
8. Dygert, M.; Gō, N.; Scheraga, H. A. Macromolecules 1975, 8, 750-761.
9. Hull, S. E.; Karlsson, R.; Main, P.; Woolfson, M. M.; Dodson, E. J. Nature 1978, 275, 206-207.
10. Deslauriers, R.; Paiva, A. C. M.; Schaumburg, K.; Smith, I. C. P. Biochemistry 1974, 14, 878-886.
11. Hadzi, D.; Bratos, S. In "The Hydrogen Bond"; Schuster, P.; Zundel, G.; Sandorfy, C., Eds.; North-Holland-Elsevier: New York, 1976; Vol. II, Chapter 12.
12. Stevens, E. S.; Sugawara, N.; Bonora, G. M.; Toniolo, C. J. Am. Chem. Soc. 1980, 102, 7048-7050.

13. Llinas, M.; Horsley, W. J.; Klein, M. P. J. Am. Chem. Soc. 1976, 98, 7554-7558.

14. Granados, E. N.; Bello, J. Biopolymers 1979, 18, 1479-1486.

15. Hawkes, G. E.; Randall, E. W.; Bradley, C. H. Nature 1975, 257, 767-772.

16. Hawkes, G. E.; Litchman, W. M.; Randall, E. W. J. Magn. Reson. 1975, 19, 255-258.

17. Levy, G. C.; Lichter, R. L. "Nitrogen-15 Nuclear Magnetic Resonance Spectroscopy"; Wiley-Interscience: New York, 1979, p. 32.

18. Llinas, M.; Klein, M. P. J. Am. Chem. Soc. 1975, 97, 4731-4737.

19. Buckingham, A. D.; Schaefer, T.; Schneider, W. G. J. Chem. Phys. 1960, 32, 1227-1233.

20. Krauss, E. M.; Cowburn, D. Biochemistry 1981, 20, 671-679.

21. Molday, R. S.; Englander, S. W.; Kallen, R. G. Biochemistry 1972, 11, 150-158.

22. Ovchinnikov, Yu. A.; Ivanov, V. T.; Bystrov, V. F.; Miroshnikov, A. I.; Shepel, E. N.; Addullaev, N. D.; Efremov, E. S.; Senyavina, L. B. Biochem. Biophys. Res. Comm. 1970, 39, 217-225.

23. Fischman, S. J.; Wittbold, W. M.; Wyssbrod, H. R., The Mount Sinai Medical Center, personal communication, 1981.

24. Hawkes, G. E.; Randall, E. W.; Hull, W. E.; Convert, O. Biopolymers 1980, 19, 1815-1826.

25. Reference 17, Chapter 6.

26. Saito, H.; Tanaka, Y.; Nukada, K. J. Am. Chem. Soc. 1971, 93, 1077-1081.

27. Kamlet, M. J.; Dickinson, C.; Taft, R. W. J. Chem. Soc. Perkin II. 1981, 353-355.

28. Marchal, J. P.; Canet, D. Org. Magn. Reson. 1981, 15, 244-246.

29. Burgar, M. I.; St. Amour, T. E., Fiat, D. J. Phys. Chem. 1981, 85, 502-510.

30. Gattegno, D.; Hawkes, G. E.; Randall, E. W. J. Chem. Soc. Perkin II 1976, 1527-1531.

31. Khaled, M. A.; Urry, D. W.; Sugano, H.; Miyoshi, M.; Izumiya, N. Biochemistry, 1978, 17, 2490-2494.

32. Kricheldorf, H. R. Org. Magn. Reson. 1981, 15, 162-177.

33. Homer, R. B.; Johnson, C. D. In "The Chemistry of Amides"; Zabicky, J., Ed.; Wiley-Interscience: London, 1970; Chapter 3.

34. Mahler, H. R.; Cordes, E. H. "Biological Chemistry"; Harper and Row: New York, 1971, p. 95.

35. Klotz, I. M.; Frank, B. H. J. Am. Chem. Soc. 1965, 87, 2721-2728.

36. Noggle, J. H.; Schirmer, R. E. "The Nuclear Overhauser Effect"; Academic Press: New York, 1971; Chapter 2.

37. Pople, J. A.; Schneider, W. G.; Bernstein, H. J. "High Resolution Nuclear Magnetic Resonance"; McGraw-Hill: New York, 1959, pp. 132-138.

38. Bystrov, V. F. Progr. N.M.R. Spectrosc. 1976, 10, 41-81.

39. Pachler, K. G. R. Spectrochim. Acta 1964, 20, 581-587.

40. Miroshnikov, A. I.; Snezhkova, L. G.; Sichev, S. W.; Chervin, I. I.; Senyavina, L. B.; Ivanov, V. T.; Ovchinnikov, Yu. A. Bioorg. Khim. 1977, 3, 180-191.

41. Waki, M.; Abe, O.; Okawa, R.; Kato, T.; Makisumi, S.; Izumiya, N. Bull. Chem. Soc. Japan 1967, 40, 2904-2909.

42. Silaev, A. B. Humboldt-Symp. Grundfragen Biol. 3, Berlin 1960 1962, 156-164; Chem. Abstr. 1963, 59, 6635f.

43. Matsuura, S.; Waki, M.; Izumiya, N. Bull. Chem. Soc. Japan 1972, 45, 863-866.

44. Aoyagi, H.; Izumiya, N. Bull. Chem. Soc. Japan 1966, 39, 1747-1753.

CHAPTER IV

COMPLEXATION AND PHASE TRANSFER OF NUCLEOTIDES BY GRAMICIDIN S

1. Introduction

Considerable attention has been given macromolecules which form stable coordination complexes with ionic substrates in solution. Through judicious placement of charged and polar groups, it has been possible to design complexing agents, or complexones, which bind substrates strongly and with considerable selectivity (1). Complexones serve as models for the study of biomolecular recognition and transport processes (1-4) and have important applications in chemical catalysis (5). Much of the recent research on anion complexones of potential biological significance (6-10) has centered on natural and synthetic polyamines which interact with nucleotides (2, 3, 7, 10, 11). Of the latter class of compounds the simplest examples are the linear amines putrescine, spermidine, and spermine, which form nucleotide complexes that may serve a regulatory function in cell growth (11). Macromonocyclic salts containing repeating units of ethylene-, propylene-, and butylenediamine bind nucleotides more tightly than the acyclic ligands (7, 9), presumably because the cyclic compounds are less conformationally mobile and possess a higher charge density. A highly constrained, lipophilic ethylenediamine congener, (N, N'-distearyl)1, 4-diazabicyclo[2.2.2]octane (DS-Dabco) has been shown to bind nucleotides and transfer them efficiently to $CHCl_3$ (2, 3). All of

these complexes involve ion pairing between the phosphate moieties of the nucleotide and the positively charged amino groups of the ligand and are stabilized by electrostatic and, where possible, hydrogen bonding interactions.

On inspection, GrS appears to be a likely candidate for an anion complexone: it is a divalent cation, and the positive charges, because of the rigidity of the peptide backbone and the relative lack of motional freedom of the Orn side chains, are constrained to occupy positions on one face of the ring, on average less than 8 Å apart (Chapter III). The side chains of the remaining hydrophobic residues are arrayed toward the opposite face of the ring (12,13), suggesting that if GrS were indeed an anion complexone it might possess phase transfer activity as well. The anion binding properties of GrS have not been investigated previously in vitro. In vivo, GrS produces remarkable effects on phosphate metabolism in microorganisms; strains of B. brevis actively synthesizing the peptide exhibit a nearly complete loss of extractable nucleoside di- and triphosphates (14,15) accompanied by a rapid loss of ^{31}P NMR signals from intracellular ATP (16). These effects were attributed to inhibition of membrane-bound respiratory enzymes by adsorption of GrS to acidic phospholipids (17) rather than to nucleotide binding. Direct evidence of such an interaction with bacterial membranes has not been obtained, however (18).

In this study it is reported that GrS efficiently binds nucleotides in water to yield a complex which partitions into organic solvents such as $CHCl_3$, establishing this molecule as the first phase transfer reagent for nucleotides which is a natural product and the first

nucleotide complexone which is not an aliphatic polyamine. GrS exhibits a pattern of selectivity similar to the synthetic complexones (4, 7) with the extraction efficiencies generally increasing in the order AMP < ADP < ATP. The interaction is primarily ionic, with little or no contribution from the nucleoside moiety, and is subject to competition by charged species. In the organic phase, the complexes associate extensively, most likely by cross-β aggregation. In contrast to the situation with the synthetic ligands, where the stoichiometry is uncertain or unknown (4) or is assumed a priori to be 1:1 (7, 9) even though other possibilities exist, the stoichiometries of the extracted complexes formed by GrS are obtained by NMR and confirmed by simulation of the extraction profiles. Knowledge of the stoichiometries permits estimation of binding constants through systematic study of the extraction, and thereby affords an understanding of the molecular basis for the observed selectivity among the nucleotides. Our observations strongly indicate that a direct nucleotide-GrS interaction underlies the anomalously low energy charge and vigorous nucleotide efflux observed in late cultures of B. brevis actively synthesizing the peptide and, possibly, the lethal effects exerted by GrS on susceptible microorganisms. The implications of GrS-induced phase transfer of nucleotides for selective nucleotide transport through biological membranes are considered.

2. Experimental Section

Materials. Gramicidin S dihydrochloride was obtained from Sigma Chemical Co. and lyophilized prior to use. It migrated as a single spot in several solvent systems on TLC. Adenosine

5′-triphosphate, disodium salt (Sigma), adenosine 5′-diphosphate, disodium salt (Sigma), adenosine 5′-monophosphate, monosodium salt (Sigma), uridine 5′-triphosphate, trisodium salt (Sigma), thymidine 5′-triphosphate, trisodium salt (Sigma), 2′-deoxythymidine 5′-triphosphate, tetrasodium salt (P-L Biochemicals), 2′,3′-dideoxythymidine 5′-triphosphate, tetrasodium salt (P-L Biochemicals), guanosine 5′-triphosphate, trilithium salt (Calbiochem), and cytidine 5′-triphosphate, disodium salt (Calbiochem) were used without further purification. Other chemicals were of reagent grade.

Spectroscopy. UV spectra were measured on a Beckman Instruments ACTA CIII or a Cary 219 spectrophotometer using 1 cm pathlength cells at 25°C. Concentrations of standard solutions of the nucleotides were determined from published molar extinction coefficients (19). Nucleotide concentration in the aqueous phase after extraction was determined by measurement of the absorbance at 270 nm, where the absorbance of the peptide is negligible.

NMR spectra were obtained on a Bruker WM-500 multinuclear spectrometer at the Southern California Regional NMR Facility. The operating frequencies were 500.13 MHz for ^{1}H and 202.49 MHz for ^{31}P.

Extraction Procedure. $CHCl_3$ constituted the organic phase for most of the extractions. The volumes of the aqueous and organic phases were equal. All operations were performed at room temperature. Aqueous solutions containing GrS, nucleotide, and (where desired) additional salts were combined in a stoppered 12 ml conical tube and adjusted to a specified pH with dilute NaOH and HCl. The

organic solvent was added and the tube shaken vigorously by hand (4 strokes sec^{-1}) for 2 min. Phase separation was hastened by brief centrifugation and the pH of the aqueous layer readjusted to the starting value, where necessary. The decrease in pH during the initial 2 min extraction was generally $<$ 1 unit at pH 7 and nil at pH 3. The tube was shaken for an additional 2 min, centrifuged, and the absorbance $\underline{A}$ of the aqueous phase determined. The extraction efficiency, $\underline{E}$, was defined (4) by Eq. 1, where $\underline{A}_{270,i}$ and $\underline{A}_{270}$ refer

$$\underline{E} = 1 - \frac{\underline{A}_{270}}{\underline{A}_{270,i}} \qquad (1)$$

to the initial and final absorbances at 270 nm. The use of longer extraction times afforded no increase in $\underline{E}$.

Whereas neutral salts were added to maintain constant ionic strength in titrimetric studies of nucleotide complexation in water (6, 7), this was not done in the present study in order to avoid competitive effects. Neutral salts were not used either in the extractions employing DS-Dabco (2-4) or in the quantitative study of the binding and extraction of alkali metal salts by macrotetralide antibiotics by Eisenman et al. (20). The concentrations of Na^+ and Cl^- present as counterions and for the purpose of pH adjustment were invariably too low ($\leq 10^{-3}$ M) to exert competitive effects in the extraction runs employing GrS.

Data Reduction. As described under Results, the variation of $\underline{E}$ with initial nucleotide concentration $[a]_i$ is, for the 1:n interaction

with $\zeta = 1$, $\underline{E}/(1-(1+\underline{K}_p^{-1})\underline{E}^{n+1} = (n[a]_i/1.2)^n \underline{KK}_p$ neglecting aggregation. Attempts to fit the extraction profiles to this equation by interative minimization of $\sum_j (\underline{E}_j^{(obs)} - \underline{E}_j^{(calcd)})^2$ were unsuccessful, since the design matrix contained explicit $[a]_i^{-n}$ dependence which spuriously weighted each datum by this factor. Successful simulation made use of the equivalent relation $\underline{Y} = n \ln(\underline{KK}_p[a]_i n/1.2) + (n+1)\ln(1 - \underline{q}/\underline{K}_p)$, where $\underline{Y} \equiv \ln(\underline{E}/(1-\underline{E})^{n+1})$, $\underline{q} \equiv \underline{E}/(1-\underline{E})$, and the algorithm minimized $\sum_j (\underline{Y}_j^{(obs)} - \underline{Y}_j^{(calcd)})^2$ with respect to $\underline{K}$ and $\underline{K}_p$. All calculations, including those outlined in the Appendix, were performed on a VAX 11/780 computer administered by the Division of Chemistry and Chemical Engineering.

3. Results

GrS promotes phase transfer into $CHCl_3$ of adenine nucleotides (Table I). As shown in Table II, the extraction efficiency $\underline{E}$ decreases significantly for ADP and AMP at pH 3, but ATP exhibits a smaller pH dependence for the extraction. Table II also compares extraction data for GrS to that obtained for DS-Dabco under similar conditions (4). At neutral pH, GrS is the more efficient phase-transfer agent, while at pH 3 the reverse holds. The abilities of these complexones to discriminate between the adenine nucleotides at either pH is qualitatively the same.

The extraction of ATP into $CHCl_3$ by GrS at pH 7 is efficient, as illustrated by the value of 0.60 measured for $\underline{E}$ when $[ATP] = 2\times10^{-6}$ M and $[GrS] = 4\times10^{-6}$ M. Purine nucleotides are extracted slightly more efficiently than pyrimidines (Table III).

Table I. Extraction Efficiencies at pH 7[a]

Nucleotide	[Nucleotide][b]	[GrS][b]	Other	E
ATP	20	40		0.88
	40	40		0.48
	10	20	0.02 M NaCl	0.75
	10	20	0.02 M P_i	0.45
	10	20	0.02 M PP_i	~0
	10	20	0.01 M $MgCl_2$	0.19
	10	20	1-octanol[c]	0.61
	100	200[d]		~0
ADP	20	40		0.78
	50	50		0.51
AMP	20	40		0.72

[a] $H_2O/CHCl_3$ system. [b] ln 10^{-6} M. [c] Substituted for $CHCl_3$.
[d] 1,5-pentanediamine.

Table II. pH Effect and Comparison with DS-Dabco[a]

	pH 7		pH 3	
	GrS	DS-Dabco[b]	GrS	DS-Dabco
ATP	0.99	0.95	0.90	0.99
ADP	0.96	0.94	0.25	0.37
AMP	0.72	0.69	0.02	0.01

[a]Extraction efficiencies for the $H_2O/CHCl_3$ system. Data for DS-Dabco from Ref. 4. Concentrations: 2×10^{-5} M nucleotide, 5×10^{-5} M complexone (pH 7); 10^{-4} M nucleotide, 2.5×10^{-4} M complexone (pH 3). [b]pH 8.

Table III. Effect of Base Moiety[a]

Nucleotide	E
ATP	0.83
GTP	0.86
CTP	0.70
UTP	0.80

[a] 10^{-5} M nucleotide, 2×10^{-5} M GrS at pH 7.

Nucleotide Binding in Water. Combining aqueous solutions of GrS and ATP at concentrations exceeding $\sim 10^{-5}$ M at pH 7 results in precipitation, demonstrating that binding occurs without the necessity of a second process involving phase transfer. Unfortunately, the very low aqueous solubility of the triphosphate-GrS complexes precluded study by titrimetry, uv, or NMR. It was, on the other hand, possible to observe by NMR the interaction between ADP and GrS when $[GrS] \leq 10^{-4}$ M. ^{1}H NMR spectra at 500.13 MHz revealed a progressive downfield shift in the central unresolved component of the Orn $C^{\delta}H_2$ multiplet, an ABXX′ system in $^{2}H_2O$, with increasing [ADP] (Fig. 1). There were no shifts in the aromatic resonances which might indicate stacking of the adenine and phenylalanine rings.

In order to obtain ^{31}P spectra it was necessary, because of the low solubility of the GrS complexes, to utilize the alkylated GrS derivative [2,2′-N^{δ}-trimethylornithyl]-GrS (Me_6GrS) (Chapter III) which binds nucleotides considerably more weakly than the native peptide. Addition of 1.5×10^{-3} M Me_6GrS to 7.5×10^{-4} M ATP at pH 7 resulted in downfield shifts of 0.5 ppm of P^{γ}, 0.4 ppm of P^{β}, and 0.1 ppm of P^{α}, with sufficient linebroadening to obscure the multiplet structure of the P^{β} resonance (Figure 2). These chemical shift changes demonstrate that an interaction with the phosphate groups has occurred; the data are unfortunately insufficient to identify preferred sites of binding on the nucleotide.

Except for minor light scattering effects, the absorption spectrum of ADP above 245 nm did not change upon addition of GrS. At shorter wavelengths absorption of the peptide group predominates.

Figure 1. 500.13 MHz ^{1}H NMR spectra of GrS in $^{2}H_2O$ under progressive addition of ADP. The Orn $C^{\delta}H_2$ and $\underline{\underline{D}}$-Phe $C^{\beta}H_2$ resonances lie in this region. For each spectrum, $[GrS]_i = 10^{-4}$ M and $[ADP]_i/[GrS]_i \equiv 1/\zeta$ is indicated above the trace; $[GrS]_i = 7.5 \times 10^{-5}$ M for $1/\zeta = 2$. The arrows indicate the position of the central unresolved component of the Orn $C^{\delta}H_2$ resonance. The grids above the chemical shift scales show the positions of the invariant $\underline{\underline{D}}$-Phe $C^{\beta}H_2$ peaks. The apparently narrower linewdith of the $1/\zeta = 2$ spectrum is the result of Gaussian multiplication of the free induction decay.

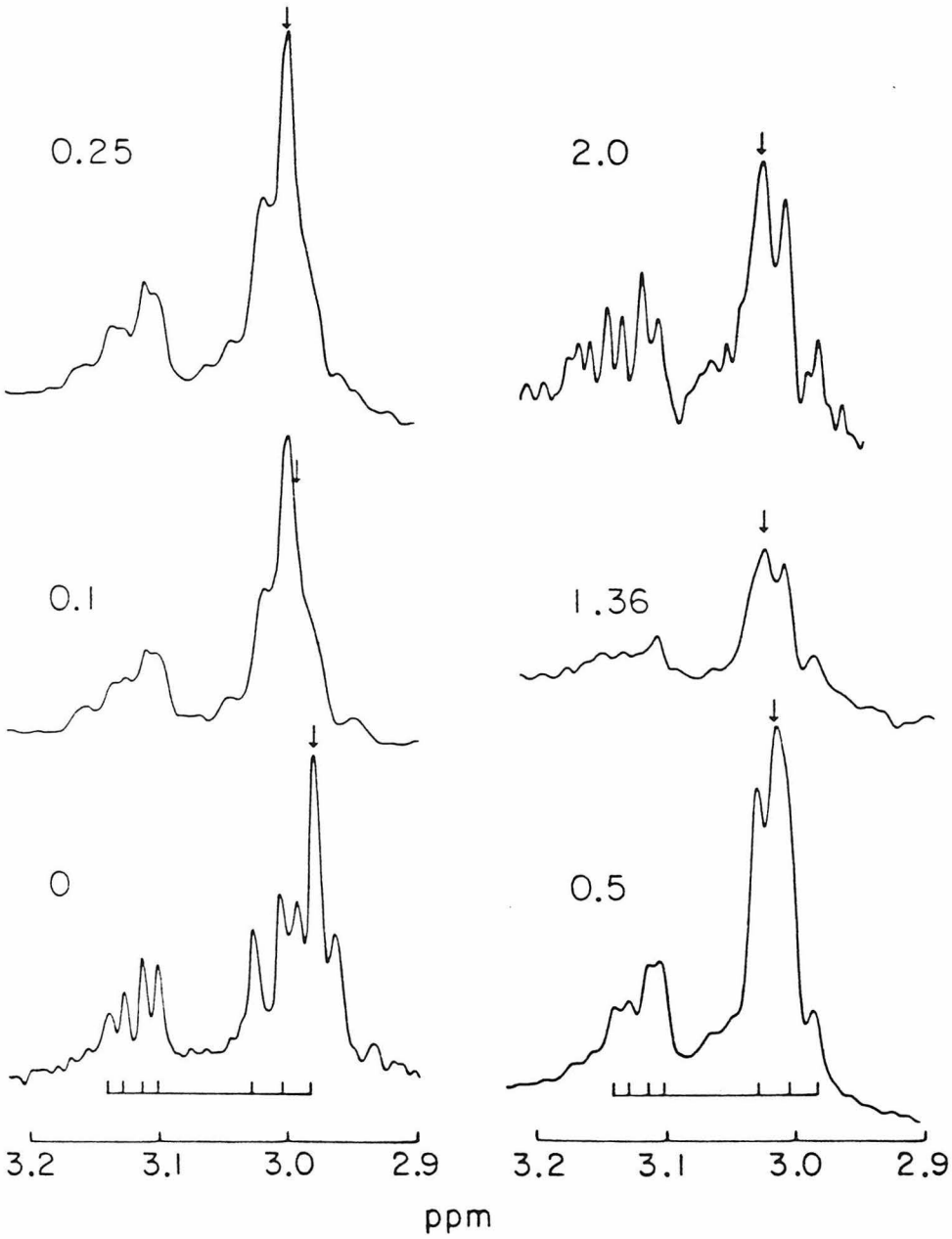
0.25
2.0
0.1
1.36
0
0.5
3.2
3.1
3.0
2.9
3.2
3.1
3.0
2.9
ppm

Figure 2. 200.49 MHz ^{31}P NMR of 7.5×10^{-4} M ATP in water containing 10% $^{2}H_2O$ at pH 7.0 in the absence (a) and presence (b) of 1.5×10^{-3} M [2,2'-N^{δ}-trimethylornithyl]-GrS. Chemical shifts are referenced to internal 5×10^{-4} M P_i (= 0.0 ppm).

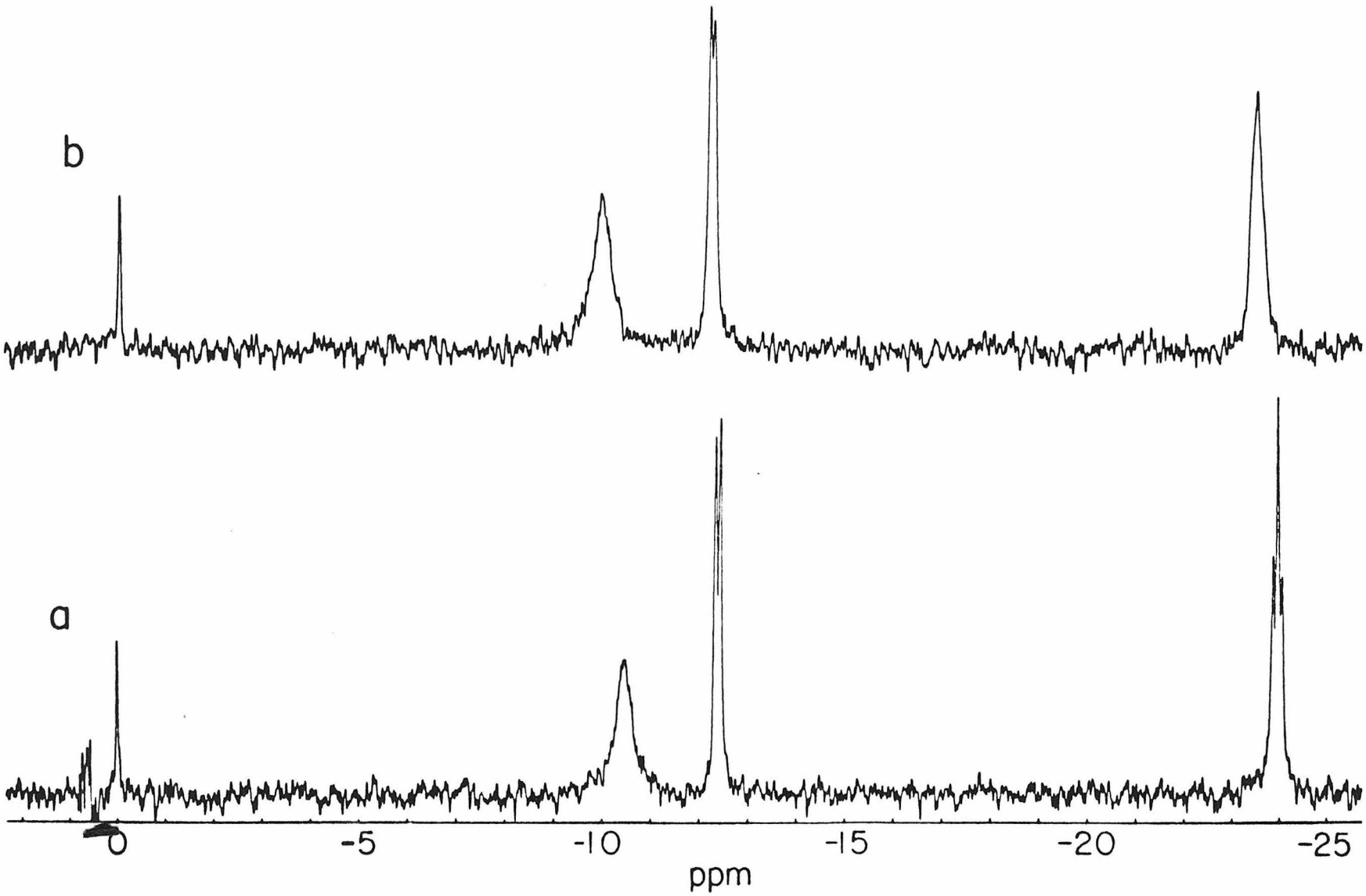
b
a
0
-5
-10
-15
-20
-25
ppm

Phase Transfer. Extraction of nearly stoichiometric solutions of GrS and nucleotides with $CHCl_3$ invariably yielded a clear aqueous phase and sharp boundary. Nucleotide removed from the aqueous phase was quantitatively transferred to the organic layer, as verified by uv. The partition coefficient of GrS into $CHCl_3$, $\underline{K}_G$, was determined independently by uv to be 0.2 in the absence of salts. Because of the low solubility of the free antibiotic in the organic phase and the high apparent affinity of GrS for the nucleotides, the concentration of free GrS in $CHCl_3$ should be relatively low after extraction. As long as GrS is not initially present to large molar excess, the organic phase should after extraction contain almost exclusively nucleotide-GrS complexes.

Use of deuterated solvents permits measurement of ^1H NMR spectra of the extracted ATP-GrS complexes in $CDCl_3$ (Fig. 3). While characteristic resonances of both components are discernible, the linewidths are too broad (>50 Hz) to allow detailed study of conformation. Some dependence of the linewidth on concentration between 2 and 40×10^{-5} M nucleotide (initial concentration in water) is apparent, suggesting that it is a concentration-dependent aggregation of complexes, rather than an intrinsically high aggregation number for the individual complex, which accounts for the broad lines. Similar spectra were obtained for the ADP complex.

Figure 3. ^{1}H NMR spectra of ATP-GrS complexes in $C^{2}HCl_3$. The numbers to the left of the traces are the initial nucleotide concentrations in water (in 10^{-6} M), prior to extraction.

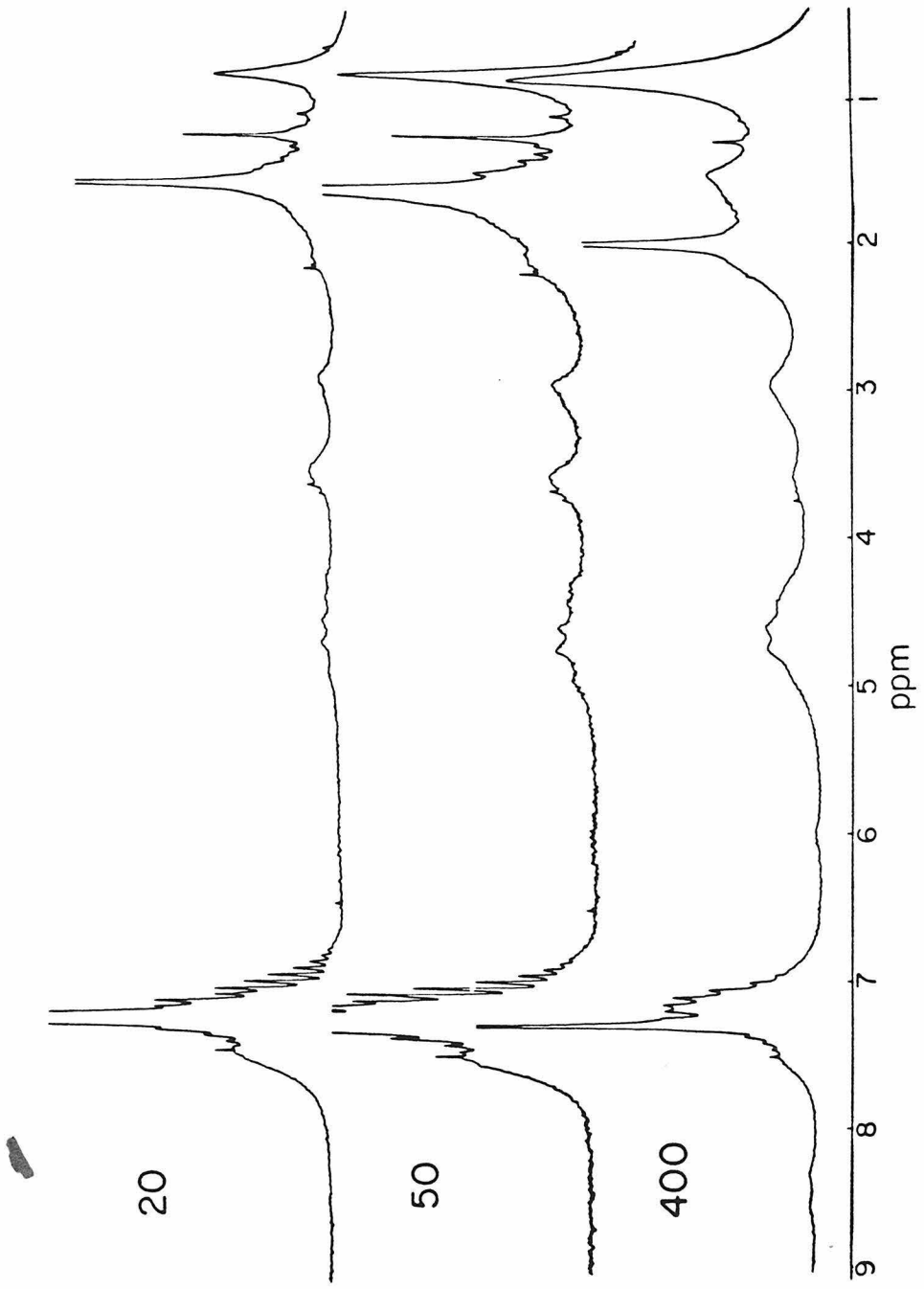
20
50
400
9
8
7
6
5
4
3
2
1
ppm

Extraction with $CHCl_3$ was facile, and the solubility of the ATP-GrS complex in this solvent exceeded 10^{-2} M. Attempts to use other organic solvents in the extraction were less successful. With 1-octanol, a slightly lower E was measured (Table I). The use of hydrocarbons or CCl_4 resulted in interfacial precipitation. However, it was possible to obtain solutions of the ATP-GrS complex in either CCl_4 (in toluene) by repeated addition of the second organic solvent to a concentrated $CHCl_3$ solution and evaporation to near dryness. The complex is soluble in $CHCl_3$-hexane mixtures but is practically insoluble in the pure hydrocarbon.

Crystals were obtained by slow evaporation of a solution of the ATP-GrS complex in EtOH-Me_2CO (1:1) (colorless needles, typically 2×0.02 mm).

Nature of the Nucleotide-Peptide Interaction. The NMR spectra in water demonstrate coordination of the ammonium and phosphoryl groups in the complex. Two other interactions are possible, (i) ring stacking of the nucleoside base and the side chain of D-Phe, and (ii) formation of additional hydrogen bonds between the nucleoside and the peptide backbone. The lack of NMR chemical shift changes indicative of ring stacking in the spectra of the ADP complex in water argues against (i), but no determination could be made in $CHCl_3$ because of the poor resolution in this solvent. The hydrogenated derivative (D-cyclohexylalanyl^4)$_2$-GrS (ChaGrS) was therefore prepared according to the method of Ruttenberg et al. (21) and its interactions compared with those of GrS. No difference in extraction efficiencies was found, and the minimum lethal concentration of ChaGrS against

Staphylococcus aureus in liquid culture was 1.6×10^{-6} M, vs. 1.5×10^{-6} M for GrS. From these observations it is concluded that base stacking contributes negligibly to the stabilization of the complex and that the aromaticity of residue 4 is unnecessary for full antibiotic potency.

To investigate (ii) further, the extraction of the thymine nucleotides TTP, 2′-deoxy-TTP, and 2′,3′-dideoxy-TTP by GrS was investigated. Again no difference was found between the analogues, suggesting that hydrogen bonds between the sugar moiety and the peptide do not form. Other hydrogen bonds between the nucleoside base and the peptide are still possible, however, and may account for the observed small differences in $\underline{E}$ between the various triphosphates.

In view of the importance of ion pairing in complex formation, it is not surprising that competitive effects are observed in the presence of other charged species. Among the anions, inorganic pyrophosphate (PP_i) at pH 7 competes most effectively, blocking 50% of transfer of 10^{-5} M ATP at a concentration of 7×10^{-5} M (Fig. 4a). The relative abilities of anions to block phase transfer of ATP at pH 7 decrease in the order $PP_i > P_i > (CH_2COO^-)_2$, Br^-, SCN^-, $ClO_4^- > Cl^-$, $CH_3COO^- > H_2BO_3^-$. Among the cations, Mg^{++}, 1,4-butanediamine (putrescine) and 1,5-pentanediamine (cadaverine), which form soluble nucleotide complexes, compete about as effectively towards nucleotides as P_i towards GrS, when added as the chlorides.

Equilibrium exchange of anions across a $CHCl_3/H_2O$ interface was mediated by GrS. In one experiment, a solution of ATP

Figure 4. (a) Competition of PP_i with 10^{-5} M ATP for 2×10^{-5} M GrS at pH 7 in the standard extraction. (b) Extraction of a 1.25×10^{-5} M ATP solution (Aqueous Layer II) with $CHCl_3$ phase which had previously been equilibrated with a solution containing 2.5×10^{-5} M GrS and the concentration of P_i indicated on the abscissa (Aqueous Layer I). $\underline{E}_{max} \approx 0.83$ is the efficiency expected for a single $CHCl_3$ extraction of a solution containing 1.25×10^{-5} M ATP and 2.5×10^{-5} M GrS; $\underline{E}/\underline{E}_{max} \sim 1$ indicates quantitative phase transfer of GrS into $CHCl_3$ in the first extraction step. The value of $\underline{E}/\underline{E}_{max} \sim 0.25$ ($[P_i] = 0$) reflects the limited $CHCl_3$ solubility of the free peptide. The pH was 7 in both aqueous layers.

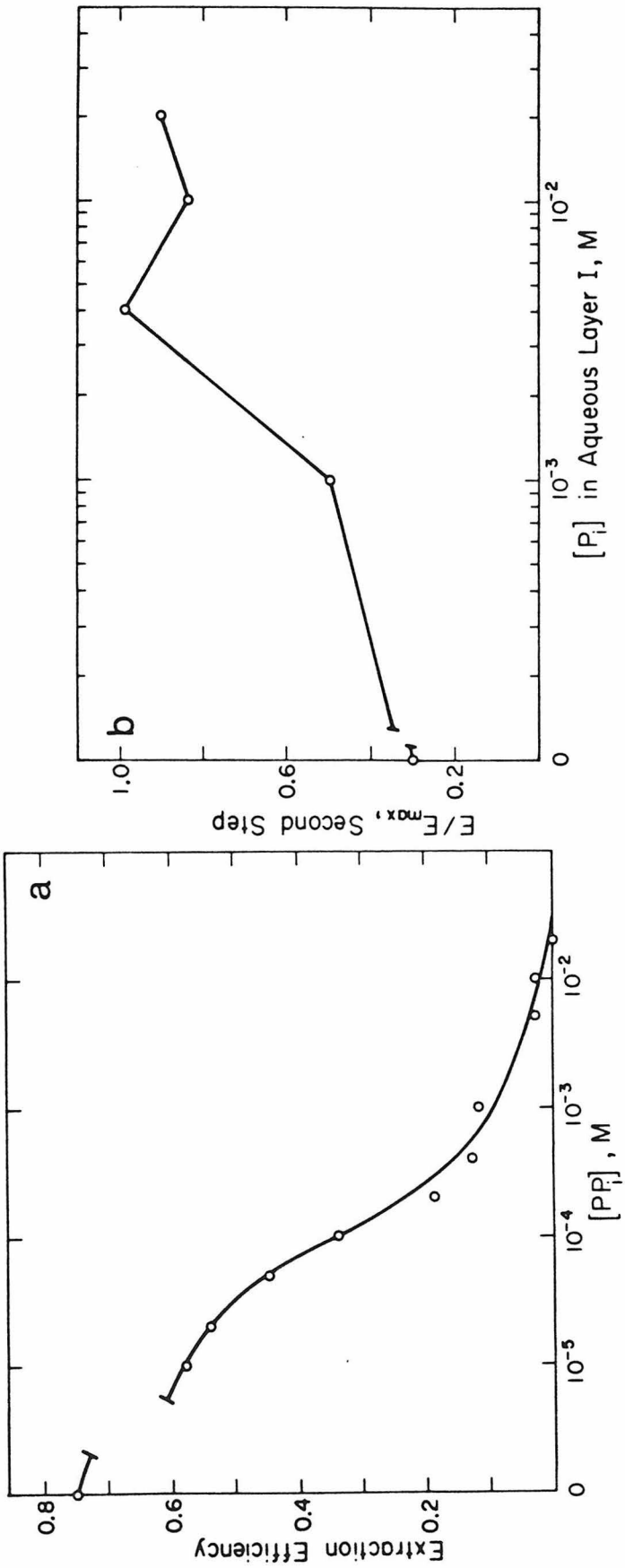
a
Extraction Efficiency
0.8
0.6
0.4
0.2
0
10^{-5}
10^{-4}
10^{-3}
10^{-2}
$[PP_i]$, M
b
E/E_{max}, Second Step
1.0
0.6
0.2
0
10^{-3}
10^{-2}
$[P_i]$ in Aqueous Layer I, M

(1.25×10^{-5} M) and GrS (2.5×10^{-5} M) was extracted with $CHCl_3$ in the usual fashion. The organic phase was withdrawn and shaken with 0.02 M phosphate buffer, pH 7. After the second extraction, ~50% of the nucleotide was present in the aqueous phase. In contrast, distilled water or saline afforded <5% back-extraction. In a second experiment a solution of 2.5×10^{-5} M GrS and a variable concentration of P_i were extracted with $CHCl_3$, the organic layer removed and shaken with a second aqueous layer containing 1.25×10^{-5} M ATP (Fig. 4b). The $CHCl_3$ phase, presumably containing a lipophilic phosphate complex of the peptide, induced phase transfer of ATP with a limiting E at high $[P_i]$ comparable to that expected for a single extraction of ATP by GrS at the same initial concentrations.

Complex Aggregation. Once formed, the nucleotide-GrS complexes appear to interact strongly with one another, as shown by the formation of precipitates in water prior to extraction and the marked NMR linebroadening in $CHCl_3$. In water, self-association is most likely directed by hydrophobic interactions, since the two charged side chains of the peptide, which confer its modest degree of aqueous solubility, are blocked. At low ($\leq 10^{-4}$ M, for ADP) concentrations, relatively small aggregates remain in solution and give rise to NMR spectra with moderately broadened lines, while bulk precipitation occurs at higher concentrations.

In $CHCl_3$, precipitation does not occur, but there is a greater degree of linebroadening than in aqueous solutions of similar concentration. The most plausible explanation for this is lateral polymerization of the complexes in the organic solvent to form linear cross-β-

aggregates (Fig. 5). Cross-β aggregation of GrS in oriented polyethoxyethylene has been shown to occur by IR dichroism (22). A maximum of four interamide hydrogen bonds can form between each pair of GrS molecules, each of which can interact similarly with the backbone of a GrS molecule in a second complex. The aggregation numbers in $CHCl_3$ are likely to be large, because interamide hydrogen bonding itself is favorable in media of low polarity (23), particularly when several bonds can form in concert between the interacting molecules. The surface properties of these large, ribbonlike aggregates ensure high solubility in organic media, while slow rotational diffusion accounts for the broad NMR linewidths. Interaction between aggregates should be weak, which may account for the large axial ratio of the crystals.

Stoichiometry and Structure of the Complexes. The molecularity of phase transfer was established directly by ^1H NMR. Following evaporation of $CHCl_3$, the extracted complexes were dissolved in MeOH-$\underline{d}_4$-Me_2SO-$\underline{d}_6$ (1:1), and the resonance of the nucleotide and peptide components integrated. It was determined that ATP and GrS form an extractable 1:2 complex at pH 7 and a 1:1 complex at pH 3. ADP and GrS form a 1:1 complex at pH 7. The measured stoichiometries did not depend on the initial concentration ratio of the components in the aqueous phase and represent an irreducible minimum exclusive of higher degrees of aggregation.

The dependence of stoichiometry on pH for ATP is the result of the change in ionization state of the nucleotide. At pH 7, ATP is predominantly tetravalent (19) and binds the charged Orn termini of

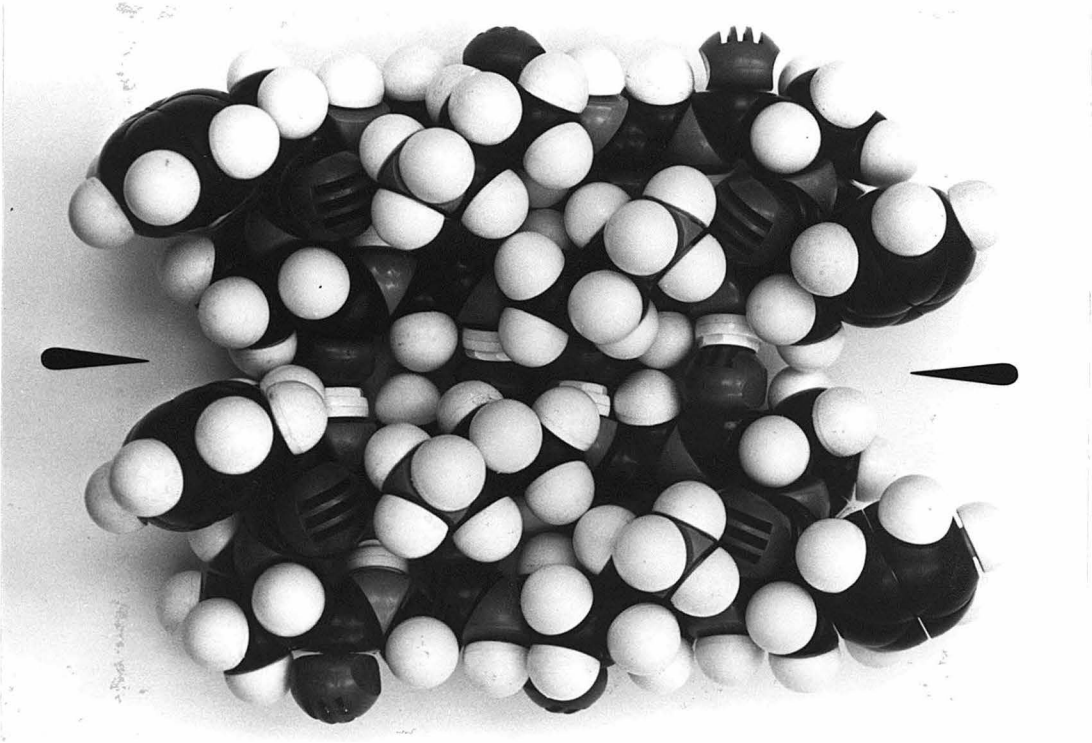

Figure 5. Cross-β association of two molecules of GrS (nucleotides omitted), viewing the polar faces (side chains of Orn, D-Phe, and Pro visible). Pointers indicate line of contact of the ring edges, where intermolecular pleating occurs.

two peptide molecules. At pH 3, the nucleotide carries an overall charge of -2 because of adenine N^1 protonation and forms a neutral 1:1 complex. The relatively low extraction efficiency measured for ADP at pH 3 (Table II) is presumably a manifestation of lower stability of complexes containing two equivalents of nucleotide per peptide (4). AMP should itself be predominantly uncharged at pH 3, and is barely extracted by GrS.

From what has been determined concerning nucleotide-GrS binding, the stoichiometries, and the colligative properties of the complexes, it is possible to propose structures for the complexes in solution. In the 1:1 complex (ATP, pH 3; ADP, pH 7), the nucleotide is apposed to the polar face of the peptide (Fig. 6), the anionic moieties in intimate contact with the NH_3^+ groups of Orn. Since polar groups remain solvent exposed over this face, the 1:1 complex clearly possesses polar and nonpolar surfaces. Four externally directed amide groups of the peptide backbone are available for hydrogen bonding in $CHCl_3$ along each ring edge.

In the 1:2 complex (ATP, pH 7; Fig. 7), two GrS molecules envelop the nucleotide. The charged groups of both components are solvent shielded, and the externally directed surfaces of the complex which are parallel to the ring planes are nonpolar. Cross-β aggregation in organic media should occur readily if the ring planes and major ring axes are parallel (Fig. 7). While this complex is expected to be more hydrophobic than the 1:1 complex by virtue of the larger number of exposed nonpolar side chains, the lateral aspect of the 1:2 complex, shown in the figure, retains considerable polar character; aggregation

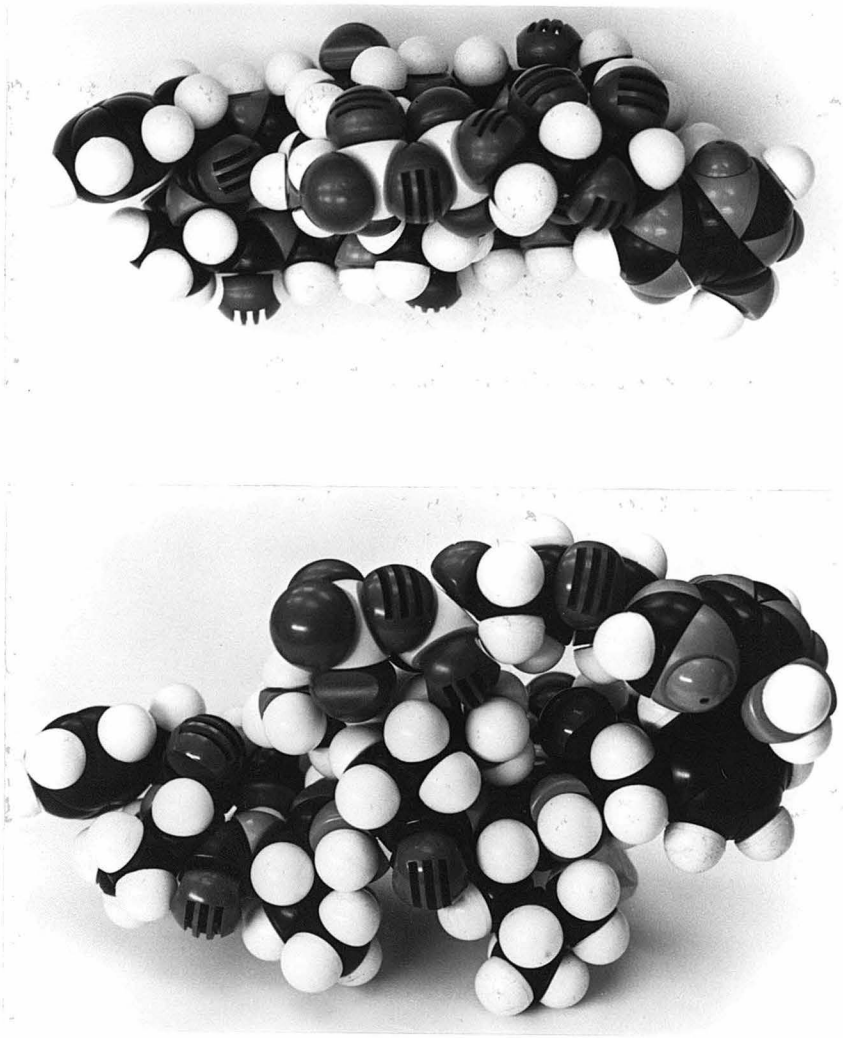

Figure 6. CPK model of the 1:1 ADP-GrS complex, viewed along (top) and perpendicular to (bottom) the symmetry axis of the peptide. The location of the adenine moiety relative to the peptide is arbitrary.

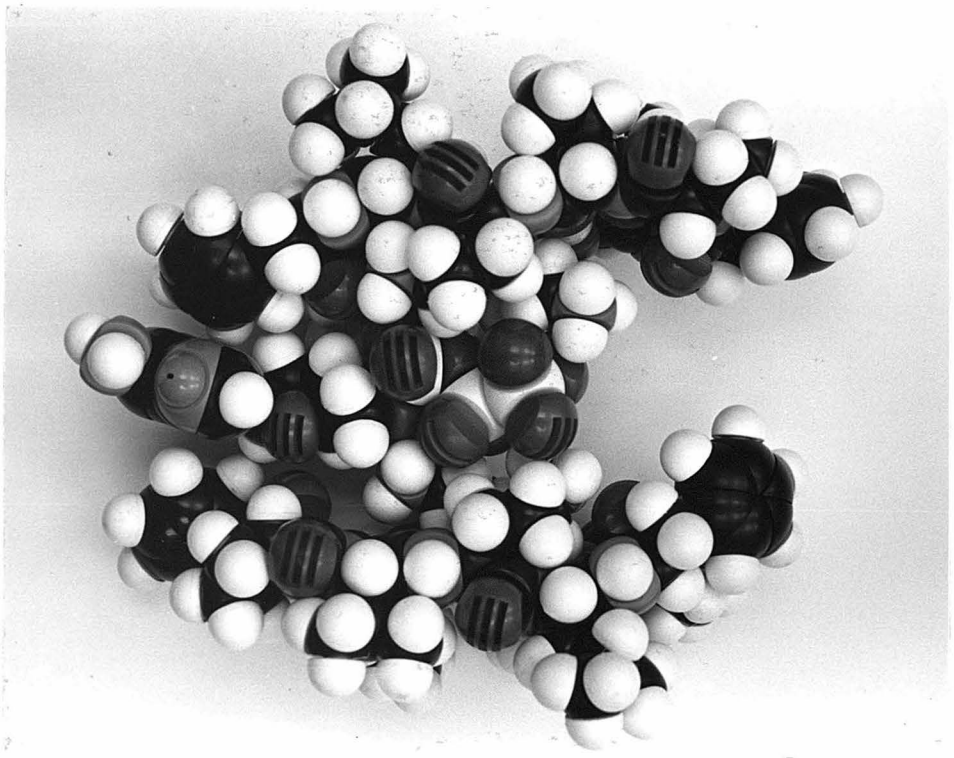

Figure 7. Lateral view of a CPK model of the 1:2 ATP-GrS complex. The nucleotide is sandwiched between the peptide molecules, which are proposed to lie with ring planes and major ring axes parallel. The exposed hydrophobic surfaces are parallel to the ring planes and perpendicular to the plane of the figure.

in water most likely proceeds via interaction of the hydrophobic surfaces, leaving the polar lateral faces, which direct aggregation in solvents such as $CHCl_3$, relatively exposed.

Whereas species such as ATP^{3-} or ADP^{3-} were generally present in solution under the conditions employed in the extractions, 2:3 stoichiometries were not observed. This is not surprising in view of the large energetic cost incurred in forming such complexes from, e.g., the interaction of a free GrS molecule with a dimer of negatively charged 1:1 complexes in which the uncomplexed residual negative charges are closely apposed. Furthermore, the GrS ring axes in 2:3 complexes cannot be aligned parallel to one another, so that self-association of the complexes in organic media is greatly hindered. Since the phase transfer stoichiometries do not reflect the equilibrium mixture of ionization states of the nucleotide, either proton shifts must occur or the extracted complexes are not uniformly neutral. That the pH decreases significantly during the initial period of extraction of ATP at pH 7 suggests that transfer of the uncharged complex is predominant.

It should be emphasized that what is transferred to $CHCl_3$ are specific nucleotide complexes or aggregates of specific complexes, and not micellar aggregates. The possibility of micelle formation must be considered in light of the large apparent size of the aggregates, inferred from the NMR linewidths in $CHCl_3$, and the known amphiphilicity of the peptide. While GrS may form a monolayer at the phase boundary (13, 25), there is no evidence that it is capable of forming or entering a micelle in the absence of other amphiphiles. The

observation of distinct and well-defined stoichiometries of phase transfer for different nucleotides eliminates the possibility of micellar entrapment.

Analysis of Phase Transfer: 1:1 Complexes. The 1:1 equilibrium extraction of monovalent cations into organic solvents by macrotetralide antibiotics has been treated previously by Eisenman et al. (20). Whereas the analysis of the extraction of nucleotides by GrS parallels this to a certain extent, there are several important differences, namely (a) the high efficiency of the extraction, which raises the possibility that the partition coefficient of the complex, rather than the binding constants, can limit $\underline{E}$; (b) multistep binding in the 1:2 complexes; (c) aggregation of the complexes in the aqueous and organic phases.

The binding constant for the 1:1 interaction in water is defined by Eq. 2, and the macroscopic partition coefficient is defined by

$$a + g \rightleftarrows ag \qquad \underline{K} \equiv \frac{[ag]}{[a][g]} \tag{2}$$

Eq. 3, where lower- and uppercase letters denote species in the

$$ag \rightleftarrows AG \qquad \underline{K}_p \equiv \frac{[AG]}{[ag]} \tag{3}$$

aqueous and organic phases, respectively. An additional parameter ζ specifies the initial ratio of GrS to nucleotide concentration and is defined for a 1:n interaction by $\zeta = [g]_i / n[a]_i$.

If complex aggregation is, for the moment, neglected, and the

volume ratio of the phases is assumed to be unity, Eqs. 2 and 3 may be solved to yield a simple expression for $\underline{E}$ which satisfactorily describes the observed extraction profiles (the variation in $\underline{E}$ with $[a]_i$) for fixed ζ:

$$\frac{\underline{E}}{(1 - \underline{P}\underline{E})(\zeta - \underline{P}\underline{E})} = [a]_i \frac{\underline{K}\underline{K}_p}{1 + \underline{K}_G} \qquad (4)$$

Here, $\underline{P} \equiv 1 + \underline{K}_p^{-1}$, and $\underline{K}_G = 0.2$ is the partition coefficient of free GrS into $CHCl_3$. Two types of saturation phenomena are clearly predicted by Eq. 4. The first, phase saturation, is encountered at high $[a]_i$ for $\zeta \geq 1$, where $(1 - \underline{P}\underline{E}) \rightarrow 0$ or $E \rightarrow \underline{P}^{-1}$, a function of $\underline{K}_p$ only. The second, stoichiometric saturation, limits $\underline{E}$ when $\zeta < 1$, since GrS can extract no more of the nucleotide than it can bind stoichiometrically. In this case, $\underline{E} \rightarrow \zeta \underline{P}^{-1}$ with increasing $[a]_i$. The two forms of saturation are discussed further in connection with the phase transfer of ATP. It should be mentioned concerning Eq. 4 that, for $\underline{K}_p$ sufficiently large and $[a]_i$ sufficiently small, the coefficients in the denominator on the left side may be taken as unity, with the resulting expression essentially equivalent to that derived for the phase transfer of cations by macrotetralides (20).

The extraction data obtained for the 1:1 interactions between ADP and GrS at pH 7 (Fig. 8) and between ATP and GrS at pH 3 (Fig. 9) are displayed with curves fitted to the data according to Eq. 4 utilizing the procedure outlined under Experimental Methods. The fitted values of $\underline{K}$ and $\underline{K}_p$ are given in Table IV. There is no significant difference in these parameters between the two types of complex.

Figure 8. Extraction of ADP by GrS at pH 7 with $\zeta = 1$. The curve was plotted according to Eq. 4 using the fitted parameters $\underline{K}$ and $\underline{K}_p$ listed in Table IV.

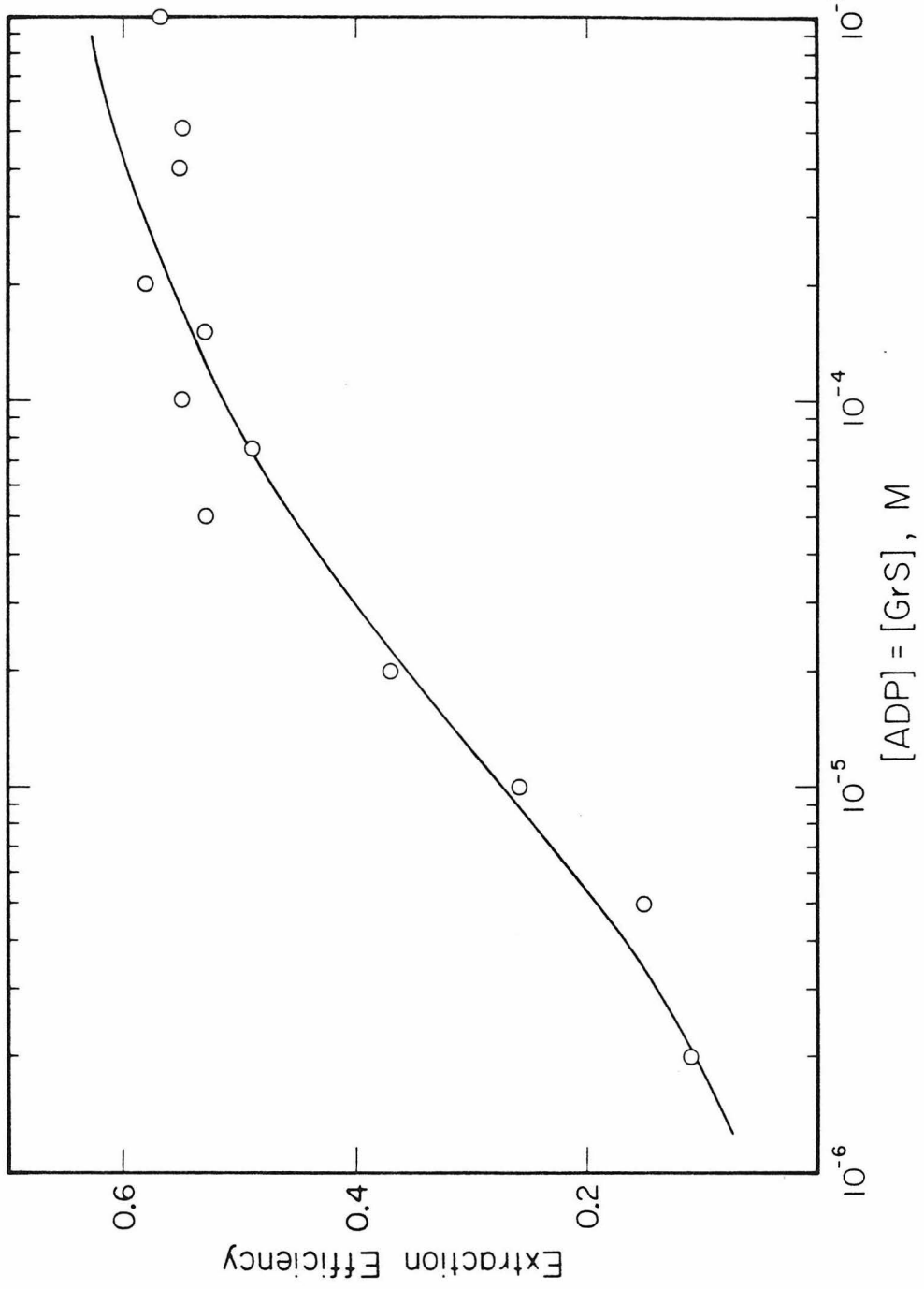
Extraction Efficiency
0.6
0.4
0.2
10^{-6}
10^{-5}
10^{-4}
10^{-3}
[ADP] = [GrS], M

Figure 9. Extraction of ATP by GrS at pH 3 (open circles, 1:1 stoichiometry) and pH 7 (closed circles, 1:2 stoichiometry) with [GrS]/[ATP] = 1, with curves plotted according to Eqs. 4 and 6, respectively. The parameters fitted to the $\zeta = 1$ profile at pH 7 by Eq. 6 (Fig. 11) were utilized for the pH 7 profile here.

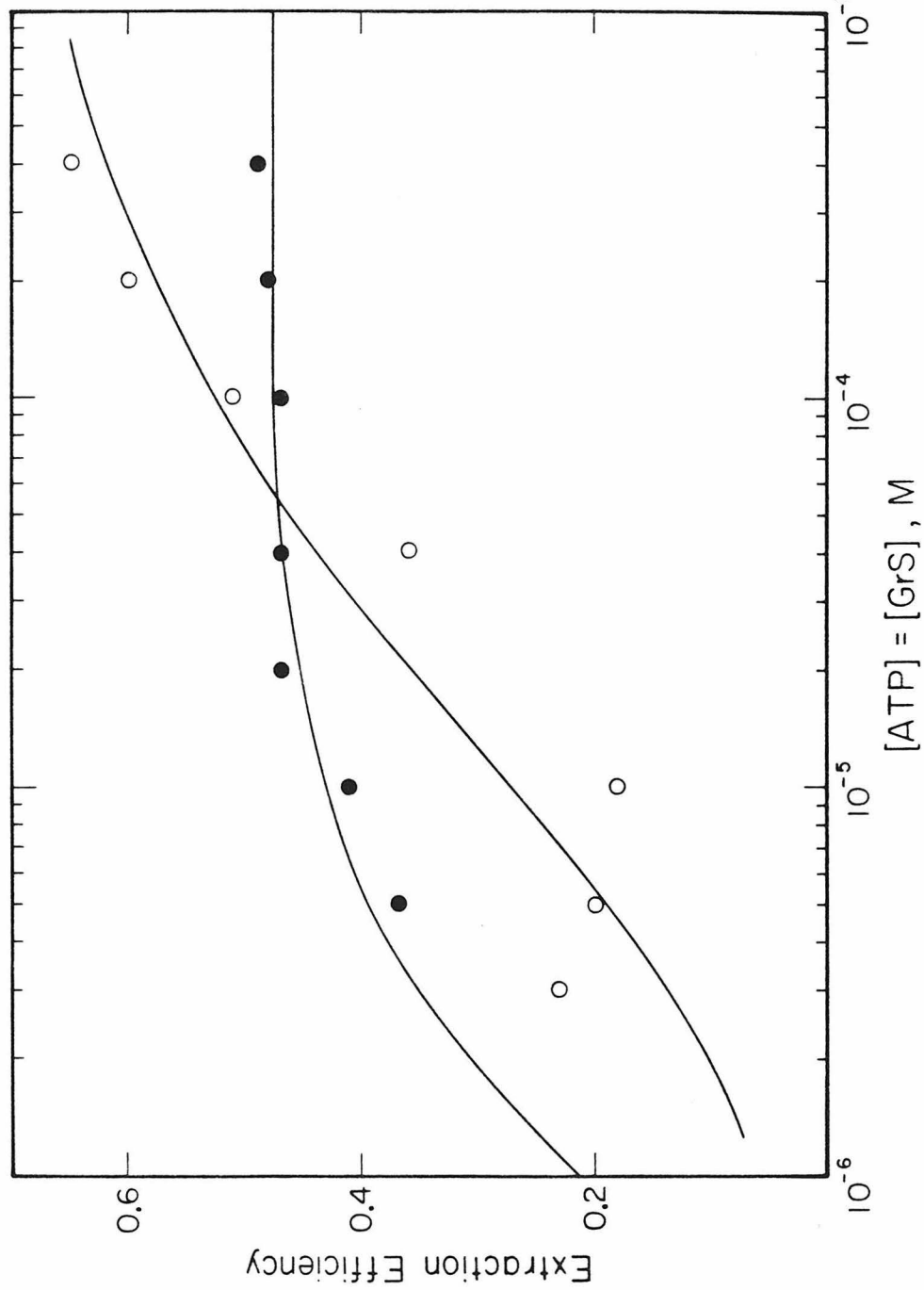
Extraction Efficiency
0.6
0.4
0.2
10^{-6}
10^{-5}
10^{-4}
10^{-3}
[ATP] = [GrS], M

Table IV. Estimated Binding and Partition Constants for GrS[a]

Nucleotide	pH	Stoichiometry	Method	log $\underline{K}_1$	log $\underline{K}_2$	log $\underline{K}_p$	log $\underline{K}_w$	log $\underline{K}_p^2\underline{K}_o$
ADP	7	1:1	Eq. 4	4.6 ± 0.2		0.4±0.1		
			Eq. 5	4.5 ± 0.5			~6	~6
ATP	3	1:1	Eq. 4	4.5±0.4		0.4± 0.2		
ATP	7	1:2	Eq. 6	10.8 ± 0.3[b]		1.3± 0.1		
			Eq. 7 (Case I)	4.5 ± 0.5	4.5 ± 0.5		~8.5	~9.5
			Eq. 7 (Case II)	4.5 ± 0.5	5 ± 1[c]		d	d

[a]In log M^{-1}, except log $\underline{K}_p$. [b]log $\underline{K}$, in log M^{-2}. [c]$\underline{K}_2/\underline{K}_1 < 100$ (see text). [d]Varies with $\underline{K}_2$ (see Fig. 13).

Here, $\underline{K}$ for ADP represents the equilibrium constant for the concerted formation of two ion pairs between the Orn $N^{\delta}H_3^+$ groups of GrS and the vicinal phosphoryl groups of the nucleotide. If the ion pairs are equivalent, a $\Delta\underline{G}^{\circ}$ of -3.1 kcal mol^{-1} is estimated for each, to which both electrostatic attraction and hydrogen bonding contribute. In the case of ATP, GrS can interact either with vicinal or (α,γ) phosphoryl groups. However, if adenine N^1 forms an intramolecular salt bridge in $CHCl_3$, as seems likely, it should most easily do so with the terminal phosphoryl; thus, in its final configuration the groups which interact with the peptide in the 1:1 ATP complex are vicinal, as in the ADP complex, and the binding constant is nearly the same. The similarity in the estimated values of $\underline{K}_p$ is also not unexpected, as the complexes possess similar surface properties.

The question of complex aggregation emerges when considering the extraction profiles for $\zeta > 1$. When $\zeta = 2$, for example, $\underline{E}$ plateaus at significantly higher values than expected for the partition coefficients estimated from Eq. 4 (>0.95 for ADP, >0.99 for ATP at pH 7). Since a significant change in stoichiometry with ζ appears ruled out by NMR, it is necessary to consider explicitly the colligative properties of the complexes. This cannot presently be done rigorously, because we lack the means for measuring the aggregation states of the complex in solution. However, by generalizing the scheme outlined above to include the noncooperative association of complexes, it is possible to reproduce the extraction profiles with reasonable accuracy while removing the artificial restriction on activity coefficients implied in Eq. 3. In the Appendix, a binding equation is derived which takes

into account the effects of aggregation (Eq. 5),

$$(1 - \underline{r})^2([a] - [a]_i) + \left[\frac{\underline{r}}{\underline{K}_w}\right](1 + \underline{K}_p) + \left[\frac{\underline{r}}{\underline{K}_w}\right]^2 \underline{K}_p(\underline{K}_p\underline{K}_o - \underline{K}_w) = 0 \tag{5}$$

where $\underline{r} = \underline{K}\underline{K}_w[a][g]$, and from which $\underline{E}$ may be computed directly. The concentrations of all species are sufficiently low ($< 5 \times 10^{-4}$ M) that activity coefficients are assumed close to unity. This derivation is based on the following provisions concerning the aggregation process: (i) Self-association occurs noncooperatively in both phases, characterized by second order association constants $\underline{K}_w$ (aqueous) and $\underline{K}_o$ (organic), $\underline{K}_w < \underline{K}_o$, and (ii) the apparent partition coefficient of an aggregate, because of structural rearrangements occurring on phase transfer which sequester solvophobic groups, is slowly varying function of the number of contained monomeric complexes. It is further proposed that excess GrS, which is largely confined to the aqueous phase, interacts weakly with the aggregates as an amphiphile and causes a decrease in the average aggregation number in water (defined in the Appendix). According to this scheme, GrS in super-stoichiometric amounts brings about a decrease in the observed $\underline{K}_w$ and, consequently, an increase in the total concentration of aggregates in water, which promotes greater transfer across the phase boundary into $CHCl_3$.

As indicated in Fig. 10, simultaneous simulation of both the $\zeta = 1$ and $\zeta = 2$ extraction profiles for ADP at pH 7 is possible only for values of the binding constant falling within a limited range. Good

Figure 10. Computed extraction profiles (Eq. 5) for the extraction of ADP by GrS with $\zeta = 1$ (a) and $\zeta = 2$ (b). The method of calculation is described in the Appendix. $\zeta = 1$: (----), $\underline{K} = 3 \times 10^3\ M^{-1}$, $\underline{K}_w = 1.5 \times 10^7\ M^{-1}$, $\underline{K}_p^2 \underline{K}_o = 2 \times 10^7\ M^{-1}$; (——), $\underline{K} = 3 \times 10^4\ M^{-1}$, $\underline{K}_w = 1 \times 10^6\ M^{-1}$, $\underline{K}_p^2 \underline{K}_o = 1.5 \times 10^6\ M^{-1}$; (. . . .), $\underline{K} = 6 \times 10^4\ M^{-1}$, $\underline{K}_w = 7 \times 10^5\ M^{-1}$, $\underline{K}_p^2 \underline{K}_o = 1 \times 10^6\ M^{-1}$; (-.-.-), $\underline{K} = 3 \times 10^5\ M^{-1}$, $\underline{K}_w = 1.5 \times 10^5\ M^{-1}$, $\underline{K}_p^2 \underline{K}_o = 2.5 \times 10^5\ M^{-1}$. $\zeta = 2$: $\underline{K}$ and $\underline{K}_p^2 \underline{K}_o$ as above; $\underline{K}_w = 1 \times 10^4\ M^{-1}$.

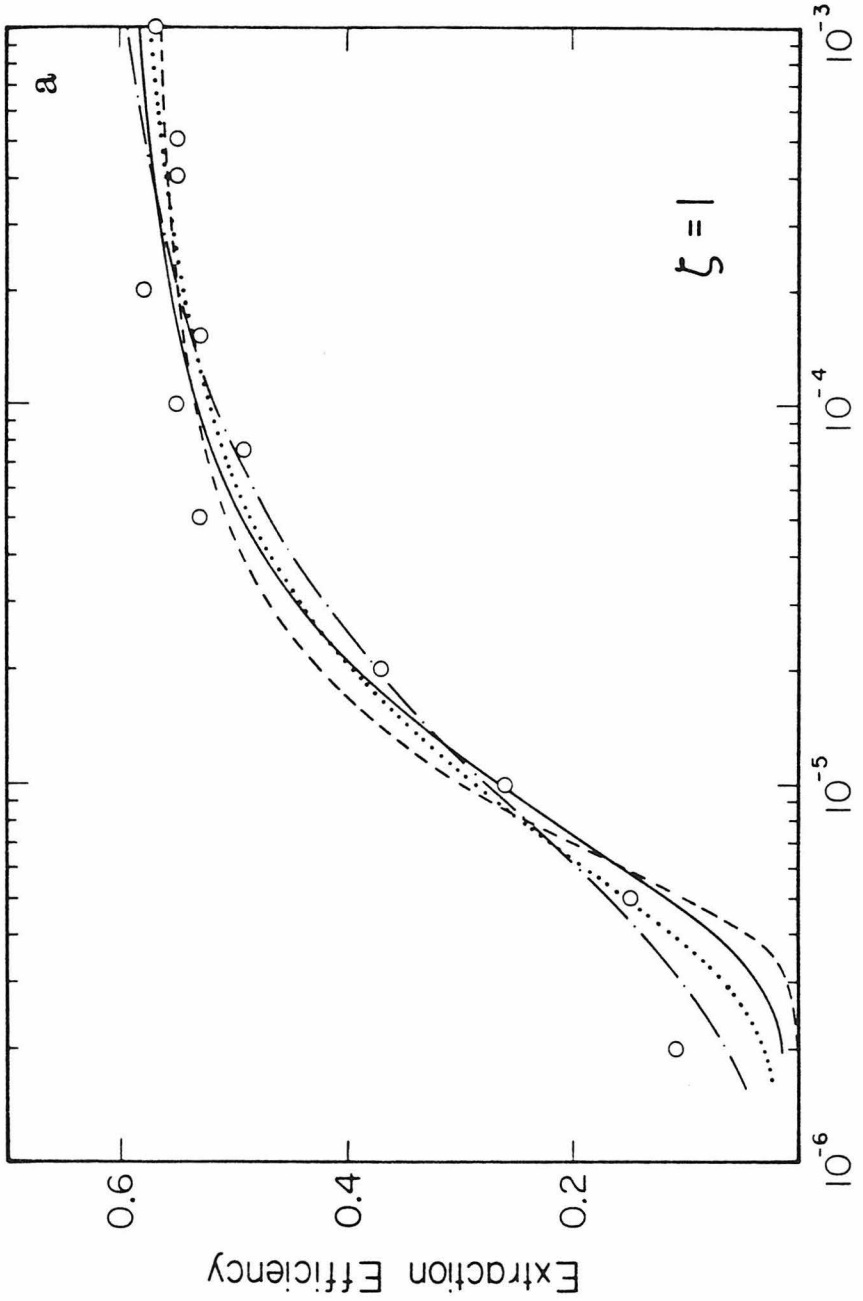
a
ζ = 1
Extraction Efficiency
0.6
0.4
0.2
10^{-6}
10^{-5}
10^{-4}
10^{-3}
[ADP] = [GrS], M

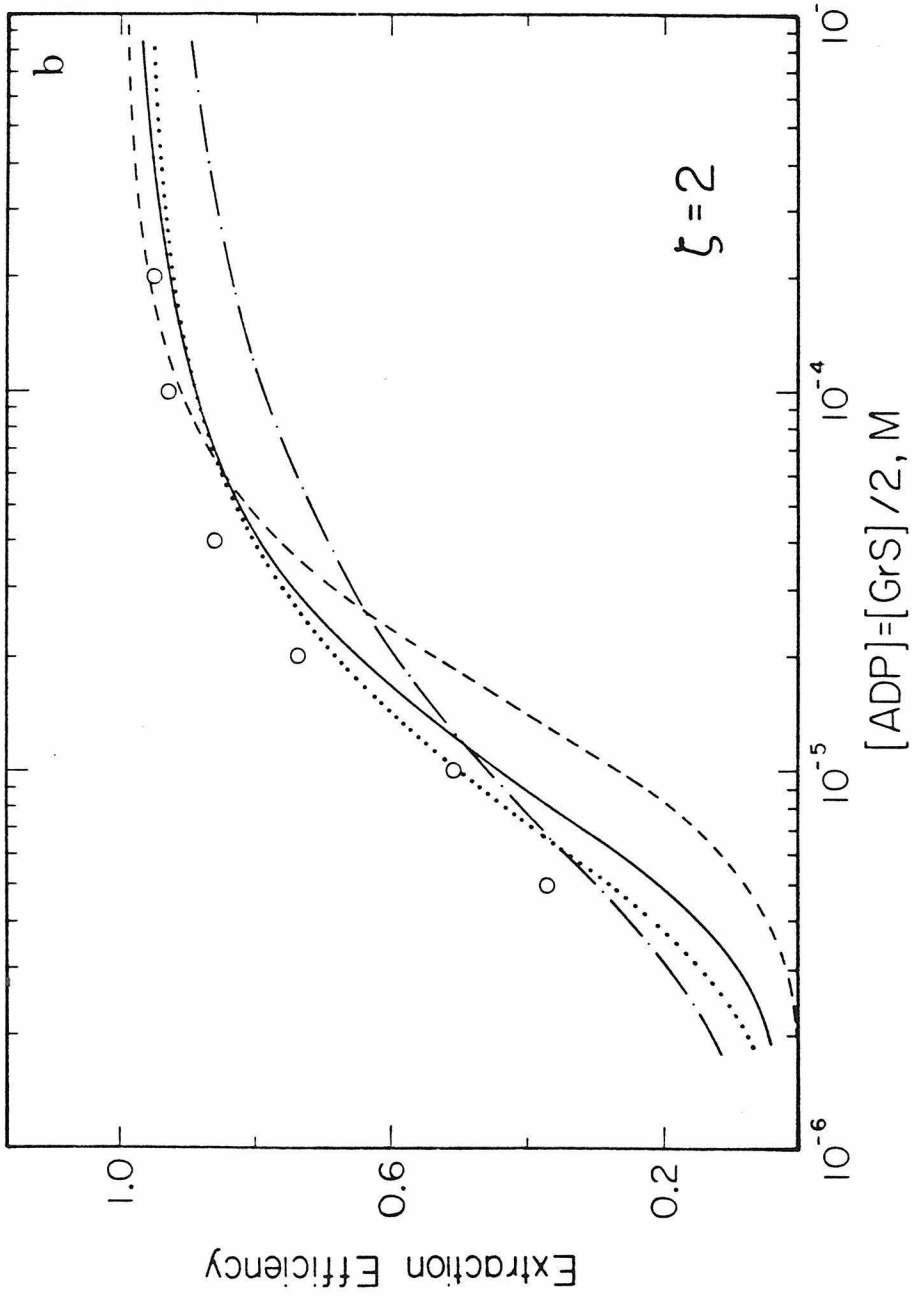
b
ζ=2
Extraction Efficiency
1.0
0.6
0.2
10^{-6}
10^{-5}
10^{-4}
10^{-3}
[ADP]=[GrS]/2, M

agreement with the experimental results is obtained when $10^4\ M^{-1} \leq \underline{K} \leq 10^5\ M^{-1}$, in which case modest (2-10) aqueous aggregation numbers are estimated. When $\underline{K}$ is too small, there is excessive curvature in both computed profiles, resulting in particularly large discrepancies between the calculated and observed values of $\underline{E}$ at low $[a]_i$. For $\underline{K} \geq 10^5\ M^{-1}$ the aggregation numbers for the aqueous phase ($\zeta = 1$) approach unity, and the $\zeta = 2$ simulation consequently fails. Thus, despite the difficulties inherent in the inclusion of complex association in the quantitative treatment of phase transfer, it is still possible to obtain a reasonably precise estimate of the 1:1 binding constant, $\underline{K}_{1:1}$. This will prove useful in the analysis of the 1:2 binding problem, since $\underline{K}_{1:1}$ should constitute a lower limit to the association constants for the interaction of GrS with ATP at pH 7. It should be noted that the concordance between the values of $\underline{K}$ estimated for the 1:1 interaction by Equations 4 and 5 is largely fortuitous, expected only if the aqueous aggregation numbers are sufficiently low. The parameter estimates obtained for the extended treatment are given in Table IV.

Extraction of 1:2 Complexes. The change in stoichiometry of the ATP extraction with pH is clearly reflected in the extraction profiles in Fig. 9. In each case, $[g]_i/[a]_i = 1$, but the curvature and limiting efficiencies differ, and the profiles intersect when $[a]_i \sim 5 \times 10^{-5}$ M. At pH 3, $\zeta = 1$ and phase saturation is encountered at high $[a]_i$, as described above, while at pH 7, $\zeta = 0.5$ and stoichiometric saturation is observed. When $[g]_i$ is not limiting, the 1:2 ATP

extraction is even more efficient than the superstoichiometric ($\zeta = 2$) ADP extraction (compare Fig. 10 and Fig. 11).

As a starting point in the analysis, the ATP data were fitted to Eq. 6, the analog of Eq. 4 for the 1:2 interaction, where $\underline{K} \equiv [ag_2]/[a][g]^2$, i.e. sequential binding with full cooperativity is

$$\frac{\underline{E}}{(1 - \underline{PE})(\zeta - \underline{PE})^2} = \left[\frac{2[a]_i}{1 + K_G}\right]^2 \underline{K}K_p \qquad (6)$$

assumed (Table IV). Not surprisingly, the estimated $\underline{K}_p$ is significantly larger than that obtained for the 1:1 complexes through application of Eq. 4. In addition, it is found that $\underline{K} > \underline{K}^2_{1:1}$; however, this estimate of $\underline{K}$ must be regarded as suspect, since Eq. 6 appears consistently to overestimate $\underline{E}$ for low $[a]_i$ (Fig. 11), where the slope and sensitivity to $\underline{K}$ of the extraction profile are greatest.

A systematic treatment of the 1:2 extraction requires inclusion of the aggregation constants $\underline{K}_W$ and $\underline{K}_O$ and, in addition, definition of separate binding constants $\underline{K}_1$ and $\underline{K}_2$ for the two binding steps. The question of two-step binding is approached by considering GrS to be a bidentate ligand which complexes one of two available pairs of charges on the triphosphate. Two limiting cases are then defined. In the first, the charge pairs constitute two independent, noninteracting sites for peptide binding, and the microscopic binding constants formally are $\underline{K}_1 \equiv [ag]/[a][g] = [ag_2]/[ag']/[g]$ and $\underline{K}_2 \equiv [ag']/[a][g] = [ag_2]/[ag][g]$ (case I). It is possible, although somewhat misleading, to regard each site as corresponding to a specific pair of phosphoryl

Figure 11. Extraction of ATP by GrS at pH 7 with $\zeta = 1$. The curve was plotted according to Eq. 6 using the fitted parameters $\underline{K}$ and $\underline{K}_p$ listed in Table IV.

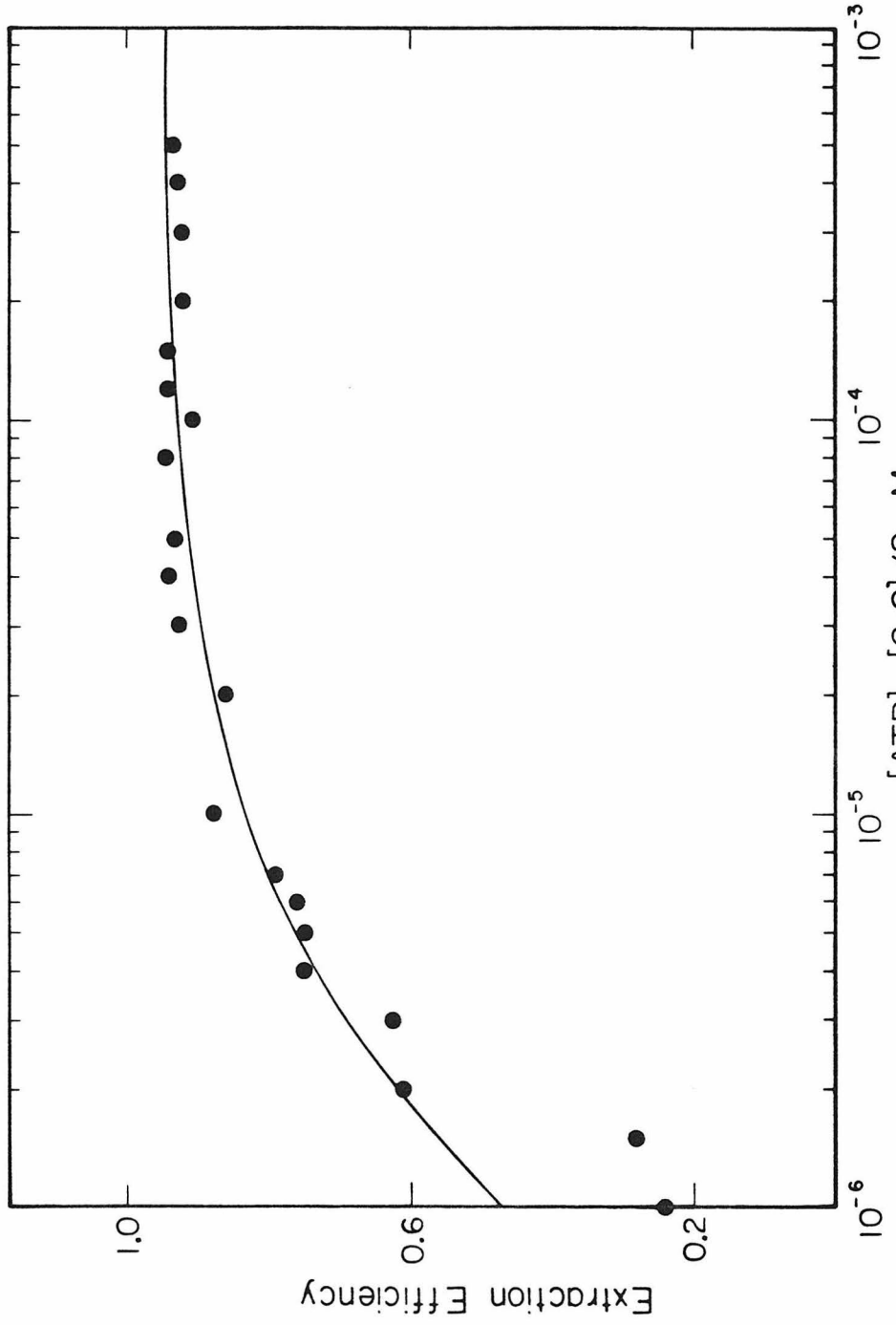
Extraction Efficiency
1.0
0.6
0.2
10^{-6}
10^{-5}
10^{-4}
10^{-3}
[ATP] = [GrS]/2, M

groups. In case II, binding is obligatorily sequential. After the first binding step, a second binding site becomes available, conceivably through facilitated deprotonation of trianionic nucleotide species present in ag complexes. Cooperative effects may arise if, after binding the second GrS molecule, rotameric isomerization within the triphosphate improves the topochemical fit with the cationic moieties of both peptides. Here, $\underline{K}_1 \equiv [ag]/[a][g]$ and $\underline{K}_2 \equiv [ag_2]/[ag][g]$. In either case, it is assumed that only ag_2 species undergo phase transfer, and that $\underline{K}_1, \underline{K}_2 \geq (\log^{-1} 4.5)\ M^{-1}$. The extended equation for binding, including complex aggregation, is (Appendix)

$$(1 - \underline{r})^2 ([a] + \underline{u}(\underline{K}_1, \underline{K}_2)[a][g] - [a]_i) + \left[\frac{\underline{r}}{\underline{K}_w}\right](1 + \underline{K}_p) + \left[\frac{\underline{r}}{\underline{K}_w}\right]^2 \underline{K}_p(\underline{K}_p\underline{K}_o - \underline{K}_w) = 0 \qquad (7)$$

where $\underline{r} = \underline{K}_w\underline{K}_1\underline{K}_2[a][g]^2$ and $\underline{u}(\underline{K}_1, \underline{K}_2) = \underline{K}_1 + \underline{K}_2$ (case I) or $\underline{K}_1$ (case II). The binding equilibria are summarized below:

$$a + g \overset{\underline{K}_1}{\rightleftharpoons} ag \ ; \ a + g \overset{\underline{K}_2}{\rightleftharpoons} ag' \qquad \text{Case I}$$

$$a + g \overset{\underline{K}_1}{\rightleftharpoons} ag \ ; \ ag + g \overset{\underline{K}_2}{\rightleftharpoons} ag_2 \qquad \text{Case II}$$

The calculated profiles are compared with the simple extraction profile for $\zeta = 1$ and a pseudotitration in which $\underline{E}$ is measured as a function of ζ ($\zeta < 1$) with $[a]_i = 10^{-4}$ M (Fig. 12,13). Use of the two sets of data make it possible to define acceptable ranges for the binding constants in each case, much as the $\zeta = 2$ profile had provided helpful

constraints on the likely values of $\underline{K}_{1:1}$. (A $\zeta = 2$ profile could not accurately be measured here since $E \sim 1$ over most of the concentration range). The pseudotitration is noteworthy in that $\underline{E} \sim \zeta$ for values of ζ as low as 0.05, which would, in the absence of colligative effects, indicate highly cooperative binding.

For case I (Fig. 12) it is found that simulation of the $\zeta = 1$ extraction profile is possible for a wide range of values of $\underline{K}_1$ and $\underline{K}_2$. This is evidently not true of the pseudotitration, however, where the calculated curves fall well short of the data unless $\underline{K}_1 \sim \underline{K}_2 \sim \underline{K}_{1:1}$. For binding constants satisfying the latter criteria the apparent cooperativity in the pseudotitration arises from efficient complex aggregation in both phases (Table IV). Case II suggests a range of $\underline{K}$'s which does not greatly differ from that deduced for case I (Fig. 13). The $\zeta = 1$ profile is well approximated if $\underline{K}_2/\underline{K}_1 \leq 10$ when $\underline{K}_1 \underline{K}_2 > 10^{11}\ M^{-2}$. For high values of the product of the binding constants with strong cooperativity, the computed and observed profiles diverge at low $[a]_i$ in a manner similar to that seen in Fig. 11. Simulation of the pseudotitration, on the other hand, requires that when $\underline{K}_1 \underline{K}_2 > 10^{11}\ M^{-2}$, $\underline{K}_2/\underline{K}_1 > 10$. The data are thus consistent with case II for the ranges of binding constants listed in Table IV, corresponding to $\underline{K}_1 \sim \underline{K}_{1:1}$ with weak cooperativity ($1 \leq \underline{K}_2/\underline{K}_1 < 100$).

Differentiation between the two cases is not possible on basis of the phase transfer data. Of them, case I appears inherently simpler, involving only stochastically independent binding to a polyanion possessing two equivalent binding sites with microscopic affinity essentially equal to that estimated for the 1:1 interaction. However,

Figure 12. Computed extraction profiles (Eq. 7) for the extraction of ATP by GrS with $\zeta = 1$ (a) and for the pseudotitration (b). The two cases are defined in the text, and the method of calculation is described in the Appendix. Case I: (——), $\underline{K}_1 = 3 \times 10^4\ M^{-1}$, $\underline{K}_2 = 3 \times 10^4\ M^{-1}$, $\underline{K}_w = 1 \times 10^9\ M^{-1}$, $\underline{K}_p \underline{K}_o^2 = 1.5 \times 10^{10}\ M^{-1}$; (-.-.-), $\underline{K}_1 = 1 \times 10^5\ M^{-1}$, $\underline{K}_2 = 1 \times 10^5\ M^{-1}$, $\underline{K}_w = 7 \times 10^7\ M^{-1}$, $\underline{K}_p \underline{K}_o^2 = 1 \times 10^9\ M^{-1}$; (----), $\underline{K}_1 = 1 \times 10^5\ M^{-1}$, $\underline{K}_2 = 1 \times 10^6\ M^{-1}$, $\underline{K}_w = 1 \times 10^7\ M^{-1}$, $\underline{K}_p \underline{K}_o^2 = 1.8 \times 10^8\ M^{-1}$; (.....), $\underline{K}_1 = 3 \times 10^4\ M^{-1}$, $\underline{K}_2 = 3 \times 10^6\ M^{-1}$, $\underline{K}_w = 3 \times 10^7\ M^{-1}$, $\underline{K}_p^2 \underline{K}_o = 5.4 \times 10^8\ M^{-1}$.

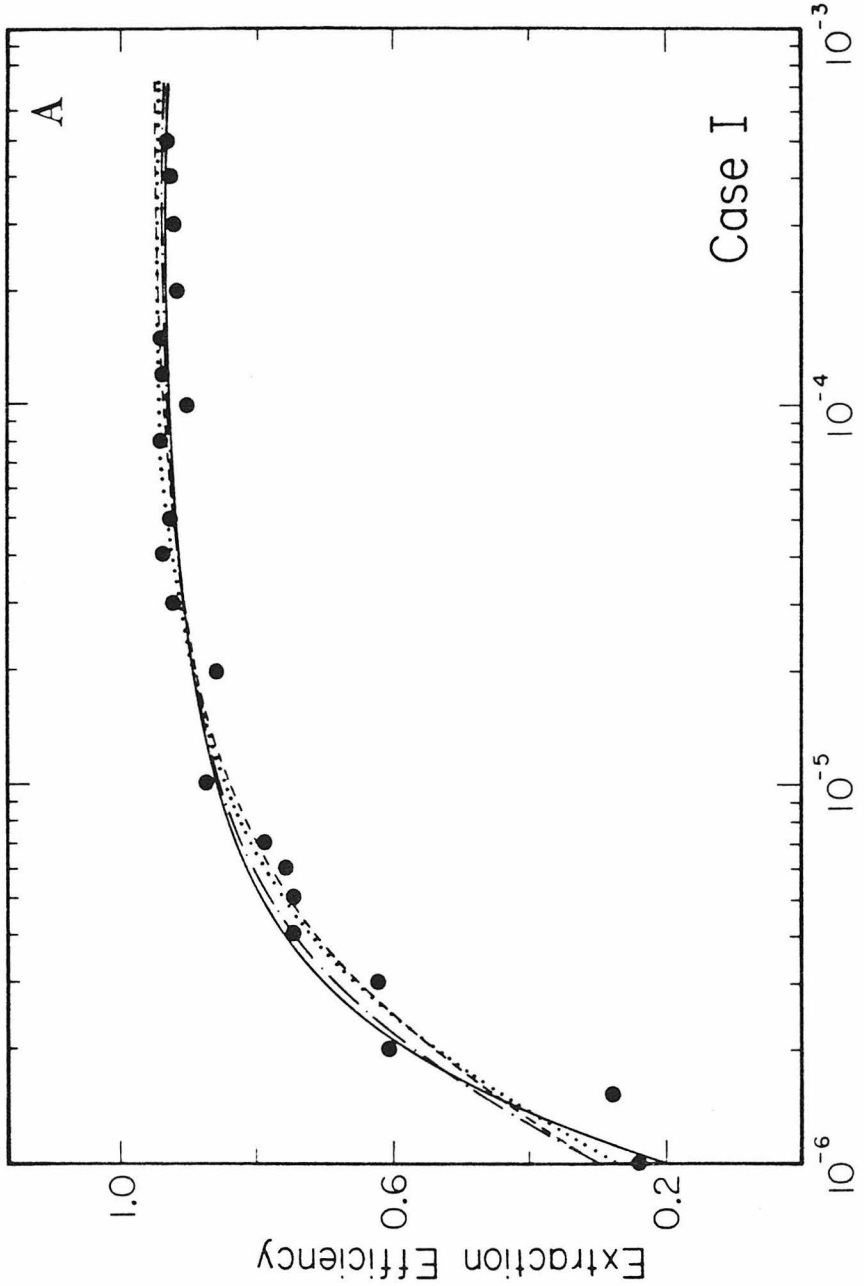
A
Case I
Extraction Efficiency
1.0
0.6
0.2
10^{-6}
10^{-5}
10^{-4}
10^{-3}
[ATP] = [GrS]/2, M

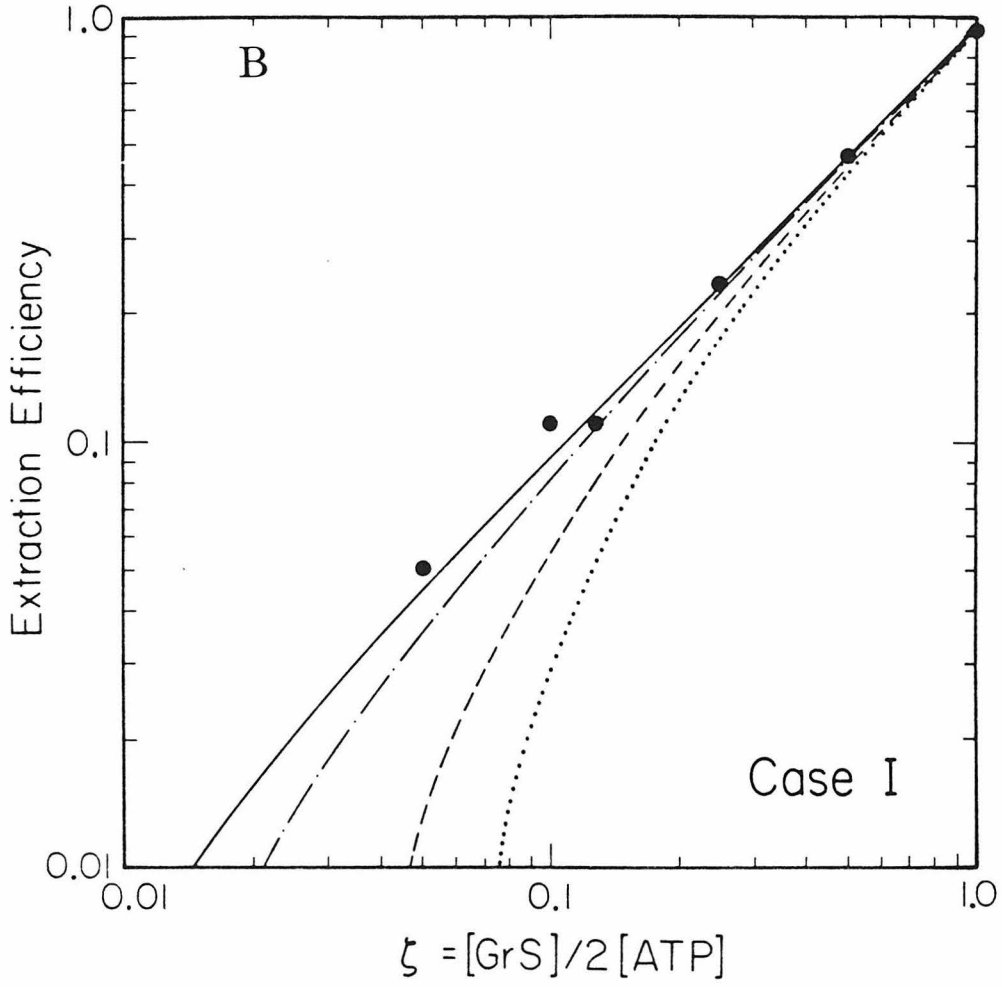
B
Case I
Extraction Efficiency
1.0
0.1
0.01
0.01
0.1
1.0
ζ = [GrS]/2[ATP]

Figure 13. Computed extraction profile (Eq. 7) for the extraction of ATP by GrS with $\zeta = 1$ (a) and for the pseudotitration (b). Case II: ($\underline{K} \equiv \underline{K}_1\underline{K}_2$, $\rho \equiv \underline{K}_2/\underline{K}_1$): (——), $\underline{K} = 3 \times 10^9\ M^{-2}$, $\rho = 1$, $\underline{K}_W = 2 \times 10^8\ M^{-1}$, $\underline{K}_p^2\underline{K}_o = 3 \times 10^9\ M^{-1}$; (-.-.-), $\underline{K} = 3 \times 10^{10}\ M^{-2}$, $\rho = 10$, $\underline{K}_W = 2 \times 10^7\ M^{-1}$, $\underline{K}_p^2\underline{K}_o = 3 \times 10^8\ M^{-1}$; (----), $\underline{K} = 3 \times 10^{11}\ M^{-2}$, $\rho = 100$, $\underline{K}_W = 3 \times 10^6\ M^{-1}$, $\underline{K}_p^2\underline{K}_o = 4.5 \times 10^7\ M^{-1}$; (.....), $\underline{K} = 1 \times 10^{11}\ M^{-2}$, $\rho = 1$, $\underline{K}_W = 7 \times 10^6\ M^{-1}$, $\underline{K}_p^2\underline{K}_o = 9 \times 10^7\ M^{-1}$.

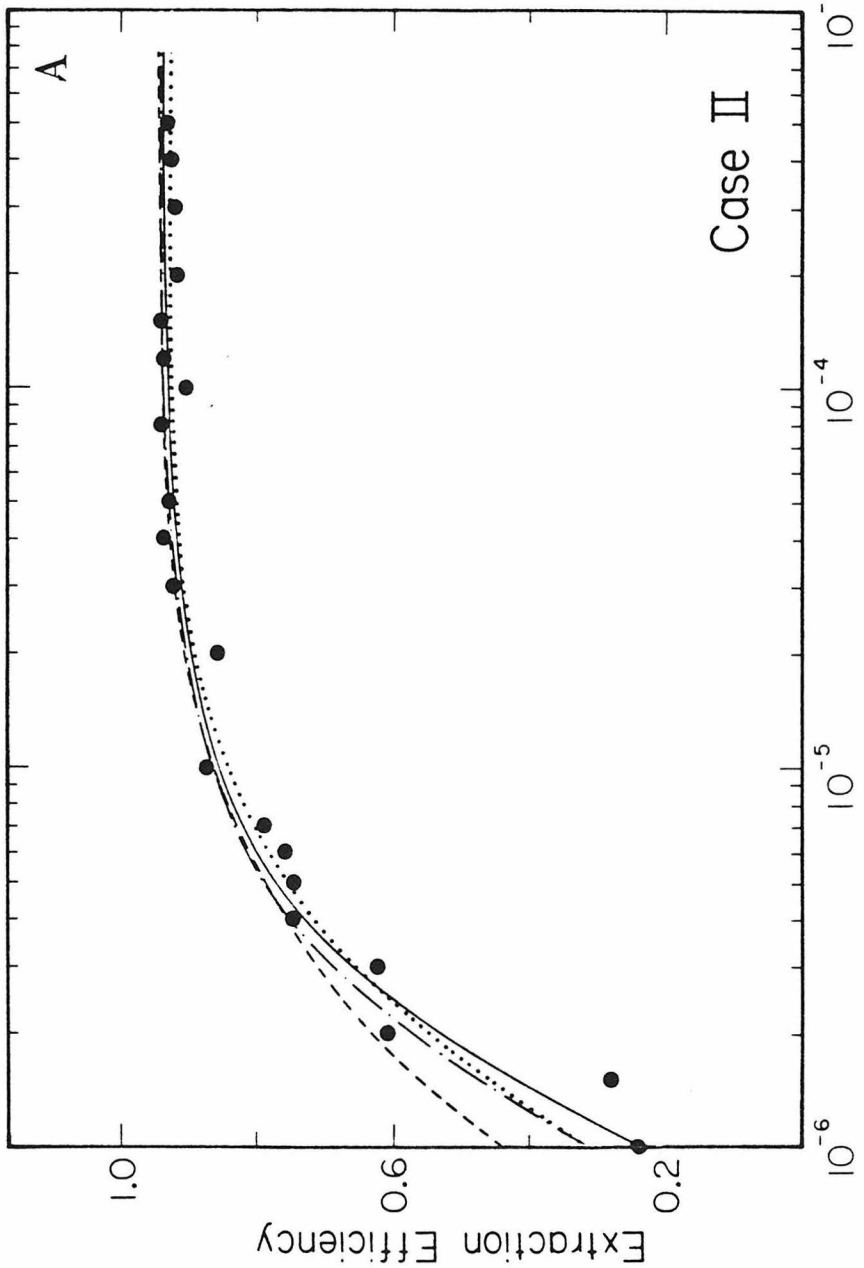
A
Case II
Extraction Efficiency
1.0
0.6
0.2
10^{-6}
10^{-5}
10^{-4}
10^{-3}
[ATP] = [GrS]/2, M

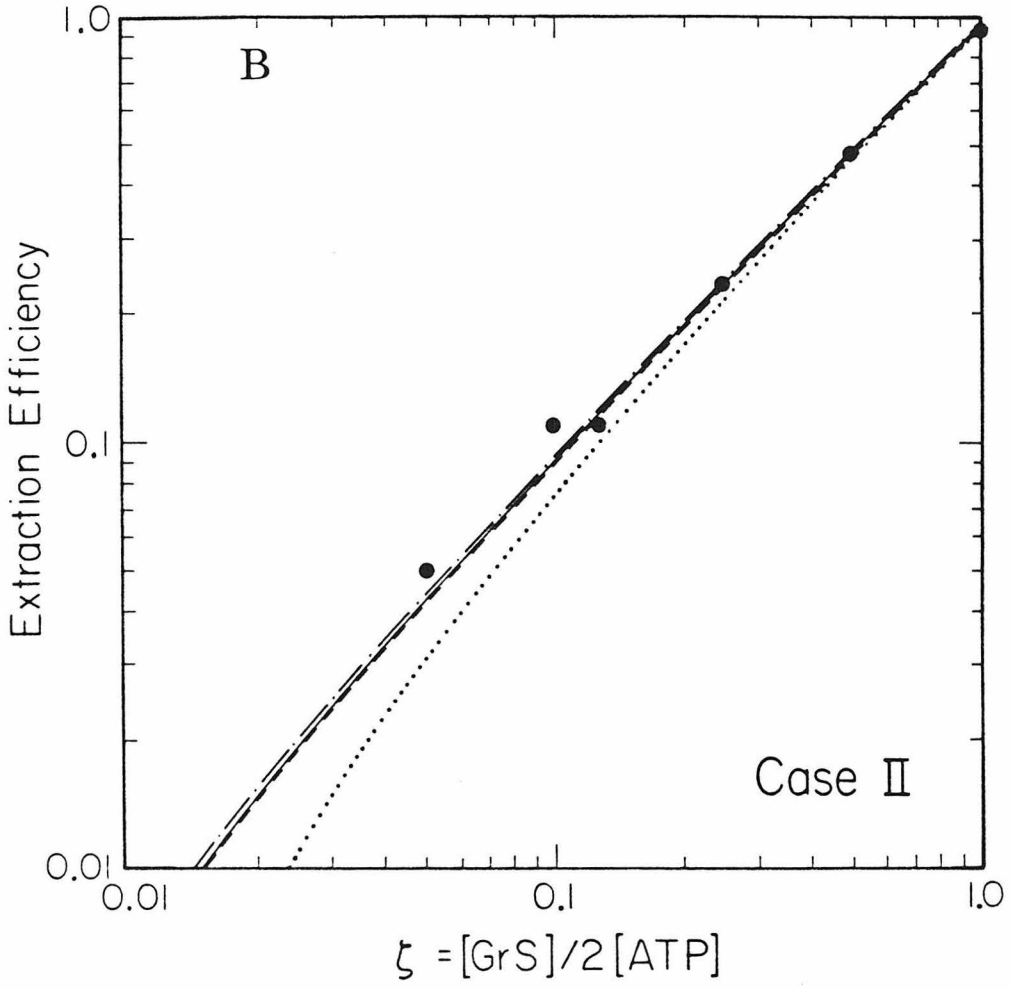
B
Case II
Extraction Efficiency
1.0
0.1
0.01
0.01
0.1
1.0
ζ = [GrS]/2[ATP]

since both cases ultimately provide estimates of $\underline{K}_1$ and $\underline{K}_2$ which are not appreciably larger than $\underline{K}_{1:1}$, the extended analysis clearly shows that complex aggregation is a major determinant of the apparent selectivity of GrS for the triphosphates in phase transfer.

Origin of Nucleotide Selectivity. Analysis of the phase transfer data has, in summary, provided similar estimates of the binding constants for the interaction between ADP and GrS at pH 7, ATP and GrS at pH 3, and the first step of the ATP-GrS interaction at pH 7, with $\Delta G_1^\circ = -\underline{RT} \ln \underline{K}_{1:1} \simeq -6.2$ kcal mol^{-1}. The binding constant for the second step of the ATP-GrS interaction is likely to be the same as or only slightly greater than this, and $\Delta \underline{G}_1^\circ - \Delta \underline{G}_2^\circ < 2$ kcal mol^{-1}. The selectivity of GrS for ATP over ADP in water at pH 7 is thus critically contingent upon the stoichiometry change, and is a consequence of differences in colligative behavior and an enhanced partition coefficient into the organic phase. It is not a manifestation of an intrinsically higher affinity of GrS for the triphosphate in the initial encounter complex.

4. Discussion

GrS is, to our knowledge, the first peptide known to possess phase transfer activity towards nucleotides. This property was suggested by the physicochemical studies described in the previous chapters which showed GrS to be a conformationally rigid, amphiphilic molecule containing two positively charged residues whose motions are limited by the formation of intramolecular hydrogen bonds to the backbone. In the present work, a combination of chemical and

spectroscopic methods have enabled us to characterize the structure, stoichiometry, and binding constants of several of the nucleotide coordination complexes of GrS which undergo transfer to organic media.

Although its solution structure is relatively well elucidated, the physiological role of GrS in the producer strain of B. brevis and the mechanism of antibiotic action against susceptible microorganisms are unclear. Concerning the latter, much consideration has been given the possibility of a direct interaction with membranes, either by insertion into the bilayer (26, 27, 28) or by electrostatic interaction with phospholipid head groups (29). Toxic effects would then result from disruption of permeability barriers (30) or inhibition of elements of the respiratory chain (17, 31). GrS is a surfactant (13, 25), and experimental evidence of its interaction with synthetic (26-28, 32, 33) or natural (34) membranes had been reported. However, the low sensitivity of the methods used to monitor GrS-membrane interactions invariably necessitates use of concentrations ~1000-fold greater than the minimum lethal concentration in vivo. Such methods have in a rigorous study by Wu et al. (28) failed to reveal any difference in membrane-binding affinity between GrS and a derivative containing a single positive charge, in contrast to the results of numerous bioassays (35). On the other hand, nucleotide binding and transport clearly occur in vitro at physiologically active concentrations of the antibiotic. The present study indicates that GrS should enter cells with little difficulty, either unassisted (possibly in monoprotonated form) or assisted by extra-

cellular P_i as the lipophilic complex. The formation of nucleotide-GrS complexes within the cell should produce a variety of toxic effects related to the depletion of high-energy phosphate metabolites; in addition, the ATP complex could partition into the membrane, conceivably as the cross-β aggregate, causing functional or structural impairment.

It has been amply demonstrated in previous investigations that GrS is associated with derangement of phosphate metabolism in microorganisms. Rapid efflux of nucleotides from a GrS-sensitive Micrococcus strain was observed to occur at antibiotic concentrations exceeding 10^{-6} M, which was the minimum lethal concentration for this organism (36). Whereas this might be attributable to a nonspecific lytic effect, rather than any direct interaction with the nucleotides, copious nucleotide secretion has been observed as well in mature cultures of B. brevis synthesizing GrS (15). Here, the effect is very likely mediated directly by GrS in its capacity as a phase transfer agent, since nucleotide efflux proceeds without evidence of destruction of the vegetative culture. Interestingly, the profile of depleted nucleotides in the producer strain (14) consists essentially of those for which GrS possesses the highest apparent selectivity. The relation of changes in the nucleotide pool to sporulation is unclear since B. brevis strains which are incapable of GrS synthesis and do not undergo nucleotide depletion nevertheless sporulate (37, 38).

Finally, study of the nucleotide-GrS interaction provides a further insight into biological transport phenomena not previously

suggested by investigations of synthetic anion complexones. Control of binding selectivity has generally been achieved through the synthesis of complexing agents which topochemically match their substrates (1). Presumably, the optimal model for a receptor site is the complexone which forms the most stable substrate complex with the highest degree of selectivity. All of the macrocyclic polyaza compounds reported (7, 9) show a greater or lesser degree of preference for ATP over ADP, however, most likely because of the critical importance of charge density in binding to these agents, and no complexone selective for ADP is presently known. The cytoplasmic terminus of the bongkrekate-sensitive ADP/ATP antiport of the inner mitochondrial membrane (39) is an example of a naturally occurring carrier site which is highly selective for ADP.

From the results of the present investigation, it is proposed that a relatively short solvent-exposed region of a membrane protein which is conformationally rigid, amphiphilic, and dicationic can function as the proximate receptor in a nucleoside diphosphate-selective carrier. Such a region is capable of binding other nucleotides, but under physiological conditions only a diphosphate will afford a neutral complex in which it is possible, by a conformational change in the membrane protein, for the nucleotide to be delivered through a hydrophobic zone to a second (cationic) acceptor or channel. Two such binding regions, closely apposed, would constitute a triphosphate-selective site; an antiport can be constructed from di- and triphosphate-selective sites on opposite sides of the membrane

which function alternately as primary and secondary acceptors. The GrS-nucleotide phase transfer paradigm suggests that selectivity in polyanion transport can be conferred, or even modulated, by dimeric association of structurally basic binding elements in membrane systems.

5. Appendix: Extended Phase Transfer Equation for Nucleotides

(a) 1:1 Association

Using the notation introduced in the text, the conservation of mass relations for nucleotide and peptide species are

$$[a]_i = [a] + \sum_j j[ag^{(j)}] + \sum_j j[AG^{(j)}] \tag{A1}$$

$$\zeta[a]_i = (1 + \underline{K}_G)[g] + \sum_j j[ag^{(j)}] + \sum_j j[AG^{(j)}] \tag{A2}$$

where the superscripts indicate the number of monomeric complexes in the aggregate. Combining Eqs. A1 and A2 provides a simple relationship between [g] and [a]:

$$[g] = ([a]_i(\zeta - 1) + [a])/(1 + \underline{K}_G). \tag{A3}$$

The binding constant $\underline{K}$ was defined by Eq. 2.

It is assumed that aggregation occurs with negligible cooperativity. Concerning the organic phase, it has been shown for the polymerization of N-methylacetamide in CCl_4 (40) that a single association constant is sufficient for all higher ($n > 2$) aggregates, and that the magnitude of this constant is ≤ 30 times that of the dimerization constant. Even this small degree of cooperativity is unlikely for GrS if, as discussed in the text, aggregation in $CHCl_3$ occurs by cross-β association through interamide hydrogen bonding, given the symmetry and rigidity of the peptide backbone. In water, where aggregation involves interaction of the apolar faces of the complexes, the relatively small size indicated for the soluble aggregates

by the observation of high resolution NMR spectral features and the total absence of precipitation after phase equilibration are noted. Second order association constants for water ($\underline{K}_w$) and the organic phase ($\underline{K}_o$) are thus defined for all $j, k = 1, 2, 3, \ldots$:

$$ag^{(j)} + ag^{(k)} \rightleftharpoons ag^{(j+k)};\ \underline{K}_w \equiv [ag^{(j+k)}]/[ag^{(j)}][ag^{(k)}]$$

$$AG^{(j)} + AG^{(k)} \rightleftharpoons AG^{(j+k)};\ \underline{K}_o \equiv [AG^{(j+k)}]/[AG^{(j)}][AG^{(k)}]$$

From these it is possible to express the sums of species in closed form:

$$\sum_j [ag^{(j)}] = \underline{r}/[\underline{K}_w(1 - \underline{r})] \tag{A4}$$

$$\sum_j j[ag^{(j)}] = \underline{r}/[\underline{K}_w(1 - \underline{r})^2] \tag{A5}$$

$$\sum_j [AG^{(j)}] = \underline{R}/[\underline{K}_o(1 - \underline{R})] \tag{A6}$$

$$\sum_j j[AG^{(j)}] = \underline{R}/[\underline{K}_o(1 - \underline{R})^2] \tag{A7}$$

where $\underline{r} \equiv \underline{K}\underline{K}_w[a][g]$ and $\underline{R} \equiv \underline{K}_o[AG^{(1)}]$. In addition, it is recalled from the definition of the extraction efficiency that

$$\sum_j j[AG^{(j)}] = [a]_i \underline{E}\ . \tag{A8}$$

These relations enable us to write Eq. A1 analytically:

$$[a]_i = [a] + \underline{r}/[\underline{K}_w(1 - r)^2] + [a]_i \underline{E}\ . \tag{A9}$$

An additional expression is necessary which relates the concentration of species across the phase boundary. It is convenient to define the aggregation number in the organic phase:

$$\langle N \rangle_o \equiv \sum_j j[AG^{(j)}] / \sum_j [AG^{(j)}] = 1/(1 - \underline{R}) \qquad (A10)$$

$\langle N \rangle_w$ may be defined analogously:

$$\langle N \rangle_w \equiv \sum_j j[ag^{(j)}] / \sum_j [ag^{(j)}] = 1/(1 - \underline{r}) \; . \qquad (A11)$$

In defining the partition coefficient, it is recalled that the forces directing aggregation, and consequently the surface characteristics of the aggregates, differ between the phases. It is useful to consider initially two limiting situations which differ in important respects from the phase transfer process at hand, in order to obtain a suitable expression for $\underline{K}_p$. (i) If aggregation proceeds in identical fashion in both aqueous and organic media, the macroscopically observed partition coefficient should simply be the ratio of total monomer concentrations, the energy of transfer of an aggregate scaling as the number of subunits, so that $\underline{K}_p = \sum_j j[AG^{(j)}] / \sum_j j[ag^{(j)}] = (\underline{R}/\underline{r})(\underline{K}_w/\underline{K}_o)(\langle N \rangle_o/\langle N \rangle_w)^2$; $\underline{E} = \underline{K}_p \underline{r}/[\underline{K}_w [a]_i (1 - \underline{r})^2]$ is then seen to be independent of $\underline{K}_o$.
(ii) If the differences between the aggregates in the two phases are so great that structural rearrangement on phase transfer is energetically equivalent to complete disaggregation in one phase and reaggregation in the second, $\underline{K}_p = [AG]/[ag] = (\underline{R}/\underline{r})(\underline{K}_w/\underline{K}_o)$. Here, it is found that $[AG^{(j)}] = \underline{K}_o^{-1} (\underline{K}_o \underline{K}_p \underline{r}/\underline{K}_w)^j$ is unbounded with increasing j, unless

$\underline{K}_o\underline{K}_p/\underline{K}_w < \underline{r}^{-1}$; but for $\langle N\rangle_w > 1$, $\underline{r}$ is $\underline{O}(1)$, and since $\underline{K}_p \geq 1$ for the monomer, this requires that $\underline{K}_o/\underline{K}_w \leq 1$, which is contrary to our observations.

Between the two extremes, neither of which appears satisfactory, are cases where aggregates undergo direct phase transfer, but with structural rearrangements which limit solvophobic contacts. Such cases correspond to $\underline{K}_p = (\underline{R}/\underline{r})(\underline{K}_w/\underline{K}_o)(\langle N\rangle_o/\langle N\rangle_w)^t$, $0 < t < 2$, where the free energy of phase transfer of $ag^{(j)}$ is between $-\infty$ and j times that of monomeric ag. Aggregates of the nucleotide-GrS complex, by virtue of the amphiphilic character and compact structure of the monomeric unit, should undergo relatively facile internal reorganization on traversal of the phase boundary in order to sequester effectively the solvophobic groups in either phase (alkyl groups in water; amide and uncharged phosphoryl groups in $CHCl_3$). The apparent partition coefficient of an aggregate should then vary slowly with the number of contained monomeric complexes, suggesting that the most appropriate expression for the macroscopic partition coefficient, corresponding to $t = 1$, is just the quotient of aggregate concentrations:

$$\underline{K}_p = \frac{\underline{R}}{\underline{r}}\frac{\underline{K}_w}{\underline{K}_o}\frac{\langle N\rangle_o}{\langle N\rangle_w} = \sum_j [AG^{(j)}]/\sum_j [ag^{(j)}]\,. \qquad \text{(A12)}$$

Combining Eqs. A6 and A10, $\sum_j [AG^{(j)}] = (\langle N\rangle_o - 1)/\underline{K}_o$, while from Eqs. A7, A8, and A10, $\underline{K}_o[a]_i\underline{E} = \langle N\rangle_o^2 - \langle N\rangle_o$; thus, solving for the aggregate concentration in the organic phase,

$$\sum_j [AG^{(j)}] = (\sqrt{4\underline{K}_o[a]_i\underline{E} + 1} - 1)/2\underline{K}_o\,. \qquad \text{(A13)}$$

Combining A4, A12, and A13,

$$\underline{E} = \frac{\underline{K}_p \underline{r}}{\underline{K}_w [a]_i (1 - \underline{r})} \left[1 + \frac{\underline{K}_p \underline{K}_o \underline{r}}{\underline{K}_w (1 - \underline{r})} \right] \tag{A14}$$

which may be combined with Eq. A9 to yield

$$(1 - \underline{r})^2 ([a] - [a]_i) + \left[\frac{\underline{r}}{\underline{K}_w} \right] (1 + \underline{K}_p) + \left[\frac{\underline{r}}{\underline{K}_w} \right]^2 \underline{K}_p (\underline{K}_p \underline{K}_o - \underline{K}_w) = 0 \tag{A15}$$

Equations A3 and A15 are solved for $\underline{r}$, and $\underline{E}$ subsequently obtained from Eq. A14 as a function of $\underline{K}$, $\underline{K}_p$, $\underline{K}_w$, $\underline{K}_o$, $[a]_i$, and ζ. The extraction profiles computed from these equations were optimized for a given $\underline{K}$ by variation of the remaining parameters. There was a high degree of correlation between $\underline{K}_p$ and $\underline{K}_o$, so that this treatment actually involves adjustment of three parameters, $\underline{K}$, $\underline{K}_w$, and $\underline{K}_p^2 \underline{K}_o$ (subject to $\underline{K}_w < \underline{K}_o$).

(b) 1:2 Association

Eqs. A9 and A3 are replaced by A16 and A17

$$[a]_i = [a] + [ag] + \underline{r}/[\underline{K}_w (1 - r)^2] + [a]_i \underline{E} \tag{A16}$$

$$[a] = [a]_i (1 - \zeta) + [(1 + \underline{K}_G)[g] - [ag]]/2 \tag{A17}$$

where $\underline{r} \equiv \underline{K}_1 \underline{K}_2 \underline{K}_w [a] [g]^2$. Equations A14, A16, and A17 are solved for $\underline{E}$ as a function of $\underline{K}_1$, $\underline{K}_2$, $\underline{K}_p$, $\underline{K}_w$, $\underline{K}_o$, $[a]_i$ and ζ, where either $[ag] = (\underline{K}_1 + \underline{K}_2)[a][g]$ (Case I) or $[ag] = \underline{K}_1 [a][g]$ (Case II).

References

1. Lehn, J.-M. Pure Appl. Chem. 1978, 50, 871-892.
2. Tabushi, I.; Imuta, J.; Seko, N.; Kobuke, Y. J. Am. Chem. Soc. 1978, 100, 6287-6288.
3. Tabushi, I.; Kobuke, Y.; Imuta, J. J. Am. Chem. Soc. 1980, 102, 1744-1745.
4. Tabushi, I.; Kobuke, Y.; Imuta, J. J. Am. Chem. Soc. 1981, 103, 6152-6157.
5. Montanari, F.; Landini, D.; Rolla, F. Topics Current Chem. 1982, 101, 147-200.
6. Dietrich, B.; Fyles, D. L.; Fyles, T. M.; Lehn, J.-M. Helv. Chim. Acta 1979, 62, 2763-2787.
7. Dietrich, B.; Hosseini, M. W.; Lehn, J.-M.; Sessions, R. B. J. Am. Chem. Soc. 1981, 103, 1282-1283.
8. Graf, E.; Lehn, J.-M. J. Am. Chem. Soc. 1976, 98, 6403-6405.
9. Kimura, E.; Kodama, M.; Yatsunami, R. J. Am. Chem. Soc. 1982, 104, 3182-3187.
10. Kimura, E.; Sakonaka, A.; Takashi, Y.; Kodama, M. J. Am. Chem. Soc. 1981, 103, 3041-3045.
11. Nakai, C.; Glinsmann, W. Biochemistry 1977, 16, 5636-5641.
12. Stern, A.; Gibbons, W. A.; Craig, L. C. Proc. Natl. Acad. Sci. U.S.A. 1968, 61, 734-741.
13. Few, A. V. Trans. Faraday Soc. 1956, 848-859.
14. Silaeva, S. A.; Glazer, V. M.; Shestakov, S. V.; Prokof'ev, M. A. Biokhimiya 1965, 30, 947-955.

15. Glazer, V. M.; Silaeva, S. A.; Shestakov, S. V. Biokhimiya 1966, 31, 1135-1141.

16. Vostroknutova, G. N.; Bulgakova, V. G.; Udalova, T. P.; Sepetov, N. F.; Sibel'dina, L. A.; Ostrovskii, D. N. Biokhimiya 1981, 46, 657-666.

17. Ostrovskii, D. N.; Bulgakova, V. G.; Zhukova, I. G.; Kaprel'yants, A. S.; Rozantsev, E. G.; Simakova, I. M. Biokhimiya 1976, 41, 175-182.

18. Kaprel'yants, A. S.; Nikiforov, V. V.; Miroshnikov, A. I.; Snezhkova, L. G.; Eremin, V. A.; Ostrovskii, D. N. Biokhimiya 1977, 42, 329-337.

19. Dawson, R. M. C.; Elliott, D. C.; Elliott, W. H.; Jones, K. M. Data for Biochemical Research (1969) Ed. 2, Oxford Press, New York.

20. Eisenman, G.; Ciani, S.; Szabo, G. J. Membrane Biol. 1979, 1, 194-345.

21. Ruttenberg, M. A.; King, T. P.; Craig, L. C. Biochemistry 1966, 5, 2857-2864.

22. Ingwall, R. T.; Gilon, C.; Goodman, M. in Peptides: Chemistry, Structure, and Biology (1975) (Walter, R., and Meienhofer, J., eds.) pp. 247-253, Ann Arbor Science, Ann Arbor, Michigan.

23. Franzen, J. S.; Stephens, R. E. Biochemistry 1963, 2, 1321-1327.

24. Susi, H.; Ard, J. S. Arch. Biochim. Biophys. 1966, 117, 147-153.

25. Melnick, E. I.; Semenov, S. N.; Miroshnikov, A. I. in Membranes Transport Processes (1978) (Tosteson, D. C., Ovchinnikov, Yu. A., and Latorre, R., eds.) pp. 261-266, Raven Press, New York.

26. Susi, H.; Sampugna, J.; Hampson, J. W.; Ard, J. S. Biochemistry 1979, 18, 297-301.

27. Nakagaki, M.; Handa, T.; Sehara, C. Yakugaku Zasshi 1981, 101, 774-779.

28. Wu, E.-S.; Jacobson, K.; Szoka, F.; Portis, A. Biochemistry 1978, 17, 5543-5549.

29. Ovchinnikov, Yu. A.; Ivanov, V. T. Tetrahedron 1975, 31, 2177-2209.

30. Hunter, F. E.; Schwartz, L. S. in Antibiotics: Mechanism of Action (1967) (Gottlieb, D., and Shaw, P. D., eds.) pp. 636-641, Springer-Verlag, New York.

31. Dergunov, A. D.; Kaprel'yants, A. S.; Ostrovskii, D. N. Biokhimiya 1981, 46, 1499-1509.

32. Finer, E. G.; Hauser, H.; Chapman, D. Chem. Phys. Lipids 1969, 3, 386-392.

33. Pache, W.; Chapman, D.; Hillaby, R. Biochim. Biophys. Acta 1972, 255, 358-364.

34. Eremin, V. A.; Sepetov, N. F.; Sibeldina, L. A.; Lordkipanidze, A. E.; Ostrovskii, D. N. Dokl. Akad. Nauk SSSR 1979, 245, 994-997.

35. Izumiya, N.; Kato, T.; Aoyagi, H.; Waki, M.; Kondo, M. Synthetic Aspects of Biologically Active Cyclic Peptides:

Gramicidin S and Tyrocidines (1979) Wiley, New York, Ch 4-6.

36. Miki, Y. Osaka Shiritsu Daigaku Igaku Zasshi 1960, 9, 4005-4017; Chem. Abstr. 1962, 55, 10587h.

37. Nandi, S.; Seddon, B. Bioch. Soc. Trans. 1978, 6, 409-411.

38. Seddon, B.; Nandi, S. Bioch. Soc. Trans. 1978, 6, 412-413.

39. Klingenberg, M. in The Enzymes of Biological Membranes, Vol. III (1976) (Martonosi, A., ed) pp. 383-438, Plenum, New York.

40. Løwenstein, H.; Lassen, H.; Hvidt, A. Acta Chem. Scand. 1970, 24, 1687-1696.

CHAPTER V

COMPLEXATION AND PHASE TRANSFER OF NUCLEIC ACIDS BY GRAMICIDIN S

1. Introduction

Little is known of the physiological role of GrS in the producer strains of B. brevis, even though the mode of biosynthesis (1) and metabolic fate (2) of the peptide are relatively well characterized. GrS is synthesized enzymatically at the end of logarithmic growth (at which time a GrS-dependent decrease in energy charge (3, 4) and nucleotide efflux are observed (5)) and is incorporated into the spore (2, 6). During germination and early vegetative growth the GrS content of the culture decreases, and products of GrS hydrolysis are detectable in the medium (2). It has also been established that GrS, while retained in the spore, is not released by the young vegetative culture as a bactericidal agent (2). Despite the temporal relation of synthesis to sporulation, GrS-deficient mutants appear to sporulate normally (6-8), indicating that GrS is unlikely to trigger dormancy. However, GrS-deficient spores grow out rapidly after germination, unlike wild-type spores (6), and it has been proposed that the peptide functions as a bacterial hormone regulating outgrowth (9). The molecular basis of this difference in outgrowth rates has not been elucidated.

In the preceding section, it was shown that GrS forms complexes with nucleotides which undergo phase transfer to organic solvents. Complexation in water is directed by coordination of the positively

charged Orn side chains of the peptide with the negatively charged phosphoryl groups of the nucleotide. The contribution of the nucleoside moiety to the stabilization of the complexes appears insignificant, and inorganic pyrophosphate was found to compete effectively with ATP for GrS in the phase transfer process. This suggested that complementary interanionic spacing might be a sufficient condition for GrS binding to polynucleotides as well. Indeed, the interanionic distance between adjacent residues in double stranded B DNA is estimated from the Corey-Pauling-Koltun model to be ~ 7 Å, which is comparable to the intercationic distance of 6 - 8 Å in the peptide in solution (Chapter III).

In the present chapter, a nucleic acid-GrS interaction is demonstrated by the direct phase transfer of nucleic acids to $CHCl_3$ in the presence of GrS and by the nucleic acid-dependent inhibition of GrS-mediated ATP phase transfer. The interaction is primarily ionic and, as was the case with free nucleotides, colligative effects are found to be a major determinant of phase transfer efficiencies. The stoichiometry of DNA-GrS binding is established; modeling of the complex suggests a close topochemical complementarity between GrS and double helical nucleic acids. In view of these results and earlier microbiological studies of spore outgrowth (2, 6, 8, 9), it is proposed that the primary function of GrS in the producer is to ensheath, and thereby protect against chemical degradation, the genetic material in the spore.

2. Experimental Section

Materials. GrS dihydrochloride (Sigma) was filtered and lyophilized prior to use. Adenosine 5'-triphosphate, disodium salt (Sigma) was used without further purification.

Preparation of Nucleic Acids. The procedure was similar to that employed by Anderson et al. (10). Ultrasonic irradiation is reported to decrease the molecular weight of calf thymus DNA toward a limiting value of 5×10^5 (11). DNA prep I: Calf thymus DNA (Sigma), 4 mg/ml in a buffer containing 0.1 M NaCl and 0.01 M tris(hydroxymethyl)aminomethane (Tris), pH = 7.0, was irradiated in an ice bath for 15 min on a Heat Systems-Ultrasonics W225R probe ultrasonicator operating at 20 KHz, 200 W maximum output (microtip, power setting = 5 (maximum = 10), 50% duty cycle; total immersion time = 30 min). The slightly turbid solution was diluted fourfold with buffer and dialyzed at 4°C against (1) 0.01 M EDTA and (2) 0.02 M NaCl + 0.01 M Tris, pH = 7.0. DNA prep II: Calf thymus DNA, 0.4 mg/ml in a buffer containing 0.08 M NaCl and 0.04 M Tris, pH = 7.0, was sonicated as above for between 0 and 5 min. Dialysis was performed as in prep I. DNA phosphate (DNA-P) concentration was determined from the absorbance at 258 nm, using ϵ_{max}(monomer) = 6.6×10^3. The increase in absorbance with sonication was less than 5 percent.

Soluble RNA, type III, from Bakers yeast (Sigma), 0.8 mg ml^{-1} in a buffer containing 0.08 M NaCl and 0.04 M Tris, pH = 7.0, was dialyzed at 4°C against (1) 0.005 M EDTA and (2) 0.02 M NaCl + 0.01 M Tris, pH = 7.0, and centrifuged briefly to remove particulate contaminants.

Synthesis of [N^{δ}-acetylornithyl^{2}]-gramicidin S (AcGrS). This was performed by the N-acetoxysuccinimide method (12), using equimolar amounts of peptide and acylating agent. N-acetoxysuccinimide (NAS) was prepared from Ac_2O and N-hydroxysuccinimide (NHS) via dicyclohexylcarbodiimide coupling (12) and recrystallized from EtOAc. An aqueous solution of GrS (220 ml, 5 mg ml^{-1}) was adjusted to pH 8.5 with NaOH and 1.9 ml of a 75 mg ml^{-1} solution of NAS in dioxane added over a period of 1.5 h at 25°C with vigorous stirring. The pH was readjusted to 8.5 after addition of each aliquot of NAS. The resulting suspension contained GrS, AcGrS, and Ac_2GrS, as well as salts, NHS, and unreacted NAS. This was lyophilized, dissolved in $CHCl_3$/MeOH (6:1), filtered, and applied to a Unisil silicic acid column (Clarkson). Ac_2GrS was eluted with the same solvent (ninhydrin-negative, R_f= 0.45 on TLC) as well as most of the NHS. The fraction eluting with 2:1 $CHCl_3$/MeOH yielded a single ninhydrin-positive spot on TLC (R_f = 0.56 in $CHCl_3$/MeOH/H_2O, 65:25:2, compared with R_f = 0.21 for GrS) and was rechromatographed on Sephadex G-15 in 60% aqueous EtOH. ^{1}H NMR spectra of the purified material at 500.13 MHz were similar to that of native GrS but contained new resonances at δ = 7.8 (Me_2SO-$\underline{d}_6$, t, 1, N$\underline{H}$COCH$_3$), δ = 2.0 (MeOH-$\underline{d}_4$, s, 3, NHCOC$\underline{H}_3$), and a decrease in intensity of the broad Orn $N^{\delta}H_3^+$ resonance from 6 to 3 protons. In Me_2SO-$\underline{d}_6$ many of the ^{1}H resonances were doubled, indicating a loss of C_2 symmetry in the peptide. This was not observed in methanol. The amino acid composition of the peptide was verified as follows: Both GrS and the acetylated derivative were dansylated by a standard

method (13). Workup consisted of LH-20 chromatography in 2:1 MeOH/$CHCl_3$, with column effluent monitoring by long wave uv illumination. Dansylornithine should be resistant to 6N HCl treatment (13) and acetylornithine should be acid-labile. Thus, the Orn content of non-dansylated GrS (or AcGrS), dansylated AcGrS, and dansylated GrS should be 2, 1, and 0 eq mol^{-1}, respectively. As expected, the Orn content of GrS and AcGrS were found after acid hydrolysis to be 1.94 and 1,90, respectively, while the Orn content of dansylated GrS was 0.28 eq mol^{-1}. The amino acid composition of the dansylated acetyl derivative was found to be: Val, 1.80; Orn, 1.06; Leu, 2.16; Phe, 1.96; Pro, 2.10. The composition, NMR spectrum, and TLC mobility were thus all consistent with acetylation of the terminal amino group of a single Orn residue as the sole modification in the peptide. The yield was 15% based on the initial quantity of GrS.

Extraction Procedure. Equilibration of each aqueous solution with $CHCl_3$ was carried out as detailed under Methods in Chapter IV. There were two differences of consequence: (i) the aqueous phase in DNA-containing extractions contained 0.01 M NaCl and 0.02 M Tris, pH = 7.0. The presence of salts lowered the maximum extraction efficiency $\underline{E}_{max}$ for the extraction of ATP by GrS at zero nucleic acid concentration ($[ATP]_i = 10^{-5}$ M, $[GrS]_i = 2 \times 10^{-5}$ M) to 0.57 from 0.83, the value obtained previously in the absence of added salts. The absolute magnitude of $\underline{E}_{max}$ was of no significance in the interpretation of the extraction-competition data. (ii) Phase transfer was generally monitored by the increase in absorbance at 270 nm of the organic layer, which is assumed proportional to the concentration of

nucleotide or nucleic acid transferred; absorbance by the peptide at this wavelength is negligible. Absorbance measurements were made on a Beckman Instruments ACTA CIII spectrophotometer using 1 cm pathlength cells at 25°C. The molar extinction coefficient of ATP is virtually unchanged by complexation and phase transfer.

When buffered solutions of DNA or RNA alone were agitated with $CHCl_3$, there was no interfacial precipitation and no absorbance change in the aqueous layer save below 245 nm, where an increase in absorbance attributable to dissolved $CHCl_3$ was detected.

3. Results

Intaction of GrS with Sonicated DNA. Figure 1 presents the results of an extraction-competition experiment in which variable quantities of sonicated calf thymus DNA were added to the aqueous phase in a standard ATP-GrS extraction at pH 7.0. The initial ATP and GrS concentrations were 10^{-5} M and 2×10^{-5} M, respectively; the stoichiometry of the ATP-GrS interaction at this pH is 1:2. The dependence of the absorbance at 270 nm in the organic phase after extraction ($A_{270,\,chl}$) on the ratio of initial concentrations $[\text{DNA monomer}]_i/[\text{GrS}]_i$ ($\equiv \underline{r}$) is as follows: For $0 < \underline{r} < 1$, $A_{270,\,chl}$ increases gradually with $\underline{r}$, achieving a maximum when $r = 1$; when $1 < \underline{r} < 2$, $A_{270,\,chl}$ decreases sharply towards a limiting value of ~ 0.005, thereafter remaining negligible for all $\underline{r} > 2$. A precipitate was evident in the aqueous phase after extraction for all $\underline{r} \geq 1$. This inhibition of ATP phase transfer by calf thymus DNA when $\underline{r} > 1$ is

Figure 1. Extraction-competition employing ultrasonically irradiated calf thymus DNA. The aqueous phase prior to extraction contained 10^{-5} M ATP, 2×10^{-5} M GrS, and DNA, pH = 7.

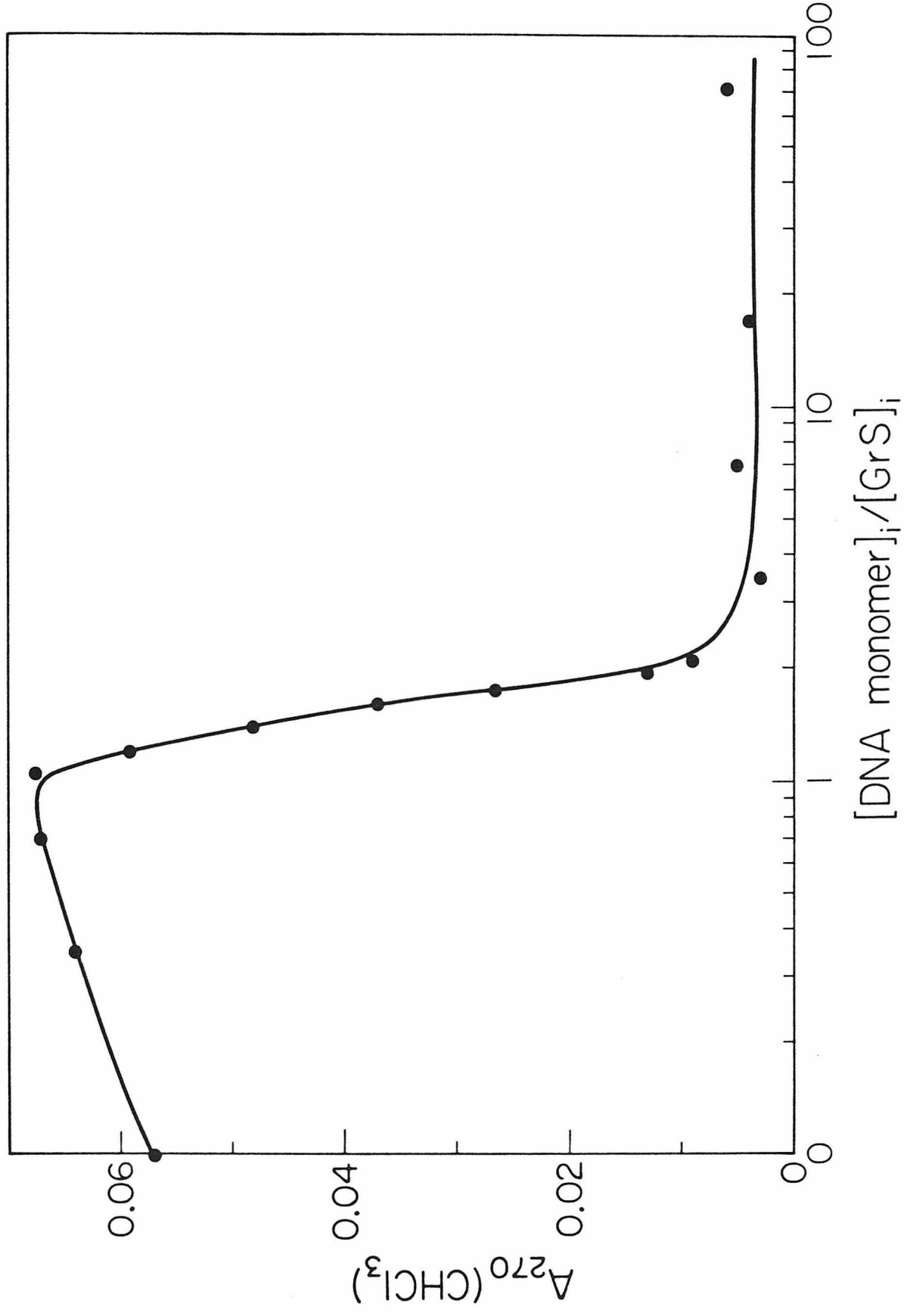
0.06
0.04
0.02
0
$A_{270}(CHCl_3)$
0
1
10
100
$[DNA\ monomer]_i/[GrS]_i$

indicative of a direct interaction between GrS and the nucleic acid. That it is just complete when $\underline{r} = 2$ is consistent with a stoichiometry of 2:1 (DNA monomer/GrS). The unexpected increase in $\underline{A}_{270,\,chl}$ with $\underline{r}$ for $\underline{r} < 1$ suggests that direct DNA phase transfer or DNA/ATP exchange may occur, assisted by the change in stoichiometry.

GrS was indeed found to mediate DNA phase transfer (Figure 2), albeit in a manner qualitatively different from the free nucleotides. With the latter, the quantity transferred by a fixed concentration of GrS increases linearly with nucleotide concentration up to the point that the ratio of initial concentrations is equivalent to the stoichiometry of the complex; the quantity transferred at higher nucleotide concentrations is simply equal to that transferred at the point of stoichiometric equivalence. In contrast, while DNA transfer increases up to $\underline{r} = 1$, a <u>decrease</u> with $\underline{r}$ is observed for higher values of this parameter. The nonlinear dependence of $A_{270,\,chl}$ on $\underline{r}$ and the appearance of a precipitate after extraction are first noted for $0.5 < \underline{r} < 1$. When the precipitate is present, the sum of the absorbances of the 2 phases is less than the initial absorbance of the aqueous phase, indicating that the precipitate contained DNA as a GrS conjugate.
In these experiments, the aqueous layer was visibly turbid prior to extraction, but the organic phase containing the DNA-GrS complex was optically clear.

Figure 1 should thus exhibit the interplay of three phenomena: (i) the direct phase transfer of DNA, which results in an increase in $A_{270,\,chl}$ for $0 < \underline{r} < 1$; (ii) competitive inhibition of the ATP extraction by DNA, assisted by the stoichiometry change, which yields a

Figure 2. Direct phase transfer of ultrasonically irradiated calf thymus DNA by GrS (2×10^{-5} M), pH = 7. Presence of a precipitate in the aqueous layer in individual runs is indicated ($\times$).

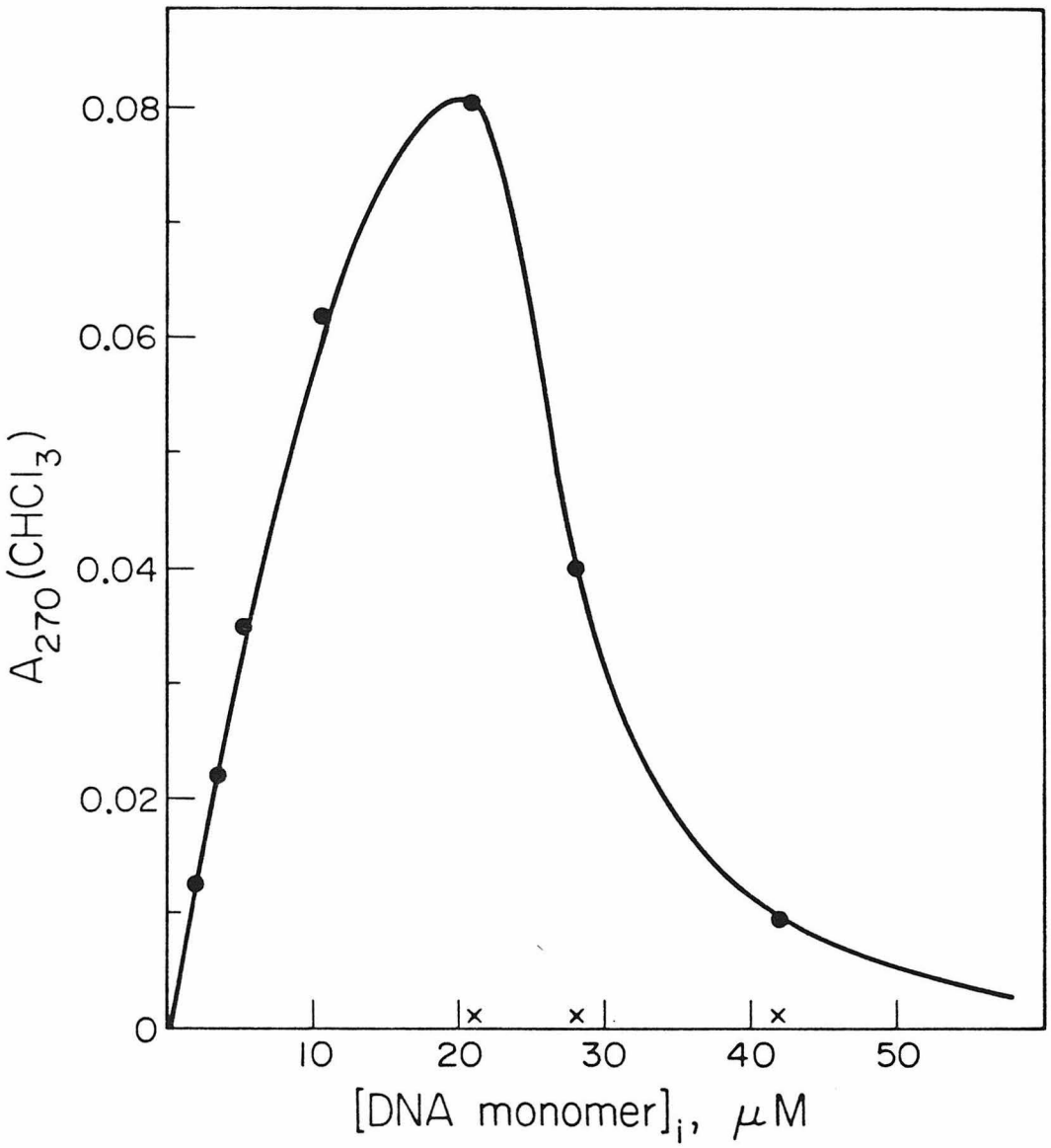
0.08
0.06
0.04
0.02
0
$A_{270}(CHCl_3)$
10
20
30
40
50
[DNA monomer]$_i$, μM

decrease in $A_{270,\,chl}$ for $\underline{r} > 0$ that partially cancels the increase attributable to (i); and (iii) a decrease in DNA transfer when $r \geq 1$ which contributes, with (ii), to the sharp decrease in $A_{270,\,chl}$ for $1 < \underline{r} < 2$. It was possible to reverse the inhibition of ATP transfer almost completely at $\underline{r} = 2$ ($[ATP]_i$ and $[GrS]_i$ as in Figure 1) by the addition of 0.005 M 1,4-butanediamine (putrescine) dihydrochloride, which should bind DNA extensively at this concentration (14). On the other hand, a 5-fold molar excess of ATP over DNA, again with $\underline{r} = 2$, afforded no reversal of the inhibition.

The presence of DNA in $CHCl_3$ after direct extraction was verified by uv spectrophotometry (Figure 3). The absorption spectrum of the transferred complex, measured between 300 nm and the solvent cutoff, 245 nm, is clearly consistent with the near uv absorption envelope of a nucleic acid. The contribution of $\underline{\underline{D}}$-Phe ($\lambda_{max}$ = 260 nm) is, in comparison, negligible, and the peptide group absorbance becomes appreciable only at shorter wavelength.

Interaction of GrS with Native DNA; Stoichiometry of the DNA-GrS Complex. Unsonicated calf thymus DNA was found to be only slightly transferred by GrS into $CHCl_3$. The native strands partition quantitatively into the precipitate, as indicated by the low absorbance of both phases. Phase transfer is markedly enhanced by brief ultrasonic irradiation (Table I).

The extraction-competition experiment was repeated with unsonicated DNA in order to measure the inhibition of ATP phase transfer as a function of DNA monomer concentration without concurrent transfer of nucleic acid. As shown in Figure 4, $A_{270,\,chl}$ decreases

Figure 3. Absorption spectrum of the $CHCl_3$ layer after extraction of an aqueous phase containing 10^{-5} M DNA monomer and 2×10^{-5} M GrS, pH = 7.

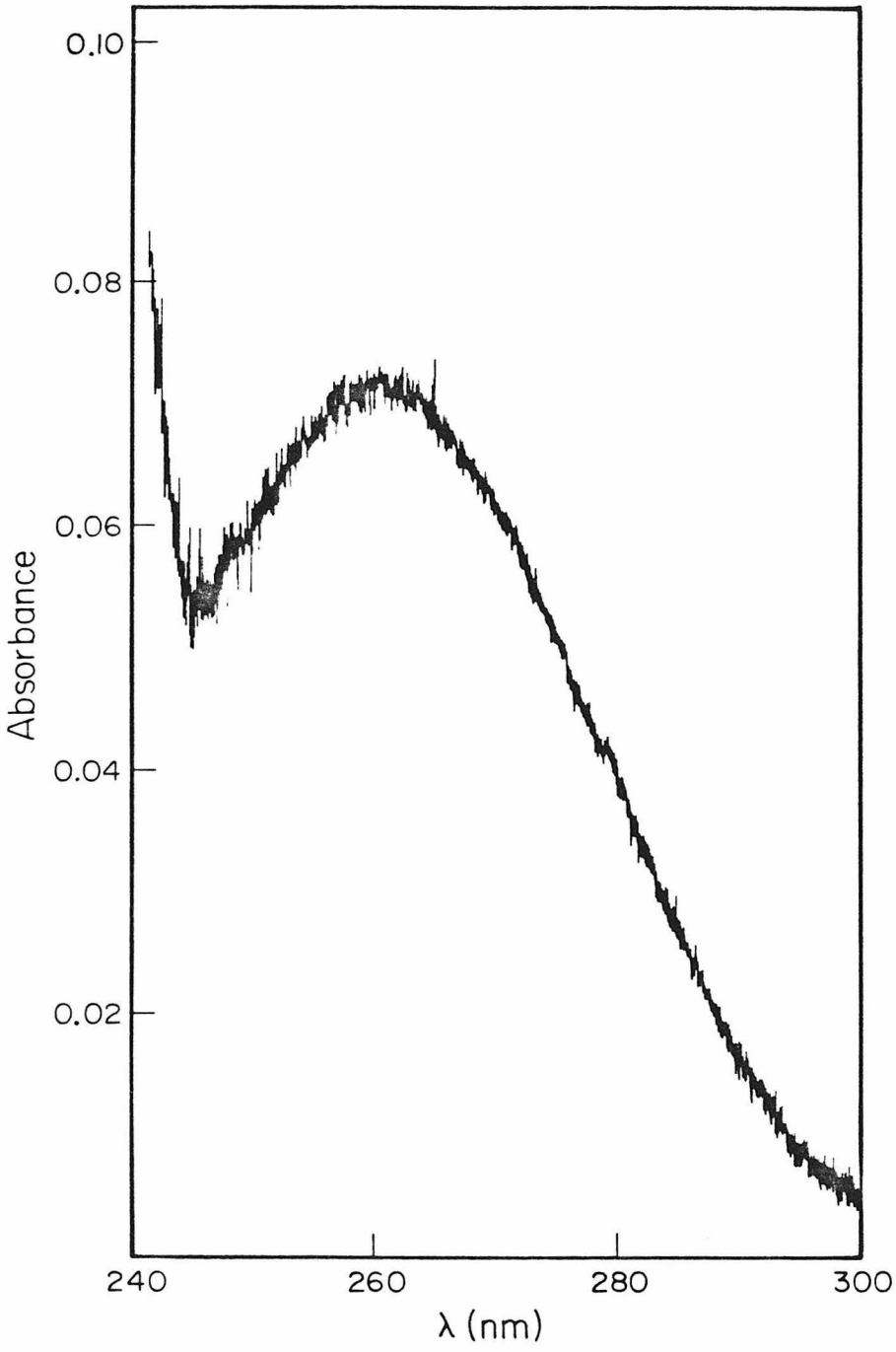
0.10
0.08
0.06
0.04
0.02
Absorbance
240
260
280
300
λ (nm)

Table I. Phase Transfer of DNA: Effect of Sonication

Sonication Time (min)[a]	$\underline{r}$[b]	Ppt[c]	$A_{270,aq}$	$A_{270,chl}$
0	0.5		0.003	0.011
0	2	+	0.002	0.000
0.5	0.5		0.002	0.040
0.5	2	+	0.005	0.004
5	0.5		0.002	0.048
5	2	+	0.007	0.004

[a]Actual time of irradiation: 50 percent duty cycle (see Methods).

[b]$\underline{r} \equiv [\text{DNA monomer}]_i / [\text{GrS}]_i$; in all instances $[\text{DNA monomer}]_i = 10^{-5}$ M. [c]Presence of a precipitate after extraction.

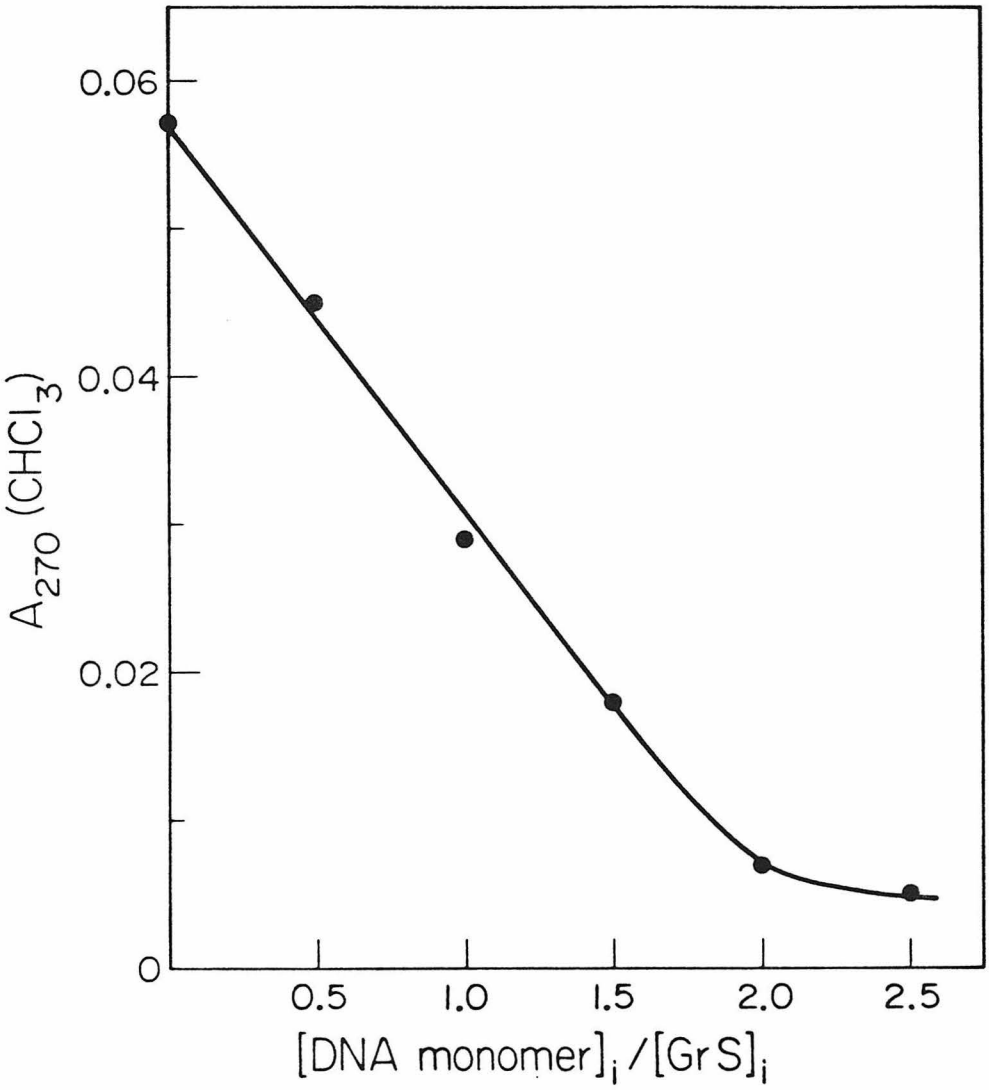

Figure 4. Extraction-competition employing native calf thymus DNA. The aqueous phase prior to extraction contained 10^{-5} M ATP, 2×10^{-5} M GrS, and DNA, pH = 7.

monotonically with [DNA] for $0 < \underline{r} < 2$, achieving a limiting value of $A_{270, chl} \sim 0.005$ when $r \geq 2$. This result provides compelling evidence that the stoichiometry of the DNA-GrS complex is indeed 2 DNA monomers per molecule of GrS, as expected for a predominantly electrostatic mode of binding. The linearity of the observed decrease in $A_{270, chl}$ suggests that the affinity of GrS for DNA is considerably higher than it is for free nucleotides.

Reexamining Figure 2, it is apparent that direct phase transfer of DNA occurs only when GrS is present in stoichiometric or higher concentrations. If GrS is randomly distributed among available (monomer) binding sites on the nucleic acid molecules and if nucleic acid transfer requires quantitative charge neutralization, then phase transfer should be negligible when the concentration of GrS is sub-stoichiometric ($\underline{r} > 2$). The decrease in DNA extraction efficiency for $1 < \underline{r} < 2$ likely derives from incomplete binding to all available polymer sites; it is also conceivable that an excess of free peptide is necessary to prevent aggregation of the DNA-GrS complexes in the aqueous phase and promote quantitative transfer, as was observed with the nucleotides.

For low concentrations of nucleic acid ($\underline{r} < 1$), sonicated DNA is transferred quantitatively to $CHCl_3$. From the initial slope of the phase transfer curve in Figure 2, one calculates $\epsilon_{270} \simeq 6 \times 10^3$ for the complex in the organic phase. If $\epsilon_{270}/\epsilon_{258} = 0.8$, as measured for calf thymus DNA in aqueous buffer, then this value of the extinction coefficient represents a hyperchromicity of between 10 and 15 percent. In water, the difference spectrum between complexed and uncomplexed DNA is complicated by light scattering effects, but the enhancement of the near-uv absorbance appears smaller (~ 4 percent). The hyperchromicity in $CHCl_3$ represents, at least in part, a change in solvation state of the nucleic acid.

Interaction of GrS with RNA. GrS was in addition found to bind soluble yeast RNA containing $tRNA^{Val}$ and $tRNA^{Tyr}$. The interaction qualitatively resembled that with sonicated calf thymus DNA: direct phase transfer was obtained (Figure 5), ATP phase transfer was blocked, and RNA transfer ceased with high $\underline{r}$, the RNA-GrS complexes instead partitioning into a precipitate. The shutoff of direct transfer at high nucleic acid concentration occurs at higher values of $\underline{r}$ than for calf thymus DNA, however, with significant phase transfer still observed when $\underline{r} = 2$. A determination of the stoichiometry of binding was not attempted here since ϵ_{max} was not known with precision.

Interaction of GrS Analogues with Sonicated DNA. In view of the importance of ion coordination in DNA binding, it was of interest to examine the affinity of the monofunctional derivative, AcGrS, for DNA. As shown in Table II, AcGrS promotes phase transfer of

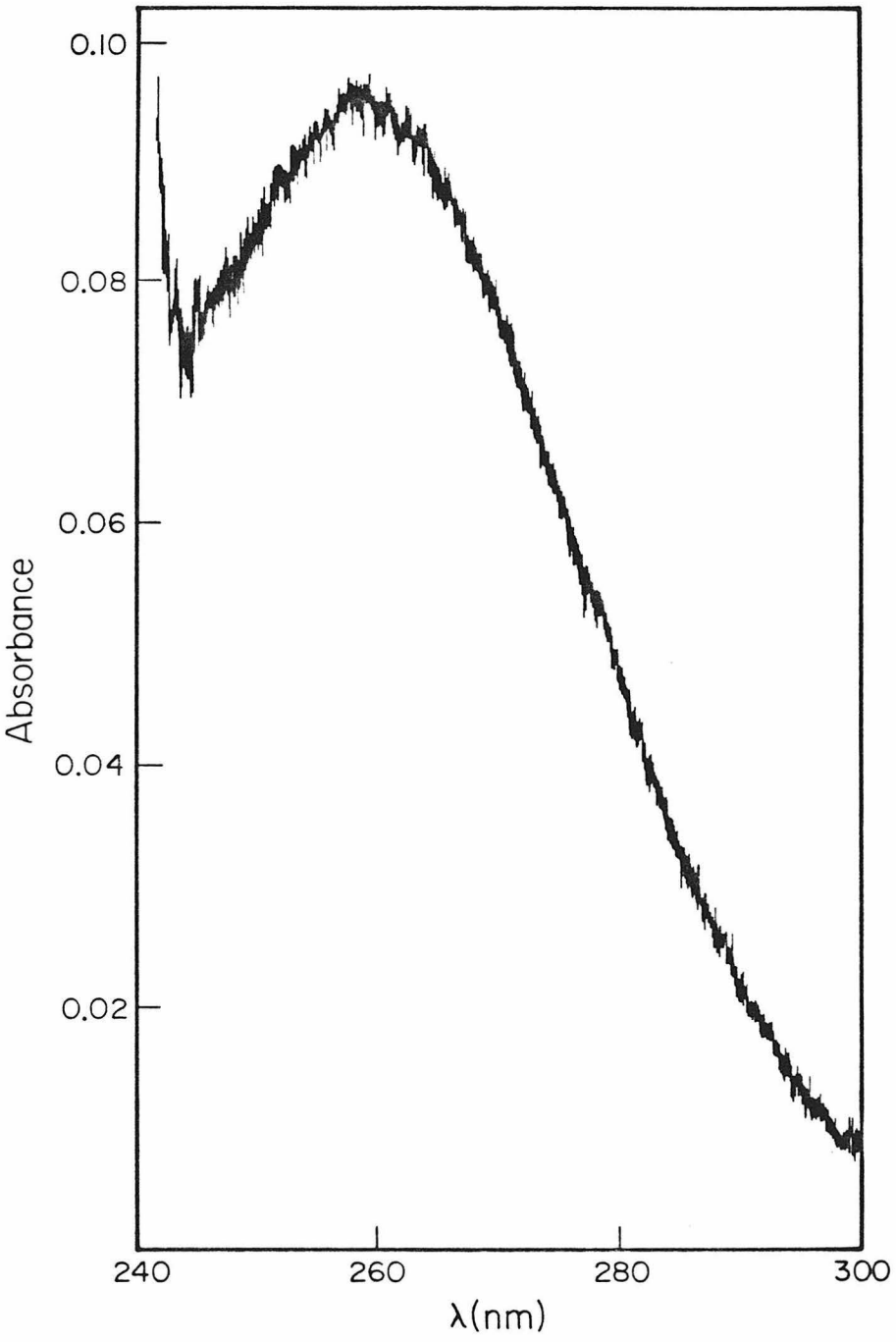

Figure 5. Absorption spectrum of the $CHCl_3$ layer after extraction of an aqueous phase containing $\sim 4 \times 10^{-5}$ M RNA monomer and 2×10^{-5} M GrS, pH = 7.

Table II. Phase Transfer of DNA by GrS Congeners[a]

Peptide	$[Peptide]_i \times 10^{-5}$ M	Ppt	$A_{270,aq}$	$A_{270,chl}$
GrS	2.0	+	0.001	0.049
AcGrS[b]	2.0		0.033	0.029
AcGrS[b]	4.0		0.019	0.056
Me_6GrS	2.0	+	0.002	0.003

[a] $[DNA\ monomer]_i = 10^{-5}$ M in all instances. [b] Added inititally to the $CHCl_3$ phase.

sonicated calf thymus DNA, albeit significantly less efficiently than the native peptide. While the separate extinction coefficients of the complex in the two phases are not known, the increase in total absorbance of the AcGrS conjugates in the two phases is consistent with a significantly larger (20 to 30 percent) hyperchromicity than was estimated for the DNA-GrS complex in $CHCl_3$.

The results of an extraction with Me_6GrS are provided in the table for comparison. In contrast to the situation with free nucleotides (Chapter VI) the degree of DNA binding, as indicated by removal of nucleic acid from the aqueous layer, is quantitatively similar for GrS and the quaternary analogue. Interestingly, Me_6GrS fails to promote measurable phase transfer.

4. Discussion

A novel interaction between GrS and nucleic acids has been discovered which, like that between GrS and nucleotides, exploits both the dicationic and amphiphilic properties of the peptide. While interactions of nucleic acids with basic polypeptides are well known (15) and have been in many instances characterized stoichiometrically (16) and thermodynamically (17,18), no instance of peptide-mediated phase transfer has heretofore been reported. Among the polypeptide antibiotics produced by other B. brevis strains, the tyrocidines, which are structurally related to GrS but monocationic, have been found to interact in aqueous media with DNA of diverse origins (19-22). The stoichiometry of the tyrocidine-DNA interaction is unknown, and neutralization of the single positive charge does not weaken the binding

(22), indicating that ion pairing contributes only secondarily to complexation, in marked contrast to GrS.

In view of the 2:1 stoichiometry of binding and the lipophilicity of the nucleic acid-GrS complexes, the only plausible mode of interaction involves apposition of the Orn side chains of GrS to adjacent phosphoryl groups of the nucleic acid backbone, with exposure of the hydrophobic face of the peptide to the solvent. While binding is not specific for a particular nucleic acid species, GrS appears particularly well adapted to the complexation of compact double stranded nucleic acids possessing 8- or 10-fold helical symmetry: For example, a mode of binding to B DNA may be postulated in which GrS binds successive phosphoryl groups, oriented with the peptide ring plane and ring minor axis parallel to the DNA helix axis. Each GrS molecule is then able to form 4 interamide hydrogen bonds with its neighbor on the opposite side of the minor groove. In this manner, the minor groove can be completely ensheathed by peptide molecules, with very little steric crowding. The major groove remains, without conformational adjustment, partially exposed. Because of the rigidity of the peptide backbone, the side chains of D-Phe are unable to engage the nucleic acid bases, but interpeptide stacking is possible. The sense of the ring twist in GrS, with the participation of the Orn^{i} amino group in internal hydrogen bonding with D-Phe $C{=}{=}O^{i+2}$ (Chapter III), may facilitate the interaction with a right-handed helix. Chiroptical studies will be helpful in elucidating the conformational changes, if any, induced in nucleic acids by GrS, although measurements below 250 nm must take into account the large Cotton effect of the peptide.

The affinity of GrS for DNA is apparently significantly higher than for free nucleotides, for which two rationales may be offered. (i) The interanionic distances in the nucleic acid are relatively fixed, and closely approximate the intercationic spacing in the peptide. The di- and triphosphate moieties of the nucleotides, in contrast, are conformationally mobile, and GrS binding selects a limited set of rotameric isomers which optimize the coordination of oppositely charged groups, an entropically unfavorable process. (ii) The monomeric nucleotide-GrS complexes in the organic phase contain exposed amide and uncharged phosphoryl groups, which are solvophobic. Association of the complexes by intermolecular hydrogen bonding (cross-β aggregation) yields ribbonlike aggregates with highly apolar surfaces; this enhances the efficiency of phase transfer, but requires diffusional encounters of the complexes in 3 dimensions. On the other hand, the nature of the GrS-nucleic acid interaction is such that interamide hydrogen bonding occurs between neighboring peptide molecules on the polynucleotide strand. The resulting complex presents, as transferred, minimal solvophobic contacts in the organic phase.

The behavior of AcGrS towards DNA differs from that of both GrS and the tyrocidines. Reflecting the lower stability of the complex involving a single ion pair, AcGrS transfers DNA to $CHCl_3$ less efficiently than does the native peptide. In addition, there is a large hyperchromic effect. If charge neutralization by the peptide is prerequisite for phase transfer, the stoichiometry should approach 1:1 (DNA-P/AcGrS) and DNA unwinding is inevitable if all the bound AcGrS is to be accommodated. Unlike AcGrS, the monocationic tyrocidines

induce significant hypochromicity (21), supporting the contention that tyrocidine-DNA interactions involve hydrogen bonding and/or base stacking through participation of the Asn, Gln, Phe, and Trp residues and thus differ fundamentally from the interactions of nucleic acids with GrS or its derivative.

Binding of nucleic acids by GrS clearly provides a molecular basis for the 8 to 10 h lag between germination and outgrowth exhibited by wild-type B. brevis Nagano or G-B spores but not by spores derived from GrS-negative mutants (6,8). Addition of GrS to mutant spores between 0 and 80 min after germination inhibited respiration and ^{14}C-uracil uptake (9) and restored the lag period (8), while extraction of GrS from wild-type spores resulted in early outgrowth as invariably observed in the mutants (9). During the lag period GrS is hydrolyzed to its constituent amino acids (2). The GrS content of a wild-type spore is 5×10^{-14} g, or 4×10^{-17} mol; $\geq 2 \times 10^{-14}$ g GrS per mutant spore is necessary to restore the lag (6,9). The DNA-P content of a Bacillus spore is typically 2 to 7×10^{-17} eq (23; data not reported for the GrS producer). The DNA-P and GrS content of the spore are thus commensurate, which would allow for near-stoichiometric binding. Removal of bound GrS is thus necessary after germination for RNA synthesis, and outgrowth, to proceed; conceivably, the hydrolytic enzymes required for this are incorporated into the spore. GrS-RNA interactions are also likely, in that Bacillus spores generally contain appreciable amounts of RNA, chiefly ribosomal and transfer (23-25). Finally, it is estimated that ~ 25 percent of the GrS synthesized in the parent cell is present in the mature spore (2). The

remainder is unaccounted for, and may be lost to the medium as nucleotide complexes during sporulation.

The primary selective advantage conferred upon the spore by GrS is, according to the results of the present study, protection of the genome. The possibility that the peptide performs a regulatory function during outgrowth (9) cannot be excluded, but there is no evidence that GrS levels after germination are endogenously modulated. Preliminary data have, on the other hand, shown diminished heat resistance among spores of several GrS-negative mutant strains (8). Stoichiometric binding by GrS ensheaths the bacterial chromosome in a dense peptide matrix possessing a highly apolar external surface, which should constitute an effective barrier against chemical degradation. Protection against uv irradiation may in addition be provided by the aromatic side chains. Further studies of the susceptibility of the wild-type and mutant dormant chromosomes to environmental damage and of the thermal and chemical stability of GrS-DNA complexes in vitro are clearly warranted.

References

1. Katz, E., Demain, A. L. Bacteriol. Rev. 1977, 41, 449-474.
2. Egorov, N. S., Vypiyach, A. N., Zharikova, G. G. Mikrobiologiya 1970, 39, 331-336.
3. Silaeva, S. A., Glazer, V. M., Shestakov, S. V, Prokof'ev, M. A. Biokhimiya 1965, 30, 947-955.
4. Vostroknutova, G. N., Bulgakova, V. G., Udalova, T. P., Sepetov, N. F., Sibel'dina, L. A., Ostrovskii, D. N. Biokhimiya 1981, 46, 657-666.
5. Glazer, V. M., Silaeva, S. A., Shestakov, S. V. Biokhimiya 1966, 31, 1135-1141.
6. Nandi, S., Seddon, B. Bioch. Soc. Trans. 1978, 6, 409-411.
7. Kambe, M., Sakamoto, Y., Kurahashi, K. J. Biochem. 1974, 75, 481-493.
8. Marahiel, M. A., Danders, W., Krause, M. Kleinkauf, H. Eur. J. Biochem. 1979, 99, 49-55.
9. Seddon, B., Nandi, S. Bioch. Soc. Trans. 1978, 6, 412-413.
10. Anderson, C. F., Record, M. T., Hart, P. A. Biophys. Chem. 1978, 7, 301-316.
11. Cohen, G., Eisenberg, H. Biopolymers 1966, 4, 429-440.
12. Lindsay, D. G., Shall, S. Biochem. J. 1971, 121, 737-745.
13. Gray, W. R. Methods Enzymol. 1972, 25, 121-138.
14. Mahler, H. R., Mehrotra, B. D. Biochim. Biophys. Acta 1963, 68, 211-233.
15. Helene, C., Maurizot, J.-C. CRC Critical Rev. Biochem. 1981 10, 213-258.

16. Seipke, G., Arfmann, H.-A, Wagner, K. G. Biopolymers 1979, 18, 855-872.

17. Latt, S. A., Sober, H. A. Biochemistry 1967, 6, 3293-3306.

18. Record, M. T., Lohman, T. M., de Haseth, P. J. Mol. Biol. 1976, 107, 145-158.

19. Schazschneider, B., Ristow, H., Kleinkauf, H. Nature 1974, 249, 757-759.

20. Ristow, H., Schazschneider, B., Bauer, K., Kleinkauf, H. Biochim. Biophys. Acta 1975, 390, 246-252.

21. Ristow, H., Schazschneider, B., Vater, J., Kleinkauf, H. Biochim. Biophys. Acta 1975, 414, 1-8.

22. Hansen, J., Pschorn, W., Ristow, H. Eur. J. Biochem. 1982, 126, 279-284.

23. Doi, R. H. in The Bacterial Spore, (Gould, G. W., Hurst, A., eds.) pp. 125-166, Academic Press, New York, 1969.

24. Vold, B. S., Minatogawa, S. in Spores V (Halvorson, H. O., Hanson, R., Campbell, L. L., eds.) pp. 254-263, American Society for Microbiology, Washington, D.C., 1972.

25. Douthit, H. A., Kieras, R. A. in Spores V (Halvorson, H. O., Hanson, R., Campbell, L. L., eds.) pp. 264-268, American Society for Microbiology, Washington, D.C., 1972.

CHAPTER VI

MICROBIOLOGICAL STUDIES OF GRAMICIDIN S ACTION

1. Introduction

In view of the implications of the work outlined in the preceding chapters for the antibacterial action of GrS, preliminary microbiological investigations were undertaken in an effort to elucidate the molecular basis for GrS toxicity in vivo.

Previous attempts to characterize the antibiotic effect, generally directed towards possible interactions of GrS with cell surface elements, cannot be considered definitive. The Ostrovskii group employed a Micrococcal preparation containing several membrane-bound oxidases which are inhibitable by GrS at absolute concentrations of antibiotic significantly higher than the minimum lethal concentration, or MLC (1-3). These workers proposed, primarily on the basis of topochemical considerations and earlier studies of model membranes, that the molecular basis for this effect was electrostatic binding of GrS to phospholipid head groups which ultimately brought about a reduction in frequency of diffusional encounters between elements of the respiratory chain. A causal connection between enzyme inhibition in this system or in extracts of the producer (4) and the bactericidal effect in vivo remains to be established, however, and evidence that a direct GrS-phospholipid interaction underlies either action of the antibiotic is not conclusive.

Yonezawa et al. (5) employed a filter-binding assay in

conjunction with a GrS congener labeled with ^{14}C at Pro to quantitate the extent of peptide binding to bacterial cells. For the more sensitive gram-positive species (Bacillus subtilis and Staphylococcus aureus, minimum inhibitory concentration (MIC) = 1.0 to 1.5 $\mu g\ ml^{-1}$) uptake of label increased linearly with GrS concentration in the culture medium, leveling off near the MIC at 1.3 to 1.4×10^6 molecules $cell^{-1}$. The time course of uptake was rapid (< 1 min). There was no uptake of label by Escherichia coli (MIC = 5 to 10 $\mu g\ ml^{-1}$) after 20 min for GrS concentrations up to 2.5 $\mu g\ ml^{-1}$; higher GrS concentrations were not employed. While the location of the cell-associated GrS was not radiautographically verified, the authors concluded that the peptide was bound by surface adsorption. By their calculation, the entire cell surface was covered by a monomolecular layer of antibiotic at the MIC. The phospholipid content of the plasma membrane is inadequate to bind this quantity of peptide (Chapter I). An alternative possibility is electrostatic binding to the phosphate residues of teichoic acid in the cell wall (6). Teichoic acids are ubiquitous in gram-positive organisms and generally absent from gram-negative organisms (7, 8) which may account for the total inability of E. coli to retain the radiolabel.

In this chapter the antibiotic potencies for GrS, [N^{δ}-trimethylornithyl$^{2,2'}$]-GrS (Me_6GrS) and [N^{δ}-acetylornithyl^2]-GrS (AcGrS) are compared. In addition, the time course of the lethal effect and the cell concentration dependence of the MLC are determined. The results obtained are used to formulate a model for GrS

action in which GrS is internalized and binds polyanionic substrates within the cell, possibly nucleoside triphosphates, to yield lipophilic complexes which are cytotoxic.

2. Experimental Section

Materials. GrS dihydrochloride (Sigma) was filtered and lyophilized prior to use. Me_6GrS (Chapter III) and AcGrS (Chapter V) were prepared as previously noted. Other chemicals were of reagent grade.

Bacterial Strain and Culture Medium. Staphylococcus aureus ATCC 25923 was the gift of Mr. Perkins Poon of Huntington Memorial Hospital. The culture was maintained on an agar plate containing, per liter, 15 g Bacto agar, 5 g Bacto yeast, 10 g Bacto tryptone, 10 g NaCl, and 50 ml thiamine HCl, 1 mg ml^{-1} stock, pH = 7.5. It was transferred to a fresh plate every two to three weeks.

Stock nutrient broths (2×) were prepared as follows: PMY medium, 10 g Bacto peptone, 3 g Bacto meat extract, 3 g Bacto yeast extract, 2 g D-glucose, and 7 g NaCl per liter, pH = 7.0; LOP medium, 5 g Proteose peptone, 6 g D-glucose, 6 g NaCl, 2 g KCl, and thiamine HCl, 1 mg ml^{-1} stock, 2 ml per liter, pH = 7.0. Prior to bioassay these were diluted twofold and sterile 0.5 M Na phosphate buffer, pH = 7.0, added to a final concentration of 0.02 M. PMY medium was similar to that employed by Yonezawa et al. (5) save that in the previous study the broth contained 10 percent MeOH. Antibiotics were delivered either as concentrated aqueous or methanolic solutions. Growth media and salt solutions were steam

sterilized at 121°C and 30 psi for 20 min. Aqueous antibiotic solutions were passed through a Millipore HA filter immediately prior to delivery.

Bioassay Procedure. An inoculum of organisms was transferred by a flame-sterilized nichrome wire from the agar plate to 4 ml of broth containing 2 ml PMY medium and 2 ml sterile distilled water. The seed culture was incubated at 30°C in a reciprocal shaker for 4 h, at which time $A_{590} \sim 2.0$ (1 absorbance unit at 590 nm = 5×10^8 cells ml^{-1}). Transfers were then made from this culture to bioassay media containing 2 ml PMY or LOP medium, 0.16 ml phosphate buffer, the desired quantity of antibiotic, and water to a final volume of 4 ml. In a typical run, antibiotic concentration increments were 10 to 20 percent between consecutive bioassay tubes. The cultures were incubated as above for 4-6 h (PMY) or 15-20 h (LOP) and final titers determined spectrophotometrically at 1:20 dilution. The MLC was defined as the antibiotic concentration above which the final titer was equal to or less than the initial titer. This is invariably greater than, but quantitatively parallels, the minimum inhibitory concentration usually reported. The MLC for GrS at a given initial cell concentration in the bioassay was found not to depend onthe following: (i) choice of LOP or PMY medium in the final propagation; (ii) the presence of MeOH up to 10 percent by volume (propagation in the MeOH-containing cultures was slowed threefold); (iii) choice of aqueous or methanolic stock solutions for delivery of the antibiotic.

3. Results

Antibiotic Potencies. The activities of GrS and congeners are given in Table I. The MLC determined for GrS is consistent with the MIC reported previously (5). The MLC of AcGrS is lower than that previously reported (40 μg ml^{-1}; 9). As the current estimate was accurately reproduced for different lots of peptide, the discrepancy must be attributed to differences in bioassay method. It should be noted that the MIC for GrS was reported to be 5 μg ml^{-1} in this earlier reference.

Me_6GrS and AcGrS are 3- to 5-fold less potents than the native peptide. It is shown in Figure 1 that both derivatives are considerably less effective phase transfer agents for ATP than GrS. The decrease in extraction efficiency is as expected, since these derivatizations substantially weaken ion pairing interactions with anions.

Time Course of the Antibiotic Effect of GrS. The effect of exposure to supralethal concentrations of GrS for varying periods of time on the viability of the culture is displayed in Figure 2. If it is assumed that GrS is primarily bactericidal, then the extent of propagation in the final step of the protocol indicates that 50 percent of the organisms are killed in 15 min and the culture is no longer viable after 90 min. The addition of 0.004 M ATP afforded no protective effect.

Dependence of MLC on Initial Cell Concentration. The routine bioassay for GrS activity was performed with varying quantities of seed culture. The MLC was found to vary linearly with the initial

Table I. Minimum Lethal Concentration of GrS and Analogues[a]

Congener	MLC (μg ml^{-1})
GrS	1.5-1.7
Me_6GrS	5-6
AcGrS	7-8

[a]Initial cell concentration = 10^8 ml^{-1}.

Figure 1. Extraction of ATP into $CHCl_3$ by Me_6GrS (closed circles) or AcGrS (open circles) at pH 7. AcGrS was added initially to the organic phase. The extraction efficiency expected for GrS under identical conditions is shown for comparison (-----). The stoichiometry of the GrS and Me_6GrS complexes is 1:2 (nucleotide:peptide). The stoichiometry of the AcGrS complex is not determined.

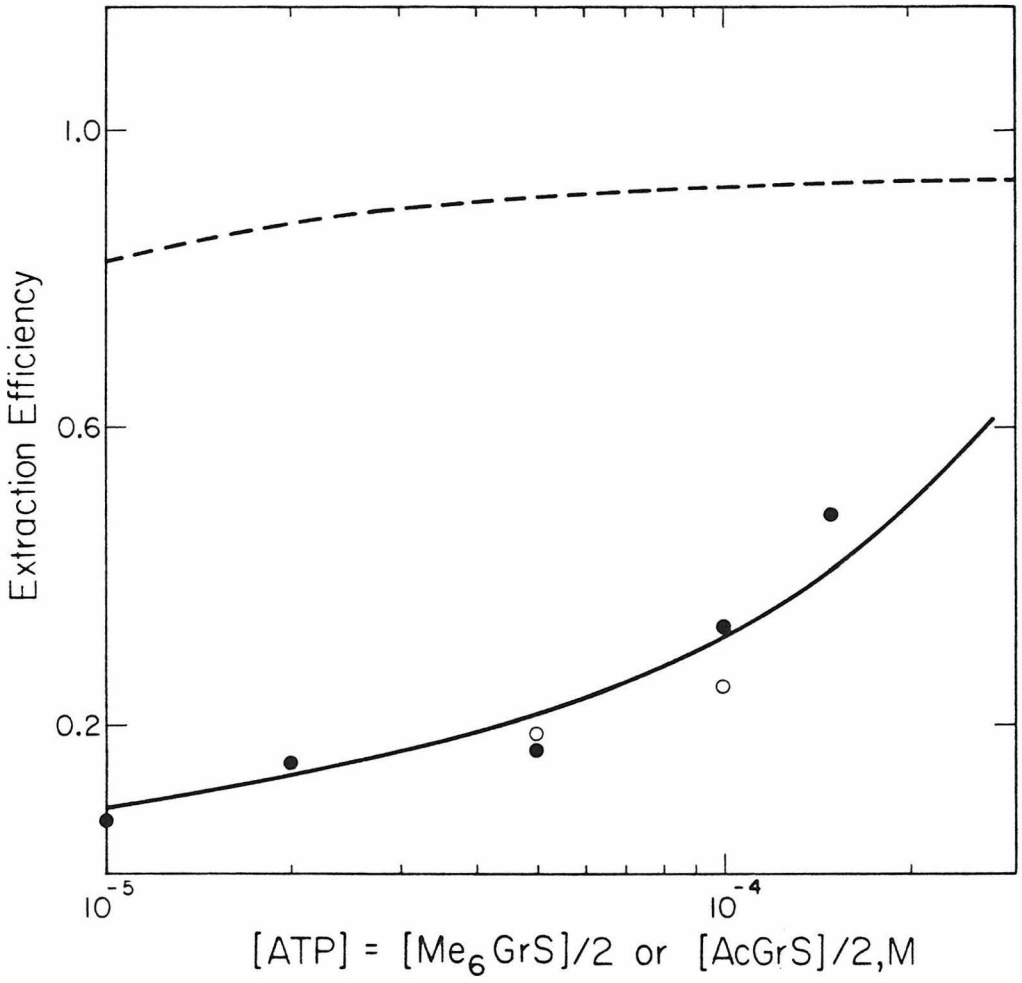
1.0
0.6
0.2
Extraction Efficiency
10^{-5}
10^{-4}
[ATP] = [Me_6GrS]/2 or [AcGrS]/2,M

Figure 2. Time course of GrS action on S. aureus. 6 ml PMY medium containing a supralethal GrS concentration of 3.5 μg ml^{-1} (exposure medium) was injected with cells from a 4 h PMY propagation culture and placed in a reciprocal shaker at 30°C. At the indicated time after injection ("Exposure Time") an 0.5 ml aliquot was withdrawn and added to a tube containing PMY without GrS (total volume = 4 ml). The final GrS concentration was therefore sublethal. The latter culture was incubated as above for 4.5 h and the final cell concentration determined spectrophotometrically. The exposure medium contained either 0.04 M P_i (● - ●) or 0.04 M P_i + 0.004 M ATP (o --- o).

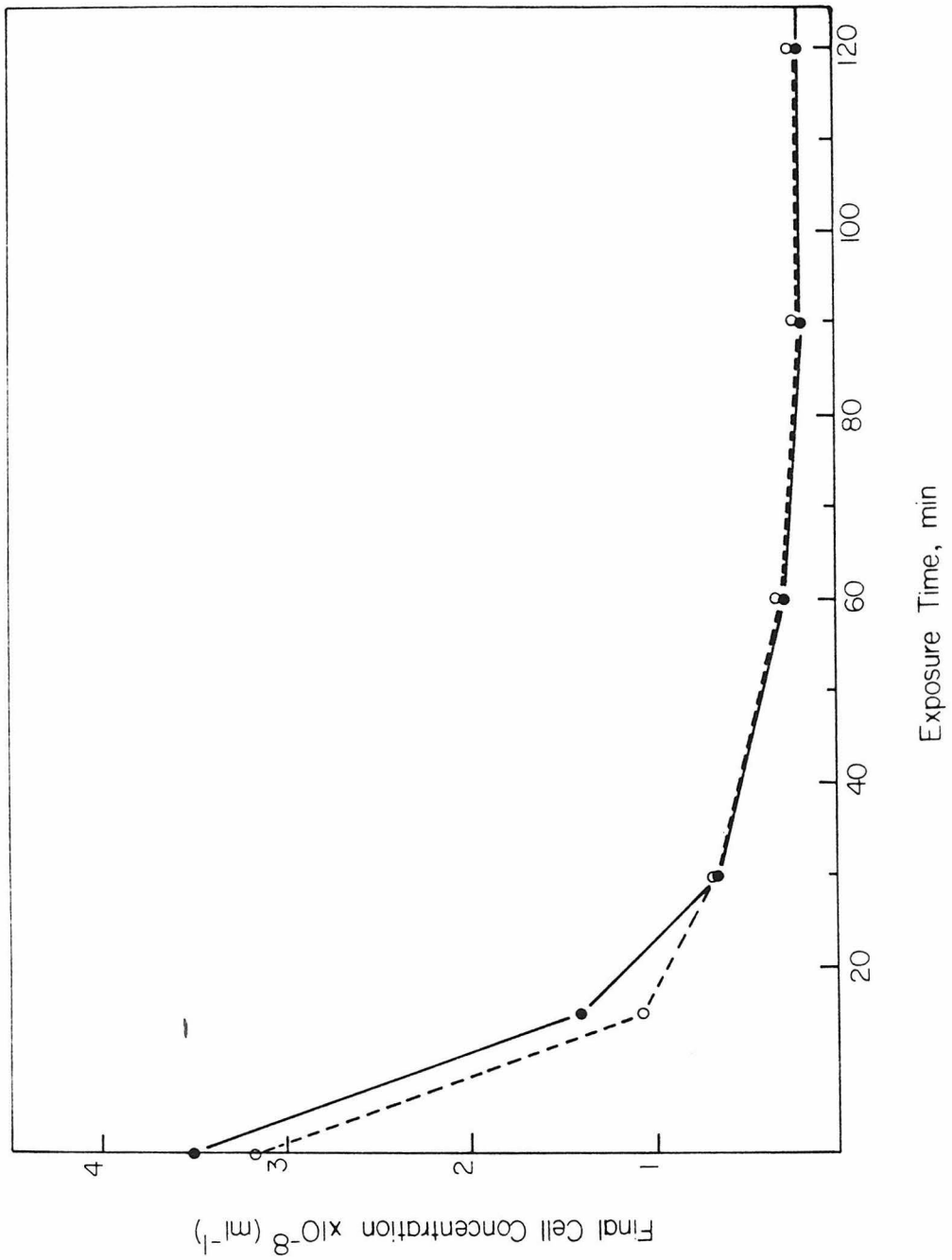
Final Cell Concentration x10^{-8} (ml^{-1})
4
3
2
1
20
40
60
80
100
120
Exposure Time, min

Figure 3. Dependence of GrS minimum lethal concentration on initial cell concentration in the bioassay. Test cultures (LOP medium) were inoculated with varying quantities of PMY seed culture.

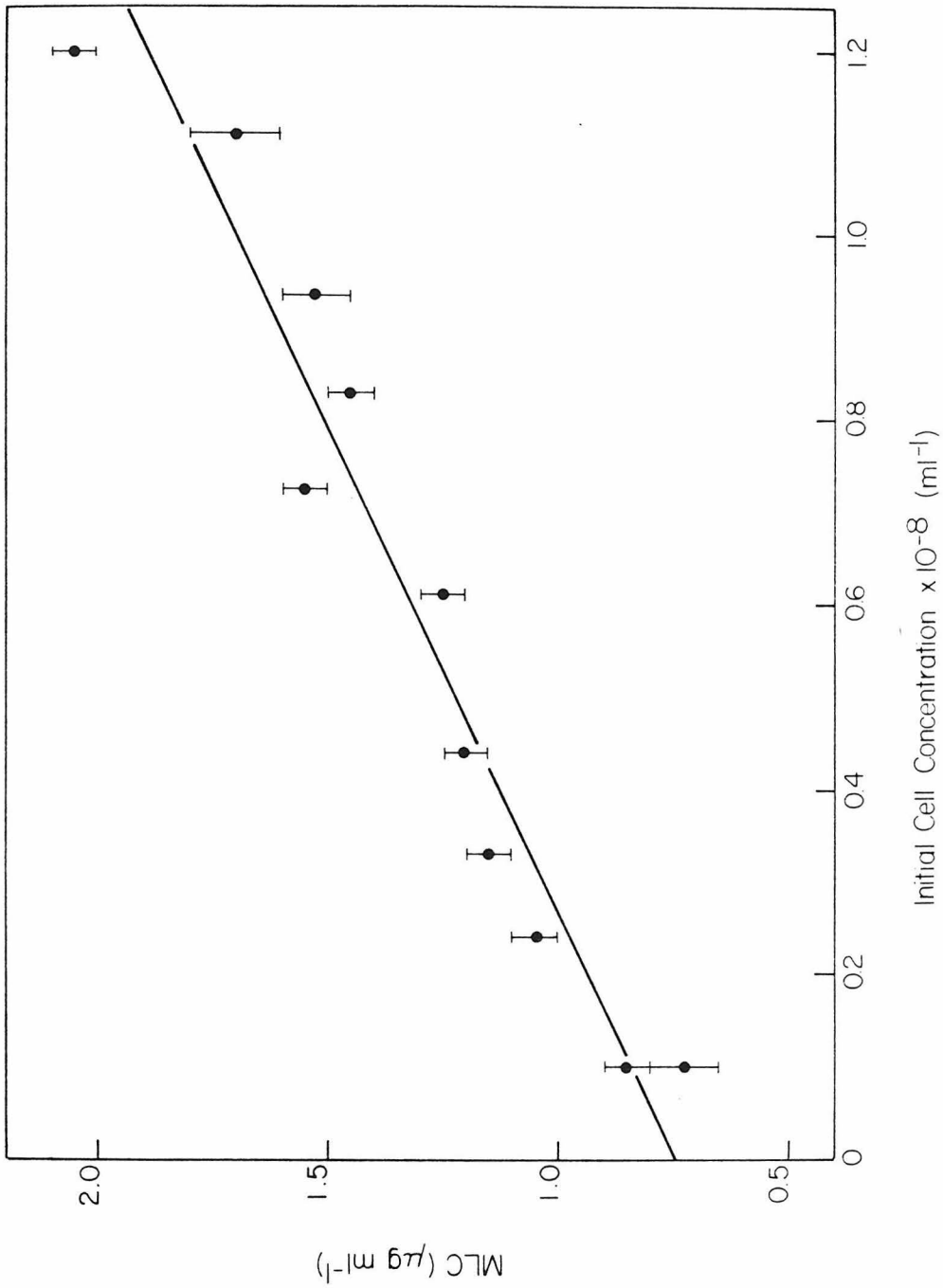
MLC (μg ml-1)
2.0
1.5
1.0
0.5
0
02
04
06
08
1.0
1.2
Initial Cell Concentration x10-8 (ml-1)

cell concentration $\underline{Y}$ according to the relation

$$\text{MLC } (\mu g\ ml^{-1}) = \underline{m}_0 + \underline{k}\underline{Y} \qquad (1)$$

(Figure 3) where $\underline{m}_0 = 0.75 \pm 0.03\ \mu g\ ml^{-1}$ and $\underline{k} = (9.5 \pm 0.8) \times 10^{-9}\ \mu g\ cell^{-1} = (4.7 \pm 0.4) \times 10^6$ molecules $cell^{-1}$. A check of the dependence of the MLC for Me_6GrS on initial cell concentration (data not shown) indicated that $\underline{k}$ was nearly identical while $\underline{m}_0 \approx 4.5\ \mu g\ ml^{-1}$.

4. Discussion

Equation 1 affords estimates of $\underline{m}_0$, which is approximately 6-fold larger for Me_6GrS than GrS. This parameter, which represents the MLC at infinite dilution, provides a basis for an analysis of the relative potencies of GrS congeners and the question of the threshold for lethality at the cellular level.

A model for GrS action is proposed in which the antibiotic equilibrates rapidly with the cytosolic compartment, such that the internal and external free peptide concentrations are nearly equal. The peptide interacts nonstereospecifically with polyanionic substrates in the cytoplasm to yield lipophilic complexes which are toxic to the cell. Here, only electrostatic binding to the nucleoside triphosphates is considered. Possible metabolic or structural lesions consequent to nucleotide complexation were discussed in Chapter IV. When the free antibiotic concentration is equal to $\underline{m}_0$, a threshold lethal concentration $\underline{b}_0$ of complexes is achieved in the cells, which is assumed to be the same to first order for the two dicationic congeners. At this stage, permeability barriers break down, and the large intracellular

pool of nucleic acids becomes available for peptide binding, most plausibly through dilutional loss of bound aliphatic polyamines (10).

Within the confines of this model, it will be shown that a consistent estimate of $\underline{b}_0$ can be calculated for GrS and Me_6GrS. Let [N] denote the total available intracellular nucleoside triphosphate concentration and K_{app} be the apparent third-order extraction constant for the 1:2 interaction between NTP and GrS estimated from the ATP phase transfer data *in vitro* ($\underline{K}_{app} \equiv \underline{E}/(4[A]_i^2(1-\underline{E})^3$, where $\underline{E}$ is the extraction efficiency and $[A]_i$ is the initial nucleotide concentration). Use of $\underline{K}_{app}$ is mandated here by lack of an exhaustive binding study for Me_6GrS; the crudeness of the approximation is somewhat lessened by the fact that $\underline{b}_0$ varies only as the square root of this parameter. Assuming that $[N] \gg \underline{b}_0$, one obtains directly

$$\underline{b}_0 = \tfrac{1}{2} m_0 - [(1 + 8\underline{m}_0 \underline{K}_{app}[N])^{\frac{1}{2}} - 1]/8\underline{K}_{app}[N] . \qquad (2)$$

From the extraction studies (Fig. 1 and Chapter IV) and bioassays, $\underline{K}_{app} = 2 \times 10^{11}\ M^{-2}$, $\underline{m}_0 = 6 \times 10^{-7}$ M for GrS and $\underline{K}_{app} = 2 \times 10^{7}\ M^{-2}$, $\underline{m}_0 = 3.5 \times 10^{-6}$ M for Me_6GrS. Investigations of the nucleotide pool of actively dividing bacteria provide estimates of 0.002 to 0.006 M for $[N]_{total}$ (11 and refs. therein; 12, 13), of which it is allowed that $\sim$50 percent is available, i.e., not tightly bound to macromolecules. If $0.001\ M \leq [N] \leq 0.003\ M$, equation 2 then yields for the intracellular threshold $1.9 \times 10^{-7} M < \underline{b}_0 < 4.2 \times 10^{-7}$ M for Me_6GrS and $2.8 \times 10^{-7} M < \underline{b}_0 < 2.9 \times 10^{-7}$ M for GrS. The estimates of $\underline{b}_0$ for the two antibiotic congeners are in agreement, corresponding to ~200 complexes

per organism, given a cellular diameter of $\sim 10^{-4}$ cm.

The present set of data is clearly at variance with the filter binding experiment (5) in showing a longer time course of action (15 min vs. < 1 min) and a greater extent of apparent binding (4.7×10^6 vs. 1.4×10^6 molecules cell^{-1}). The difference between the time course of uptake of radiolabeled GrS as determined by filter binding and of attenuation of the culture as determined by the bioassay raises the possibility that the two phenomena are unrelated. In the filter binding assay, the first data point in the graph of adsorbed radioactivity vs. time (for gram-positive strains) is observed to be within 10 percent of the limiting value (5). Ultrafiltration of bacteria whose cell walls are rich in teichoic acid should confer a substantial negative charge (7) to the filter, which will in turn trap an appreciable quantity of the cationic peptide. The amount adsorbed will reflect the total available cell surface area if the local charge density is sufficiently high, and the process should not require prior incubation of GrS with the cells. Because of the small surface charge, E. coli will under the same conditions induce negligible retention of label regardless of incubation time, as observed (4). In view of these considerations, the form of binding detected by filtration may be unrelated to the antibacterial action. The timescale of the bactericidal effect at the cellular level is thus judged to be more accurately represented by the time course of attenuation reported herein.

The value of k estimated by Equation 1 is too large to represent surface adsorption and suggests almost certain association of GrS

with cytosolic components. It is possible to regard this quantity as either (i) a minimum number of bound GrS molecules which is bactericidal or (ii) uptake of peptide by components of the dead, and presumably lysed, cell which have come in contact with the external medium. Two observations are inconsistent with (i): the lack of correlation of $\underline{k}$ for GrS and Me_6GrS with potency, and the absence of positive curvature in the graph in Figure 3 as $\underline{Y} \rightarrow 0$), which suggests that any true threshold for lethality is much smaller than MLC/$\underline{Y}$. On the other hand, release of nucleic acids once the cell has been killed will make available $\geq 10^7$ binding sites, with which GrS or Me_6GrS should interact with comparable affinity (Chapter V). It is therefore more reasonable to ascribe $\underline{k}$ to peptide binding to dead cell residua with a smaller contribution from passive surface binding to viable cells.

While the analysis presented cannot provide a firm estimate for the bactericidal threshold at the cellular level or identify target molecules in the cell, it has been established that the behavior of GrS congeners as bactericidal agents and as complexones is consistent with a scheme for GrS action involving intracellular formation of a relatively small number of cytotoxic macromolecular complexes, possibly of the types experimentally demonstrated <u>in vitro</u>, with subsequent cell lysis and uptake of additional peptide by the residua. Such a position contrasts markedly with the traditionally held view that GrS is a surface-active agent which is toxic by virtue of a bulk interaction with membrane phospholipid, so that a high local concen-

tration is needed to achieve the bactericidal effect. It is anticipated that future microbiological studies will address the possibility that internalization and anion complexation underlie the mechanism of action of this antibiotic.

References

1. Ovchinnikov, Yu. A., Ivanov, V. T. Tetrahedron 1975, 31, 2177-2209.
2. Ostrovskii, D. N., Bulgakova, V. G., Zhukova, I. G., Kaprel'yants, A. S., Rozantsev, E. G., Simakova, I. M. Biokhimiya 1976, 41, 175-182.
3. Kaprel'yants, A. S., Nikiforov, V. V., Miroshnikov, A. I., Snezhkova, L. G., Eremin, V. A., Ostrovskii, D. N. Biokhimiya 1977, 42, 329-337.
4. Vostroknutova, G. N., Bulgakova, V. G., Udalova, T. P., Sepetov, N. F., Sibel'dina, L. A., Ostrovskii, D. N. Biokhimiya 1981, 46, 656-666.
5. Yonezawa, H., Kaneda, M., Tominaga, N., Higashi, S., Izumiya, N. J. Biochem. 1981, 90, 1087-1091.
6. Yonezawa, H., Izumiya, N. Kyushu University, Japan, personal communication, 1981.
7. Archibald, A. R., Baddiley, J. Adv. Carbohydrate Chem. 1966, 21, 323-375.
8. Heptinstall, S., Archibald, A. R., Baddiley, J. Nature (London) 1970, 225, 519-521.
9. Izumiya, N., Kato, T., Aoyagi, H., Waki, M. Kondo, M. Synthetic Aspects of Biologically Active Cyclic Peptides: Gramicidin S and Tyrocidine, 1979, pp. 60-61, Wiley, New York.
10. Tabor, C. W., Tabor, H. Annu. Rev. Biochem. 1976, 45, 285-306.

11. Fynn, G. H., Davison, J. A. J. Gen. Microbiol. 1976, 94, 68-74.

12. Scarborough, G. A. Biochem. Biophys. Res. Commun. 1971, 43, 968-975.

13. Slayman, C. L. J. Bacteriol. 1973, 114, 752-766.

CHAPTER VII

CONCLUSION

Since the report of its discovery in 1944, GrS has been the subject of numerous physicochemical and pharmacologic studies inspired by its elegant pleated-sheet structure, amphiphilic character, and high antibiotic activity. In recent years it became a virtual prototype in the development of methods for peptide synthesis and conformational analysis. Notwithstanding the large body of accumulated knowledge, major gaps persisted in our understanding of the structure and function of this molecule. These may be summarized as follows: the number, disposition, and strength of the internal hydrogen bonds; the conformation of the functionally essential ornithyl side chains; the molecular basis for antibiotic activity; and the physiological role in the produce organism.

The initial phase of this investigation addressed the role of hydrogen bonding in the secondary structure of GrS. Little refinment of the conformation, known to be of the β-pleated type, was warranted here. However, a protocol was developed which provided the first site-selective characterization of intramolecular hydrogen bonds in a heteropolypeptide in solution. The possibility therefore exists to expand greatly our understanding of the role of hydrogen bonds in proteins in general, through both the unambiguous identification of donor moieties and the characterization of the potential in which the H atom under observation resides.

The study of the ornithyl residues necessitated that the often intractable problem of rapid averaging of NMR parameters sensitive to conformation be circumvented. Rather than proceed segmentally outward from the backbone, which by classical NMR methods rarely, if ever, yields meaningful information beyond the first dihedral angle for amino acid residues, we sought to establish initially the location relative to the ring of the terminal side chain segment. Once this was accomplished, the delineation of the solution structure was relatively straightforward, despite the presence of motional averaging. Two conclusions emerged from this work. First, it should not be assumed with proteins that a solvent-exposed hydrophilic residue cannot participate in an intramolecular polar interaction with a suitable, spatially proximate acceptor moiety; such interactions may be crucial in modulating biological activity. Second, GrS, rather than a simple amphiphile, appeared to possess singular topochemical properties which might enable it to function as an anion complexone.

Observation that nucleotide phase transfer was mediated by GrS established the molecule as the first peptide known to be either a nucleotide complexone or phase transfer agent; GrS possessed both properties. This was, in addition, the first molecular recognition process in which GrS was demonstrated to participate <u>in vitro</u> at physiologically active concentrations. The relevance of nucleotide binding to the cytotoxicity of GrS and to the enigmatic depletion of high-energy phosphate compounds observed in GrS-producing strains actively synthesizing the peptide were discussed. A model for the

antibiotic action was proposed involving internalization of GrS and formation of cytotoxic complexes with polyanionic substrate. The results of preliminary microbiological experiments were consistent with this model.

Finally, GrS was found to bind and induce phase transfer of nucleic acids. This was not unexpected, in view of its interaction with nucleotides; however, in its ability to transfer nucleic acids to apolar media as soluble complexes, GrS is apparently unique among natural and synthetic compounds. Knowledge of the stoichiometries of the nucleotide complexes greatly facilitated the determination of that of the DNA-GrS conjugate. DNA binding may at last provide a rationale for the presence of GrS in the dormant spore of the producer.